Publication No. U-1494

SPACE SYSTEMS OPERATIONS

SUMMARY

MARINER B CAPSULE STUDY

Submitted to: Jet Propulsion Laboratory
California Institute of Technology
Pasadena, California

18 December 1961

AERONUTRONIC
A DIVISION OF Ford Motor Company
FORD ROAD / NEWPORT BEACH, CALIFORNIA

TABLE OF CONTENTS

	Page	to Page
Summary	1	21
Appendices		
A. Separation and Attitude Control	A-1	A-36
B. Space Trajectories and Error Analysis	B-1	B-37
C. Entry Trajectories	C-1	C-15
D. Stability Analysis	D-1	D-15
E. Capsule Heating and Heat Protection	E-1	E-26
F. Communication System	F-1	F-81
G. Capsule Missions and Mission Experimentation	G-1	G-35
H. Capsule Structure; Weight, Power and Propulsion Requirements	H-1	H-16
I. Space Environment and Planet Physical Characteristics	I-1	I-23

Ford Motor Company AERONUTRONIC DIVISION

Intra-Company Communication

AL-164

14 December 1961

To: R. F. Nease

From: J. E. Kemmerly

Subject: ~~SUMMARY OF~~ MARINER B CAPSULE STUDY

1. Introduction

This memorandum presents a summary of the results of a feasibility study regarding a Mariner B probe which may be launched late in 1964 to gather scientific data about the planet Mars during a close fly-by. The major part of this study has been devoted to an instrumentation capsule which would be carried by the spacecraft to a point about 200,000 miles from the planet, and then propelled into a new trajectory which would allow the capsule to penetrate the atmosphere and ultimately land in a sub-solar equatorial region. Two kinds of capsules have been considered, one of which permits survival of the capsule after impact. The general purpose of the capsule is to gather scientific and engineering data about the Martian surface and atmosphere, and data about the space environment in the vicinity of the planet. Such information would not be available to the unaided spacecraft and would help to insure the success of future exploratory missions. Following this summary is a set of eight appendices, each of which is an informal collection of technical memoranda which discuss a major area of interest in the study. Throughout the summary, a superscript notation such as $^{(B-14)}$ will be used to indicate, for example, that reference is being made to Appendix B, page 14.

The study which will be summarized here is definitely not intended to constitute a proposal to design or build the capsule, nor should it be interpreted as a preliminary design because most of the technical investigations are cursory ones which include little in the way of detailed optimization. The investigations have been carried far enough, however, to conclude that at least one of the Mariner B spacecrafts should carry a capsule for atmospheric penetration, and that there is considerable assurance of a valuable and successful capsule mission which will not endanger the simultaneous success of the spacecraft mission itself. Hence a detailed description of a possible capsule mission will be given here, along with a delineation of event sequence, instrumentation, and capsule configuration. Certain capabilities of the spacecraft, which were not known during this study, may dictate major changes in the capsule design; thus the following discussion only constitutes a tentative capsule design and associated mission objectives.

2. Capsule Mission (General)

During this study there has been considerable discussion among the various investigators as to what the scientific objectives of the entry capsule might be. (G-16 to G-35) Of course the opinions are dependent upon whether or not the capsule is to survive the impact on the Martian surface. The following represents a consensus concerning the capsule objectives:

(a) To measure magnetic fields and radiation belts, if any, in the region up to a few hundred miles above the atmosphere.

(b) To obtain photographs at altitudes ranging from points near the surface to points in the high atmosphere.

(c) To obtain data about the atmosphere ... pressure, density, and temperature, as functions of altitude, as well as information about gaseous constituents.

(d) To measure diurnal temperature variations and search for the existence of life forms at the planet surface.

These objectives are all useful in insuring the success of future Mars missions, but it is difficult to say which ones are the most important without some sort of differentiation between purely scientific value and political propaganda value.

Several of the objectives listed above can be attained by the spacecraft alone, regardless of whether or not it carries an entry capsule. It can, for example, carry a spectrophotometer with which to investigate the existence of vegetation on the planet. It can also measure emission and absorption spectra of the stratosphere, thereby determining information regarding the gaseous constituents in the high-altitude part of the atmosphere. Radiometric measurements could provide surface temperature data, and photographs could be taken at ranges down to a few thousand miles from the surface. Also the spacecraft would be capable of gathering large amounts of data regarding the Earth-to-Mars interplanetary environment. But if the spacecraft were designed to carry an instrumentation capsule, considerable enhancement of the data-gathering capability would be made possible. Naturally the additional data would depend upon the type of capsule carried. In this study, two major types of capsule have been considered. One, which shall be called the LAT (Land And Terminate) capsule, gathers, and transmits to the spacecraft, data describing radiation belts and magnetic fields, while on its way toward the planet; enters the atmosphere from which it transmits drag deceleration data, altimeter data and information about the atmospheric profile; sends information gathered from several vidicon pictures taken at altitudes reached after undergoing peak deceleration and heating; and finally impacts on the Martian surface

where its useful life ends. This is the capsule to which most of the attention is devoted in this summary. Another type of capsule which has been given lesser consideration will be called the LAS (Land And Survive) capsule. This one differs from the LAT capsule in that it deploys a parachute at an altitude of roughly 50,000 feet, and then descends to a relatively soft landing on the surface where it can continue, for a few hours, to gather and transmit information (at fairly low data rates) about the planetary environment and provide a picture taken from very low altitude.

One obvious advantage of the LAT capsule is that it is not dependent upon the successful deployment of a parachute in an atmosphere which is not well defined at this time. (I-12 and I-16) Thus the weight contributed by the chute and associated deployment hardware can either be eliminated completely, or can be allotted to additional systems for scientific measurements. The major disadvantage, however, lies in the relatively high velocities experienced by the capsule during the terminal portion of atmospheric descent, making the determination of a static temperature profile of the atmosphere virtually impossible and complicating measurements of atmospheric density and pressure as functions of altitude. It is easier for the measurements to be made with the LAS capsule, which is capable of obtaining pictures from altitudes of a few hundred feet and transmitting the picture data to the spacecraft before landing if necessary. Although it is not completely clear that one capsule type is preferable to the other, there is little doubt that one of the two, by virtue of its penetration of the atmosphere and its ultimate proximity to the surface of the planet, can make valuable scientific and engineering measurements that could not be made from the spacecraft itself.

3. Specific Outline for a Possible Capsule Mission

Since we have been given very little *a priori* information regarding engineering constraints which may be imposed on the capsule by the spacecraft, such as weight, volume, allowable data rates and so forth, any specific capsule mission which we describe must necessarily involve some guesswork. Hence the mission outline which follows can only be a description of a mission which *might* be attempted, *if* a number of assumptions are found to be valid. These assumptions are:

1) The spacecraft and capsule will be on a fly-by trajectory prior to separation. The approach velocity and altitude of closest approach to Mars will be 4-6 km/sec (B-1) and 6000-10,000 km, respectively, depending upon the geocentric launch energy and guidance errors.

2) The weight and ballistic modulus of the capsule will be W = 300 lbs and $M/C_DA = 1$, respectively. The latter value is a compromise (C-1) between high capsule velocities in the atmosphere and excessive volume of the capsule.

3) At about 320,000 km from Mars (or less, depending upon trajectory errors) the spacecraft will orient the capsule so that it can be propelled into the desired impact trajectory by a fixed velocity-impulse provided by a solid-propellant capsule rocket motor.

4) The capsule velocity at time of entry into the atmosphere will not exceed 26,000 ft/sec.

5) A gross knowledge of the temperature and density profiles of the atmosphere is assumed.

6) A major objective of the capsule mission is to obtain pictures of the planet's surface. Hence, the angle between the Mars-Sun line and the local vertical at the impact point must be held within the range 20-40 degrees.

7) To minimize the errors in location of the impact point, the entry angle must be near vertical, in the range 75-105 degrees.[B-24]

8) No auxiliary drag devices will be employed.

9) The spacecraft will be able to receive, store and transmit to Earth whatever data is transmitted by the capsule, whose useful life will end upon impact. No constraint will be placed upon the data rate that can be handled by the spacecraft's data storage system.

The capsule configuration chosen is a 300-pound, blunt-nosed 10° half angle cone having a base diameter of 47 inches and a length of 38.5 inches.[H-1] This capsule has a ballistic modulus (M/C_DA) of approximately one slug/ft^2. To provide adequate thermal protection during atmospheric entry an ablative heat shield made of phenolic nylon, with J-M/MIN-K2000 backup insulation, is provided. The following major components then comprise this LAT capsule:

(a) Event timer

(b) A low-thrust, spin motor to provide post-separation attitude stabilization of the capsule.

(c) Solid-propellant rocket motor to provide the fixed velocity increment (approximately 900 ft/sec) required to place the capsule on the desired impact trajectory.

(d) One accelerometer to measure longitudinal acceleration; and another to measure the square of spin rate so as to monitor spin-up and spin-down.

(e) Magnetometer and charged-particle detector for measuring Martian magnetic field and "Van Allen" belts prior to atmospheric entry.

(f) A g-switch to signal atmospheric entry.

(g) A cageable gyro to measure atmospheric entry angle and to provide information regarding the trajectory of the capsule while in the atmosphere.

(h) Spin-down yo-yo mechanism to insure capsule stability in the atmosphere, and to facilitate taking pictures with reasonably long exposure times.

(i) Instrumentation for determining atmospheric pressure and density after capsule velocity has been reduced to about Mach 1.

(j) A 100 Mc pulsed altimeter.

(k) Three vidicon cameras with appropriate color filters.

(l) Three wideband transmitters and data encoders to handle the vidicon picture data.

(m) A narrow-band transmitter for all other engineering and scientific data, commencing with capsule/bus separation.

(n) Antenna system.

(o) Power supply composed of chemical batteries and a dc-to-dc converter.

The event sequence associated with a LAT capsule having the components listed above would then be similar to the following:

(1) Just before separation the spacecraft orients the capsule in the direction required for launching into the desired impact trajectory.

(2) Turn-on is signalled for the capsule power system, the narrow-band transmitter, the event timer, the magnetometer and the charged-particle detector.

(3) The spacecraft signals the beginning of separation at a time determined by its knowledge of the capsule's velocity-impulse capability and its computation of position and velocity relative to a Mars-centered coordinate system.

(4) A spring-actuated separation system imparts a small velocity increment (about one foot per second) to the capsule. Event sequencing in the timer begins.

(5) About two seconds after separation the event timer signals capsule spin-up to about 100 RPM. The spin motors may possibly be canted slightly to provide a larger linear velocity increment if further investigation shows that this will cause no unfavorable interaction with the spacecraft.

(6) Approximately ~~ten~~ 5 minutes after separation the capsule will be sufficiently far from the spacecraft (about 300 feet) to allow firing of the main rocket. The firing signal will be delivered by the event timer, and the rocket motor will continue to burn until its propellant is exhausted.

(7) Immediately after burnout, the g-switch is armed in preparation for signalling atmospheric entry.

(8) During the spacecraft-to-Mars transit (which will require between 15 and 20 hours, depending on the velocity with respect to Mars at time of separation) magnetic field and charged particle data are transmitted from the narrow-band transmitter to the spacecraft.

(9) Capsule enters the atmosphere with a nominal entry angle (measured between the velocity vector and the local vertical) of approximately 0°. The force due to linear deceleration of the capsule actuates the g-switch which signals atmospheric entry.

(10) Actuation of the g-switch simultaneously initiates several events: uncaging and spin-up of the gyro; cutoff of power to the magnetometer and charged-particle detector; and application of power to the vidicons, wideband transmitters and altimeter.

(11) Immediately after gyro spin-up, the yo-yo spin-down mechanism is actuated, reducing the angular velocity of the capsule from 100 RPM to approximately 10 RPM.

(12) During the time from spin-down to impact, data from the accelerometers and gyro pickoff will be transmitted from the narrow-band transmitter to the spacecraft via antennas in the aft end of the capsule.

(13) Approximately 40 second after atmospheric entry the capsule will experience its maximum deceleration which may range from 40 g to 135 g at an altitude of approximately 150,000 feet. These numbers are very dependent on assumed values of entry velocity, atmospheric parameters, entry angle and so forth. At this time the angle-of-attack envelope will be less than 5° and the capsule will move along a trajectory that is essentially vertical. The output of the accelerometer aligned along the spin axis will be differentiated to determine the time at which peak deceleration occurs, and the accelerometer output will be used to determine the time at which the picture-taking mission may be initiated with safety.

(14) Altitude data, which will become available at the time of peak deceleration, will also be transmitted to the spacecraft from the narrow-band transmitter. As soon as the capsule velocity is sufficiently low (about Mach 1) the camera lens cover in the capsule nose is blown off, and the access ports covering the atmospheric pressure - and density-measuring instruments are blown off to allow the beginning of the terminal instrumentation phase of the mission.

(15) After removal of the lens cover and access ports, the event timer immediately initiates the taking of color pictures (3 simultaneous vidicon pictures) of the Martian surface, producing and transmitting the information regarding a single picture every six to ten seconds up to time of impact on the surface. The picture data and the data regarding atmospheric pressure and density are fed through a multiplexer, along with all other engineering and scientific data, to a common transmitting antenna in the aft end of the capsule.

(16) Impact of the capsule on the Martian surface terminates the mission.

A more detailed discussion of some of the details of the LAT mission described above, such as the separation maneuver, trajectories, communications and so forth appears in the following sections.

4. Capsule/Spacecraft Separation and the Capsule Approach Trajectory

In order to accomplish the picture-taking portion of the LAT capsule mission, the capsule should separate from the spacecraft and move along a trajectory which will allow it to impact in a sub-solar equatorial region, such that the angle between the Mars-Sun line and the local vertical is approximately $\emptyset_S = 30^\circ$. This will assure well-illuminated pictures with good contrast.

There are other requirements which must be considered. The line-of-sight data transmission path between the capsule and spacecraft must not be broken by the planet during the terminal portion of atmospheric entry. The capsule propulsion requirements should be made as small as possible. Errors between the desired impact location and the actual impact location should be minimized. The total heat load due to atmospheric penetration should be minimized, and the separation maneuver must be accomplished in a manner which does not upset the spacecraft. After considering three nominal capsule trajectories, we have chosen one (described below) which is most likely to meet the above requirements.

It is assumed that the separation maneuver will be made at a distance of approximately 3.2×10^5 km from Mars; that the angle between the Mars-Sun line and the approach velocity vector $\overline{v}_A$ is within the range

$20^{\circ} \leq \Lambda_s \leq 40^{\circ}$; that the approach velocity has been measured by the spacecraft, and is within the range 4 km/sec $\leq v_A \leq$ 6 km/sec; and that, at a time just before separation, the spacecraft will be able to predict its altitude of closest approach to the planet with an error no greater than Δh = 500 km. The expected altitude of closest approach is assumed to be in the interval 6000 km $\leq h \leq$ 10,000 km.(B-2)

Just prior to separation the spacecraft will point the capsule in a direction that is roughly perpendicular to v_A, but pointed slightly toward the planet (about 20° off normal) to decrease the capsule's transit time and to insure an unbroken communication path up to time of impact. If the measured value of v_A and the predicted value of h were both to have their maximum expected values of 6 km/sec and 10,000 km, respectively, then the velocity change v_C, required to place the capsule on an approach trajectory which would pass through the planet center, would also have a maximum value. That is, $v_{C\ max}$ = 0.28 km/sec.(B-20) However, if either the predicted h or the measured v_A (or both) is reduced, then one of two corrections must be made. Either v_C must be reduced or (if v_C is not changed) the time of separation must be delayed by an amount which is dependent on the predicted h and the measured v_A. In the mission described here the latter alternative has been selected. That is, the capsule will carry a solid-propellant rocket motor which produces a fixed velocity change of 0.28 km/sec, initiated about 5 minutes after separation. The five-minute delay is necessary to assure that the capsule's rocket exhaust does not disturb the spacecraft. Thus the spacecraft will be required to provide a signal at the computed time of separation.

The particular approach trajectory mentioned above has been chosen because the smallest values of error in the impact location are associated with it.(B-24)

On the following two pages a summary of typical weight and power requirements are shown, along with a tentative version of the structural details of the capsule. Approximate physical parameters for a capsule of this configuration are:

Roll moment of inertia	J_R = 14.6 slug-feet^2
Pitch moment of inertia	I_P = 10.6 slug-feet^2
Weight	W = 300 pounds (including rocket propellant)
Base diameter	d = 47 inches
Length	L = 38.5 inches

Using these parameters it is concluded that approximately 30 pounds of solid propellant with an I_{SP} of 280 seconds will produce the desired v_C, using a rocket motor whose total weight is 36 pounds, including propellant.(H-13)

LAT CAPSULE WEIGHT SUMMARY

Ablative Shield and Insulation	113 pounds
Aft Mounting Ring and Closure Diaphragm	16½
Conical Motor Support	4
Crossed-Slot Antenna	3
Altimeter Antenna	10
Equipment Support Structures	7
Spin-Despin Mechanism	4
Cameras and Camera Control Units	15
Wideband Transmitters and Power Amplifiers	21
Narrow-Band Transmitter	1½
Event Controller	5½
Television and Telemetry Synchronizers and Encoders	6½
Camera Control	½
Accelerometers and g-Switch	1
Gyro	2
Altimeter	4
Density and Pressure Sensors	1½
Mass Spectrometer (including Electronics)	10
Magnetometer	6
Scintillation Counter (including Electronics)	4
Multiplexer	4
Main Rocket Motor	35
Power Supply (including dc-to-dc Converter)	26
Total	301 pounds

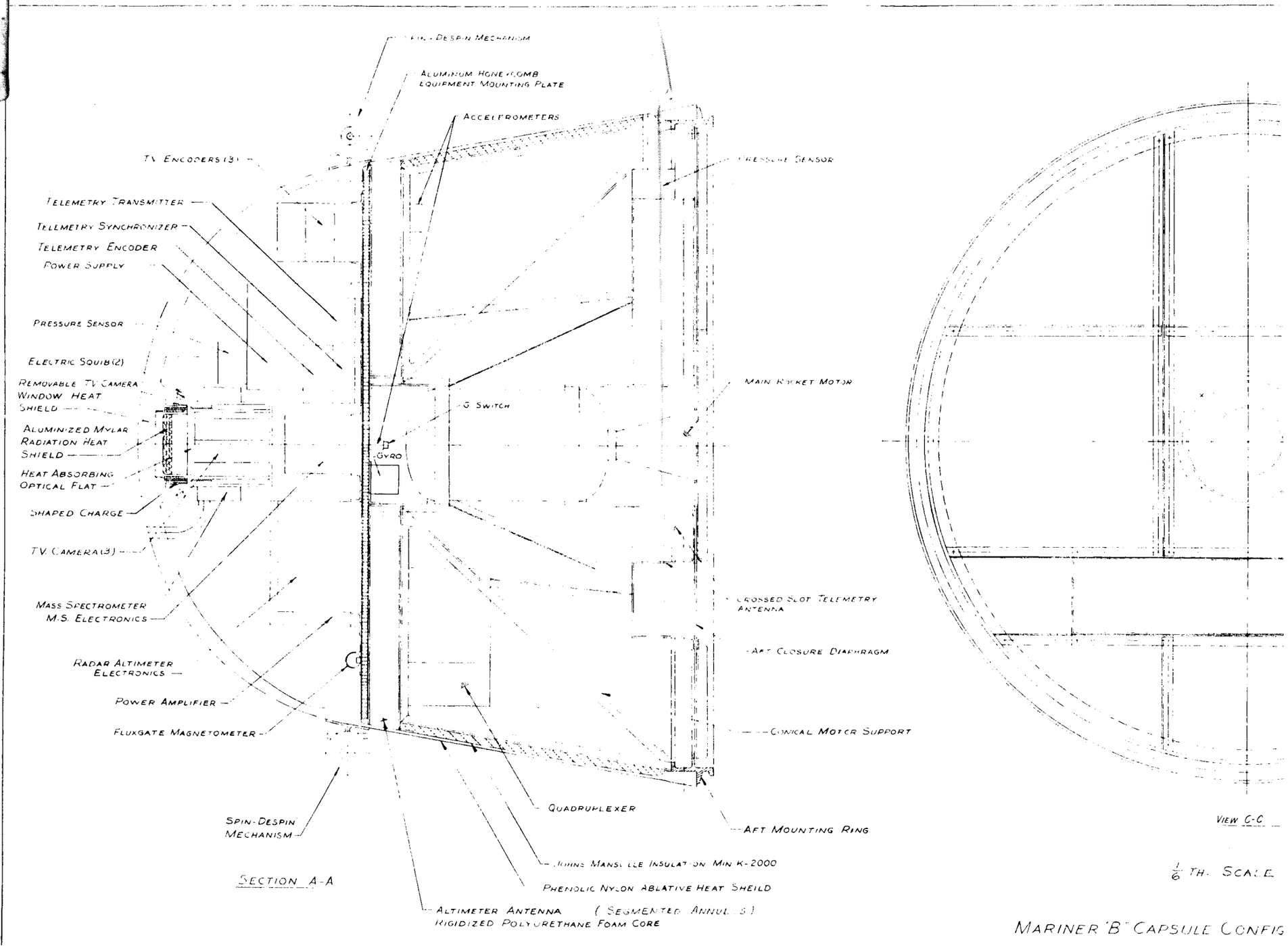

Mariner "B" Capsule Config

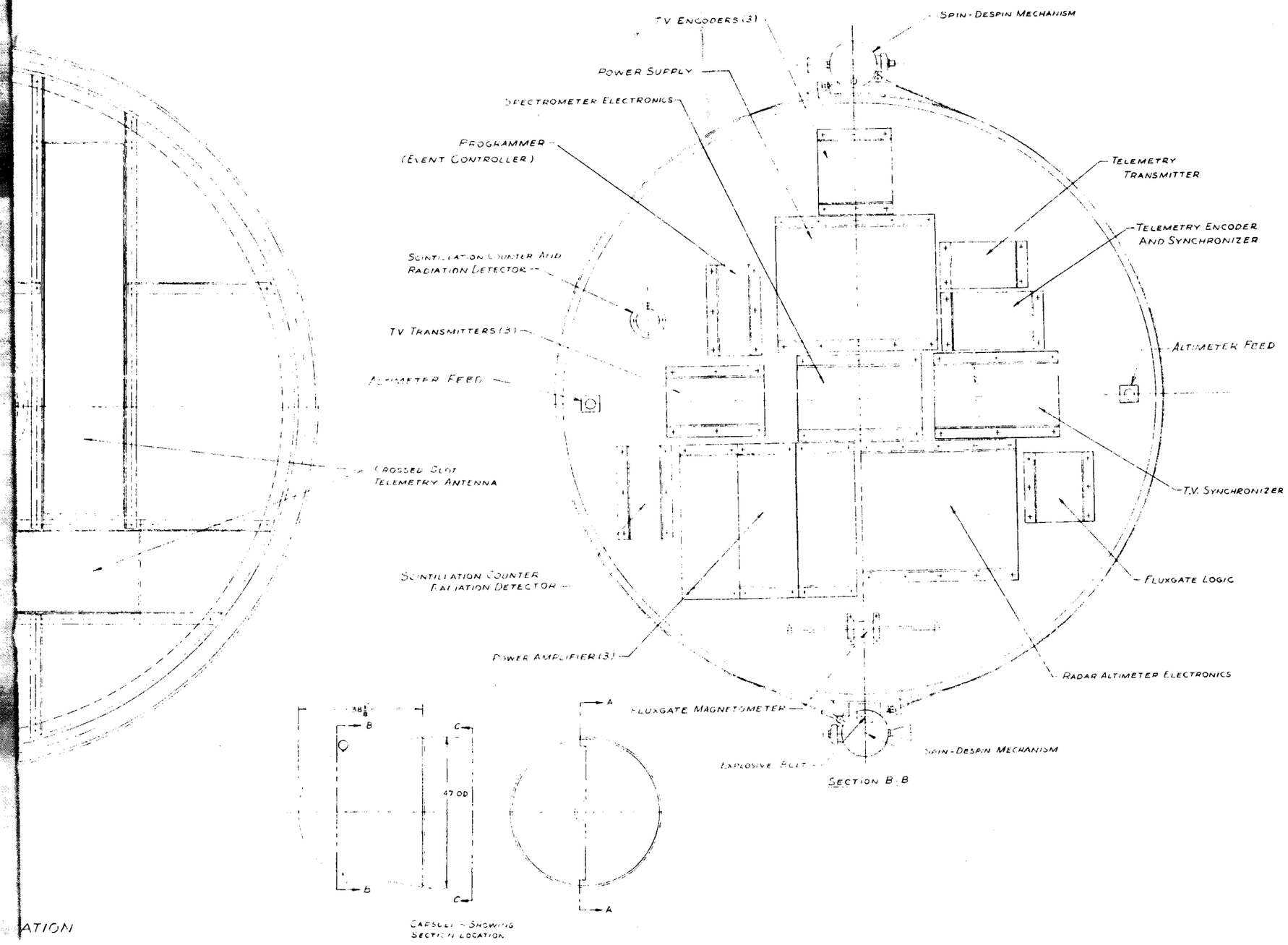
TV ENCODERS (3)
SPIN-DESPIN MECHANISM
POWER SUPPLY
SPECTROMETER ELECTRONICS
PROGRAMMER
(EVENT CONTROLLER)
TELEMETRY
TRANSMITTER
TELEMETRY ENCODER
AND SYNCHRONIZER
SCINTILLATION COUNTER AND
RADIATION DETECTOR
TV TRANSMITTERS (3)
ALTIMETER FEED
ALTIMETER FEED
CROSSED SLOT
TELEMETRY ANTENNA
T.V. SYNCHRONIZER
SCINTILLATION COUNTER
RADIATION DETECTOR
FLUXGATE LOGIC
POWER AMPLIFIER (3)
RADAR ALTIMETER ELECTRONICS
FLUXGATE MAGNETOMETER
SPIN-DESPIN MECHANISM
EXPLOSIVE BOLT
SECTION B-B
38½
B
B
C
C
47 OD
A
A
CAPSULE - SHOWING
SECTION LOCATION

ATION

From various methods of controlling the attitude of the capsule after separation, there are three that have been considered in detail. These are:

(1) Spin stabilization, with spin-up prior to separation.

(2) Stabilization with an inertia wheel mounted in the capsule along the axis of symmetry, with wheel spin-up prior to separation.

(3) Spin stabilization, with capsule spin-up initiated immediately after separation.

The first two of these schemes, which require capsule or wheel spin-up before separation, are found to be undesirable, however, because of the gyroscopic cross coupling which they exert on the spacecraft's attitude control system. The third method was examined, and was found to be satisfactory.(A-4 to A-6) In using this method of attitude control the capsule is given a velocity separation impulse v_0 which is sufficiently small (about 1 ft/sec) so that the spacecraft is not adversely disturbed by the separation. Then the capsule is spun up by a pair of low-thrust jets about 2 seconds after the instant of separation, and finally given the required velocity change v_c about 5 minutes after separation when the capsule is sufficiently far removed from the spacecraft (approximately 300 feet).

The capsule spin rate required for adequate stabilization is found to be approximately 10 radians/sec. Spinup to this rate can be accomplished by delivering 3.33 pounds of thrust for 15 seconds from each of two spin jets mounted on opposite sides of a 3-foot ring which is perpendicular to the spin axis and whose center is coincident with the mass center of the capsule. Although a detailed analysis of the effect of capsule spinup on the spacecraft is not possible, because of a lack of knowledge of the structural details of the spacecraft (particularly the solar panels), it was estimated that this low thrust level would not produce any significant spacecraft disturbance.(A-5)

The torque impulse experienced by the spacecraft due to separation of the capsule is held to a low value by keeping the capsule's separation velocity v_0 down to one foot per second. It is assumed that a Marmon clamp secures the capsule to the spacecraft and, at time of separation, the clamp is released and a spring-loaded ram imparts a velocity v_0 to the capsule. If it is assumed that Δ, the distance from the line of action of the spring force to the mass center of the capsule, is no greater than 0.01 feet, then it has been shown that the resultant torque impulse imparted to the spacecraft is approximately 0.15 ft-lb-sec. Since this value has been permissible for Ranger-type spacecraft, it is assumed that it will not be excessive for a Mariner spacecraft.

Five minutes after separation and spinup the capsule's main rocket will ignite and burn for approximately ten seconds, delivering a thrust of about 900 pounds. The capsule will then be on the desired impact trajectory and will enter the Martian atmosphere sometime between 14.5 and 21.5 hours later, depending upon the value of v_1 and the distance from Mars at time of separation. The nominal entry angle (with respect to local vertical) is zero degrees, and the entry velocity will be in the range $21{,}000 \leq v_M \leq 26{,}000$ ft/sec depending, once again, upon v_1. The actual point of impact on the Martian surface may be in error by approximately 15° in latitude and longitude, corresponding to an 800-mile error in the point of impact.

5. Atmospheric Entry and Impact

In attempting the design of a Martian entry vehicle an a priori knowledge of the gaseous constituents of the atmosphere and the variation (as a function of altitude) of atmospheric temperature, pressure and density are vitally important. One or more of these parameters will strongly influence the capsule configuration, the design of the heat shield, the design of the communication system, and the prediction of aerodynamic behavior during entry. Some of the parameters can be measured directly, and others deduced on the basis of a number of assumptions; but, unfortunately, our knowledge of the Martian atmosphere is currently subject to some rather large uncertainties, especially at high altitudes. A summary of this knowledge is available in RAND report RM-2817-JPL, dated June 30, 1961. Memos I-12 and I-16 discuss some of the topics in this report which are of immediate interest, and graphical data are presented which indicate the bounds on our evaluation of the density and temperature profiles of the atmosphere. In the discussion which follows, reference will be made to several of these atmospheric models, and comment will be made regarding particular ones which impose the most severe constraints on the tentative design of the LAT capsule.

Since one of the major purposes of the LAT capsule is to obtain low-altitude pictures of the Martian surface, a primary consideration in the capsule design is the maximization of the time T spent in subsonic flight prior to impact. The stipulation on subsonic flight is made because of the inadvisability of uncovering the lens of the camera system when moving at higher velocities. The upper bound on T is dependent on entry velocity and angle, the atmospheric model assumed, and the nominal ballistic modulus M/C_DA. Near-vertical entry angles, high entry velocities, and large values of M/C_DA all tend to produce an undesirable reduction in T; and the smallest values of T are found to be associated with atmospheric models B, D and E. (C-15)

Capsule size limitations in mating of the capsule to the spacecraft dictate that M/C_DA cannot be made appreciably smaller than unity, however.

Hence unity is chosen as a nominal value and shall be used in all subsequent discussions. Atmosphere D appears to impose the most severe limitation on the maximum value of T. Therefore, an analysis was made to determine a range of possible values of T assuming the worst possible atmosphere (D), the highest expected entry velocity (26,000 ft/sec) and a vertical entry angle. Even in this most pessimistic case it was found that a capsule having a base diameter of 47 inches (assumed non-rotating), and having a variable drag coefficient, would remain in subsonic flight for approximately T = 30 seconds. The altitude at which the capsule reaches Mach 1 is about 22,000 feet; and the corresponding impact velocity is approximately 650 ft/sec. A peak longitudinal deceleration of 131 Earth g's is experienced at an altitude of approximately 122,000 feet, but it is important to note that these performance data are the most severe that may be expected. Values of T up to 100 seconds and maximum decelerations as low as 66 g's have been predicted using different model atmospheres and entry angles. (C-11 and C-12)

Heat protection for the capsule during atmospheric entry has been provided to restrict the maximum inner wall temperatures to the range from 300 to 400 degrees F. This is accomplished by use of a phenolic nylon (P-N) ablative material which completely covers the nose and skirts of the capsule, varying in thickness from 1.2 inches at the stagnation point on the nose to 0.2 inches at the aft end of the skirts. (E-22 and E-23) In addition a layer of backup insulation (Johns-Manville MIN K-2000) about 0.4 inches thick is provided beneath the ablative material covering the capsule skirt. The total P-N weight is 100 pounds, and the weight of the insulation is 13 pounds. This heat-protection system gives adequate protection even during the most severe entry conditions, e.g., a vertical entry into atmosphere C or E at 26,000 feet/sec.

It is unfortunate that 113 pounds out of the total payload weight of 300 pounds allotted to the capsule must be devoted to heat protection. Indeed this <u>is</u> excessive if only convective heat transfer rates are considered. However, it has been found that radiant heat transfer from the cyanide band must also be considered because of its significant contribution to the total heating at the stagnation point, due to the CN formed in the shock layer during a high-velocity, vertical entry. (E-1)

A preliminary assessment of the dynamic stability of the capsule during atmospheric entry has been made, because of the influence of stability on both the design of the capsule structure (and heat shield) and on the feasibility of taking pictures of the Martian surface during subsonic flight. (D-12) The angle-of-attack <u>envelope</u>, rather than instantaneous angle of attack, has been computed for the LAT capsule as it follows a point-mass trajectory through several different hypothetical atmospheres. The variation of this envelope with time (or altitude) is dependent upon

several parameters such as the estimated damping coefficient C_{M_q}, the capsule spin rate ω_S, the entry velocity v_E, the entry angle θ_E measured with respect to the local vertical, the initial angle of attack α_E, and the atmospheric model which is assumed. Consequently the effect of variations in these parameters on the convergence of the angle-of-attack envelope has been investigated. In a typical computation the C_{M_q} is estimated to be approximately -1, ω_S is 10 RPM, v_E is 26,000 ft/sec, θ_E is zero, θ_E is 90°, and the E atmosphere is assumed. Using these parameters the angle-of-attack envelope decreases to 5° at an altitude of approximately 225,000 feet, and becomes essentially zero for altitudes less than 100,000 feet.(D-15) Thus the picture-taking portion of the capsule mission could conceivably be initiated at these altitudes if the corresponding capsule velocity were found to be sufficiently low. The capsule will also have passed through the region of peak dynamic pressure at these altitudes, but there is still some question as to whether or not the region of peak heating will be passed.

Convergence of the angle-of-attack envelope is delayed somewhat if some of the parameters are varied. For example a decrease in v_E, an increase in ω_S, an increase in α_E or a decrease in the magnitude of C_{M_q} will delay the convergence. A more detailed knowledge of the variation of C_{M_q} with capsule velocity will be required before a more careful assessment of dynamic stability can be made.

6. Capsule Communications System

The preliminary analysis which has been undertaken for the Mariner B communications system has been divided into two parts, one for the LAT capsule and one for the LAS capsule. The following commentary is mostly concerned with the LAT capsule.

One of the first questions which must be answered in considering a capsule communication system is to decide whether the capsule will transmit its information via the capsule-spacecraft-Earth link, or the simpler capsule-Earth link. Transmission of information directly to Earth from the capsule is found to be extremely impractical, however, for the picture-taking mission considered here. By 1964 the state of the deep space telemetry art, for mean Mars-to-Earth distances, will almost certainly limit information rates to something on the order of a few hundred bits per second, even if the transmitting antenna has a gain of 18-20 db over isotropic. Not only would these bit rates be inadequate for transmitting (during descent) the information to describe one picture taken from the descending LAT capsule, but the transmission capability would be limited even further by the inability of the capsule to carry a directional antenna that could be continuously oriented toward Earth during atmospheric entry. In addition the actual transmission distances will very likely exceed the mean Mars distance, which is approximately one astronomical unit. For these reasons, only transmission over the capsule-to-spacecraft link has been seriously considered here.

The LAT capsule transmitting equipment consists of three 100-watt, 250-megacycle wideband transmitters which transmit video data from the three vidicon cameras mounted in the nose of the capsule, and a single two-watt, narrow-band transmitter which transmits the information from all other engineering and scientific experiments. The data transmission system is divided into four separate transmitting and receiving subsystems ... a subsystem to handle the video data from each of the three vidicon cameras, and a subsystem to handle all other engineering and scientific data. This redundancy increases the liklihood of obtaining pictorial information regarding the Martian surface, and permits the use of lower transmitter power.(F-1 to F-5) The following discussion applies to a single data-handling subsystem.

The transmitter power required for a given information rate has been determined, using the following assumptions:

(1) Data power (at the spacecraft receiver input terminals) is about half of the total power received.

(2) The signal-to-noise power ratio at the receiver input terminals is 8 db. This should be quite adequate if a PCM/PSK/PM modulation scheme and coherent detection are used.(F-2)

(3) The system noise power spectral density is -199 dbw/cps, corresponding to a receiver noise figure of 5 db and an effective noise temperature of 900°K.(F-3)

(4) The free-space transmission loss is 164 db. This assumes a transmitter carrier frequency of 250 Mc and a maximum capsule-to-spacecraft distance of 9000 statute miles.

(5) The polarization loss is 3 db, and miscellaneous system losses total 2 db.

(6) The total antenna gain, for the transmitting and receiving antennas taken together, is 10 db.

(7) A design margin of 8 db is used to absorb errors in the above assumptions and deficiencies in system performance.

Using these assumptions it is readily shown that data rates of 12,500 bits/sec and 250 bits/sec are allowable for the 100-watt wideband transmitters and the two-watt nearrow-band transmitter, respectively.(F-5) If a 200-line resolution capability is assumed for a single vidicon, and one of eight gray levels is used to specify the intensity of each of the 40,000 resolvable elements, then a maximum of 120,000 bits of information is needed to characterize a single picture. The time required to transmit

one picture is approximately ten seconds, which includes the time required for vidicon erasure and for the transmission of synchronizing signals. Thus it follows that, even under the most adverse conditions, there will be sufficient time during subsonic flight of the capsule in the atmosphere for the transmission of at least three color pictures of the Martian surface.

The capsule must carry two separate transmitting antenna systems ... one for the transmission of video, scientific and engineering data to the spacecraft, and the other for use with the radar altimeter. The former system must be pointed out the aft end of the capsule and have a radiation pattern that is symmetrical about the longitudinal axis, because the capsule will be spinning during entry. It should also provide an angular coverage of approximately $\pm 60^{\circ}$, measured with respect to the longitudinal axis. These requirements can be met by use of a crossed-slot antenna (F-31) for which each slot weighs roughly 1.5 pounds and has dimensions of 24" x 5" x 5". This antenna is located in the base of the capsule so that it always remains pointed in the approximate direction of the spacecraft. The altimeter antenna system is composed of two circumferential slots having 62" x 2" apertures, located under the ablative material in the capsule skirt approximately half way between the nose and base. Since the altimeter antenna will be subjected to severe heating during atmospheric entry, a study must be made to determine the most appropriate material that can be used to fill and cover the slots.

In transmitting from the altimeter antenna and the crossed-slot antenna, two problem areas must be considered. These are the possibility of antenna breakdown due to high radiated power, and communication blackout due to plasma sheath attenuation. A preliminary investigation of antenna breakdown (F-28) shows that transmission from the crossed-slot antenna can be safely initiated at altitudes less than 120,000 feet with no likelihood of antenna breakdown. Since this altitude is greater than the altitude at which subsonic velocities are reached and picture-taking is initiated (about 70,000 feet), the possibility of breakdown of the crossed-slot antenna is of no concern. A further analysis may be necessary to obtain similar assurance with regard to the altimeter antenna, which may be required to radiate at altitudes as high as 150,000 feet. Attenuation of radiated signals, arising from high electron concentrations in the plasma sheath, are found to be troublesome only for forward transmission from the altimeter antenna. (F-25) It has been shown that transmission from this antenna is impractical in the altitude range from 800,000 feet to 150,000 feet; (F-55) but below 150,000 feet the altimeter will be able to transmit adequately through the sheath. Conditions for transmitting out the aft end of the capsule are not so severe, however, and it is estimated that no appreciable attenuation will be experienced, due to the presence of the plasma sheath, at any altitude.

The design of the capsule, and decisions regarding its mission objectives are strongly influenced by the ability of the spacecraft to relay to Earth the information collected by the capsule after separation. Special attention must be given to the demands which are placed on the spacecraft with regard to the receiving antenna system, the data receivers and the data storage system.

It is very important that the spacecraft's receiving antenna be circularly polarized because the incoming energy may be of any polarity, due to the unpredictable motion of the capsule and to the use of a crossed-slot transmitting antenna. (F-32) Furthermore it is desirable that the receiving antenna power gain be at least 10 db, so that the power which must be radiated from the capsule transmitters can be held to a reasonably low value. The Space Program Summaries from JPL have indicated that the Mariner B spacecraft may utilize a Mars-oriented boom to point scientific instruments, such as a radiometer, at the planet. Hence it is assumed that such a boom could be made available for the mounting of a receiving antenna which would accept capsule data. Then the above requirements can be adequately met by using a collapsible helical antenna which (when erected) is approximately four feet long, 15 inches in diameter, and employs a two-foot-by-two-foot ground plane. This antenna would give the desired 10 db gain at 250 Mc, and would have a 50° beam width. The capsule would lie in the beam, once it has approached to within about 4000 miles of the planet. (F-32 and F-37)

The spacecraft receiving system utilizes four separate receivers fed from a common antenna ... three wideband receivers for handling video information from the capsule's vidicons, and a single narrow-band receiver for the reception of all other engineering and scientific data. Fundamentally the four receivers are identical, with the exception of the required changes in filtering circuitry. Each is a double superheterodyne, PM receiver employing phase-lock-type discriminator circuitry. (F-69) The redundancy associated with using completely separate receivers provides increased reliability of obtaining <u>some</u> important data in the event of a partial failure in the communication system. However, the final design criteria may dictate a sharing of some circuitry (e.g., RF preselector, RF amplifier, first mixer and first IF stage) by the four receiving channels to reduce the power and weight requirements imposed on the spacecraft.

A facility for data storage must be provided on the spacecraft because the rate at which the capsule gathers and transmits video data during atmospheric entry far exceeds the rate at which the spacecraft is able to transmit data back to Earth. For example, the capsule may transmit data describing as many as eight color pictures to the spacecraft in 80 seconds. Since each picture requires approximately 4×10^5 bits (including sync signals) to describe it, the spacecraft must be able to accept and store information at a rate of about 4×10^4 bits per second. The rate at which information can be relayed to Earth is about 100 bits per second, however; hence the ratio of data rates is about 400:1. If

we assume that a magnetic-tape storage device is used, and that the device has ½ inch per second as a practical lower limit on its playback tape speed, then the tape speed while recording must be 200 inches per second if only a single recording channel is utilized. (F-50) This speed is impractically large. Reduction of the recording speed can be accomplished, however, by arranging the data on the tape in nine parallel tracks (three tracks per wideband receiving channel) so that the recording speed can be reduced to a more reasonable 22 inches per second. After all the video data from the capsule has been stored, the tape transport is rewound and the nine tracks are read out in serial fashion at ½ inch per second for transmission to Earth. For the handling of the remaining engineering and scientific data from the capsule, there is no appreciable storage problem. These data rates are sufficiently low that they may be relayed by the spacecraft to Earth in real time, i.e., no storage at all, if it is convenient to do so.

It is estimated that the equipment which must be carried by the spacecraft to support the capsule mission, exclusive of the capsule itself, will weigh about 25 pounds and require approximately 15 watts of electrical power for its operation.

7. Scientific Data Accumulation

In the LAT capsule mission, data is to be gathered which will describe capsule altitude and velocity; atmospheric pressure and density profiles; color pictures of the Martian surface; charged-particle belts and magnetic fields outside the atmospheric envelope; and capsule system performance. Major attention has been given to the picture-taking portion of the mission in this study because this portion presents the most challenging problems in implementation and data transmission. Our investigation has included a study concerned with obtaining pictures of the planetary surface prior to atmospheric entry, as well as pictures taken in the atmosphere from altitudes less than 60,000 feet. For simplification in this summary, however, only the taking of in-atmosphere pictures is discussed.

The camera subsystem consists of three completely independent vidicon cameras (with appropriate color filters) mounted in a cluster in the capsule nose. The cameras look outward along the axis of symmetry, and are exposed to view by the process of removing the lens cover. Each camera has its own data transmission equipment, but all three share a common programming control, multiplexer and transmitting antenna.

No optimum choice of vidicon type has been made thus far in this study. However it has been determined that a vidicon similar to the Westinghouse WX4530 may be suitable, except for the possible necessity of increased ruggedization. Some typical vidicon characteristics that are found to be desirable are the following:

(1) Tube dimensions: 5 inches long, one inch diameter

(2) Shock: greater than 150 g

(3) Total weight of vidicon and control equipment: less than 6 pounds

(4) Resolution: 200 x 200 TV lines

(5) Gray levels: 8

(6) Format dimensions: 0.45 inches, square

(7) Picture retention time: greater than 10 seconds

(8) Minimum exposure: 0.1 foot-candle-seconds

The exposure time required for a particular tube is dependent on several factors ... color of the filter with which it is associated, the wavelength of its spectral peak, characteristics of the lens being used, and on the brightness of the surface which is viewed. It has been shown that a vidicon having the characteristics listed above, employing an F/1.4 lens and an exposure of 1/200 second, will be amply illuminated by the Martian surface at mid-day.(G-8 and I-4) Ground resolutions in the range from 245 feet to 16 feet would be obtained for capsule altitudes from 50,000 feet down to 4000 feet. Corresponding fields of view would vary from 45,000 feet down to about 3000 feet.(G-6)

By utilizing the data obtainable from the altimeter, accelerometer and gyro, it should be possible to reconstruct the geometry of the entry trajectory as well as a history of capsule velocity, altitude and attitude. A 100 Mc altimeter has been tentatively chosen, with a capability of radiating a peak power of 100 watts.(G-15) This choice has been made in order that the altimeter may be completely transistorized and the weight, volume and power requirements held to a minimum. Since the ablative heat shield is not to be removed during atmospheric descent, the altimeter antenna must be mounted under the shield. This creates a problem which must be resolved, because it is unlikely that the antenna will be able to radiate energy through phenolic-nylon ablative material after it has been charred by heating. Thus it becomes necessary to examine the possibility of covering the altimeter antenna aperture with some other ablative material such as teflon which is more transparent to rf radiation.

There is little doubt that the determination of atmospheric pressure, density, temperature and composition is of great importance in a capsule mission. The required instrumentation should not be radically different from that used in upper air soundings of our own atmosphere. One major

complication may be the very high velocities attained by the LAT capsule, however; hence the determination of some of these parameters (especially temperature) may dictate the use of a drag chute. This instrumentation has not been studied in detail, as yet, but allowances have been made for types of instruments which may be appropriate. The capsule structural diagram on page 10 shows, for example, the presence of a flux gate magnetometer and a scintillation counter for the pre-entry measurement of magnetic fields and charged-particle belts. A mass spectrometer is indicated for determining information about the composition of the atmosphere, and two sensors are located with access to the atmosphere (one near the nose and one at the rear of the skirt) for the determination of dynamic pressure. Data from these sensors and the two accelerometers may be correlated with our knowledge of the capsule structure and velocity to ascertain the pressure and density profiles.

8. Problem Areas

A substantial number of technical problems have been uncovered during the course of this study, many of which would require more careful investigation before a preliminary capsule design could be completed. The following is a partial list of problem areas:

(1) The possibility of directing both the spacecraft and capsule on an impact trajectory prior to separation, and then propelling the spacecraft off this trajectory and into a fly-by trajectory should be investigated further to see what advantages may be obtained.

(2) The separation and spin-up scheme must be examined more closely, once a more definite idea of the spacecraft structure is obtained. Every precaution must be taken to insure that the spacecraft is not upset by the separation maneuver.

(3) The total number of bits of information obtained from the mission described here is very high, producing a correspondingly large capsule weight. A less ambitious mission should possibly be considered in which fewer pictures are obtained if it is necessary to reduce the capsule weight radically. Weight savings can also be obtained by optimization of the capsule configuration.

(4) The use of some other heat protection material, such as pyrographite, should be investigated in an effort to reduce capsule weight.

(5) Determination of the time of entry into the atmosphere is a problem that needs further examination. Also the determination of capsule velocity history and the proper time for removal of the vidicon lens port need more attention.

(6) If the temperature and shock environment are too severe for state-of-the-art vidicons, a special vidicon may have to be developed.

J. E. Kemmerly

J. E. Kemmerly

JEK:clm

APPENDIX A

SEPARATION AND ATTITUDE CONTROL

Ford Motor Company

AERONUTRONIC DIVISION

Intra-Company Communication

AL-148

13 November 1961

To: J. E. Kemmerly

From: R. R. Auelmann

Subject: SPIN-UP OF THE MARINER CAPSULE WITH MINIMUM DISTURBANCE TO THE BUS

SUMMARY

It has been proposed that the thrust vector which accelerates the capsule be controlled by spin stabilization of the capsule. The main difficulty is to spin-up the capsule without disturbing the bus. Because of the tip-off rate which is expected to accompany separation, the capsule must be stabilized either before separation or immediately thereafter.

Schemes which require that the capsule or an inertia wheel be spun up prior to separation are shown to be unacceptable because of the gyroscopic crosscoupling which these schemes impose on the bus attitude control system.

The recommended approach is to spin-up the capsule shortly after separation (similar to the procedure used on the Ranger capsules). Two spin rocket nozzles will be used. Thus, the torque produced on the bus due to spurious gas particles from one spin nozzle acting on one solar panel will (in the ideal case) be balanced by the torque due to gas particles from the other nozzle acting on the other solar panel. In the actual case the thrusts and gas flow profiles will be slightly different for the two nozzles (due to machining tolerances, etc.). Hence, some small torque will be produced on the bus. Therefore it seems advisable to use low thrust levels (and long burning times) for the spin-up system. We show that spin torque levels as low as 5 ft lb can limit the pointing error resulting from an initial tip-off rate to acceptable values. We expect that the torques and torque impulses on the bus (which result from small errors in the spin-up system) to be negligibly small.

177A

INTRODUCTION

Prior to separation, the capsule and the bus are on a "fly-by" trajectory relative to Mars. After capsule-bus separation an impulse is imparted to the capsule thereby placing it on an impact trajectory. Spin-stabilization is the simplest scheme for insuring that the thrust impulse vector is applied in the desired direction. The problem is to spin-up the capsule without significantly disturbing the bus. The maximum torque impulses which can be sustained by the Ranger bus during antenna deployment (Ref. 1) are

0.15 ft lb sec (pitch and yaw axes)
0.09 ft lb sec (roll axis)

In this memo we assume that the same specifications hold for the Mariner bus during separation and spin-up of the Mariner capsule. Since a transverse torque impulse (about the pitch and/or yaw axes of the capsule) is expected to accompany separation, the capsule must be stabilized either prior to separation or shortly after separation.

From Ref. 2, a .84 meter/sec error in the velocity change vector $\bar{v}_C$ normal to the plane of the approach trajectory results in a 1 degree error in the impact site. This is the critical error. The magnitude of $\bar{v}_C$ is taken as 277 meters/sec. Hence, a pointing error of $.84/277 \simeq 3 \times 10^{-3}$ rad in $\bar{v}_C$ can produce a 1 degree error in latitude. We will assume that the latitude error resulting from the initial tip-off rate at separation may not exceed 10 degrees.

THREE POSSIBILITIES

Scheme (1): Spin-up the capsule prior to separation by either slowly torquing the capsule against the bus or by use of very low thrust spin rockets.

Scheme (2): Spin-up an inertia wheel (with spin axis fixed to the capsule centerline) prior to separation. The wheel is torqued against the bus. After separation the wheel is clutched to the capsule thereby transferring the angular momentum to the capsule.

Scheme (3): Spin-up the capsule after separation. Relatively low thrust, slow burning spin-up system is required.

Schemes (1) and (2)

We will show that both of these schemes may be eliminated from further consideration. The tip-off rate ω_T for the Ranger Lunar Hard Landing capsule is taken as .01 rad/sec (Ref. 3). The inertia data Ranger and Mariner B capsules at separation are:

Item	Ranger Capsule	Mariner B Capsule
Mass m	9.0 slugs	9.3 slugs
Roll moment of inertia, J	2.45 slug ft^2	14.6 slug ft^2
Pitch (and yaw) moment of inertia, I	9.40 slug ft^2	10.6 slug ft^2

If the Mariner capsule were not spun-up prior to separation, the tip-off rate would scale as follows

$$(\omega_T)_{MARINER} = \frac{I_{RANGER}}{I_{MARINER}} (\omega_T)_{RANGER}$$

Hence, the expected ω_T for the Mariner capsule would be approximately .01 rad/sec. Since in schemes (1) and (2) the capsule is spinning prior to separation, the tip-off rate would most likely be greater than .01 rad/sec. Hence, if we use ω_T = .01 rad/sec, we are being optimistic. The transverse impulse is given by

$$I\omega_T = (10.6 \text{ slug ft}^2)\ (.01 \text{ rad/sec}) \simeq .11 \text{ ft lb sec}$$

This impulse is imparted to both the bus and the capsule. Since this impulse is less than .15 ft lb sec maximum for the bus, we may not as yet eliminate schemes (1) and (2).

The spin angular momentum (for either the capsule or the inertia wheel) must be sufficient to insure that the latitude error due to ω_T does not exceed 10 degrees. This represents a peak pointing error α of .03 rad. After separation the capsule centerline will precess about a new angular momentum vector which is displaced from the nominal direction by the angle α. The required spin angular momentum is

$$Js = \frac{I\omega_T}{\alpha} = \frac{(10.6 \text{ slug ft}^2)\ (.01 \text{ rad/sec})}{.03 \text{ rad}} = 3.5 \text{ ft lb sec}$$

where s is the spin rate. The spin momentum Js is achieved prior to separation. Since the bus must precisely orient the capsule immediately before separation, the spin momentum Js must be resisted by the bus control system in any pitch and yaw maneuvers. Clearly Js represents a disturbance to the bus far in excess of the acceptable torque impulse levels. Hence, schemes (1) and (2) are eliminated from further consideration.

Scheme (3): Spin-up After Separation

At "separation" the mechanism (Marmon clamps or explosive ring), which secures the capsule to the bus, will be released and a spring loaded ram will impart a small velocity v_0 to the capsule relative to the bus. Suppose that the tip-off rate ω_T is due entirely to misalignment of the impulse producing force (spring). Then

$$\omega_T = \frac{mv_0\Delta}{I} \qquad \text{or} \qquad v_0 = \frac{I\omega_T}{m\Delta}$$

where Δ is the distance from the line of action of the spring force to the mass center of the capsule. Let τ be the time interval between separation and the start of spin-up. The distance r which the capsule has traveled during τ is given by

$$r = v_0\tau = \frac{I\omega_T}{m\Delta}\tau$$

Using the relation

$$\tau = \alpha/\omega_T$$

where α is the "tumble" angle, we obtain

$$r = \frac{I\alpha}{m\Delta}$$

If we allow α to reach .02 rad in the interval τ and assume $\Delta \leq .01$ ft, we have

$$r = \frac{(10.6 \text{ slug ft}^2)\ (.02 \text{ rad})}{(9.3 \text{ slug})\ (.01 \text{ ft})} \simeq 2 \text{ ft}$$

We now assume that, even if Δ were zero, the tip-off rate at separation due to preload and alignment of the separation clamps would be .01 rad per sec. Then allowing α to reach .02 rad we find

$$\tau = \frac{\alpha}{\omega_T} = 2 \text{ sec}$$

Hence,

$$v_0 = s/\tau = 2 \text{ ft}/2 \text{ sec} = 1 \text{ ft/sec}$$

We now check whether the impulse imparted to the bus will exceed .15 ft lb sec.

$$I\sqrt{\omega_{T_1}^2 + \omega_{T_2}^2} = \sqrt{2}(10.6 \text{ slug ft}^2)\ (.01 \text{ rad/sec}) = .15 \text{ ft lb sec}$$

where ω_{T_1} is the tip-off rate due to the spring misalignment and ω_{T_2} is due to the separation mechanism.

We consider the spin-up phase next. Suppose that spin-up is accomplished instantaneously. After spin-up the angular momentum vector remains fixed in direction but is misaligned (from the nominal direction) by an amount

$$\alpha = \frac{I\omega_T}{Js}$$

Taking the spin rate s as 10 rad/sec and $\omega_T = \sqrt{2}(.01 \text{ rad/sec})$, we obtain

$$\alpha = \frac{(10.6 \text{ slug ft}^2)\ (.014 \text{ rad/sec})}{(14.6 \text{ slug ft}^2)\ (10 \text{ rad/sec})} \simeq 10^{-3} \text{ rad}$$

which is negligibly small compared to .03 rad.

Actually spin-up will not be accomplished instantaneously. Since the cone angle of the gas particles from the spin rockets may easily approach 90 degrees in a vacuum, some of the gas particles will impact on the bus. We suggest using an even number of spin rocket nozzles so that the gas particles impacting on one solar panel (of the bus) will be compensated by the gas particles impacting on the other panel. Even though no torque will be produced

on the bus in the ideal case we would prefer to use a low thrust spin-up system which has a long burning time. An analysis of the capsule motion during spin-up with an initial tip-off rate is presented in the appendix. A plot of the tip-off angle as a function of the initial tip-off rate for specific values of spin torque T and time t_1 to spin up to 10 rad/sec is given in Fig. 1. Even if T is as small as 5 ft lb, the tip-off angle due to a tip-off rate of .014 rad/sec will be less than .03 rad. Suppose that we select T = 10 ft lb and use two spin rocket nozzles which are mounted on a 4 ft diameter ring. The thrust at each nozzle will be approximately 2.5 lb. It is not thought that errors in this low thrust level will create any significant disturbance to the bus. A detailed analysis is not feasible at this time since the dimensions of the bus, particularly the solar panel dimensions, are not known.

R. R. Auelmann

RRA:clm

Attachments

Distribution

J. R. Ambrose
T. A. Bergstrahl
I. F. Blifford
M. G. Boobar
P. B. Bower
M. Caldwell
D. M. Conrad
E. Durand
R. M. Foster
A. A. Gammal
N. P. Gluth
K. C. Harder
W. W. Hawley
V. H. Henderson
J. Housego
J. A. Jansen
S. Lampert
W. T. Lemm
F. A. Losee
G. R. Miczaika
R. P. Nagorski
R. F. Nease
T. W. Neumann
J. J. Oslake
D. Rodriquez
W. H. Schilling
I. F. Sobczak
D. Stimpson

FIG. 1. Angle Error vs Tip-off Rate

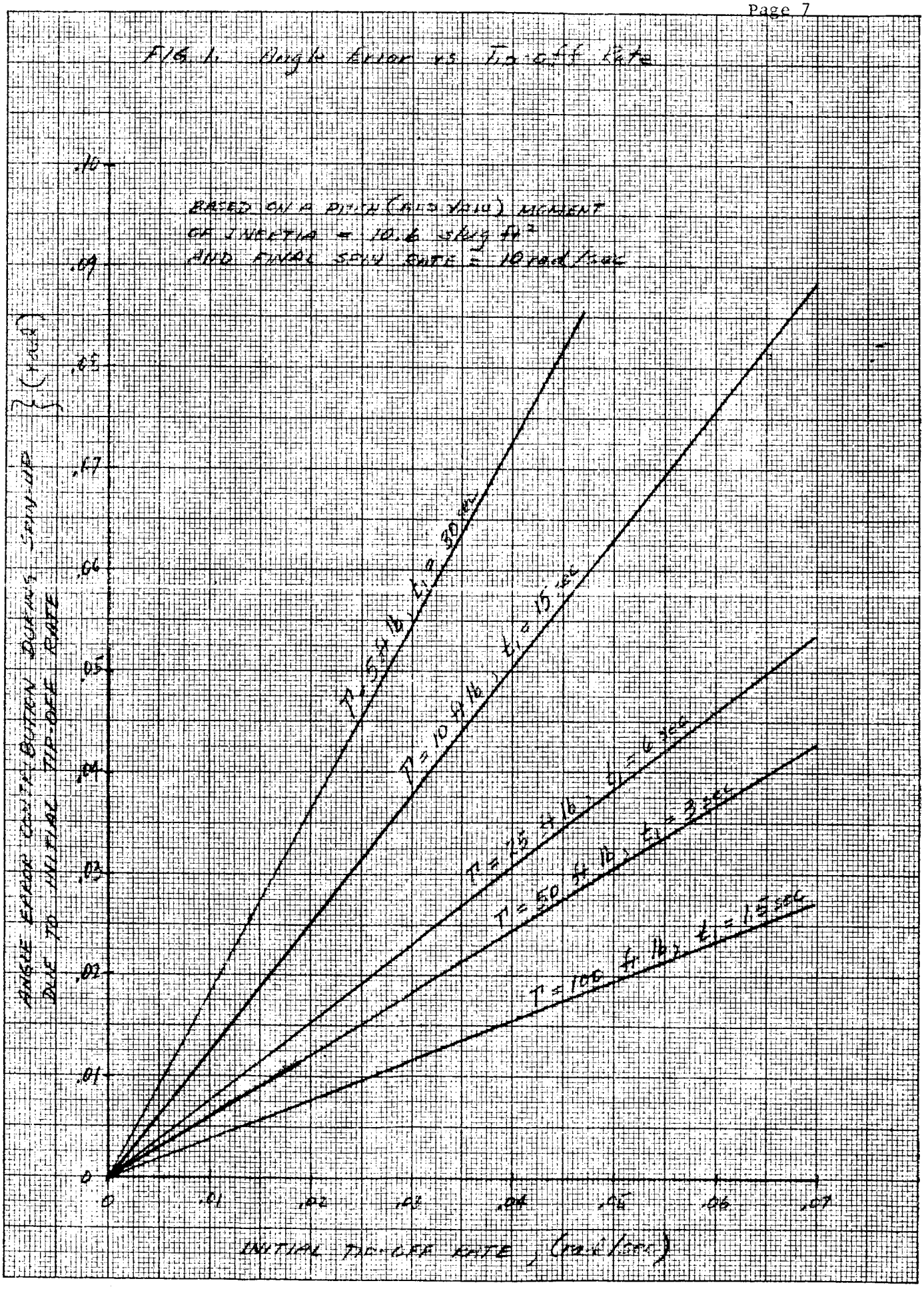

REFERENCES

1. Specification LCS-301, "Specification for Altimeter Support and Erection Assembly", April 15, 1961

2. AL-145, "Mariner Capsule Impact Trajectory Study", Auelmann to Kemmerly, October 26, 1961

APPENDIX: SPIN-UP WITH AN INITIAL TUMBLE RATE

Let A, B and C be three Cartesian coordinate systems with origins at the mass center of the body:

A - nonrotating system

B - body fixed system which rotates relative to A at rate $\bar{\omega}$

C - a system which rotates relative to A at rate $\bar{\Omega}$

The coordinate axes of C are x, y and z, where z coincides with the body axis of symmetry. We require that $\Omega_x = \omega_x$, $\Omega_y = \omega_y$ and $\Omega_z = 0$.

Let J be the moment of inertia of the body about the axis of symmetry and I be the moment of inertia about a transverse axis through the mass center of the body.

The equations of motion resolved along C are

$$\begin{pmatrix} I\dot{\omega}_x \\ I\dot{\omega}_y \\ J\dot{\omega}_z \end{pmatrix} + \begin{pmatrix} 0 & 0 & -\omega_y \\ 0 & 0 & \omega_x \\ \omega_y & -\omega_x & 0 \end{pmatrix} \begin{pmatrix} I\omega_x \\ I\omega_y \\ J\omega_z \end{pmatrix} = \begin{pmatrix} 0 \\ 0 \\ T \end{pmatrix}$$

where T is the spin-up torque. These equations reduce to

$$\dot{\omega}_x - \frac{J}{I}\omega_z\omega_y = 0, \qquad \dot{\omega}_y + \frac{J}{I}\omega_z\omega_x = 0, \qquad \omega_z = \frac{Tt}{I}$$

Then

$$\dot{\omega}_x - \frac{Tt}{I}\omega_y = 0, \qquad \dot{\omega}_y + \frac{T}{I}t\omega_x = 0$$

Multiplication of the first equation by ω_x and the second equation by ω_y, and addition of the resulting equations provides

$$\omega_x\dot{\omega}_x + \omega_y\dot{\omega}_y = \frac{1}{2}\frac{d}{dt}(\omega_x^2 + \omega_y^2) = 0$$

which yields an integral of motion:

$$\omega_x^2 + \omega_y^2 = \alpha^2 \text{ (a constant)}$$

The equation for $\dot{\omega}_x$ may now be reduced to quadrature:

$$\left(\frac{\Gamma}{I}\right) t\, dt = \frac{d\omega_x}{\sqrt{\alpha^2 - \omega_x^2}}$$

$$\frac{\Gamma}{2I} t^2 = \int \frac{d\omega_x}{\sqrt{\alpha^2 - \omega_x^2}} + C = \sin^{-1}\left(\frac{\omega_x}{\alpha}\right) + C$$

or

$$\omega_x = \alpha \sin\left[\frac{\Gamma}{2I} t^2 + \sin^{-1}\left(\frac{\omega_{x_0}}{\alpha}\right)\right]$$

Suppose that the x and y axes are selected so that $\omega_{x_0} = 0$. Then $\alpha = \omega_{y_0}$ and

$$\omega_x = \omega_{y_0} \sin\left(\frac{\Gamma t^2}{2I}\right), \qquad \omega_y = \omega_{y_0} \cos\left(\frac{\Gamma t^2}{2I}\right)$$

We now assume that the z axis departs from the initial direction by only an infinitesimal angle at all times. Then

$$\dot{\phi}_x \simeq \omega_x \qquad \text{and} \qquad \dot{\phi}_y \simeq \omega_y$$

where ϕ_x and ϕ_y are tip-off angles of the z axis. We have

$$\phi_x = \omega_{y_0} \int \sin\left(\frac{\Gamma t^2}{2I}\right) dt + \phi_{x_0}$$

$$\phi_y = \omega_{y_0} \int \cos\left(\frac{\Gamma t^2}{2I}\right) dt + \phi_{y_0}$$

Defining the new variable

$$u = \sqrt{\frac{\Gamma}{\pi I}}\, t$$

we have

$$\int_0^{t_1} \sin\left(\frac{\Gamma t^2}{2I}\right) dt = \sqrt{\frac{\pi I}{\Gamma}} \int_0^{u_1} \sin\left(\frac{\pi}{2} u^2\right) du = \sqrt{\frac{\pi I}{\Gamma}}\, S(u_1)$$

$$\int_0^{t_1} \cos\left(\frac{\Gamma t^2}{2I}\right) dt = \sqrt{\frac{\pi I}{\Gamma}} \int_0^{u_1} \cos\left(\frac{\pi}{2} u^2\right) du = \sqrt{\frac{\pi I}{\Gamma}}\, C(u_1)$$

where $C(u_1)$ and $S(u_1)$ are Fresnel integrals. Thus at the end of spin-up (denoted by the subscript 1)

$$\phi_{x_1} = \omega_{y_0}\sqrt{\frac{\pi I}{T}}\, S(u_1)$$

$$\phi_{y_1} = \omega_{y_0}\sqrt{\frac{\pi I}{T}}\, C(u_1)$$

where we have taken ϕ_{x_0} and ϕ_{y_0} as zero.

Next we will describe the motion after spin-up. The angles between the angular momentum vector (which is fixed in space after spin-up) and the z axis is defined by the infinitesimal angles θ_{x_1} and θ_{y_1}:

$$\theta_{x_1} = -\frac{I\omega_{y_1}}{Js}, \qquad \theta_{y_1} = \frac{I\omega_{x_1}}{Js}$$

where s is the spin rate. Since ϕ_x, ϕ_y, θ_x and θ_y are infinitesimals, we may represent them as vectors in the xy plane as shown below.

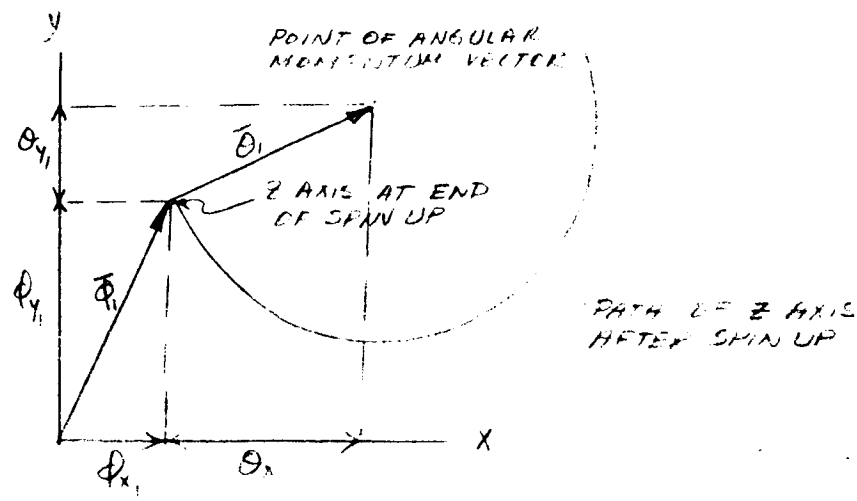

The magnitude of $\bar{\theta}_1$ is $I\omega_{y_0}/Js$. The pointing angle α of interest is the angle between the reference direction 0 and the angular momentum vector. We have

$$\alpha = \sqrt{(\phi_{x_1} + \theta_{x_1})^2 + (\phi_{y_1} + \theta_{y_1})^2}$$

Ford Motor Company AERONUTRONIC DIVISION

Intra-Company Communication

3 October 1961

TO: John Housego

FROM: Russell P. Nagorski

SUBJECT: Attitude Control of the Mariner Capsule

CC: H. H. Hall
G. R. Miczaika
J. L. Arsenault
R. Avelman
F. Dennison
A. Gammel
J. Kemmerly
E. W. Onstead

ABSTRACT

Four probable modes of attitude control for the Mariner Capsule are analyzed with the common evaluation criteria the influence of thrust malalignment during powered flight. The four modes considered are:

1) a spin-stabilized vehicle
2) a stabilizing inertia wheel mounted along the vehicular axis of symmetry (Ref 1)
3) a momentum exchange scheme
4) thrust vector control

A brief discussion of the dynamics of a spinning body under "free-fall" conditions is presented in order to define the contributing factors to vehicular attitude dispersion after burnout.

TECHNICAL DISCUSSION

The general concept of attitude control by spin-stabilization of a body of symmetry can be analyzed by considering a modified form of Euler's dynamical equations*:

$$
\begin{aligned}
I_x \dot{\omega}_1 + I_z \dot{\phi} \omega_2 &= M_1 (t) \\
I_x \dot{\omega}_2 - I_z \dot{\phi} \omega_1 &= M_2 (t) \\
I_z \dot{\omega}_3 &= M_3 (t)
\end{aligned}
\qquad (1)
$$

*Detailed derivation is contained in Appendix A.

177

where the following definitions apply:

I_z = principal moment of inertia about the axis of symmetry

I_y = principal moment of inertia about the transverse axis

ω_n = components of the total rotation vector - angular rotation referred to a quasi-inertial axis

$M_n(t)$ = components of the impressed torque again referred to a quasi-inertial axis

Subscripts 1, 2, 3 refer to a quasi-inertial set of coordinates such that 1, 2 define a pair of axes orthogonal to the third (3) which is in turn aligned along the nominal axis of spin of the vehicle.

Considering first the case of a spin-stabilized vehicle (case 1) the equations shown above have the particular form:

$$\begin{aligned} I_x \dot{\omega}_1 + H_z \quad \omega_2 &= M_m \cos \phi \\ I_x \dot{\omega}_2 - H_z \quad \omega_1 &= M_m \sin \phi \\ I_z \dot{\omega}_3 \qquad\quad &= 0 \end{aligned} \tag{2}$$

These equations have the solutions:

$$\omega_1(t) = \frac{M_m}{H_z\ (1-\rho)} \left\{ \rho \sin \dot{\phi}\ t - \sin \rho\ \dot{\phi}\ t \right\}$$

$$\omega_2(t) = \frac{M_m\ \rho}{H_z\ [1-\rho]} \left\{ \cos \dot{\phi}\ t - \cos \rho\ \dot{\phi}\ t \right\} \tag{3}$$

and, upon integration

$$\theta_1(t) = \frac{M_m}{H_z\ \dot{\phi}\ (1-\rho)} \left\{ \rho\,(1 - \cos \dot{\phi}\, t) - \frac{1}{\rho}\,(1 - \cos \rho\ \dot{\phi}\ t) \right\}$$

$$\theta_2(t) = - \frac{M_m\ \rho}{H_z\,\dot{\phi}\ [1-\rho]} \left\{ \sin \dot{\phi}\ t - \frac{1}{\rho} \sin \rho\ \dot{\phi}\ t \right\} \tag{4}$$

where M_x = represents the disturbing body-fixed moment due to the thrust malalignment

$$\rho = \frac{I_z}{I_x}$$

$$H_z = I_z\ \dot{\phi} = \text{constant}$$

These equations represent the angular rotations of the body about two mutually perpendicular axes which are in turn normal to the axis of spin and which remain <u>fixed in space relative to the spin axis</u>.

The effect of this thrust malalignment is seen to produce a two-frequency curlicue motion bounded by a circle whose radius is

$$\frac{2M_m\ (I_x \pm I_z)}{H_z^2}$$

Hence, the outstanding characteristic of this form of stabilization is the absence of secular terms, e.g. the **position** is harmonic, and the condition of instability of the spherical configuration ($I_x = I_z$).

The resultant variation magnitude of the nominal velocity vector (ΔV_o) may be determined the integration of the appropriate acceleration vector:

$$(\Delta V_o) = \int_0^t \frac{T}{m}(1 - \cos\theta)\,dt = \frac{1}{2}\int_0^t \frac{T}{m}\,\theta^2\,dt \qquad (5)$$

and the deviation normal to the nominal flight path $(\Delta V_o)_n$ may be found

$$(\Delta V_o)_n = \frac{\int_0^t \frac{T}{m}\,\theta(t)\,dt}{\int_0^t \frac{T}{m}\,dt} \qquad (6)$$

where T/m represents the instantaneous thrust to mass ratioof the vehicle.

These two integrals may be utilized in the final quantitative evaluation of the selected system. Obviously these integrals are contingent on the magnitude of the body attitude (θ) and so are not expanded in detail here. For purposes of preliminary design one may approximate the T/m function by an average value, hence, considerable simplification of the integrals occurs.

Considering the case of stabilization by means of an inertia wheel (case 2) equations (1) have the particular form

$$
\begin{aligned}
I_x \dot{\omega}_1 + H_z \omega_2 &= M_m \\
I_x \dot{\omega}_2 - H_z \omega_1 &= 0 \\
I_x \dot{\omega}_3 &= 0
\end{aligned}
\tag{7}
$$

which, in turn, can be integrated to yield

$$
\begin{aligned}
\omega_1 &= \frac{M_m}{H_z} \sin \rho \dot{\phi} t \\
\omega_2 &= - \frac{M_m}{H_z} (1 - \cos \rho \dot{\phi} t)
\end{aligned}
\tag{8}
$$

It follows that

$$
\begin{aligned}
\theta_1 &= \frac{M_m I_x}{H_z^2} (1 - \cos \rho \dot{\phi} t) \\
\theta_2 &= \frac{M_m}{H_z} (t - \frac{1}{\rho \dot{\phi}} \sin \rho \dot{\phi} t)
\end{aligned}
\tag{9}
$$

The latter of equations (9) reveals a secular term, as expected, and because of this inherent feature is rarely used for payload stabilization.

In a comparative sense, the spin-stabilized vehicle (case 1) has a distinct advantage over the inertia wheel (case 2) in minimizing the influence of probably the most predominant disturbance: thrust malalignment. However, the desirability of a "non-rotating" case during the entry portion of the trajectory should be considered as well.

In order to retain the desirable features of both schemes described above, a suggested approach would be to use another form of control -- that based on a principal of momentum exchange (case 3). The concept is simply based on the use of spin-stabilization (case 1) mode of control during the powered flight and upon burnout the angular momentum of the vehicle transferred to an inertia wheel in order to stabilize the case. Increased sophistication (and complexity) may be considered where the attitude of the vehicle may commanded by an appropriate impressed torque on the body case.

The last mode of control considered, that of thrust vector control, can be represented by the single control loop as shown:

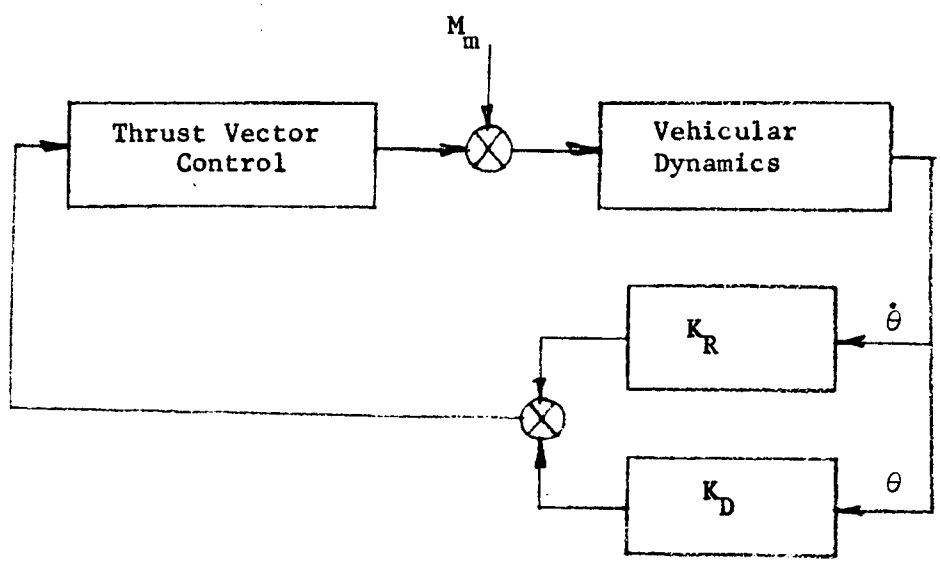

Figure 1

The system represented by Figure 1 can be expressed by a simple second order differential equation

$$I_x \ddot{\theta} + K_R \dot{\theta} + K_D \theta = M_m \tag{10}$$

where K_D, K_R represent the displacement and rate gains of the controller respectively.

In the quasi-steady state condition it can be seen that

$$\theta = \frac{M_m}{K_D} \tag{11}$$

Obviously the angular deviation can be reduced by a judicious choice of the dynamic gain constant (K_D), however, there is a limit. It can be shown that, for this type of control, that the dynamic gain is related to the prescribed control frequency which, in turn, is limited in magnitude by the fundamental bending mode of the body (among other things). Hence a relatively flexible structure (as anticipated for this capsule) could limit the effectiveness of this form of control.

Finally, the kinematics of the capsule after burnout and prior to atmospheric entry can be analyzed by considering the solutions to the basic Euler equations for a symmetrical body:

$$\begin{aligned} I_x \dot{\omega}_x + [I_z - I_x]\omega_y \omega_z &= 0 \\ I_x \dot{\omega}_y + [I_x - I_z]\omega_z \omega_x &= 0 \\ I_z \dot{\omega}_z &= 0 \end{aligned} \tag{12}$$

and the principle of the conservation of angular momentum. For a detailed discussion of the motion of a spinning body under free fall conditions refer to Appendix B.

Basically the body will exhibit a coning motion about the total momentum vector ($\bar{H}$), the included half-angle of the vertex of which is given by the equation

$$\theta = \cos^{-1} \frac{H_z}{H} = \text{constant} \tag{13}$$

where

$$H_z = I_z \dot{\phi} = \text{constant, and}$$

$$H = [H_z^2 + H_x^2 + H_y^2]^{1/2} = \text{constant.}$$

Note that the total momentum H can be found from the initial conditions (in the case considered, the residual angular momentum normal to the body orientation at burnout):

$$H^2 = (I_z \dot{\phi})^2 + (I_x \omega_0)^2 \tag{14}$$

ω_0 = the residual velocity normal to the body attitude at end of powered flight (see equations 3 and 8).

The motion of the vehicle is illustrated below:

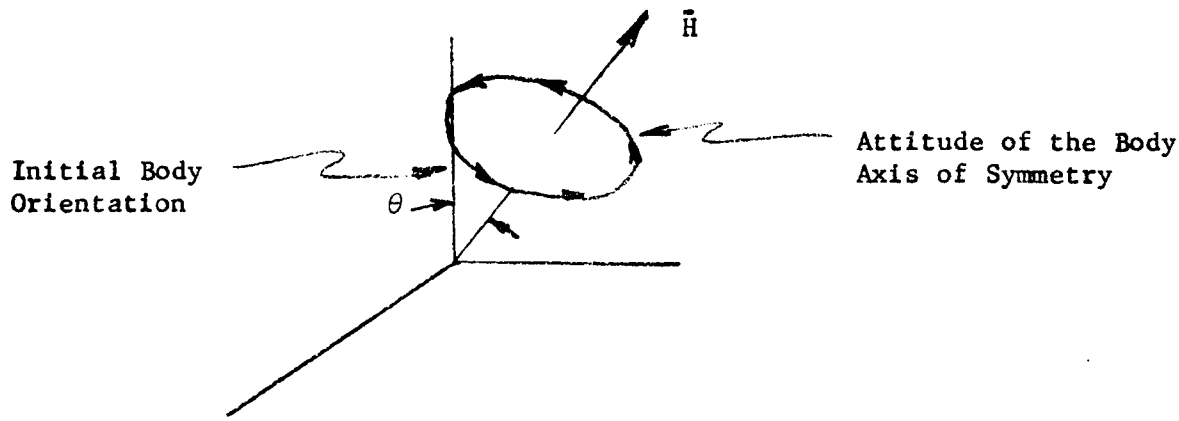

Figure 2

It is evident from the illustration above that the maximum angular excursion of the body is simply 2θ which is the maximum resultant attitude error.

CONCLUSIONS AND RECOMMENDATIONS

A summary of the significant kinematic relationships are presented in Table I for the two forms of spin-stabilization considered. While it is

recognized that the dynamics of the body are subject to influences other than thrust malalignment (e.g., body angular rates evolved during separation, jet damping and variations of the principal axes, among others) the primary system error may be expected from thrust malalignment and thus has been established as the criteria of evaluation.

It is the recommendation of the author that capsule stabilization be attained by initially spinning the entire capsule prior to separation. If it be deemed necessary to (a) "stop" the spin of the case, or (b) re-orient the attitude of the capsule then the momentum exchange scheme is most advantageous. In any event, the usage of a stabilizing inertia wheel alone or attitude control by thrust vectoring during the powered portion of the trajectory have definite dynamical disadvantages for this application.

R. P. Nagorski

SUMMARY

I. ANGULAR RATES

Case 1

$$\omega_1(t) = \frac{M_m}{H_z\ (1-\rho)} \left\{ \rho \sin \dot{\phi}\ t - \sin \rho\ \dot{\phi}\ t \right\}$$

$$\omega_2(t) = \frac{M_m\ \rho}{H_z\ (1-\rho)} \left\{ \cos \dot{\phi}\ t - \cos \rho\ \dot{\phi}\ t \right\}$$

Case 2

$$\omega_1(t) = \frac{M_m}{H_z} \sin \rho\ \dot{\phi}\ t$$

$$\omega_2(t) = \frac{M_m}{H_z} (1 - \cos \rho\ \dot{\phi}\ t)$$

II. ANGULAR ROTATIONS

Case 1

$$\theta_1(t) = \frac{M_m}{H_z\ \dot{\phi}\ (1-\rho)} \left\{ \rho(1 - \cos \dot{\phi}\ t) - \frac{1}{\rho} (1 - \cos \rho\ \dot{\phi}\ t) \right\}$$

$$\theta_2(t) = - \frac{M_m\ \rho}{H_z \dot{\phi}\ [1-\rho]} \left\{ \sin \dot{\phi}\ t - \frac{1}{\rho} \sin \rho\ \dot{\phi} t \right\}$$

d

Case 2

$$\theta_1(t) = \frac{M_m}{H_z\ \rho\ \dot{\phi}} (1 - \cos \rho\ \dot{\phi}\ t)$$

$$\theta_2(t) = \frac{M_m}{H_z} (t - \frac{1}{\rho\ \dot{\phi}} \sin \rho\ \dot{\phi}\ t)$$

TABLE A

APPENDIX A

THE EQUATIONS OF MOTION OF SPINNING BODY WITH A DISTURBING MOMENT APPLIED

Consider the basic Euler equations (Ref. 2) given below:

$$\begin{aligned} I_x \dot{\omega}_x + [I_z - I_x]\omega_y \omega_z &= M_x = M_m \\ I_x \dot{\omega}_y + [I_x - I_z]\omega_z \omega_x &= M_y = 0 \\ I_z \dot{\omega}_z &= M_z = 0 \end{aligned} \tag{15}$$

The latter equation can be integrated immediately to give

$$I_z \omega_z = \text{constant} - H_z = I_z \dot{\phi} \tag{16}$$

Next, consider a coordinate set such that the triad is aligned along the axis of spin ("Z" axis) and remains inertially fixed except for rotations about the two axes normal to the spin axis. These axes, called the pseudo-stability axes, will be denoted by the subscripts 1 and 2 while the subscripts x, y, and z will be retained as referencing to a body-fixed coordinate system.

From Figure 3 shown below several significant relationships may be noted:

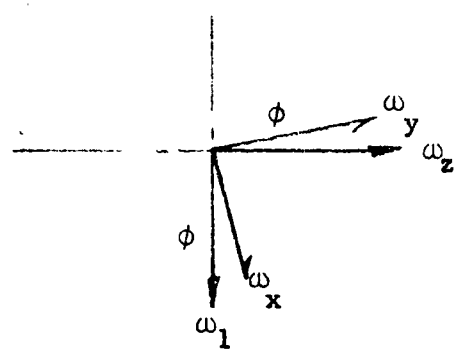

Figure 3

$$\omega_x = \omega_1 \cos \phi + \omega_2 \sin \phi$$
$$\omega_y = - \omega_1 \sin \phi + \omega_2 \cos \phi \tag{17}$$

similarly

$$M_m = M_1 \cos \phi + M_2 \sin \phi$$
$$0 = - M_1 \sin \phi + M_2 \cos \phi \tag{18}$$

substituting the relations above into (15) yields:

$$I_x \dot{\omega}_1 + I_z \phi \omega_2 = M_1 = M_m \cos \phi$$
$$I_x \dot{\omega}_2 - I_z \phi \omega_1 = M_2 = M_m \sin \phi \tag{19}$$

For the situation where the thrust malalignment (M_m) rotates with the vehicle (or in other words referenced to body-fixed coordinates) these equations are of the form

$$I_x \dot{\omega}_1 + H_z \omega_2 = M_m \cos \phi$$
$$I_x \dot{\omega}_2 - H_z \omega_1 = M_m \sin \phi \tag{20}$$
$$H_z = \text{constant}$$

If the disturbing torque appears along the pseudo-stability axes then

$$I_x \dot{\omega}_1 + H_z \omega_2 = M_m$$
$$I_x \dot{\omega}_2 - H_z \omega_1 = 0 \tag{21}$$
$$H_z = \text{constant}$$

APPENDIX B

THE EQUATIONS OF MOTION OF A "FREE" SPINNING BODY

Euler's Equations again will express the dynamics of the spinning body, i.e.,

$$\begin{aligned} I_x \dot{\omega}_x + [I_z - I_x]\, \omega_y \omega_z &= 0 \\ I_x \dot{\omega}_y + [I_x - I_z]\, \omega_z \omega_x &= 0 \\ I_z \dot{\omega}_z &= 0 \end{aligned} \tag{22}$$

The last equation yields:

$$I_z \omega_z = \text{constant} = H_z \tag{23}$$

Since the total momentum vector $\bar{H}$ cannot change (no impressed torques) it follows that

$$H^2 = H_x^2 + H_y^2 + H_z^2 = \text{constant} \tag{24}$$

The angular position of the momentum vector can be seen from Figure 4 given below:

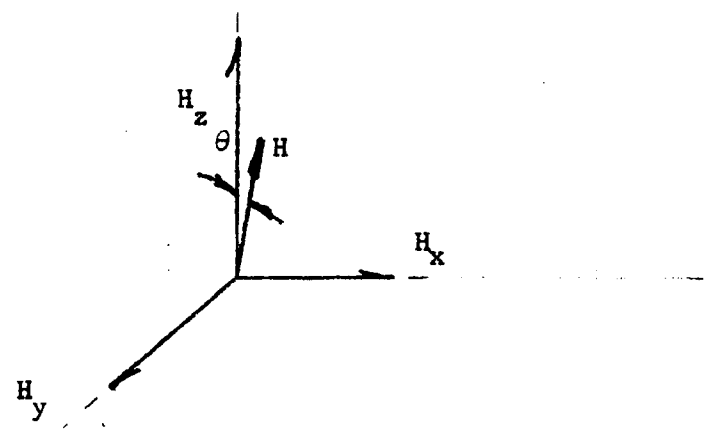

Figure 4

It is seen that

$$\cos \theta = \frac{H_z}{H} = \text{constant} \tag{25}$$

Thus the body will rotate in space about the $\bar{H}$ vector, the so-called invariant line and will reach a maximum deviation of 2θ. The normal momentum components may be easily evaluated in terms of initial rates imparted to the body.

The rate ($\dot{\psi}$) that the body will precess in the coming motion about the invariant line is given by (Ref. 3)

$$\dot{\psi} = \frac{H_z}{(I_x - I_z) \cos \theta} \tag{26}$$

REFERENCES

1. R. R. Anelman to R. F. Nease — "Propulsion Capability of the Mariner Capsule with Inertia Wheel Attitude Control" 7 September 1961, AL-131

2. J. Ames and F. Murnagham — "Theoretical Mechanics" Dover Publications page 198

3. J. Ames and F. Murnagham — "Theoretical Mechanics" Dover Publications page 218

Intra-Company Communication

TO: J. Housego

FROM: R. Nagorski

SUBJECT: Further Notes on the Attitude Control of the Mariner Capsule.

REFERENCE: (1) "Attitude Control of the Mariner Capsule", (Nagorski to Housego), 3 October, 1961

ABSTRACT

Subsequent to the publication of Reference 1, a tentative definition of the mode of control for the Mariner capsule was made. The capsule is to be separated from the parent craft; spun up by a suitable array of spin rockets with engine ignition to occur shortly thereafter. The velocity increment is imparted approximately normal to the nominal flight path of the parent craft and the moment of inertia distribution is such that the lateral moment of inertia is slightly larger than that about the axis of symmetry.

The analysis of the kinematics of the spin-stabilized Mariner capsule has been extended in this memorandum to define qualitatively the several possible sources of error including initial rates. A quantitative solution is presented, using selected arbitrary parameters, to illustrate the required spin rate as a function of the ratio of moment of inertias.

TECHNICAL DISCUSSION

The Equations of motion of a spin-stabilized symmetrical body under thrust were shown in a previous memorandum (Reference 1) to have the form:

$$
\begin{aligned}
I_x \dot{\omega}_1 + H_z \omega_2 &= M_m \cos \dot{\phi} t \\
I_x \dot{\omega}_2 - H_z \omega_1 &= M_m \sin \dot{\phi} t \\
I_z \dot{\omega}_3 &= 0
\end{aligned}
\tag{1}
$$

The solutions to these equations have been extended to include the influence of the separation kinematics:

177

$$\omega_1 = \frac{M_M}{H_z(1-\rho)}\left[\rho \sin \dot{\phi}\tau - \sin \rho \dot{\phi}\tau\right] + \omega(0) \cos \rho \dot{\phi}\tau$$

$$\omega_2 = \frac{M_M \rho}{H_z(1-\rho)}\left[\cos \dot{\phi}\tau - \cos \rho \dot{\phi}\tau\right] + \omega(0) \cos \rho \dot{\phi}\tau \tag{3a}$$

$$\theta_1 = \frac{M_M}{H_z(1-\rho)\dot{\phi}}\left[\rho(1-\cos \dot{\phi}\tau) - \frac{1}{\rho}(1-\cos \rho \dot{\phi}\tau)\right] + \frac{\omega(0)}{\rho \dot{\phi}} \sin \rho \dot{\phi}\tau$$

$$\theta_2 = -\frac{M_M \rho}{H_z(1-\rho)\dot{\phi}}\left[\sin \dot{\phi}\tau - \frac{1}{\rho} \sin \rho \dot{\phi}\tau\right] + \frac{\omega(0)}{\rho \dot{\phi}} \sin \rho \dot{\phi}\tau \tag{3b}$$

where the previous nomenclature applies and $\omega(0)$ represents the initial rate imparted to the vehicle.

These angular deviations are related to the variations in the velocity vector since the instantaneous acceleration vector is defined in terms of the instantaneous body attitude. The variation in the velocity magnitude is given by the following equation :

$$\Delta V_0 \cong \frac{1}{2} \int_0^t \frac{T}{M} \theta^2 \, d\tau \tag{4}$$

and the variation normal to the nominal flight path is simply

$$(\Delta V_0)_N = \int_0^t \frac{T}{M} \theta \, d\tau \tag{5}$$

Because of the relatively large error expected from thrust cutoff, the velocity magnitude error due to the variation in body attitude, equation (4), may be neglected and the error determined by the cutoff equation:

$$\Delta V_o = \frac{T}{M_{BO}} \Delta t \tag{6}$$

where T = nominal thrust

M_{BO} = vehicular mass at burnout

Δt = uncertainty in cutoff time

Equation (5) may be simplified to a fair degree of accuracy with the conservative assumption that the attitude angle θ remain a constant maximum value throughout the thrusting period, hence:

$$(\Delta V_o)_N \cong V_o \, \theta(MAX) \tag{7}$$

where

V_o = applied velocity increment

The maximum angular excursion that would occur may be extracted from equations 3a and 3b for the condition $\rho \cong 1$;

$$\theta(MAX) = \frac{1}{\dot{\phi}} \left[\frac{2M_m}{H_z(1-\rho)} + \omega(0) \right] \tag{8}$$

The two dynamic parameters, thrust malalignment (M_m) and initial rates ($\omega(0)$), of equation (8) are discussed in detail in the following sections.

THRUST MALALIGNMENT

The malalignment of the thrust vector is of a two-fold

nature, e.g., angular and linear variations of the line of thrust with respect to the center of mass. The expression for the overturning moment due to these random contributions is

$$M_M = T\left[(\ell_F \lambda)^2 + (\Delta R)^2\right]^{1/2} \tag{9}$$

where

T = thrust

ℓ_F = distance from exit plane of rocket nozzle to the capsule c.m.

ΔR = lateral displacement of the engine axis of symmetry to the c.m.

λ = inclination of the engine centerline to the vehicular axis of symmetry.

An appropriate combination of these two malalignments would also produce a roll moment; however, this contribution is neglected for the purposes of this study.

INITIAL RATES

The initial angular velocities are the residual velocity of the parent vehicle at time of separation (ω_i) and the angular impulse applied about a transverse axis during spin up. Based on an assumed cruxiform array of spin rockets about the periphery of the capsule, the several transverse moment components imparted to the vehicle during spin up are (Figure 1)

(a) A moment generated about a transverse axis due to malalignment of the spin rockets about a radial line:

$$M_\alpha = \sqrt{2}\, F R \alpha \tag{10}$$

(b) Malalignment from the true tangency produces

$$M_\beta = \sqrt{2}\, F \ell_s \beta \tag{11}$$

(c) Variations of the locations of the spin rockets

$$M_{l_s} = \sqrt{2}\, F \Delta l_s = \sqrt{2}\, F l_s k_1 \tag{12}$$

(d) Variations in thrust level

$$M_F = \sqrt{2}\, l_s \Delta F = \sqrt{2}\, F l_s k_2 \tag{13}$$

If these moments are random in nature then

$$M_s^2 = \left[M_\alpha^2 + M_\beta^2 + M_{l_s}^2 + M_F^2 \right] \tag{14}$$

where M_s is the moment applied to the vehicle about a transverse axis. The resulting angular rate is simply:

$$\omega = \frac{M_s t}{I_x} = \frac{M_s}{M} \rho \dot{\Phi} \tag{15}$$

where M is the nominal torque applied during spin up:

$$M \triangleq 4FR \tag{16}$$

and since from the previous equations

$$M_s = \sqrt{2}\, F \left[(R\alpha)^2 + l_s^2 (\beta^2 + k_1^2 + k_2^2) \right]^{1/2} \tag{17}$$

substitution into equation 15 yields

$$\omega = \frac{\rho \dot{\Phi} \left[\alpha^2 + \left(\frac{l_s}{R}\right)^2 (\beta^2 + k_1^2 + k_2^2) \right]^{1/2}}{2\sqrt{2}} \tag{18}$$

if the placement of the spin rocket assemblies is very close to the center of mass of the vehicle, then $\frac{\ell_2}{R} \rightarrow 0$ and

$$\omega \cong \frac{\rho \dot{\phi} \alpha}{2\sqrt{2}}$$

An additional rate would be generated from a spin rocket misfire or a time delay in reaching full thrust; however, if the vehicular spin center of mass is very close to the rocket plane, then this effect may be negligible.

Therefore, to a very close approximation, the initial rate can be found from

$$\omega(0) = \left[\left(\frac{\rho \dot{\phi} \alpha}{2\sqrt{2}} \right)^2 + \omega_i^2 \right]^{1/2}$$

SPIN RATE REQUIREMENTS

In order to illustrate the relationship of the ratio of moment of inertias, to the required spin rate, a selected set of vehicular parameters were used in conjunction with the several equations established earlier in this memorandum. The results are shown in Figure 2. The restriction was established that $\rho \cong 1$ to conform to the expected inertia distribution of the Mariner capsule.

A NOTE ON JET DAMPING

If a rocket rotates about a transverse axis during burning, the gas must be accelerated laterally as it flows through the case. The net effect of this change of momentum is to provide a damping term on the resulting oscillatory motion as will be shown below:

Consider the case of planar motion where

$$\frac{d}{dt}(I_x \omega) = 0$$

To this equation must be added the momentum lost as the gas leaves the nozzle:

$$\frac{d}{dt}(I_x \omega) - \frac{d}{dt}(M_g \ell^2 \omega) = 0$$

where M_g = mass of gas

ℓ = lever arm from c.g. to nozzle exit plane

Expanding this equation:

$$k^2 \dot{m} \omega + I_x \dot{\omega} - \dot{m}_g \ell^2 \omega = 0$$

where k = radius of gyration

It follows then, if $\dot{m}_g \triangleq \dot{m}$

$$I_x \dot{\omega} = \dot{m} \omega (\ell^2 - k^2)$$

Since $\dot{m}$ is a negative number and if the lever arm (ℓ) is greater than the radius of gyration (k) (as is generally the case) then it can be shown that the resulting motion will decay exponentially.

The net effect, therefore, is not detrimental to the vehicular kinematics and will not be considered in this analysis.

R. Nagorski

R. NAGORSKI

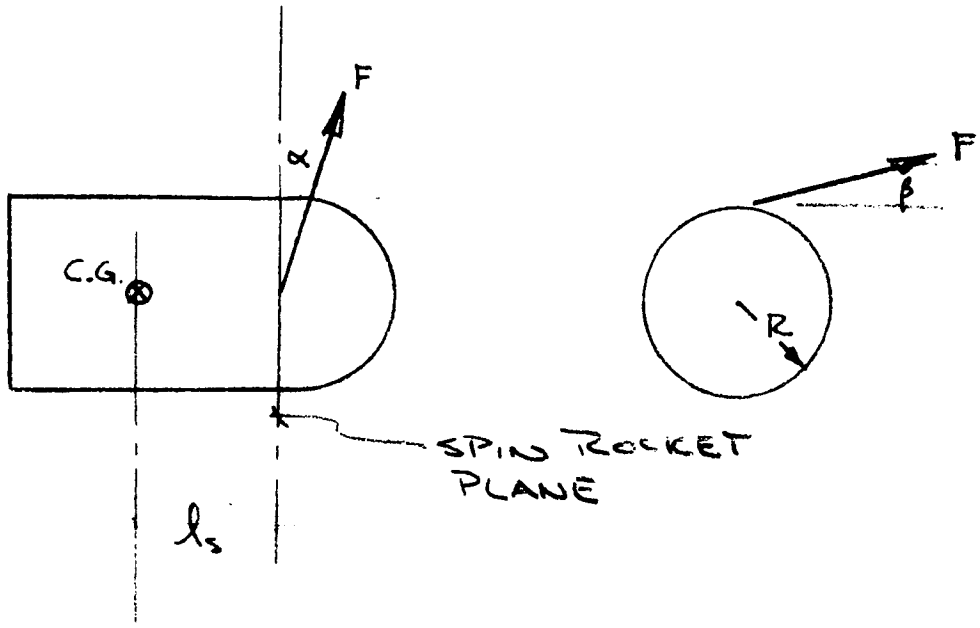

FIGURE 1

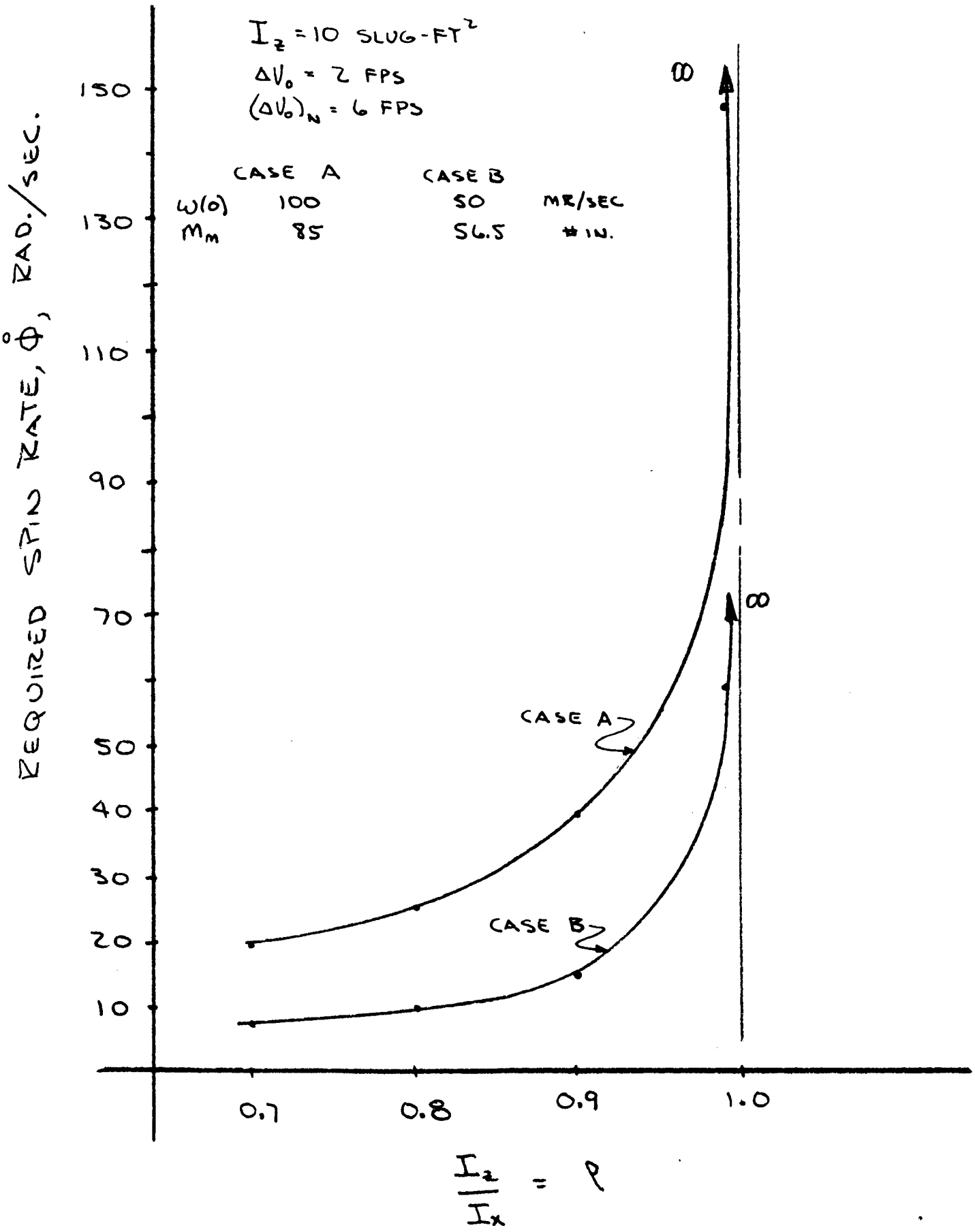
$I_z = 10$ SLUG-FT^2
$\Delta V_0 = 2$ FPS
$(\Delta V_0)_N = 6$ FPS
CASE A
CASE B
$\omega(0)$ 100 50 MR/SEC
M_m 85 56.5 # IN.
REQUIRED SPIN RATE, $\dot{\phi}$, RAD./SEC.
150
130
110
90
70
50
40
30
20
10
0.7
0.8
0.9
1.0
∞
∞
CASE A
CASE B
$\frac{I_z}{I_x} = \rho$

FIGURE 11

APPENDIX B

SPACE TRAJECTORIES AND ERROR ANALYSIS

Ford Motor Company AERONUTRONIC DIVISION

Intra-Company Communication

AL-145

26 October 1961

To: J. E. Kemmerly

From: R. R. Auelmann

Subject: MARINER CAPSULE IMPACT TRAJECTORY STUDY

Note: This document supercedes: AL-134, 138, 139, 141

SCOPE OF STUDY

We define the "capsule impact trajectory" as the path travelled by the capsule between the points of capsule-bus separation and impact on Mars. In particular we are interested in the relations between the end points of such trajectories.

The initial conditions (the velocity and position at separation) are selected to be consistent with relatively low energy launch conditions between November 10, 1964 and December 10, 1964. Transfer orbits between planets are not evaluated.

The atmosphere of Mars is ignored in this study, since the path length in the atmosphere ($\sim$ 300 km) is small when compared to the overall distance travelled from the point of separation ($\sim 3 \times 10^5$ km).

The primary purpose of this study was to establish one or more criteria for selecting nominal capsule impact trajectories. The factors which were considered are;

a) illumination of the surface of Mars before and during atmospheric entry

b) bus-capsule communication link

c) atmospheric entry angle

177A

d) propulsion requirements

e) error sensitivity

Three different sets of nominal trajectories are proposed and are critically evaluated.

R. R. Auelmann

RRA:clm

Distribution
J. R. Ambrose
T. A. Bergstrahl
I. F. Blifford
M. G. Boobar
P. B. Bower
M. Caldwell
D. M. Conrad
E. Durand
R. M. Foster
A. A. Gamma
K. C. Harder
W. W. Hawley
V. H. Henderson
J. Housego
J. A. Jansen
S. Lampert
W. T. Lemm
F. A. Losee
G. R. Miczaika
R. P. Natorski
R. F. Nease
T. W. Neumann
J. J. Oslake
D. Rodriquez
W. H. Schilling
I. F. Sobczak
D. Stimpson

CONTENTS

Section	Page
Scope of Study	i
A. VELOCITY AND POSITION AT SEPARATION	1
1. Nominal Interplanetary Trajectories	1
2. Uncertainties	1
B. IMPACT TRAJECTORIES	3
1. Parameters for Defining the Impact Trajectories	3
2. Parameters in the Plane of $\bar{v}_1$ and $\bar{s}$	3
3. The velocity Change Vector $\bar{v}_C$	4
4. Errors Normal to the Nominal Plane of $\bar{v}_1$ and $\bar{s}$	10
C. CRITERIA FOR THE SELECTION OF NOMINAL TRAJECTORIES	14
1. The Approach Trajectory Prior to Separation	14
2. Three Sets of Nominal Impact Trajectories	15
3. Illumination Requirements	15
4. Bus-Capsule Communication Distance and Line of Sight	17
5. Atmospheric Penetration	18
6. Propulsion Requirements	19
7. Error Sensitivity	20
8. Summary Comparison of Nominal Trajectories	22
REFERENCES	25
APPENDICES	26
A. Expected Values for Λ_s	26
B. Motion in the Plane of $\bar{v}_1$ and $\bar{s}$	28
C. Error in the Magnitude of $\bar{v}_C$	32
D. Time and Position Relations Impact	34
E. Change in Transit Time Due to Δv_1	36

A. VELOCITY AND POSITION AT SEPARATION

1. Nominal Interplanetary Trajectories

The range of asymptotic approach velocities v_A with respect to Mars is taken between 4 and 6 km/sec. This range is consistent with values of C_3 between 0.1 and 0.12 x 10^8 meters^2/sec^2 for launch dates between November 10 and December 10, 1964 (Ref. 1, Fig. 1). C_3 is twice the geocentric energy per unit mass.

The angle Λ_s measured clockwise (as viewed from north ecliptic pole) from the Sun-Mars line to the vector $\bar{v}_A$ will vary between 20 and 40 degrees for the range of values for C_3 which were considered (see Appendix A).

2. Uncertainties

We assume that the spacecraft and capsule are on a "fly-by" trajectory prior to separation. The altitude h of closest approach of the fly-by trajectory to the surface of Mars is a sensitive parameter. Dispersions in h on the order 10^5 km result from injection guidance errors (Ref. 2, p. 40).

After midcourse correction, the dispersion in h may be on the order of 4000 km (Ref. 2, p. 39*). The dispersion is due to errors in pointing, shutoff and velocity resolution. We have assumed that the 4000 km corridor lies between h = 6000 and 10,000 km.

Next we will consider the requirements for a successful capsule mission. Clearly a 4000 km uncertainty in h is unacceptable for carrying out an impact on a planet with a radius of 3310 km. Presumably an approach guidance scheme will be activated perhaps at a distance of 10^6 km from the planet. This scheme, which measures the angle diameter of Mars at successive time intervals, can be used to locate h to within a few hundred kilometers in the corridor between 6000 and 10,000 km. In our study we have assumed that, if no other errors were introduced, the 3σ dispersion at impact due to errors in the approach guidance scheme are $\pm$ 15 degrees in both latitude and longitude.

---

* The numbers quoted in Ref. 2 pertain to a Venus probe, however, the dispersions should also be representative for a Mariner B mission.

The expected uncertainties in h are summarized below:

Immediately after injection: $h \sim 10^5$ km

After midcourse correction: $h \sim 8000$ km $\pm$ 2000 km

Knowledge of h after use of approach guidance: $\Delta h \sim 500$ km

The initial conditions for the approach "fly-by" trajectories are taken as follows:

$$4 \text{ km/sec} \leq v_A \leq 6 \text{ km/sec}$$

$$20 \text{ deg} \leq \Lambda_s \leq 40 \text{ deg}$$

$$6000 \text{ km} \leq h \leq 10{,}000 \text{ km}$$

We also assume that the capsule cannot separate from the bus at distances greater than 3.2×10^5 km from Mars.

B. IMPACT TRAJECTORIES

1. Parameters for Defining the Impact Trajectories

The initial conditions are taken immediately after the capsule has been placed on an impact trajectory. We assume that the gravitational field strength due to the Sun is uniform in the region of interest, near Mars. Hence, we may regard the motion of the capsule as a simple central force problem. We also assume that the potential energy of the capsule at the initial point on the impact trajectory is zero. As a consequence, the trajectory is (to a first approximation) independent of the position vector from Mars to the initial position, and only five initial conditions are needed to define the problem.

Let $\bar{v}_1$ be the velocity of the capsule relative to Mars at the initial point and let $\bar{s}$ be the radius vector from the center of Mars to the line of action of $\bar{v}_1$ such that $\bar{v}_1 \cdot \bar{s} = 0$. The six components of $\bar{v}_1$ and $\bar{s}$ completely define the orbit. The constraint, $\bar{v}_1 \cdot \bar{s} = 0$, reduces the number of initial conditions to five.

2. Parameters in the Plane of $\bar{v}_1$ and $\bar{s}$

The geometry for motion in the plane of $\bar{v}_1$ and $\bar{s}$ is given in Fig. 1. The subscript M denotes quantities at the surface.

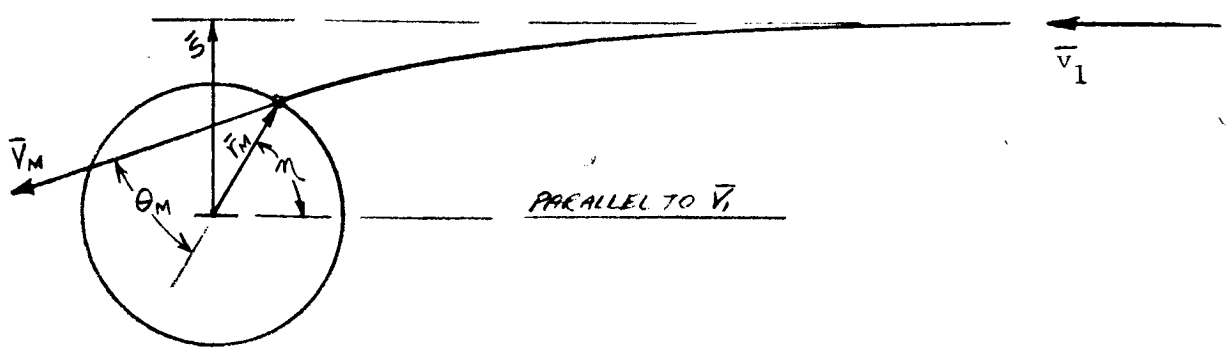

Fig. 1 Geometry for In-Plane Motion

v_M is the magnitude of the impact velocity, θ_M is the angle between $\bar{v}_M$ and the local vertical at impact and η is the in-plane impact location angle referenced to $\bar{v}_1$. The dependence of v_M on v_1, and θ_M and η on v_1 and s is established in Appendix B. v_M, θ_M and η are plotted in Figures 2, 3 and 4.

The error coefficients which relate small changes in v_M, θ_M and η due to v_1 and s are derived in Appendix B and are plotted in Figs. 2, 5 and 6.

3. The Velocity Change Vector $\bar{v}_c$

At some distance less than 3.2×10^5 km from Mars an impulse will be imparted to the capsule. The capsule approach velocity vectors before and after the impulse are denoted by $\bar{v}_A$ and $\bar{v}_1$, respectively. The vector difference $\bar{v}_1 - \bar{v}_A$ is $\bar{v}_C$. The main purpose of $\bar{v}_C$ is to reduce the angular momentum γ_Z of the capsule (assume a unit mass) relative to Mars. Let $\bar{s}_A$ be the perpendicular distance between the mass center of Mars and $\bar{v}_A$ ($\bar{s}_A$ is to $\bar{v}_A$ as $\bar{s}$ is to $\bar{v}_1$) and let r_1 be the distance between the mass center of Mars and the point at which the impulse is applied. Then, since $v_C s \ll v_c r_1$, $\bar{v}_C$ should be applied approximately perpendicular to $\bar{v}_1$. Since $v_C \ll v_A$, $\bar{v}_C$ is approximately perpendicular to $\bar{v}_A$ too. The angular momentum γ_Z and v_C are related as follows:

$$\gamma_z = -r_1 V_c \quad , \qquad \Delta\gamma_z = \gamma_z \left(\frac{\Delta V_c}{V_c}\right) - V_c \Delta r_1$$

Since the altitude of closest approach h for a fly-by trajectory may vary by as much as 4000 km, the desired value for γ_Z (as calculated from data obtained from the approach guidance system) will be unknown until just prior to separation. The implication is that γ_Z will be a variable, and that either r_1 or v_C must be capable of change. Thus two schemes suggest themselves; a variable impulse v_C at a fixed r_1 or a fixed impulse v_C at a variable distance r_1. The maximum value for v_C will be the same for both schemes. If we assume that both $\Delta v_C/v_C$ and Δr_1 are the same for both

schemes, then the variable v_C scheme will, in many cases, produce smaller errors in γ_Z. However, the maximum value for $\Delta\gamma_Z$ will be the same for both systems. From the viewpoint of system mechanization the fixed impulse scheme is probably easier.

We define Λ as the angle between the nominal direction of $-\bar{v}_1$ and the actual (perturbed) direction of $\bar{r}_M$. The error coefficients which relate small errors in Λ and θ_M due to $\Delta\gamma_Z$ are derived in Appendix C and are plotted in Fig. 7.

4. Errors Normal to the Nominal Plane of $\bar{v}_1$ and $\bar{s}$

Let xyz be a Cartesian coordinate system with origin at the mass center of Mars. The x axis is parallel to the nominal direction to $-\bar{v}_1$, the y axis is parallel to the nominal direction of $\bar{s}$, and the z axis is normal to the nominal orbit plane as shown in Fig. 8. We are interested in the effects due to the error sources v_{1_Z} and s_Z. For small values of v_{1_Z}/v_1 and s_Z/s, the latitude error of the impact point is given by

$$\lambda \simeq \frac{\partial\lambda}{\partial s_z} s_z + \frac{\partial\lambda}{\partial v_{1_z}} v_{1_z}$$

where

$$\frac{\partial\lambda}{\partial s_z} = \frac{\sin\eta}{s}, \qquad \frac{\partial\lambda}{\partial v_{1_z}} = \frac{-\cos\eta}{v_1}$$

These error coefficients are plotted in Fig. 9.

If the velocity change vector $\bar{v}_C$ has an error component $v_{C_Z} = v_{1_Z}$, the error s_Z is given by

$$s_z = \gamma_y / v_1 \quad \text{where} \quad \gamma_y = -r_{1_x} v_{1_z} \simeq -r_1 v_{1_z}$$

Then, if $r_1 >> s$, we have

$$\lambda \simeq \frac{\partial\lambda}{\partial\gamma_y} \gamma_y \quad \text{where} \quad \frac{\partial\lambda}{\partial\gamma_y} = -\frac{\sin\eta}{v_1 s}$$

FIG. 2. V_M and $\partial V_M/\partial V_1$ as functions of V_1

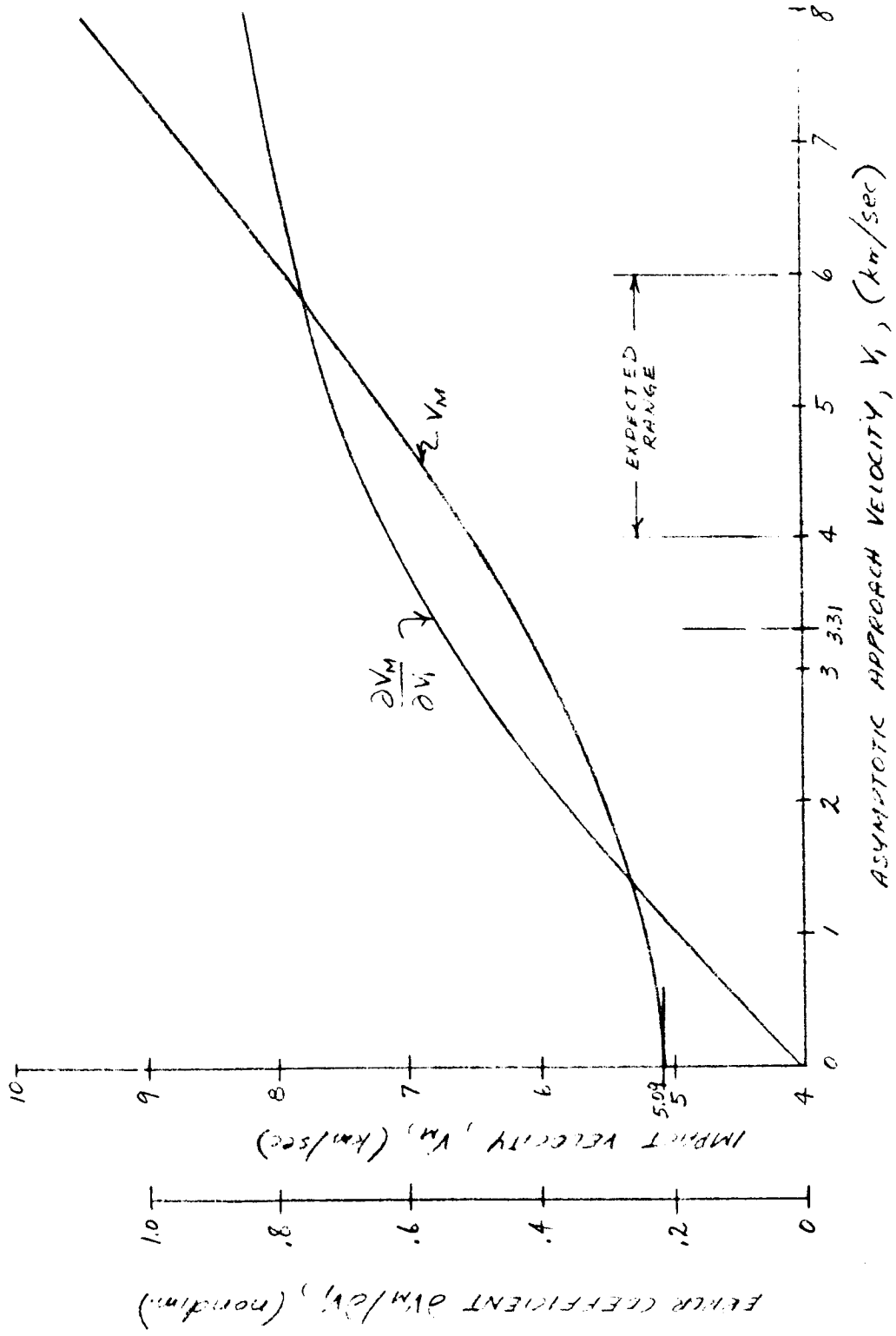

FIG. 3. θ_M as a function of s for 3 values of v_1

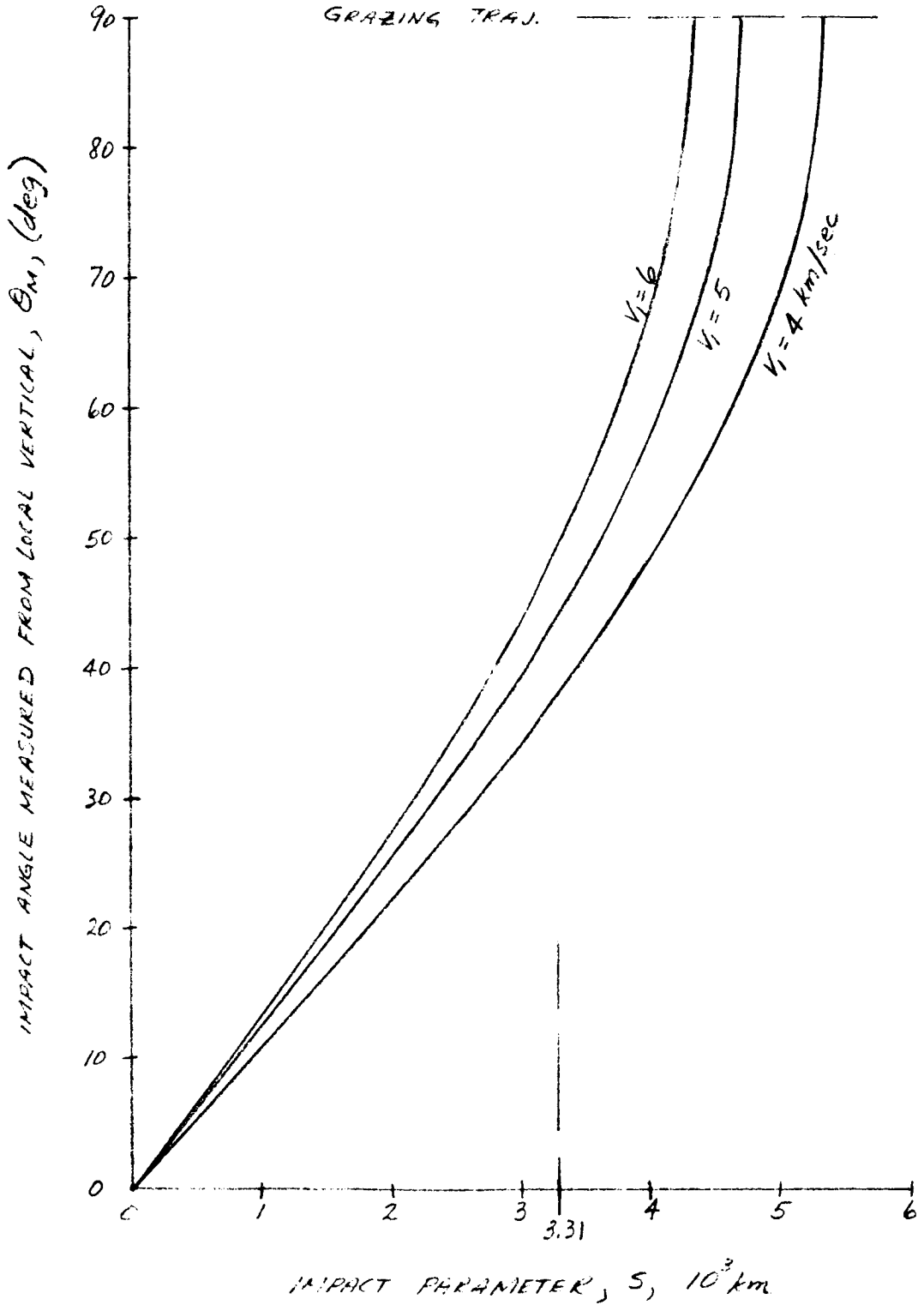

FIG. 4. η as a function of s for 3 values of V_1

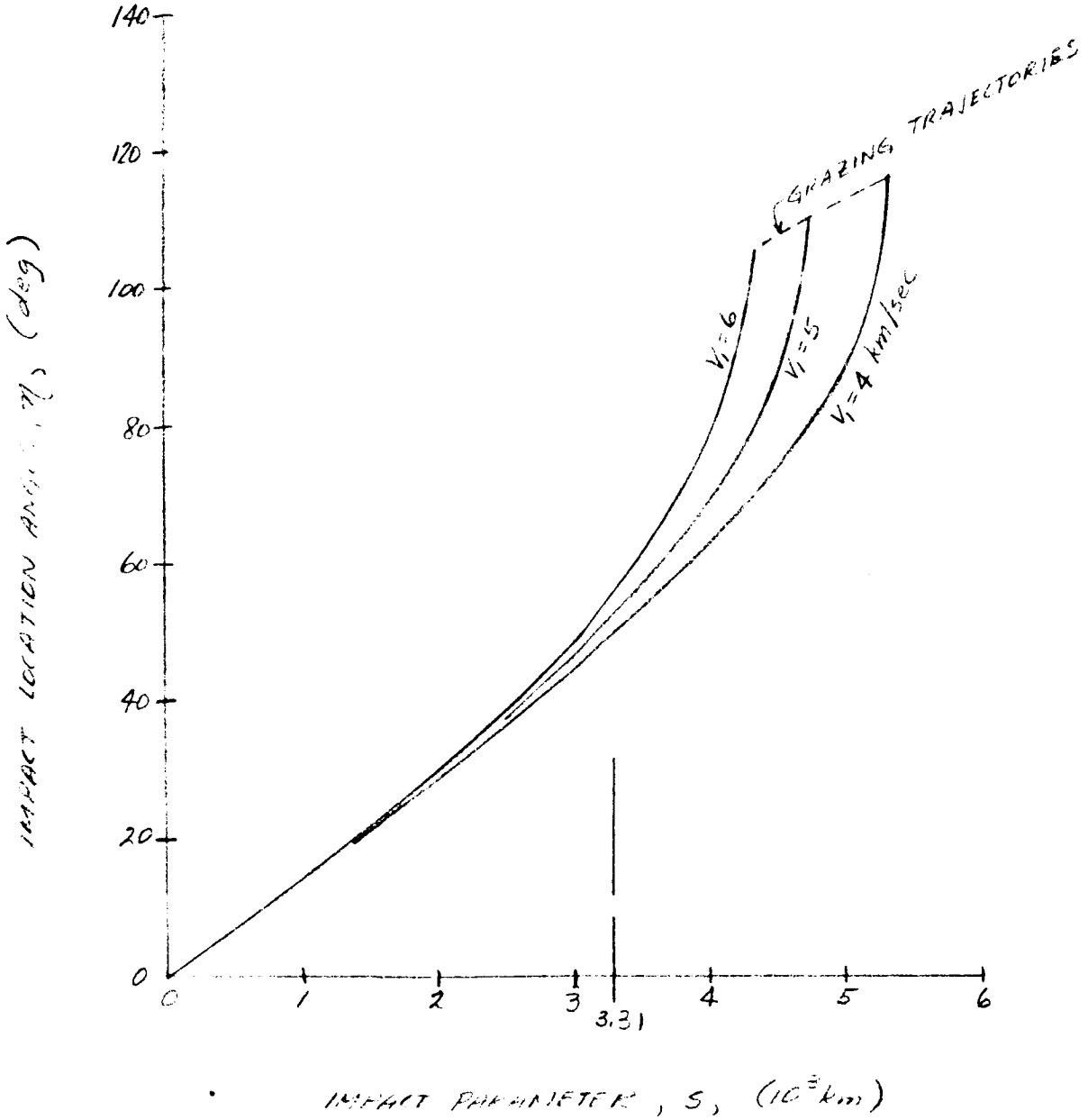

FIG. 5. $\partial\eta/\partial v_1$ and $\partial\theta_M/\partial v_1$ as functions of s for 3 values of v_1

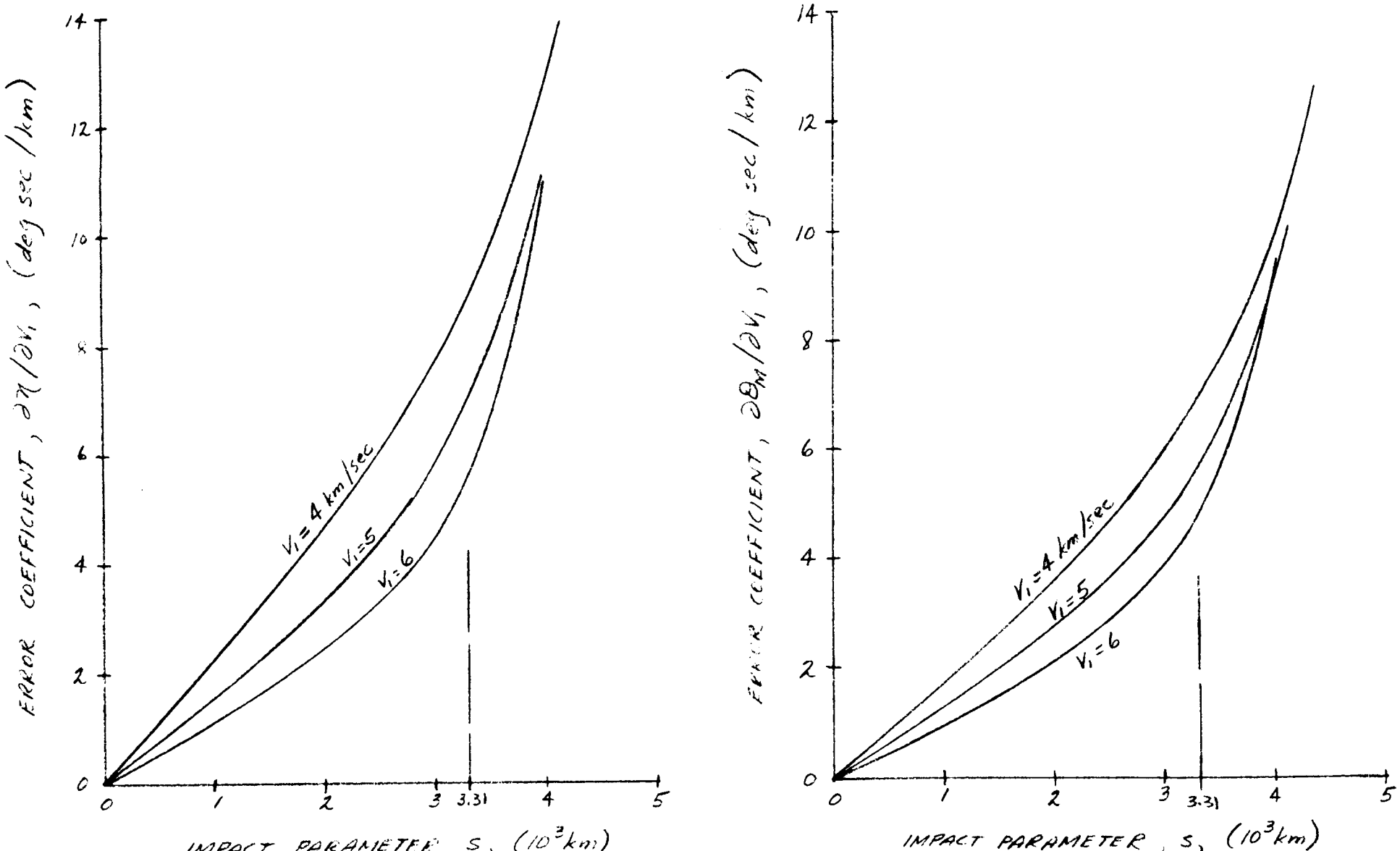

FIG. 6. $\partial\eta/\partial s$ and $\partial\theta_M/\partial s$ as functions of s for 3 values of V_1

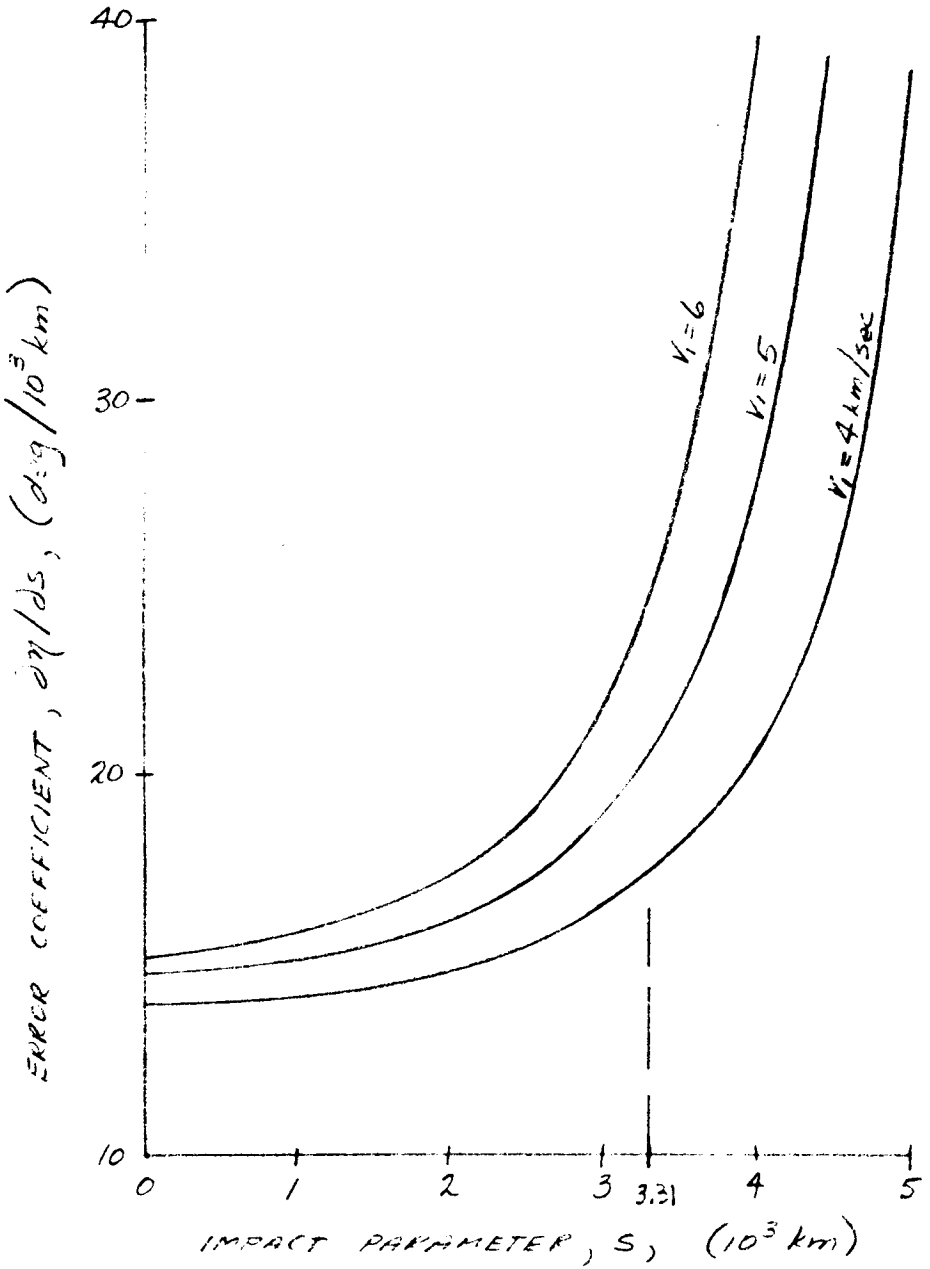

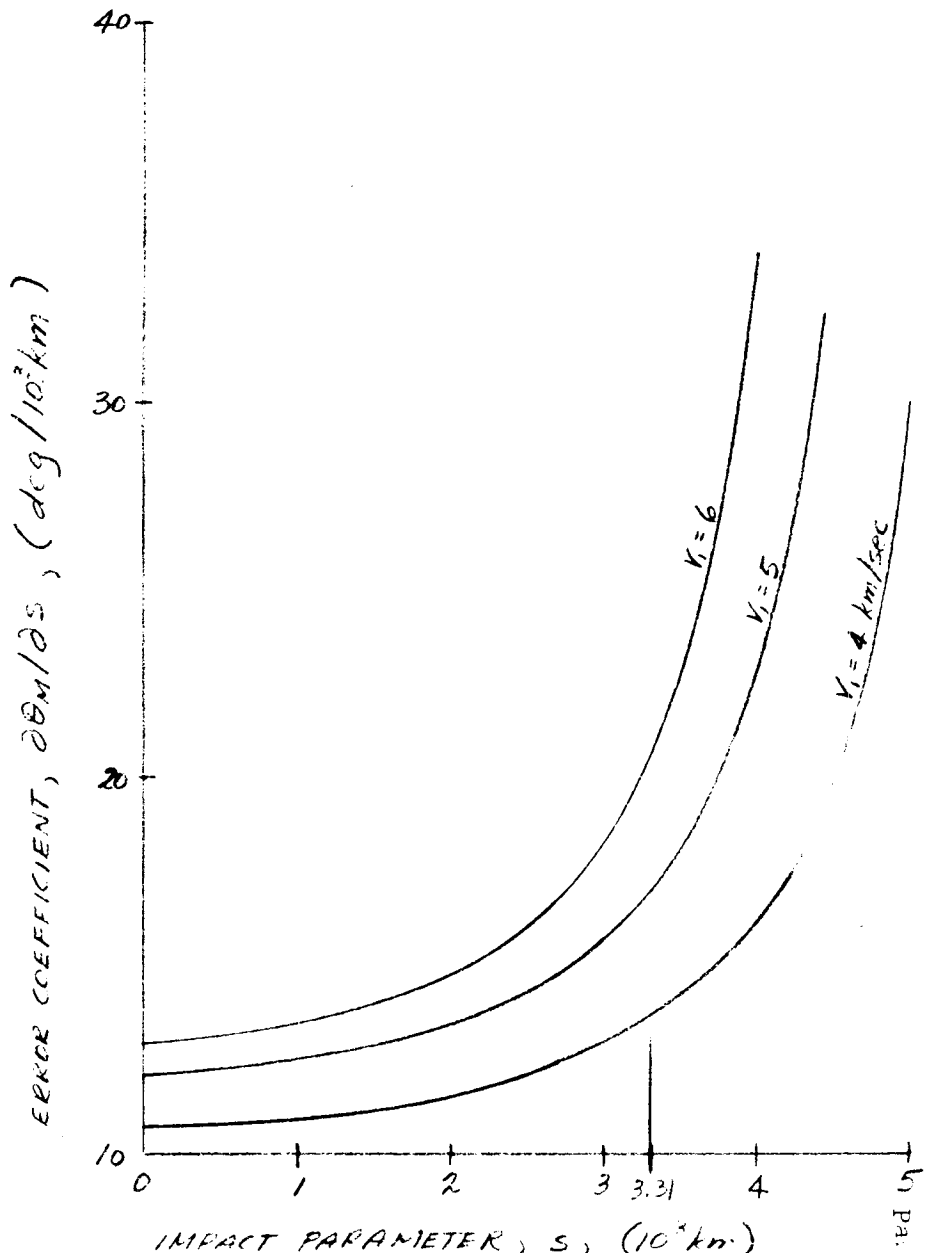

FIG. 7. $\partial L/\partial \gamma_2$ and $\partial \theta_M/\partial V_r$ as functions of s for 3 values of V_1

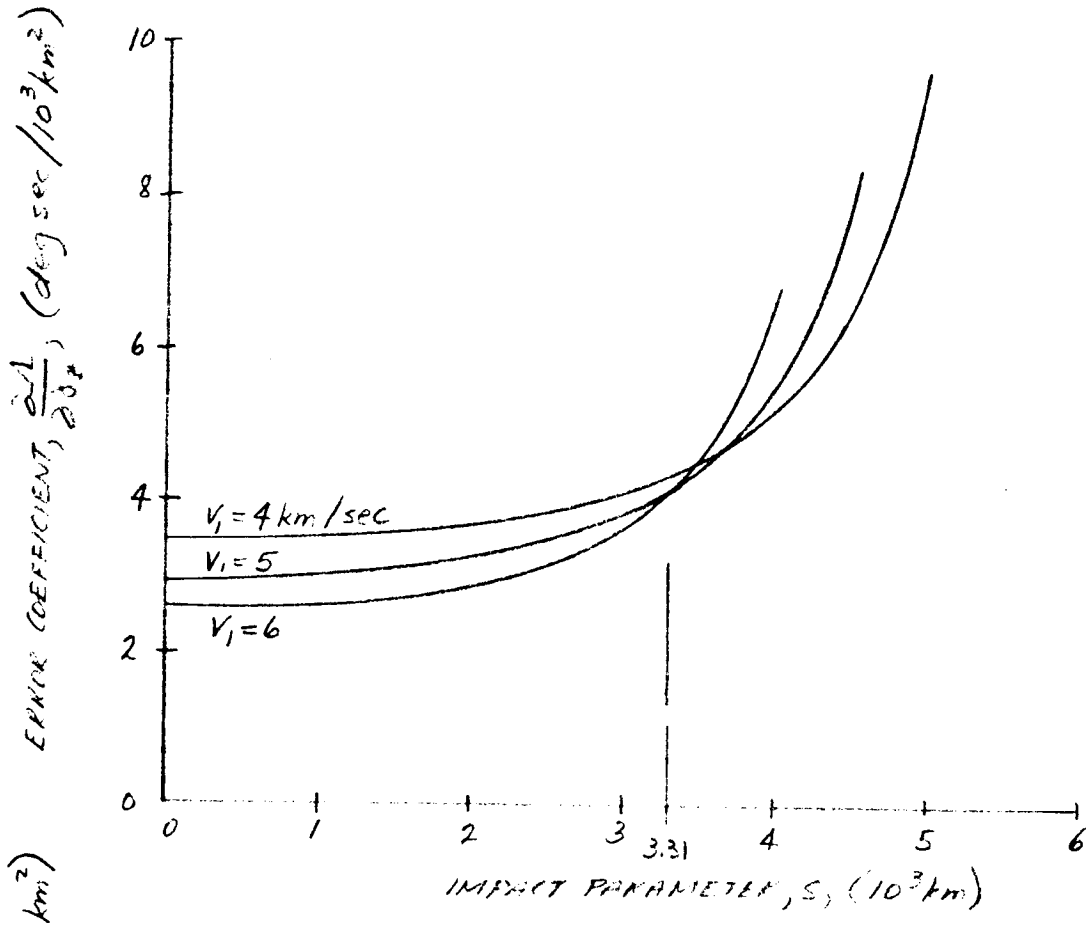

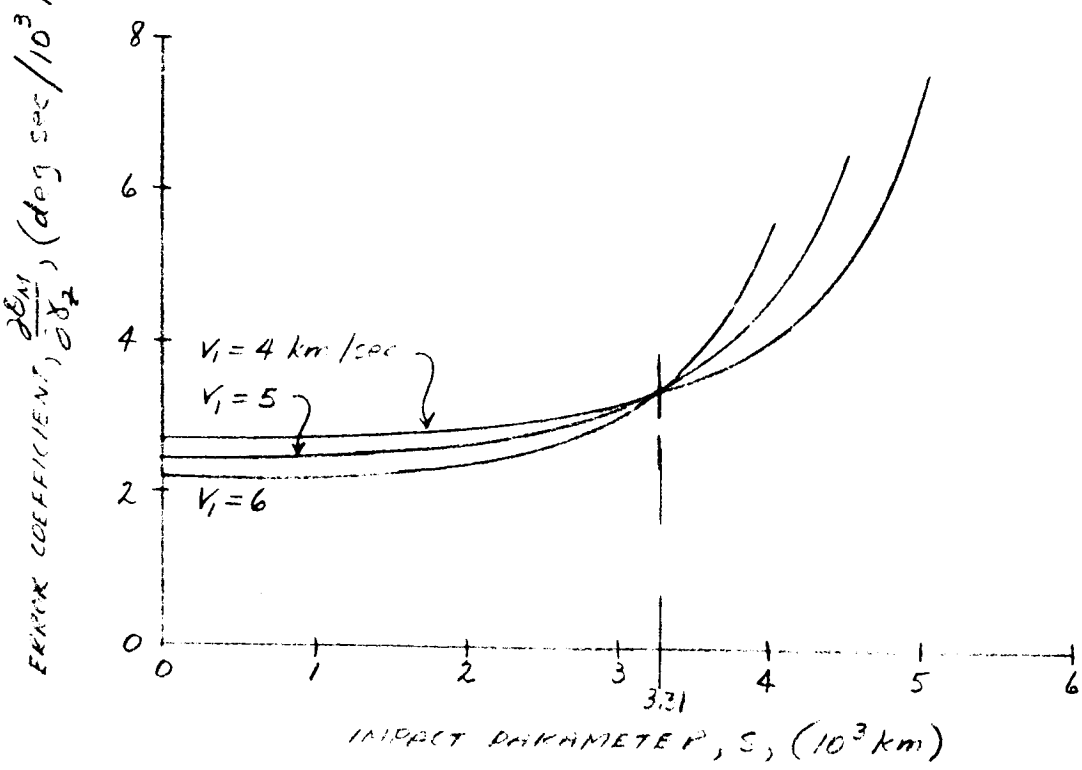

FIG. 8. Geometry for Errors Normal to the Nominal Impact Trajectory

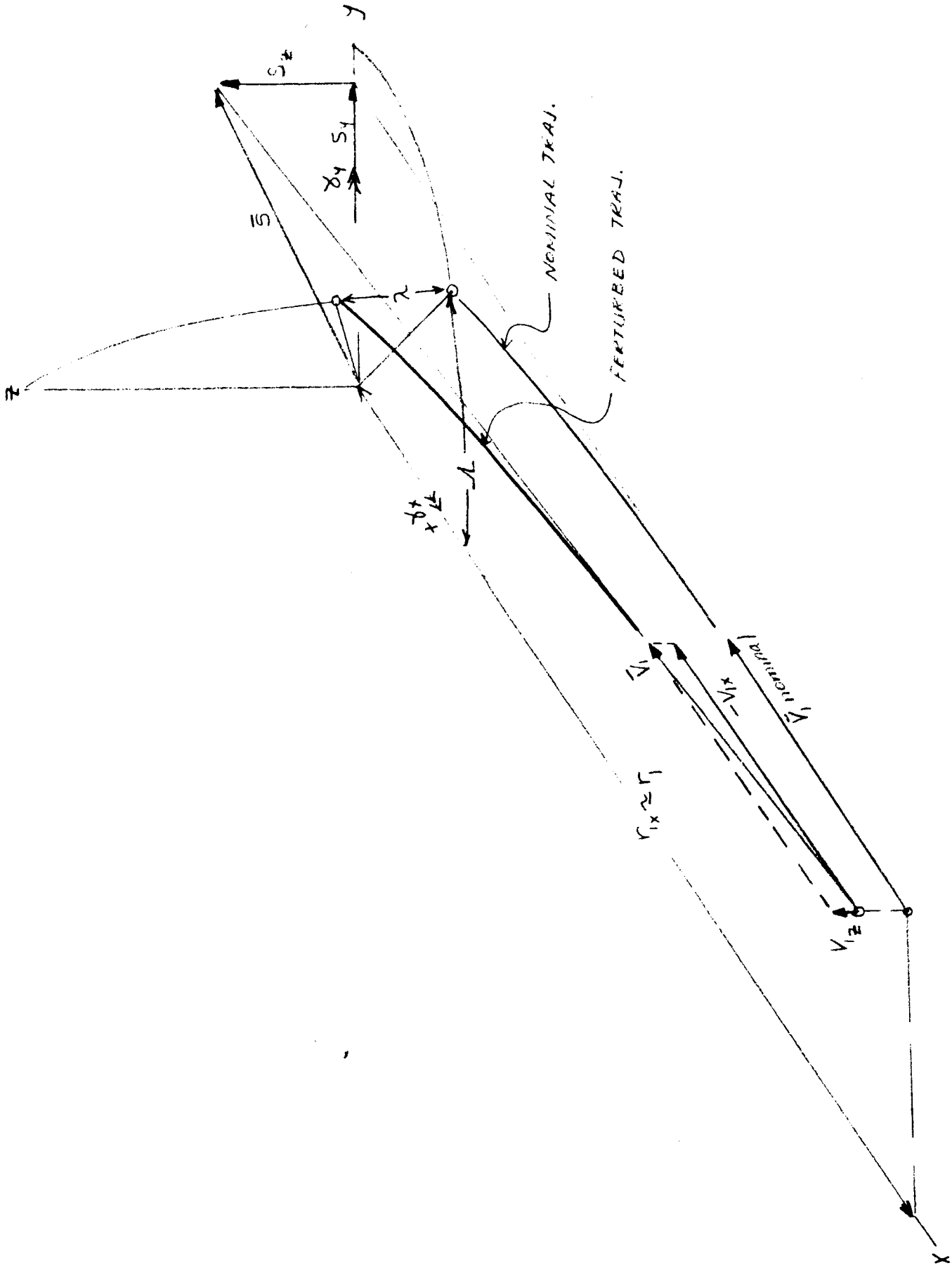

FIG. 9. $\frac{\partial\lambda}{\partial V_{1z}}$ and $\frac{\partial\lambda}{\partial S_z}$ as functions of s for 3 values of V_1

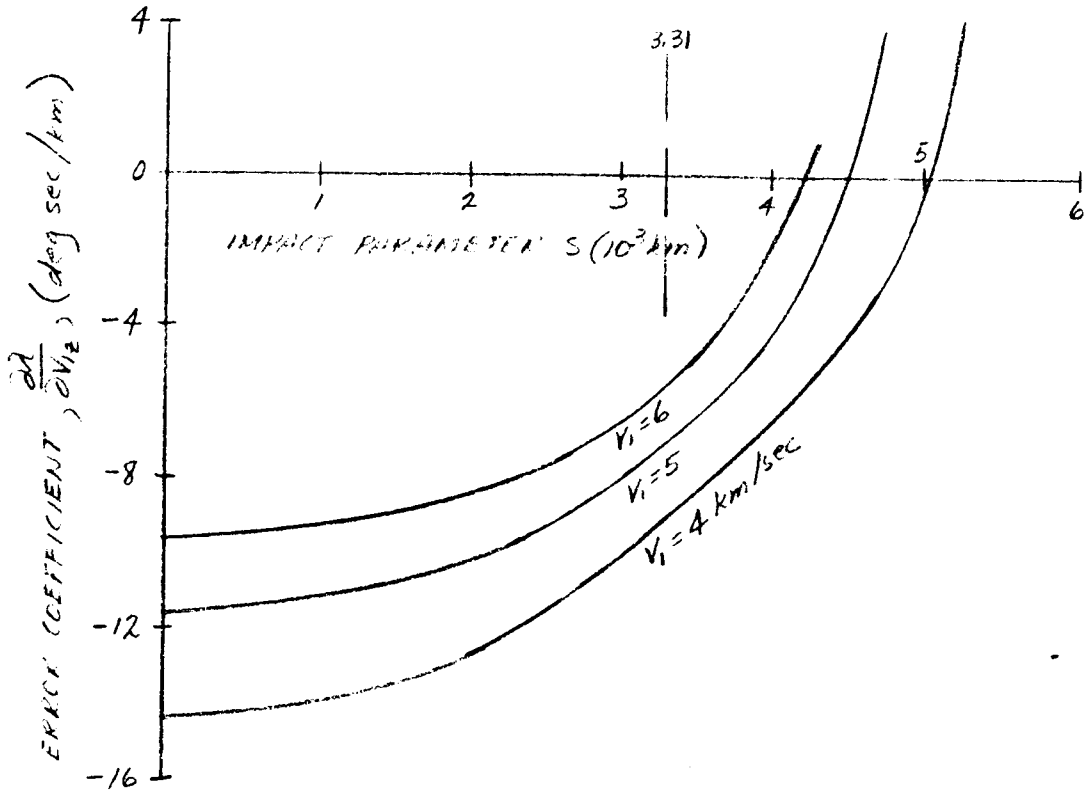

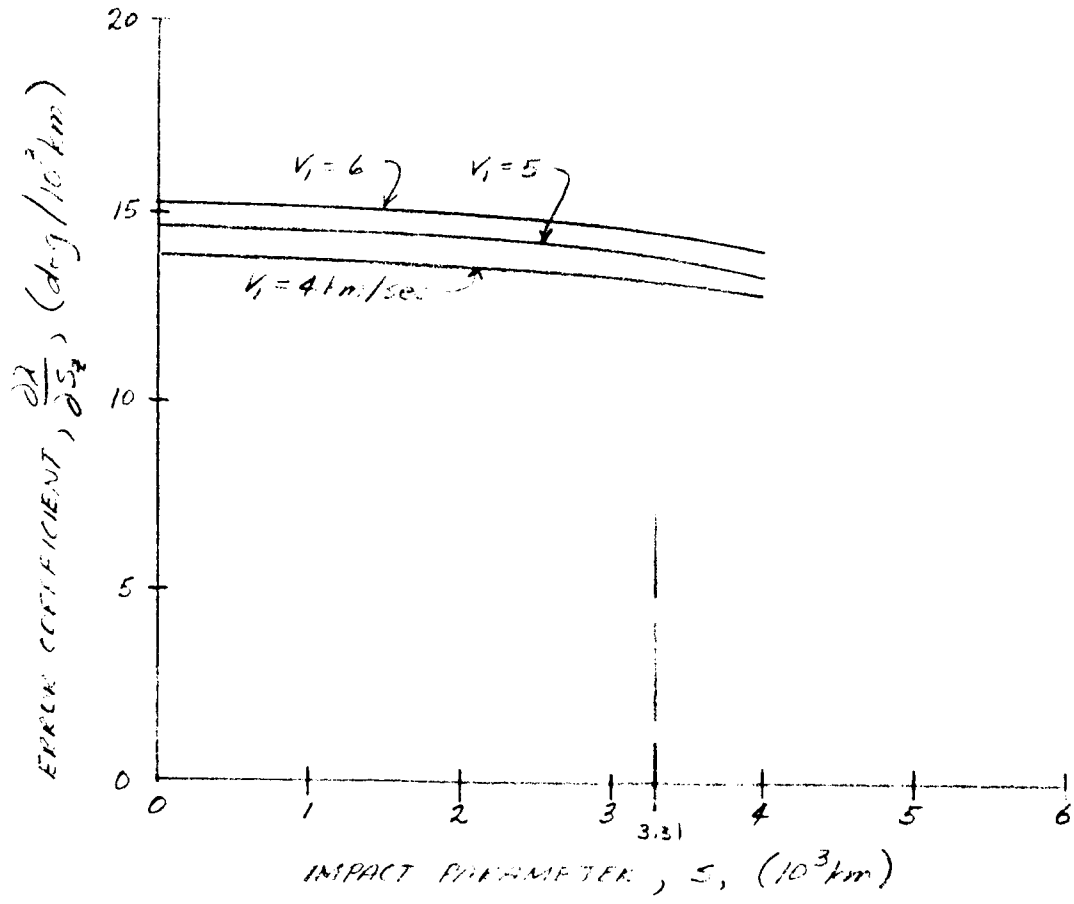

C. CRITERIA FOR THE SELECTION OF NOMINAL TRAJECTORIES

1. The Approach Trajectory Prior to Separation

We have assumed that the combined spacecraft and capsule are on a Mars "fly-by" trajectory prior to separation and that an impulse is imparted to the capsule after separation to achieve capsule impact. This scheme differs from the one proposed by Gates (Ref. 3) of JPL wherein the combined vehicles are initially on an impact trajectory and an impulse is imparted to the bus after separation to achieve a fly-by trajectory. It should be pointed out that the selection of nominal impact trajectories can be made independent of the above consideration.

We have already pointed out that the expected angle Λ_s between the spacecraft approach velocity vector $\bar{v}_A$ and the Sun-Mars line is between 20 and 40 degrees. First, let us consider the bus fly-by trajectory. The question arises whether the bus should intersect the Martian orbit before or after the planet (see Fig. 10). Presumably pictures will be taken from the

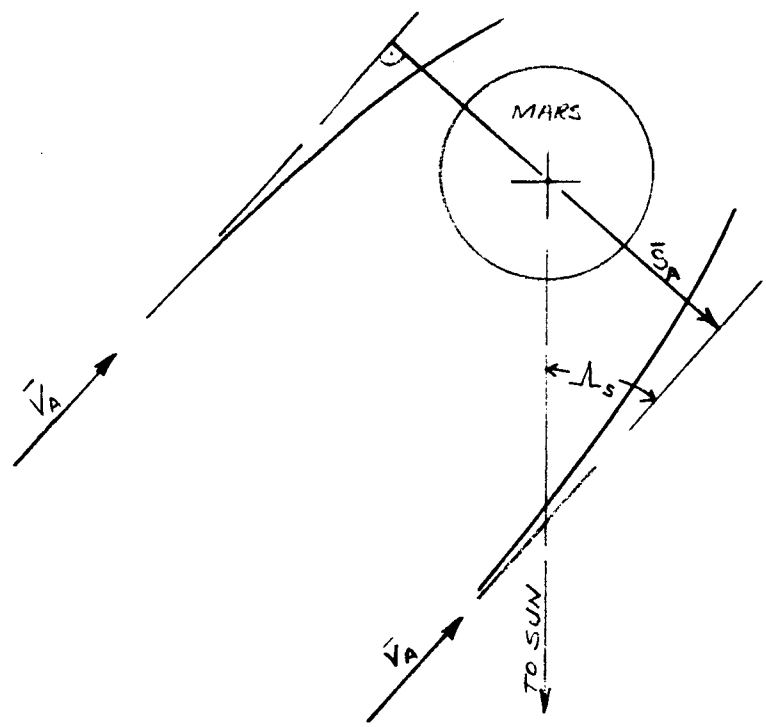

Fig. 10 Fly-By Trajectories Viewed from the North Ecliptic Pole

bus as it passes near Mars. Since Λ_s is expected to be positive, the surface of Mars adjacent to a trajectory which passes behind Mars will be better illuminated than the surface adjacent to a trajectory which passes ahead of Mars.

If the capsule is to transmit to the spacecraft after impact, we have another reason for selecting a fly-by trajectory which passes behind Mars; namely, the capsule (on the surface of Mars) will rotate "towards" the spacecraft. Gates (Ref. 3) shows that the capsule-bus communication link will be interrupted for a period on the order of two hours and will subsequently be open again for more than twelve hours.

On the basis of the above two considerations, we recommend that only fly-by trajectories which pass behind Mars be investigated.

2. Three Sets of Nominal Impact Trajectories

Three criteria for selecting nominal capsule impact trajectories have been studied in detail:

a) $\phi_s = 30^\circ$, b) $\phi_s = 0^\circ$ c) $s = 0$

The angle ϕ_s is measured counterclockwise from the Mars-Sun line to the local vertical at impact. Trajectories typical of each of the three requirements are sketched in Fig. 11. All are assumed to be launched from a bus, fly-by trajectory which passes behind Mars.

The three sets of nominal trajectories are evaluated and compared on the following factors; illumination of the Martian surface, bus-capsule communication link, atmospheric penetration, propulsion requirements and error sensitivity.

3. Illumination Requirements

The angle ϕ_s is significant from the viewpoint of illumination. Picture taking from the capsule may be divided into two distinct regions; from a distance of approximately 10^4 km from Mars up to atmospheric entry, and during atmospheric penetration.

Illumination of the surface during the first region should be adequate for nearly all trajectories which impact on Mars for the reason that Λ_s is not expected to approach 90 degrees (the unlikely case of a Hohmann transfer). Thus ϕ_s is not particularly critical for this region of picture taking.

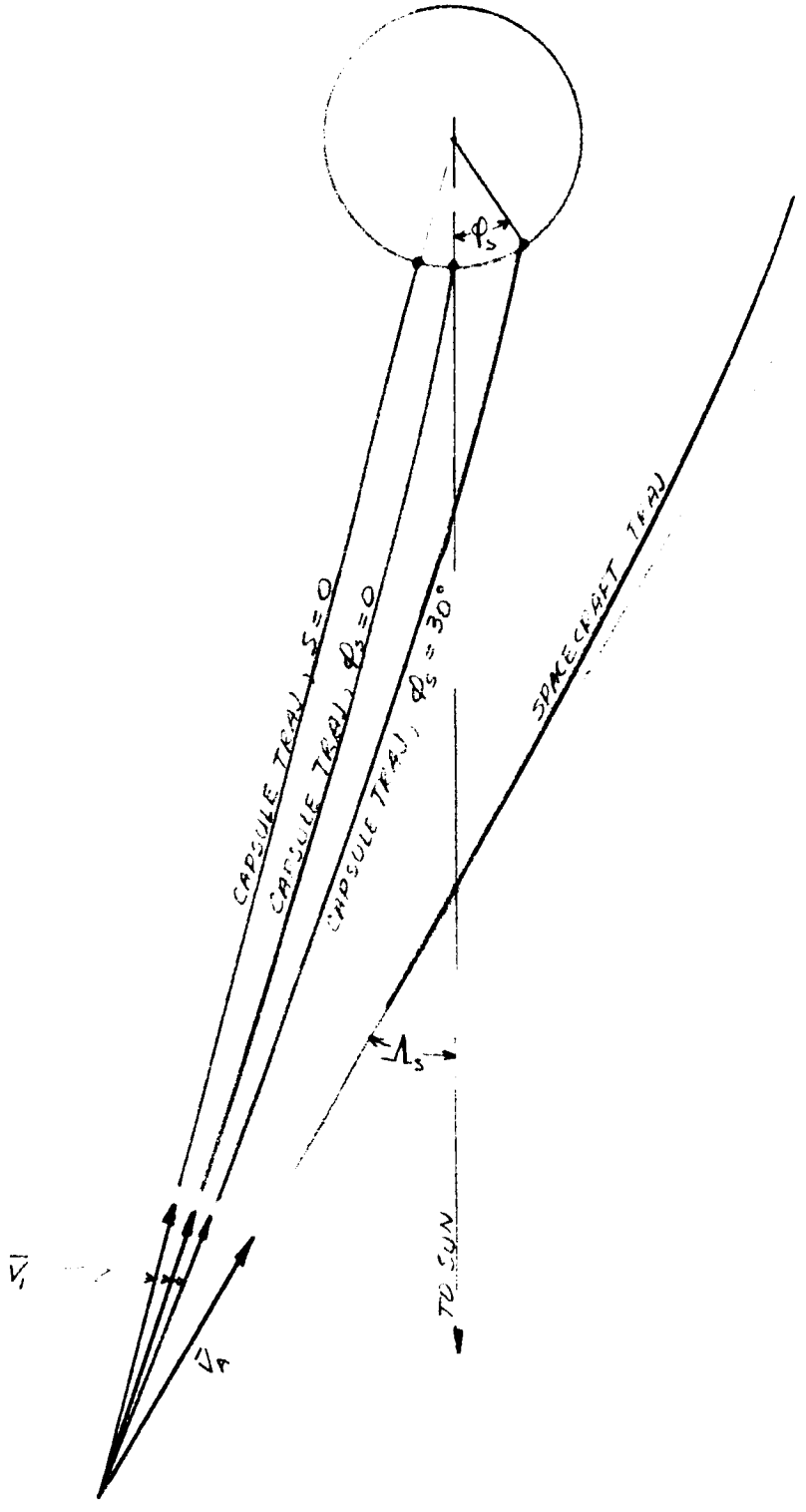

FIG. 11. Three Sets of Capsule Trajectories Viewed From North Ecliptic Pole

The final descent portion of the capsule trajectory through the atmosphere will be along the local vertical. The angle ϕ_s is significant because it is indicative of the illumination of the impact region. We have assumed that a 30 degree illumination angle ($\phi_s = \pm 30^o$) is ideal for taking pictures of the impact region.

The first set of nominal impact trajectories are designed to satisfy the nominal requirement $\phi_s = 30^o$, identically.

The second set of nominal trajectories ($\phi_s = 0^o$) all have direct sunlight on the impact site and the shadow contrast is not ideal. On the other hand deviations from the nominal impact site will improve the shadow contrast.

The third set (s = 0) of nominal trajectories are not linked directly to ϕ_s. However, since the angle between the $\bar{v}_1$ and $\bar{v}_A$ is small ($\sim$2 deg) we have the relation $\phi_s \simeq -\Lambda_s$. Whence, the expected range of ϕ_s for these trajectories will lie between -20 and -40 degrees.

4. <u>Bus-Capsule Communication Line of Sight</u>

We assume that the capsule will transmit to the spacecraft rather than to the earth, directly. Hence, the angle ψ between the local vertical at impact and the capsule-bus line of sight vector $\bar{\rho}$ must not exceed 90 degrees and preferably be less than 80 degrees (see Fig. 12).

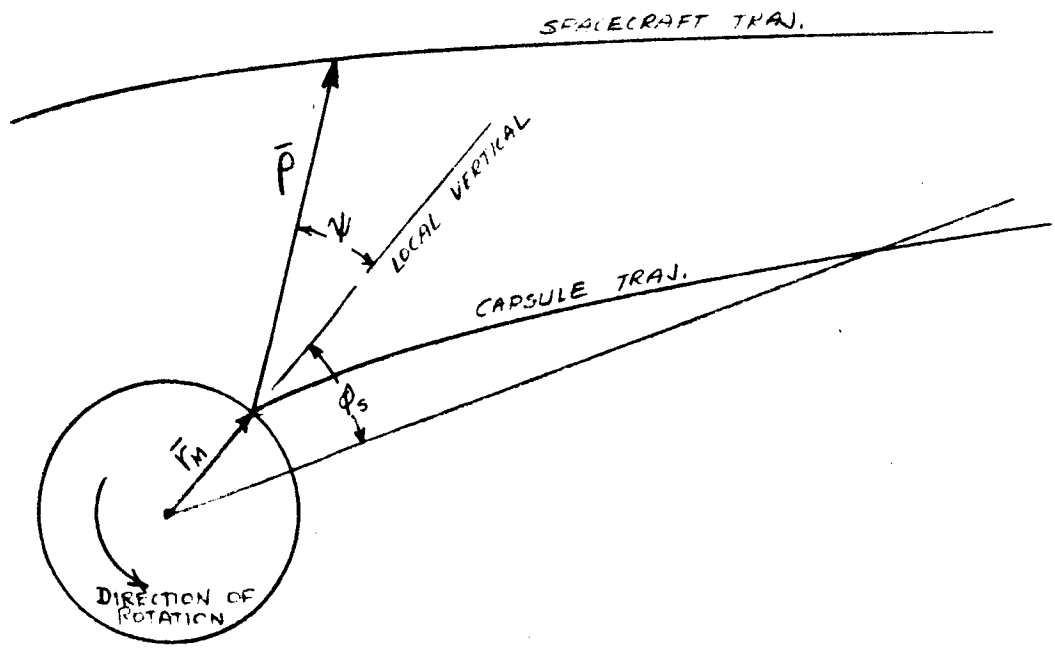

Fig. 12 Capsule to Bus Line of Sight Vector

Of the three sets of nominal trajectories, which we are considering, the maximum value of ψ is the largest ($\sim$75 deg) for the sets (s = 0), and the smallest ($\sim$ 55 deg) for the sets (ϕ_s = 30 deg). For all sets, the maximum value occurs when v_1 = 4 km/sec and h = 6000 km. The analytical development, upon which these conclusions are based, is presented in Appendix D.

Atmospheric effects were ignored in the above calculations. If we assume that, using a parachute, the total descent time through the atmosphere may be as long as 15 minutes, then the maximum values for ψ for the sets (s = 0) may approach 90 deg. On the basis of calculations made in Appendix E, we find that, if v_1 (for the capsule alone) is increased by .1 km/sec, the capsule time of flight will be

reduced by $\begin{Bmatrix} 14 \\ 20 \\ 30 \end{Bmatrix}$ minutes for $v_1 = \begin{Bmatrix} 6 \\ 5 \\ 4 \end{Bmatrix}$ km/sec.

The increase in $\bar{v}_1$, but not in $\bar{v}_A$, may be accomplished by pointing $\bar{v}_C$ slightly towards Mars for the sets (s = 0). This represents a small penalty in propulsion; however, it is a necessary maneuver to insure that $\bar{\rho}$ will not dip below the local horizon prior to impact.

If data is to be transmitted to the spacecraft after impact, as discussed by Gates (Ref. 3), then the set of nominal trajectories (ϕ_s = 30 deg) is preferable to the other two sets. The reason is that the time interval for which $\bar{\rho}$ is below the horizon is a minimum for this set.

5. Atmospheric Penetration

The heat transfer problem associated with the penetration of the Martian atmosphere is not expected to be as critical as the corresponding problem associated with the penetration of the atmosphere of the earth. Nevertheless, the relations between peak heating rate and entry angle θ_M, and total heat absorbed and θ_M should be considered when selecting nominal trajectories.

In general the peak heating rate will be a maximum when $\theta_M = 0$ (vertical entry) and the total heat load will be a maximum for grazing trajectories. On the basis of heat transfer considerations alone, a vertical entry would probably be preferred.

Note that θ_M is the velocity angle at impact and only approximately represents the atmospheric entry angle.

The third set (s = 0) of nominal trajectories are characterized by $\theta_M = 0$.

The range of expected values for θ_M for the first two sets of nominal trajectories (ϕ_s = 30 and 0°) may be obtained from the following approximate relations

$$\eta \simeq \Lambda_s + \phi_s$$

and

$$\theta_M \simeq \frac{\Delta\theta_M}{\Delta\eta}(\Lambda_s + \phi_s)$$

Here we have made use of the approximate linearity between θ_M and η, and the fact that the angle between $\bar{v}_A$ and $\bar{v}_1$ is relatively small. The values may be obtained from Appendix B. Using the above relations we obtain

$$39^o \leq \theta_M \leq 60^o \qquad \text{when } \phi_s = 30^o$$

$$15^o \leq \theta_M \leq 34^o \qquad \text{when } \phi_s = 0^o$$

for the range $20^o \leq \Lambda_s \leq 40^o$. It is of interest to note that the range of θ_M studied by Gates (Ref. 3) was between 40 and 60 degrees.

The range of atmospheric entry velocities (approximately equal to the impact velocities v_M) is between 6.5 and 7.9 km/sec for all three sets of nominal trajectories.

6. Propulsion Requirements

For each of the three sets of nominal trajectories the largest required velocity change v_C arises when both v_A and h are the maximum expected values; 6 km/sec and 10^4 km, respectively. For the first two sets of nominal trajectories ($\phi_s = 30^o$ and 0°), v_C is also a function of Λ_s. v_C is maximized by selecting the minimum expected value for Λ_s.

For the nominal trajectories (s = 0) we have

$$v_C r_1 = v_1 s_A(v_1, h)$$

For the nominal trajectories ($\phi_s = 30^o$ and 0°)

$$v_C r_1 = v_1\left[s_A(v_1, h) - s(\Lambda_s, \phi_s)\right]$$

where

$s = s\ (\Lambda_s, \phi_s)$ is plotted in Fig. 13.

$$s_A = \sqrt{(r_M + h)^2 + \frac{2\mu_M (r_M + h)}{v_1^2}}$$

r_M is the radius of Mars

μ_M is the product of the universal constant of gravitation and the mass of Mars

Taking $r_1 = 3.2 \times 10^5$ km we obtain the following maximum values for v_C:

$v_C = .215$ km/sec for $\phi_s = 30$ deg

$v_C = .247$ km/sec for $\phi_s = 0$ deg

$v_C = .258$ km/sec for $s = 0$

In order to insure that the line of sight between the capsule and the bus does not fall below the horizon during a "slow" penetration of the Martian atmosphere, it was suggested that the vector $\bar{v}_C$ be pointed slightly towards Mars for the cases when s = 0. It was shown that, if the component of $\bar{v}_C$ along $\bar{v}_1$ were .1 km/sec, the time of flight could be decreased by at least 14 minutes. This reduction in flight time of the capsule is enough to insure that the capsule-bus communication link is not broken prior to impact. Thus for the sets of nominal trajectories (s = 0)

$$v_C(\text{total}) = \sqrt{(.258)^2 + (.1)^2} = .277 \text{ km/sec}$$

7. Error Sensitivity

The impact parameter s is the critical quantity when comparing the error sensitivity of the three sets of nominal trajectories. Normal impacts are defined by s = 0 and are expected to be the least sensitive to errors. The range of expected values for s for the first two sets of nominal trajectories may be determined from Fig. 13. The relation between Λ_s and s is given by

$$\Lambda_s = \eta(v_1, s) - \phi_s + \frac{v_c}{v_1} \simeq \eta(v_1, s) - \phi_s$$

FIG. 13. s as a function of Λ_s for $\phi_s = 30$ and 0 deg.

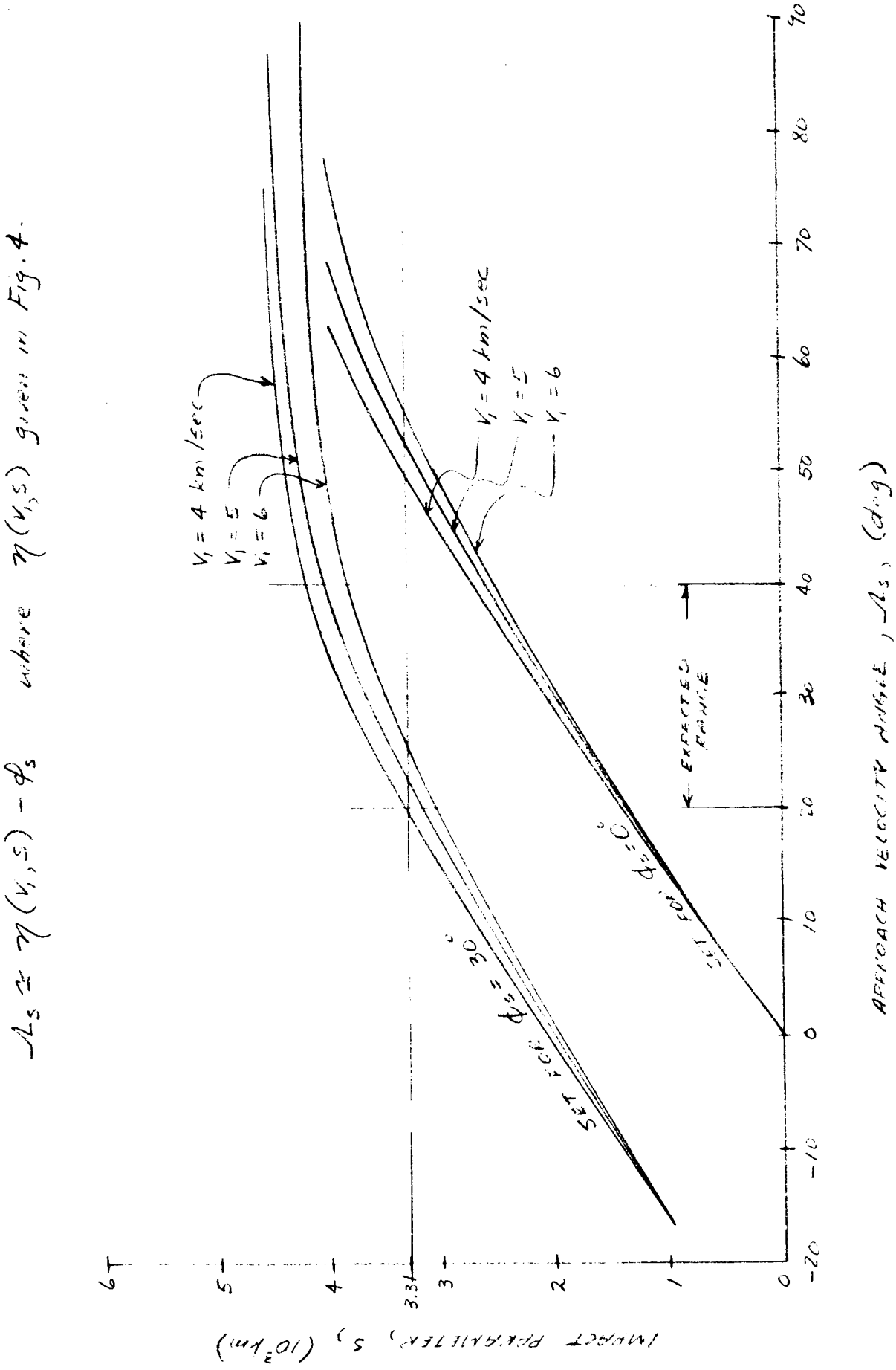

where $\eta(v_1, s)$ is given in Fig. 4. From Fig. 13 the expected ranges for s for the two sets $\phi_s = 30^\circ$ and 0° are given by:

$$\left.\begin{array}{lll} 3.05 \leq s(10^3 \text{ km}) \leq 4.20 & \text{when} & \phi_s = 30^\circ \\ 1.35 \leq s(10^3 \text{ km}) \leq 2.70 & \text{when} & \phi_s = 0^\circ \end{array}\right\} \text{ for } 20^\circ \leq \Lambda_s \leq 40^\circ$$

The maximum (positive or negative) expected values for all of the error coefficients are tabulated in Table 1 for the three sets of nominal trajectories.

8. Summary Comparison of Nominal Trajectories

The essential characteristics of the three sets of nominal trajectories are summarized and compared in Table 2.

TABLE 1. Maximum Expected Error Coefficients

ERROR COEFFICIENT SYMBOL AND DIMENSIONS	CRITERIA FOR NOMINAL TRAJ.		
	$\phi_s = 30°$	$\phi_s = 0°$	$s = 0$
$\frac{\partial V_M}{\partial V_1}$, nondimensional	.78	.78	.78
$\frac{\partial \theta_M}{\partial V_1}$, deg sec / km	11.1	5.1	0
$\frac{\partial \theta_M}{\partial s}$, deg / 10^3 km	> 34	16.7	13.0
$\frac{\partial \eta}{\partial V_1}$, deg sec / km	14.0	6.6	0
$\frac{\partial \eta}{\partial s}$, deg / 10^3 km	> 40	20.0	15.2
$\frac{\partial \theta_M}{\partial \gamma_z}$, deg sec / 10^3 km^2	> 6	3.1	2.7
$\frac{\partial \Lambda}{\partial \gamma_z}$, deg sec / 10^3 km^2	$\simeq 8$	4.0	3.5
$\frac{\partial \lambda}{\partial V_{1z}}$, deg sec / km	−5.6	−10.8	−14.4
$\frac{\partial \lambda}{\partial s_z}$, deg / 10^3 km	14.0	14.7	15.2
$\frac{\partial \lambda}{\partial \gamma_y}$, deg sec / 10^3 km^2	−3.3	−3.4	−3.5

Maximum values for $\phi_s = 30°$ based on $s = 4.2$
Maximum values for $\phi_s = 0°$ based on $s = 2.7$

ITEM OF COMPARISON	NOMINAL SETS OF TRAJECTORIES		
	$\phi_s = 30$ deg	$\phi_s = 0$ deg	$s = 0$
Impact Parameter, s	$3.05 \leq s(10^3 \text{ km}) \leq 4.20$	$1.35 \leq s(10^3 \text{ km}) \leq 2.70$	$s = 0$
Illumination of impact site. Angle between local vertical and Mars-Sun line at impact	30 deg	0 deg	Between -20 and -40 deg
Capsule-to-bus communication link prior to impact. Angle ψ between $\bar{\rho}$ and $\bar{r}_M$	No problem: $\psi < 90$ deg	No problem: $\psi < 90$ deg	$\bar{v}_C$ must be pointed slightly towards Mars to insure $\psi < 90$ deg
Communication to bus after impact	Shortest period of interruption		Longest period of interruption
Atmospheric entry angle, θ_M and heating problems	$39 \leq \theta_M \leq 60$ deg Highest heat load	$15 \leq \theta_M \leq 34$ deg compromise	$\theta_M = 0$ deg Peak heat rate
Propulsion requirements characterized by v_C (maximum values)	.215 km/sec	.247 km/sec	.277 km/sec with components .1 km/sec along $\bar{v}_1$ and .258 km/sec perpendicular to $\bar{v}_1$.
Error Sensitivity (See Table 1)	Out-of-plane errors approximately the same for all three sets		
	Very sensitive to in-plane errors	Moderately sensitive to in-plane errors	Least sensitive to in-plane errors

Table 2 Summary Comparison of Nominal Sets of Trajectories

REFERENCES

1. JPL Research Summary No. 36-6, Vol. 1, Dec. 15, 1960, pp 4-5.

2. JPL Research Summary No. 37-10, Vol. 1, August 1, 1961, pp 39-40.

3. Gates, C. R., "A Description of a Mars Spacecraft with a Landing Capsule", presented at the National IAS-ARS joint meeting in Los Angeles, Calif., June, 1961.

4. Plummer, An Introductory Treatise on Dynamical Astronomy, Dover.

APPENDIX A

(by E. Onstead)

Expected Values for Λ_s

The essential characteristics of an Earth to Mars trajectory are defined by the geocentric energy (the energy of the spacecraft immediately after injection taken with respect to the mass center of the earth) and the launch date. Most of the critical parameters for low geocentric energies and launch dates in November and December of 1964 are presented in Fig. 1 of Ref. 1. The asymptotic approach velocity $\bar{v}_A$ is the vector difference between the heliocentric velocity $\bar{u}$ of the spacecraft and the heliocentric velocity $\bar{w}$ of Mars (see sketch). The magnitude of $\bar{v}_A$ as a

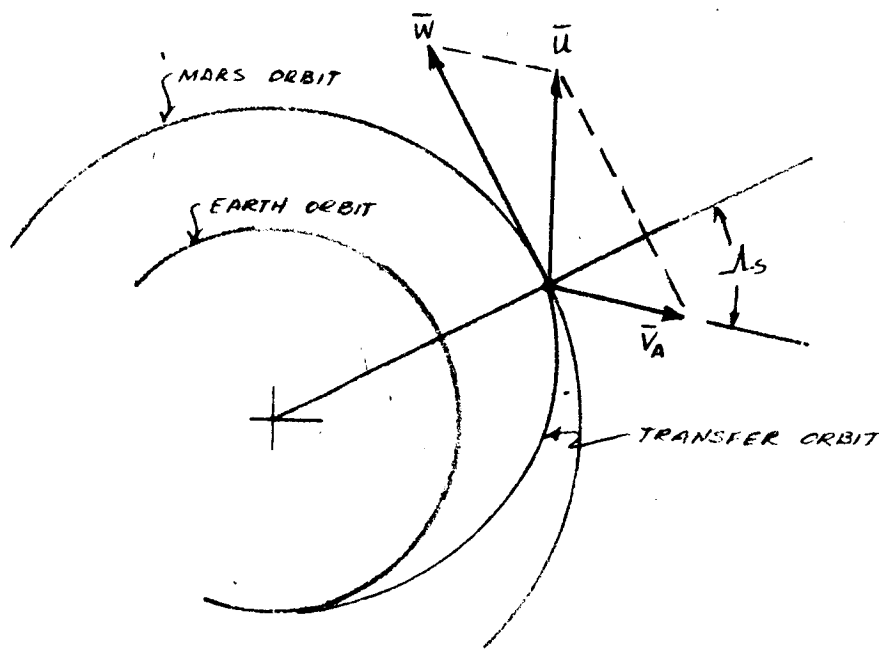

function of the geocentric energy and the launch date is given in Ref. 1; however, the angle Λ_s between $\bar{v}_A$ and the Sun-Mars line is not given.

Using the data given in Ref. 1 and taking the eccentricity of the Martian orbit into consideration, we were able to determine Λ_s as a function of the geocentric energy and the launch date (see accompanying graph). The curves were generated as follows. First the date of intercept was determined for a given geocentric energy and launch date by adding the time of flight (from Fig. 1 of Ref. 1) to the launch date. Using a standard ephemeris, the Mars-Sun distance was determined for the date of intercept. The corresponding orbit velocity $\bar{w}$ of Mars was obtained from the energy integral. Next, the velocity of the spacecraft relative to the earth was added to the heliocentric velocity of the earth to obtain the heliocentric velocity of the spacecraft in the vicinity of the earth. Using the energy integral we could calculate $\bar{u}$. Knowing v_A, w and u, and using the cosine law we were able to find Λ_s. The inclination of the plane of the transfer orbit to the plane of the ecliptic was not taken into consideration.

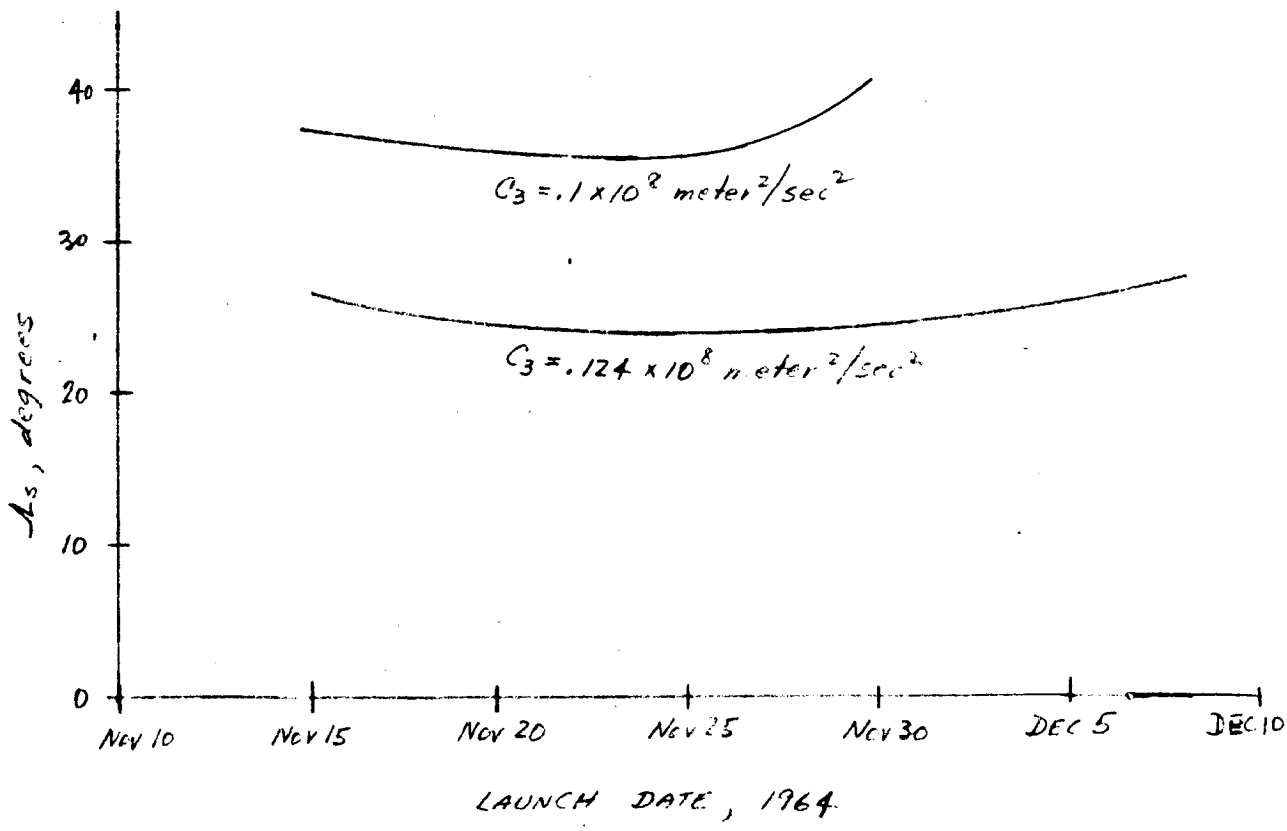

APPENDIX B

Motion in the Plane of $\bar{v}_1$ and $\bar{s}$

1. Notation and Geometry

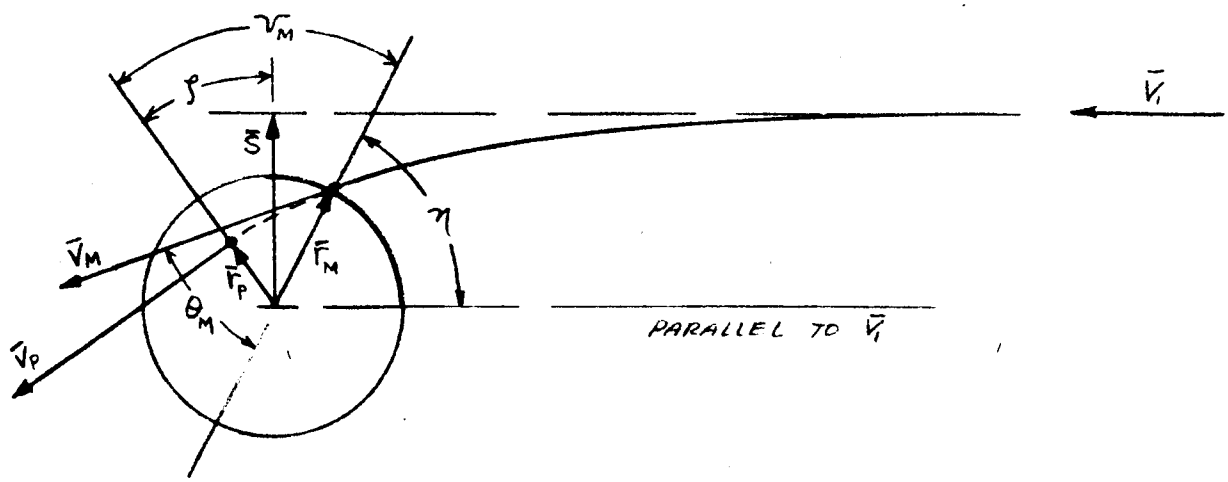

v_1 - asymptotic approach velocity

v_M - impact velocity

v_P - velocity at the perifocus

s - impact parameter

r_M - radius vector of the point of impact (3310 km)

r_P - radius vector of the perifocus

θ_M - angle between $\bar{v}_M$ and $-\bar{r}_M$

η - angle between $-\bar{v}_1$ and $\bar{r}_M$

ρ - true anomaly of $\bar{s}$

ν_M - true anomaly of $\bar{r}_M$

μ_M - produce of the universal constant of gravitation and the mass of Mars ($\mu_M = 4.29 \times 10^4$ km^3/sec^2)

2. Relation Between v_M and v_1

The magnitude of $\bar{v}_M$ is uniquely determined by the magnitude of $\bar{v}_1$ through the energy equation:

$$V_M = \sqrt{V_1^2 + \frac{2\mu_M}{r_M}} \tag{1}$$

Here we have assumed that the potential energy at the initial point is zero. For small variations in v_1 we have

$$\frac{\partial V_M}{\partial V_1} = \left(1 + \frac{2\mu_M}{V_1^2 r_M}\right) = \frac{V_1}{V_M} \tag{2}$$

3. The Dependence of θ_M Upon v_1 and s

The angular momentum of the capsule (we assume a unit mass) about an axis through the mass center of Mars and normal to $\bar{v}_1$ and $\bar{s}$ is a constant equal to $v_1 s$. Whence,

$$\theta_M = \sin^{-1}\left(\frac{V_1 S}{V_M r_M}\right) \tag{3}$$

For small variations in v_1 and s (we must remember that v_M is functionally dependent upon v_1) we have

$$\frac{\partial \theta_M}{\partial V_1} = \frac{1}{V_1}\left(1 - \frac{V_1^2}{V_M^2}\right)\left[\left(\frac{V_M r_M}{V_1 S}\right)^2 - 1\right]^{-1/2} \tag{4}$$

$$\frac{\partial \theta_M}{\partial S} = \frac{1}{S}\left[\left(\frac{V_M r_M}{V_1 S}\right)^2 - 1\right]^{-1/2} \tag{5}$$

4. The Dependence of η Upon v_1 and s

Using the energy and momentum integrals, we may express v_P in terms of v_1 and s:

$$V_P = \frac{\mu_M}{V_1 S}\left[1 + \sqrt{1 + \left(\frac{V_1^2 S}{\mu_M}\right)}\right]$$

The eccentricity e and the semi-major axis a of the impact hyperbola are given by

$$e = \frac{v_1^3 s}{\mu_M v_p} + 1, \qquad a = \frac{\mu_M}{v_1^2}$$

The angle ρ is equal to one-half of the "scattering" angle between the incoming and outgoing asymptotes of the hyperbola. Thus

$$\rho = \sin^{-1}\left(\frac{1}{e}\right)$$

The true anomaly ν_M of $\bar{r}_M$ is obtained from the parametric equation of the hyperbola:

$$\nu_M = \cos^{-1}\left\{\frac{1}{e}\left[\frac{a(e^2-1)}{r_M} - 1\right]\right\}$$

Finally,

$$\eta = \frac{\pi}{2} + \rho - \nu_M \tag{6}$$

Observe that, when ν_M is zero, the hyperbola is tangent to the surface of Mars.

When η is plotted against θ_M a surprising result is obtained; η appears to vary linearly with θ_M. The slopes $\Delta\eta / \Delta\theta_M$ are independent of s and vary with v_1:

$$\frac{\Delta\eta}{\Delta\theta_M} \simeq \begin{cases} 1.29 & \text{for } v_1 = 4 \text{ km/sec} \\ 1.21 & \text{" } v_1 = 5 \text{ km/sec} \\ 1.17 & \text{" } v_1 = 6 \text{ km/sec} \end{cases}$$

η is zero when θ_M is zero. The linearity is only approximate. One can show that

$$\frac{d\eta}{d\theta_M} = 2\left(\frac{v^2}{v^2 - v_1^2}\right)$$

where v is the instantaneous velocity along the path. Using an average value for v one can rationalize that $\Delta\eta / \Delta\theta_M$ will approach 2 as v_1 approaches zero and $\Delta\eta / \Delta\theta_M$ will approach 1 as v_1 approaches infinity.

The approximate linearity, which was established emperically, can be used to obtain error coefficients for $\Delta\eta$ due to ΔV_1 and ΔS :

$$\frac{\partial \eta}{\partial V_1} \simeq \frac{\Delta \eta}{\Delta \theta_M} \frac{\partial \theta_M}{\partial V_1} \tag{7}$$

$$\frac{\partial \eta}{\partial S} \simeq \frac{\Delta \eta}{\Delta \theta_M} \frac{\partial \theta_M}{\partial S} \tag{8}$$

APPENDIX C

Error in the Magnitude of $\bar{v}_C$

An error Δv_C produces both an error in the velocity angle θ_M and in the angle coordinate Λ of the impact point (in the plane of the nominal impact trajectory). The geometry is shown below for a negative Δv_C.

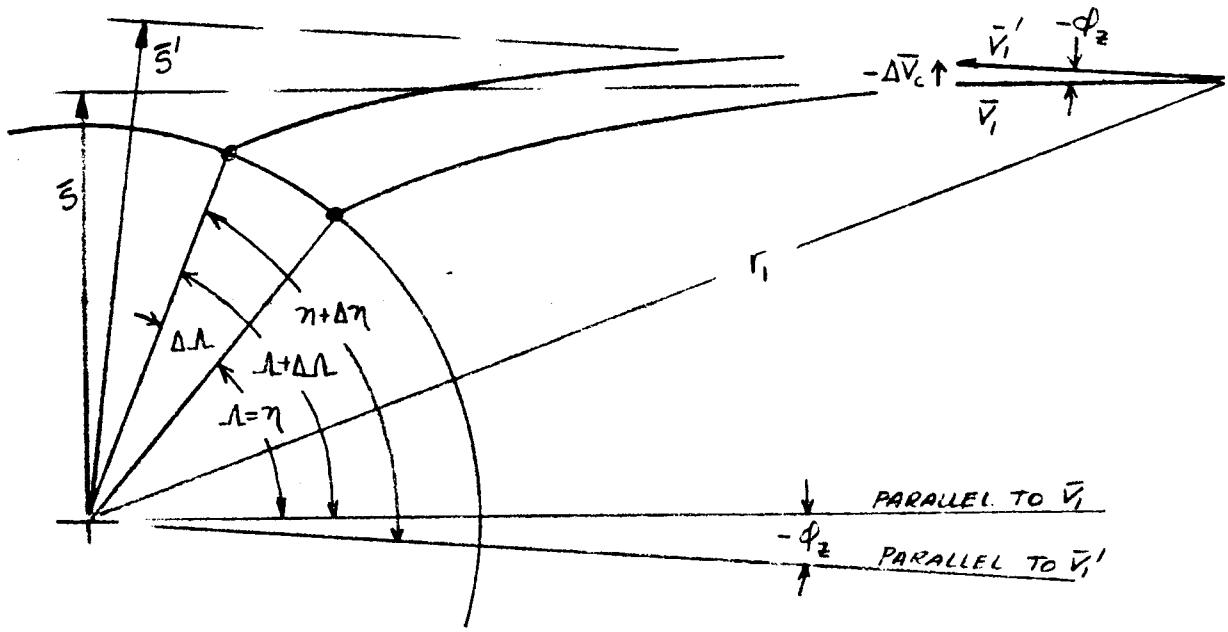

$\bar{v}_1'$ and $\bar{s}'$ refer to the perturbed values of $\bar{v}_1$ and $\bar{s}$. Note the distinction between Λ and η. From the above figure

$$\Delta\Lambda = \Delta\eta + \phi_z \simeq \frac{\partial\eta}{\partial s}\frac{\partial s}{\partial\gamma_z}\Delta\gamma_z$$

where

$$\gamma_z = -r_1 V_c, \qquad \Delta\gamma_z = \gamma_z\left(\frac{\Delta V_c}{V_c}\right) - V_c\,\Delta r_1$$

$$\frac{\partial s}{\partial\gamma_z} = \frac{1}{r_1}, \qquad \frac{\partial\eta}{\partial s} \text{ from Fig. 6.}$$

Similarly

$$\Delta\theta_M = \frac{\partial\theta_M}{\partial s}\frac{\partial s}{\partial \gamma_z}\Delta\gamma_z$$

where $\partial\theta_M/\partial s$ is given in Fig. 6.

APPENDIX D

(by E. W. Onstead and J. L. Arsenault)

Time and Position Relations at Impact

The problem, which we have considered, is to determine the angle γ between the local vertical and the capsule to bus line-of-sight vector $\bar{\rho}$ at impact. We have assumed that the approach velocity magnitude v_A of the spacecraft is equal to the approach velocity magnitude v_1 of the capsule. We proceeded as follows:

1. The difference in time between the events of "capsule at perifocus" and "spacecraft at perifocus" was determined by treating the capsule trajectory as a nominal path and the spacecraft trajectory as the perturbed path. The appropriate error coefficients were determined from Lambert's theorem for hyperbolic trajectories (Ref. 4).
2. The hypothetical time interval to travel between the impact point and the point of closest approach on the capsule trajectory was determined from Kepler's equation.
3. Again using Kepler's equation, the location of the bus on the perturbed trajectory was determined for the instant of capsule impact.

The determination of the error coefficients from Lambert's theorem (step 1) is the critical step. The time of flight from the initial point to the perifocus is given by

$$t_1 = \sqrt{\frac{a^3}{\mu_M}}\left[-(\alpha - \sinh\alpha) + (\beta - \sinh\beta)\right]$$

where

$$\sinh\frac{\alpha}{2} = \frac{1}{2}\sqrt{\frac{r_1 + r_2 + C}{a}}, \qquad \sinh\frac{\beta}{2} = \frac{1}{2}\sqrt{\frac{r_1 + r_2 - C}{a}}$$

where r_2 is the radius of perifocus. r_1, C and a are defined in Appendix E. Both r_2 and C are treated as variables.

Thus

$$\Delta t_1 = \sqrt{\frac{a^3}{\mu_M}} \Big[(\cosh\alpha - 1)(2a\sinh\alpha)^{-1}(\Delta r_2 + \Delta c)$$
$$- (\cosh\beta - 1)(2a\sinh\beta)^{-1}(\Delta r_2 - \Delta c) \Big]$$

However, ΔC is expected to be much less than Δr_2. Therefore,

$$\Delta t_1 = \sqrt{\frac{a^3}{\mu_M}} \left[\frac{\cosh\alpha - 1}{2a\sinh\alpha} - \frac{\cosh\beta - 1}{2a\sinh\beta} \right] \Delta r_2$$

The second partial of t_1 with respect to r_2 is identically zero.

APPENDIX E

Change in Transit Time Due to Δv_1

Let t_1 be the time interval between thrust termination (for v_C) and impact on the Martian surface. We will assume that the path of the particle is rectilinear, that is, s = 0. Then t_1 is given by Lambert's theorem for hyperbolic orbits (Ref. 4):

$$t_1 = \sqrt{\frac{a^3}{\mu_M}}\left[-(\alpha - \sinh\alpha) + (\beta - \sinh\beta)\right] \tag{1}$$

where

$$\sinh\frac{\alpha}{2} = \frac{1}{2}\sqrt{\frac{r_1 + r_M + c}{a}}, \qquad \sinh\frac{\beta}{2} = \frac{1}{2}\sqrt{\frac{r_1 + r_M - c}{a}}$$

r_1 is the distance from the center of Mars to the initial point
r_M is the distance from the center of Mars to the impact point
C is the distance between the initial point and the impact point

$$a = -\mu_M / v_1^2 \tag{2}$$

It is reasonable to set $r_M = 0$ since the hypothetical time of flight between the surface of Mars and the center of Mars is at least an order of magnitude less than t_1. With this simplification

$$c = r_1, \quad \sinh\frac{\alpha}{2} = \sqrt{\frac{r_1}{2a}}, \quad \alpha = 2\sinh^{-1}\sqrt{\frac{r_1}{2a}}$$

$$\sinh\alpha = 2\sinh\frac{\alpha}{2}\cosh\frac{\alpha}{2} = \frac{1}{a}\sqrt{r_1(2a + r_1)}$$

$$\sinh\frac{\beta}{2} = 0, \qquad \beta = 0$$

Thus, equation (1), reduces to

$$t = \sqrt{\frac{a^3}{\mu_M}}\left[-2\sinh^{-1}\sqrt{\frac{r_1}{2a}} + \frac{1}{a}\sqrt{r_1(2a+r_1)}\right.$$

$$= -2\sqrt{\frac{a^3}{\mu_M}}\sinh^{-1}\sqrt{\frac{r_1}{2a}} + \sqrt{\frac{r_1}{\mu_M}}\sqrt{a(2a+r_1)} \tag{3}$$

From equations (2) and (3) we have

$$\frac{\partial t}{\partial v_1} = \frac{\partial t}{\partial a}\frac{\partial a}{\partial v_1} \tag{4}$$

where

$$\frac{\partial t}{\partial a} = -3\sqrt{\frac{a}{\mu_M}}\sinh^{-1}\sqrt{\frac{r_1}{2a}} + \left(3a + \frac{r_1}{2}\right)\sqrt{\frac{r_1}{\mu_M a(2a+r_1)}} \tag{5}$$

$$\frac{\partial a}{\partial v_1} = -2\frac{\mu_M}{v_1^3} \tag{6}$$

APPENDIX C

ENTRY TRAJECTORIES

Ford Motor Company AERONUTRONIC DIVISION

Intra-Company Communication 24 October 1691

TO: J. Housego cc: Distribution

FROM: A. A. Gammal

SUBJECT: Mariner-B Capsule Entry Trajectories

I. INTRODUCTION

A study has been made to determine the effect of the ballistic parameter, m/C_DA (symbol list in appendix), and the various postulated Mars atmospheres on entry trajectory characteristics of the Mariner-B capsule. The intent of the study was to provide a basis for specifying an acceptable m/C_DA, or range of m/C_DA, and providing the trajectory information required for structural and thermodynamic design of the capsule and defining of the constraints within which the capsule experiments must be carried out.

Three of the five postulated model atmospheres presented in Reference 1, B, C, and E, were considered in this study, it being assumed that these three would impose the most stringent design requirements upon the capsule. The density and temperature variation with altitude of these three atmospheres is presented in Figures 1 and 2 respectively. The constants $\bar{\rho}_o$ and β used in the expression for density, $\rho = \bar{\rho}_o e^{-\beta h}$, are given in Table I, together with the speed of sound.

II. DESIGN m/C_DA

The first phase of the study attempted to determine the bounds upon design m/C_DA, the primary criterion being capsule flight duration from M = 1 down to impact (M = 1 being dictated by picture quality considerations). Though the duration required for adequate picture taking of Mars during the terminal portion of the entry trajectory was rather tenuous, the minimum feasible value was taken to be of the order of 100 seconds. Consideration was to be given to both a capsule that would survive the impact and one which need not.

A summary of pertinent trajectory information is presented in Table II for Atmosphere E, a nominal entry velocity of 22,000 ft/sec (at an altitude of 10^6 ft), entry angles of -20, -40, and -90°, and m/C_DA = 1, 2, 4. Variation of subsonic flight duration as a function of m/C_DA is presented in Figure 3. Choice of m/C_DA values was made on the basis of an assumed capsule weight of 250 pounds, possible packaging densities, and a relatively high drag configuration. It is to be noted that an entry angle of -10° did not allow direct impact, i.e., impact in less than one orbit about Mars.

It is apparent from Table II and Figure 3 that an m/C_DA of one for the basic capsule would yield approximately the desired subsonic flight duration for the worst possible entry angle condition, however, m/C_DA cannot be much greater than one if no auxiliary drag device, such as a parachute, is used. Even if a parachute is used, m/C_DA still cannot much exceed one, for with M = 1 occurring at 52,000 ft for $m/C_DA = 1$ but only 11,000 ft for $m/C_DA = 2$ (entry angle = -90°), a subsonic parachute may be deployed at a reasonable altitude only if m/C_DA is not much greater than one. A supersonic parachute would involve added complexities over those of a subsonic chute, including that of weight.

For the capsule that must survive impact, an $m/C_DA = 1$ yields a reasonable impact speed of 312 ft/sec. It should be noted, however, that the values presented involve a certain degree of approximation in that the trajectory computations assumed constant mass and constant C_D throughout entry.

Capsule size considerations and mating of the capsule to the spacecraft indicate that m/C_DA cannot be much less than one.

In view of the above, $m/C_DA = 1$ was taken as a nominal (within close tolerances) design specification for the remainder of the study. Trajectory characteristics for $m/C_DA = 1$, entry angles of -20° and -90°, entry velocity of 22,000 ft/sec, and Atmosphere E are presented in Figure 4. It may be seen from Figure 4 that increasing the Mach number at which picture taking is initiated has limited value in increasing picture-taking time, for such time is increased by only 13 seconds if Mach number for picture initiation is increased from one to two for an entry angle of -90°.

III. EFFECT OF ATMOSPHERE ON m/C_DA

An investigation was made to determine what effect the existence of an atmosphere other than "E" might have on the picture-taking experiment and the required m/C_DA. The comparative results for Atmospheres B, C, and E are presented in Table III for the worst possible situation relative to entry angle (-90°) and entry velocity. A value of 26,000 ft/sec was chosen for the latter rather than the previously used 22,000 to allow for a greater latitude in spacecraft launch date.

Of the three atmospheres, "B" is the most critical from both the standpoint of flight time below M = 1, 94 seconds, and altitude at which M = 1, 38,500 ft, possible parachute deployment altitude. Impact velocity is not much different for Atmosphere B from that for "E" and is even improved in the case of "C", from the standpoint of capsule impact survivability.

The "most probable" subsonic flight time duration is in excess of 94 seconds inasmuch as the 94 results from the worst possible set of circumstances (presumably). Consideration of the data in Table II and comparison with those of Table III indicates that the degree by which the "most probable" time exceeds 94 seconds depends primarily on the "most probable" entry angle, for the time is quite sensitive to entry angle, definitely less so to atmosphere--2 of the atmospheres, B and E, giving relatively similar results--and insensitive to entry velocity.

IV. A REITERATION ON m/C_DA

A further investigation was made to determine the sensitivity of the subsonic flight time duration to m/C_DA for m/C_DA less than one and for the "worst" conditions: Atmosphere B, entry angle of -90°, entry velocity of 26,000 ft/sec. The result is the curve presented in Figure 5.

V. VARIABLE C_D

Entry trajectory characteristics heretofore obtained were based on the assumption of constant m/C_DA. To evaluate this assumption, trajectory computations were made for the current capsule design, employing a 47-inch body, and for a similar one having a 53-inch body. The estimated drag coefficient (Figure 6) used in the computations was that presented in Reference 2. Capsule mass at entry was taken to be 8.35 slugs (269 lbs), the latest estimate available; mass was assumed constant throughout the entry trajectory.

The subsonic flight time durations for the two capsule sizes considered are shown in Figure 5. Corresponding m/C_DA values were taken to be those for the high-speed flight region and were based on a C_D of .72, to allow comparison with the constant m/C_DA results. When a variable C_D is considered, its substantially lower average in the subsonic compared to the hypersonic speed range produces a marked decrease in picture-taking time--from 99 to 74 seconds for the 47-inch capsule. For the same capsule, impact velocity rises from approximately 310 ft/sec to 456 ft/sec. A 53-inch diameter body would give a picture-taking time of 101 seconds under the "most adverse" conditions, including actual C_D, and an impact velocity of 406 ft/sec.

REFERENCES

1. Blifford, I. H.: Mariner B Capsule Study, Memo dated 9-28-61.
2. Stimpson, L.D.: Mariner B Capsule Aerodynamic Coefficients.

Abraham O. Hammond

Distribution:

R. Auelmann	R. Nagorski
M. Boobar	T. Neumann
R. Foster	J. Oslake
J. Kemmerly	D. Rodriguez
S. Lampert	L. Stimpson
F. Losee	

APPENDIX

LIST OF SYMBOLS

a = speed of sound

a_t = tangential acceleration

A = capsule drag reference area

C_D = capsule drag coefficient (at zero lift)

g_e = earth gravity constant, $g_e = 32.2$ ft/sec^2

h = altitude

m = capsule mass

M = Mach number

q = dynamic pressure

t = time

V = velocity

β = atmospheric density decay parameter, $\rho/\rho_o = e^{-\beta h}$

γ = flight path angle

ρ = density

ρ_o = zero-altitude intercept of $\ln \rho$ vs h for specified altitude range

subscript

E denotes "entry"

TABLE I

MARS ATMOSPHERE CHARACTERISTICS

ATMOSPHERE MODEL	10^{-3} h / ft	$10^4 \bar{\rho}_o$ / slug/cu ft	$10^4 \beta$ / per ft	a / ft/sec
B	45-1000	4.30	0.241	885
	0-45	2.70	0.1380	1002-885
C	70-1000	14.00	0.342	750
	0-70	4.30	0.1740	965-750
E	0-1000	2.70	0.1697	1000

TABLE II

TRAJECTORY CHARACTERISTICS - EFFECT OF m/C_DA

Atmosphere E $h_E = 10^6$ ft $V_E = 22{,}000$ ft/sec

γ_E deg	m/C_DA slug/sq ft	$t_{h=o}$ sec	$t_{h=o} - t_{M=1}$ sec	$10^{-3} h_{M=1}$ ft	q_{max} psf	$V_{h=o}$ ft/sec
-20	1	513	240	118	306	312
	2	422	131	78	580	459
	4	366	55	38	1052	676
-40	1	292	181	79	937	312
	2	186	73	39	1844	456
	4	114	-	-	3617	1038
-90	1	186	118	52	1570	312
	2	84	14	11	3152	625
	4	54	-	-	4633	3154

TABLE III

TRAJECTORY CHARACTERISTICS - EFFECT OF ATMOSPHERE

$h_E = 10^6$ ft $V_E = 26{,}000$ ft/sec $\gamma_E = -90^\circ$ $m/C_DA = 1$ slug/sq ft

ATMOSPHERE MODEL	$t_{h=o}$ sec	$t_{h=o} - t_{M=1}$ sec	$10^{-3} h_{M=1}$ ft	q_{max} psf	$a_{t_{max}}$ ge	$V_{h=o}$ ft/sec
E	173	112	49.5	2137	-66.0	312
B	149	94	38.5	3017	-93.2	310
C	198	145	47.8	4347	-134.7	244

Fig. 1

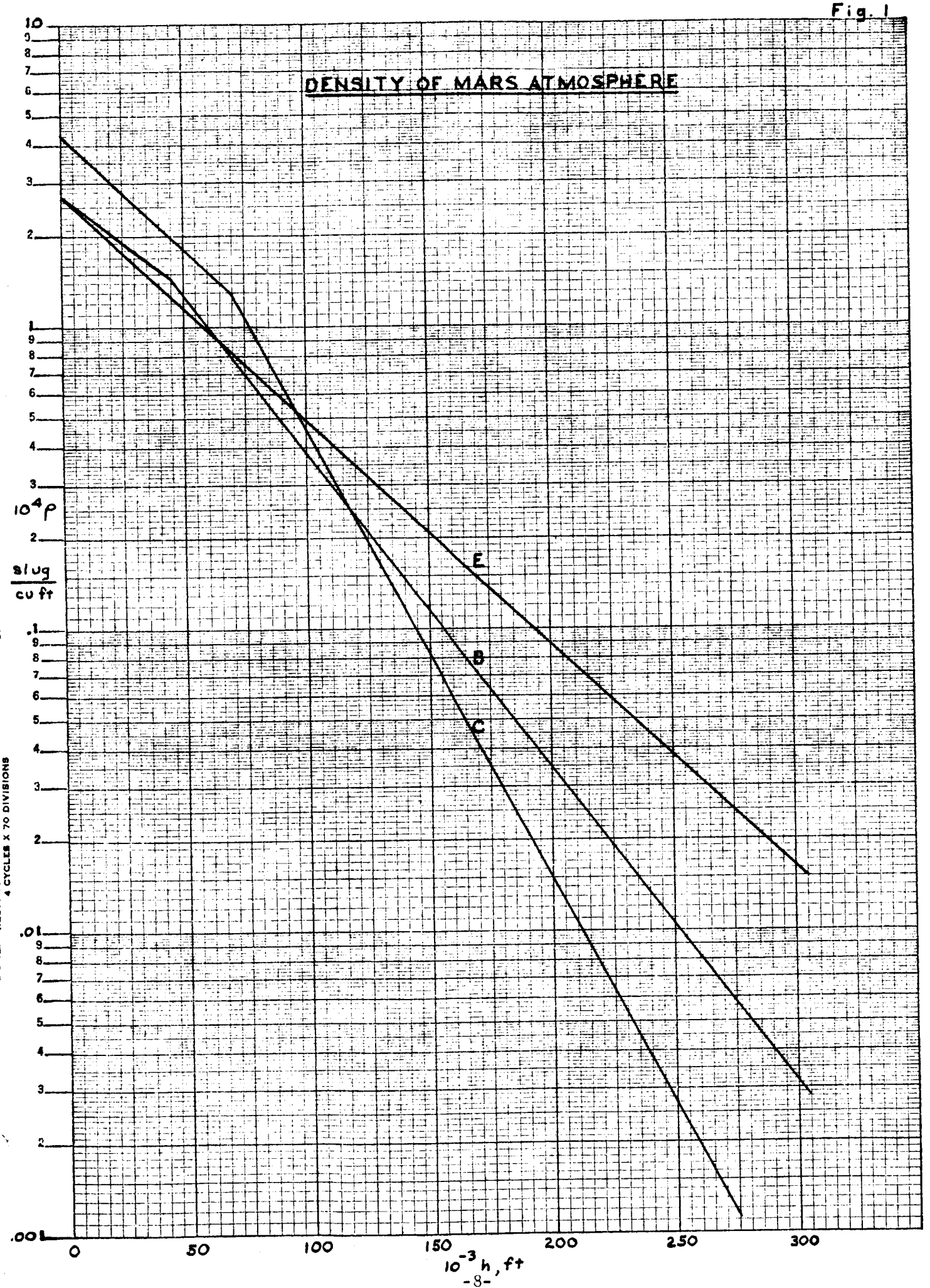
DENSITY OF MARS ATMOSPHERE
$10^4 \rho$
slug / cu ft
10
1
.1
.01
.001
E
B
C
0
50
100
150
200
250
300
10^{-3} h, ft
K+E SEMI-LOGARITHMIC 359-81
KEUFFEL & ESSER CO. MADE IN U.S.A.
4 CYCLES X 70 DIVISIONS

Fig. 2

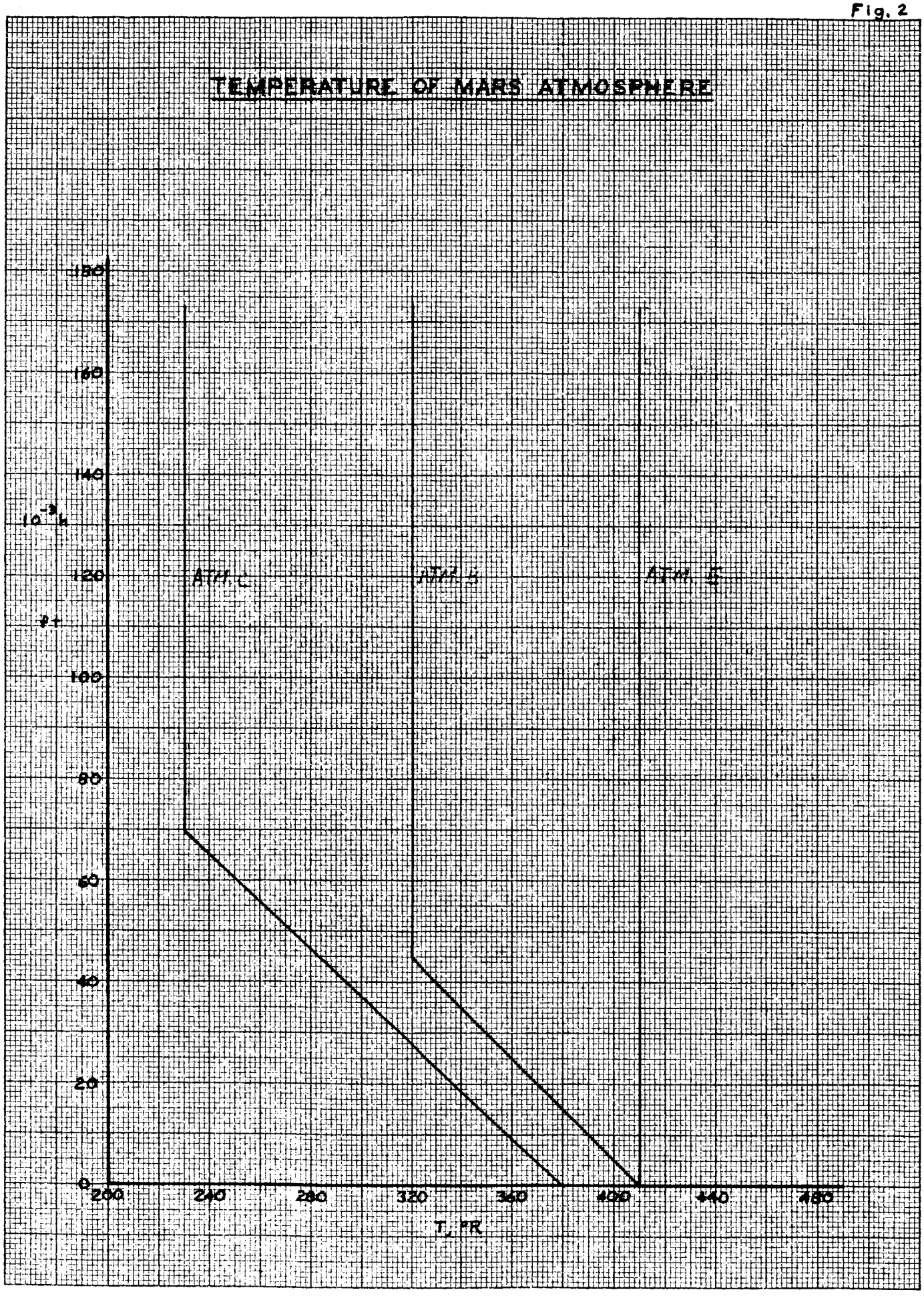
TEMPERATURE OF MARS ATMOSPHERE
180
160
140
10^{-3} h
120
ft
100
80
60
40
20
0
200
240
280
320
360
400
440
480
T, °R
ATM. C
ATM. L
ATM. G

Fig. 3

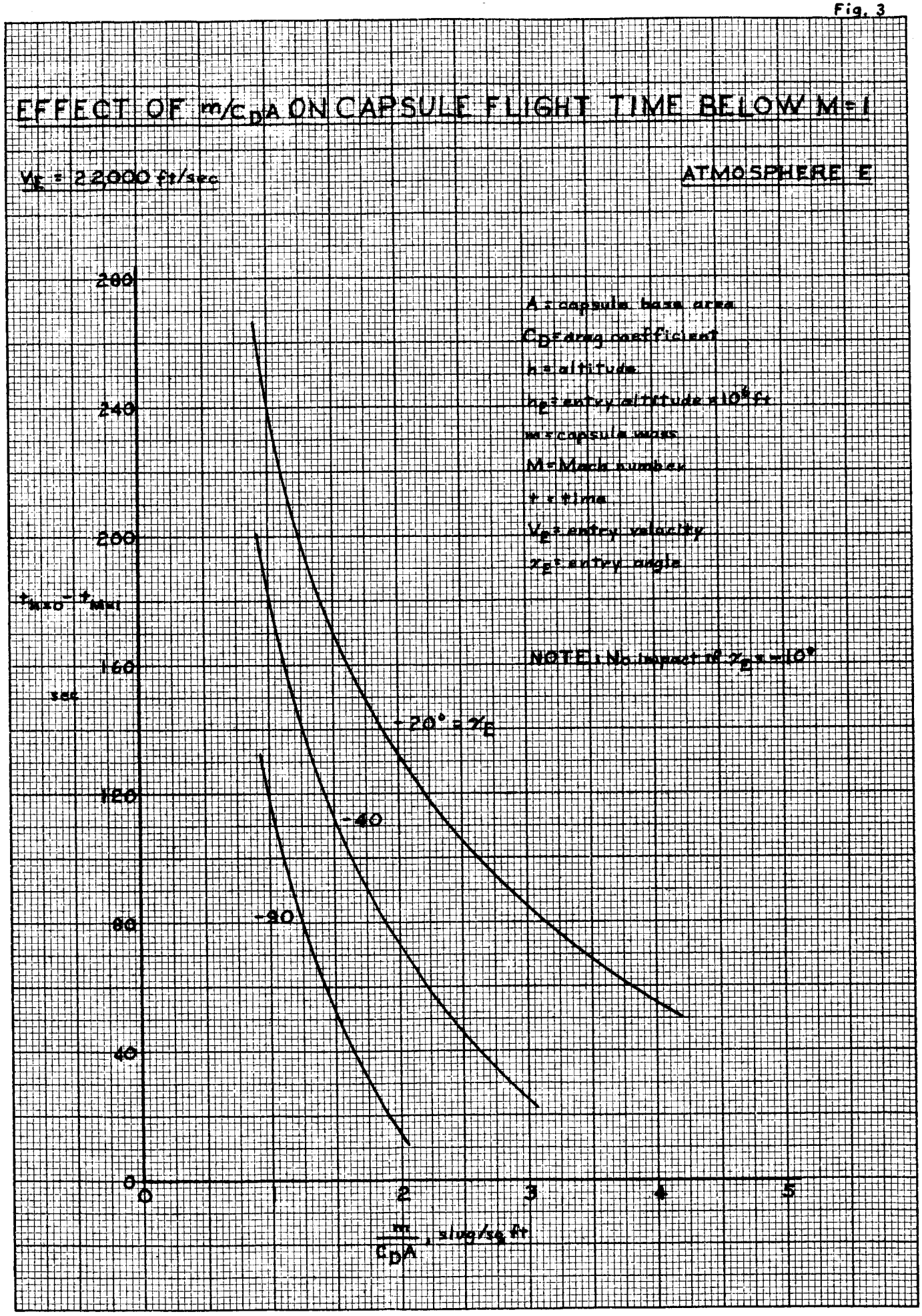
EFFECT OF m/C_DA ON CAPSULE FLIGHT TIME BELOW M=1
V_E = 22,000 ft/sec
ATMOSPHERE E
A = capsule base area
C_D = drag coefficient
h = altitude
h_E = entry altitude = 10^5 ft
m = capsule mass
M = Mach number
t = time
V_E = entry velocity
γ_E = entry angle
NOTE: No impact if γ_E = -10°
-20° = γ_E
-40
-90
280
240
200
160
120
80
40
0
t_M=0 - t_M=1
sec
0
1
2
3
4
5
m/C_DA, slug/sq ft

Fig. 4a

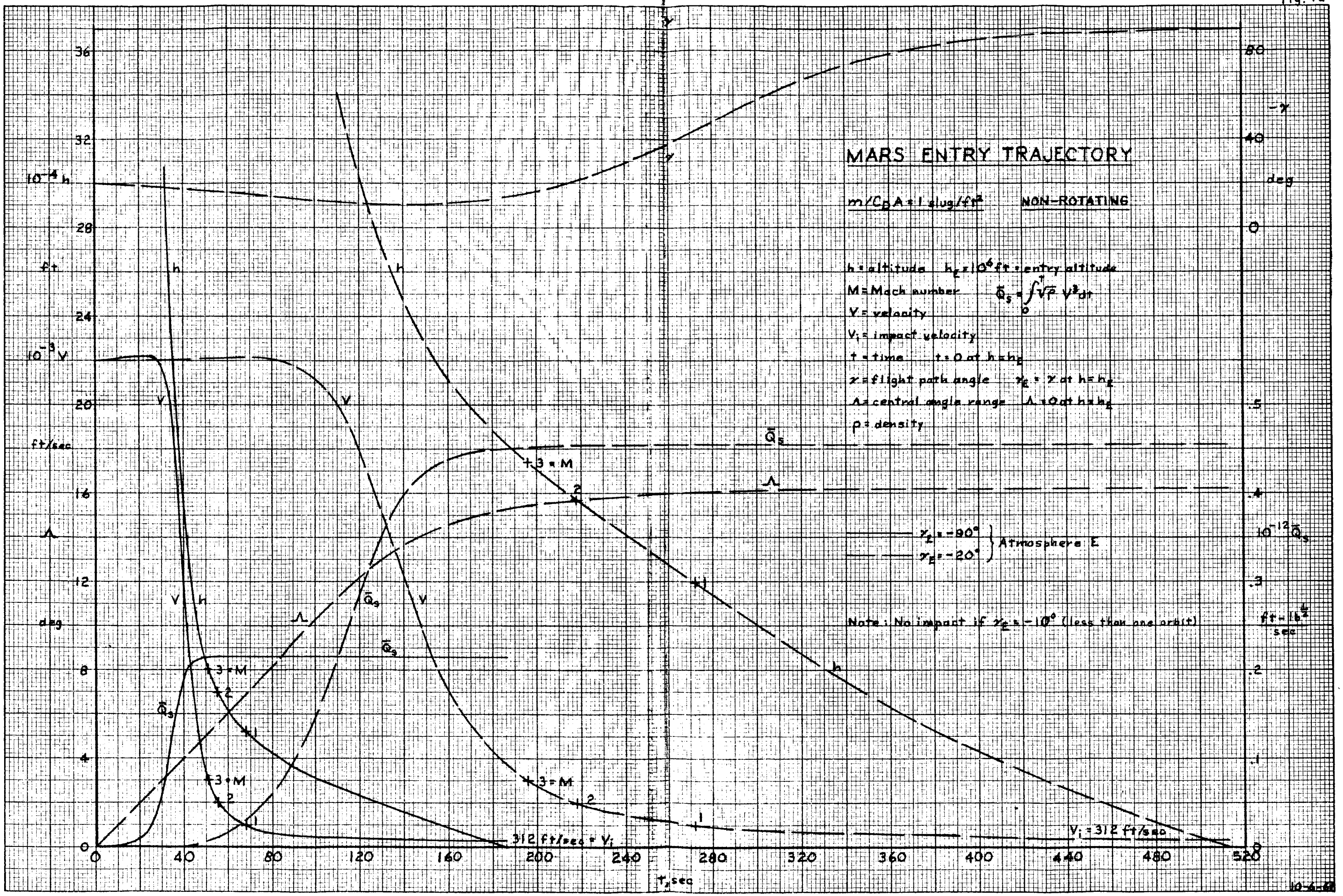
MARS ENTRY TRAJECTORY
m/C_D A = 1 slug/ft² NON-ROTATING
h = altitude h_E = 10⁶ ft = entry altitude
M = Mach number Q̄_s = ∫₀^t √ρ V³ dt
V = velocity
V_i = impact velocity
t = time t = 0 at h = h_E
γ = flight path angle γ_E = γ at h = h_E
Λ = central angle range Λ = 0 at h = h_E
ρ = density
γ_E = -90°
γ_E = -20°
Atmosphere E
Note: No impact if γ_E = -10° (less than one orbit)
312 ft/sec = V_i
V_i = 312 ft/sec
10⁻⁴ h
ft
10⁻³ V
ft/sec
Λ
deg
-γ
deg
10⁻¹² Q̄_s
ft-lb^½/sec
t, sec
10-6-61

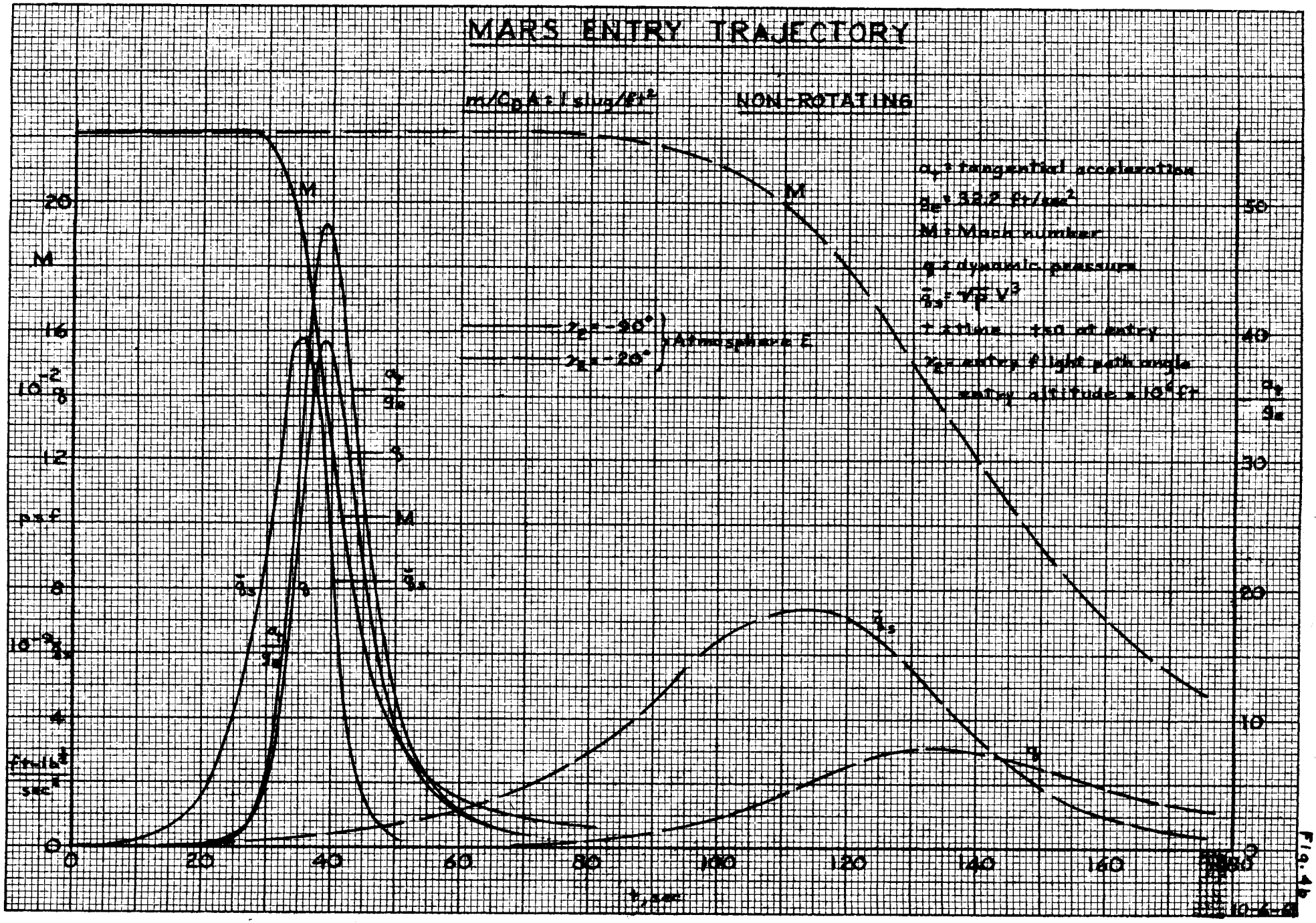
MARS ENTRY TRAJECTORY
m/C_D A = 1 slug/ft²
NON-ROTATING
a_T = tangential acceleration
g_E = 32.2 ft/sec²
M = Mach number
q = dynamic pressure
q_s = ½ρV³
t = time, t=0 at entry
γ_E = entry flight path angle
entry altitude = 10⁶ ft
γ_E = -90°
γ_E = -20°
Atmosphere E
M
q/q_s
a_T/g_E
t, sec

Fig. 4b

Fig. 5

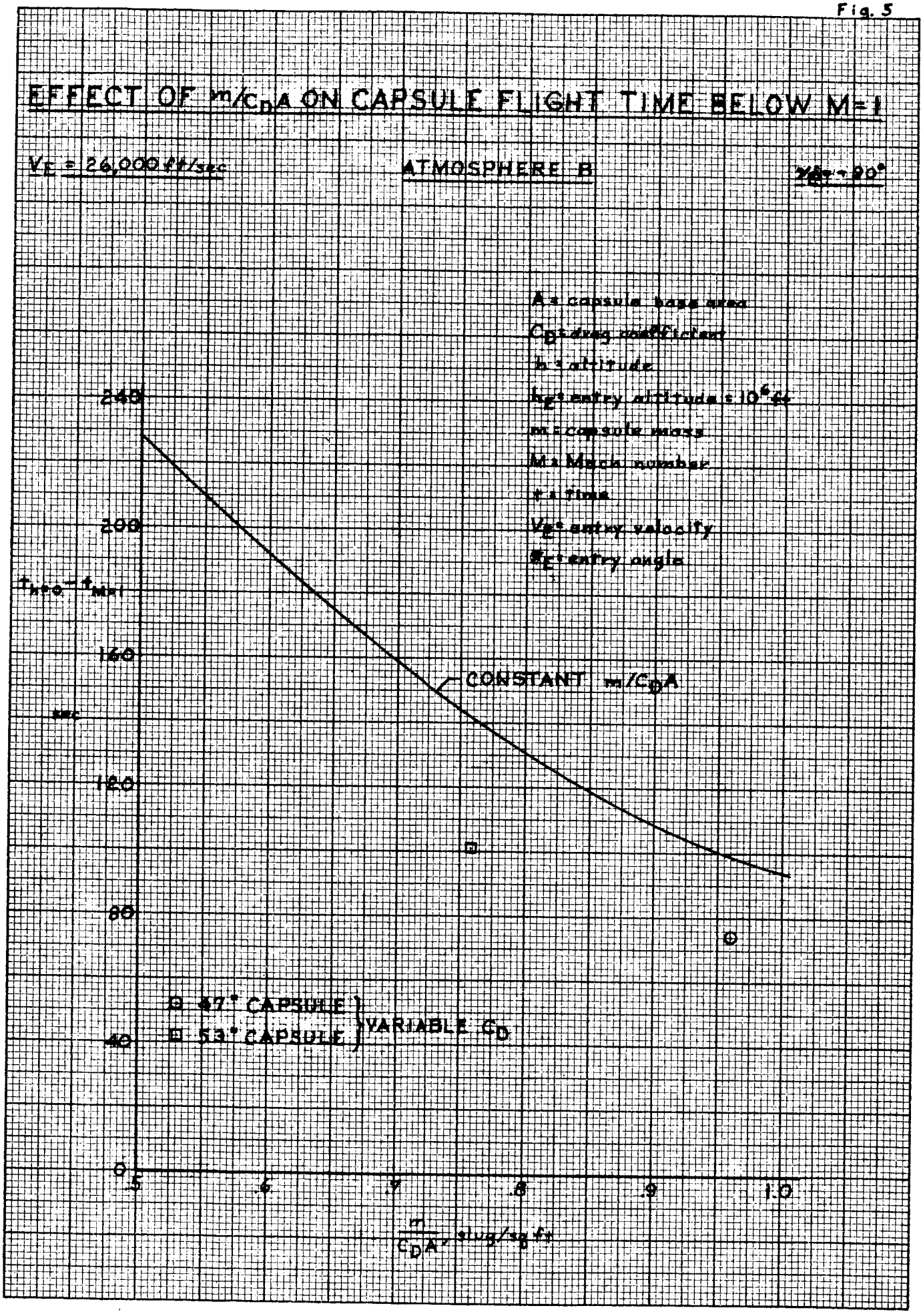
EFFECT OF m/CDA ON CAPSULE FLIGHT TIME BELOW M=1
VE = 26,000 ft/sec
ATMOSPHERE B
γE = 90°
A = capsule base area
CD = drag coefficient
h = altitude
hE = entry altitude = 10^6 ft
m = capsule mass
M = Mach number
t = time
VE = entry velocity
γE = entry angle
240
200
160
120
80
40
0
th=0 − tM=1
sec
CONSTANT m/CDA
47° CAPSULE
53° CAPSULE
VARIABLE CD
.5
.6
.7
.8
.9
1.0
m/CDA, slug/sq ft

K+E 10 X 10 TO THE ½ INCH 359-11
KEUFFEL & ESSER CO. MADE IN U.S.A.

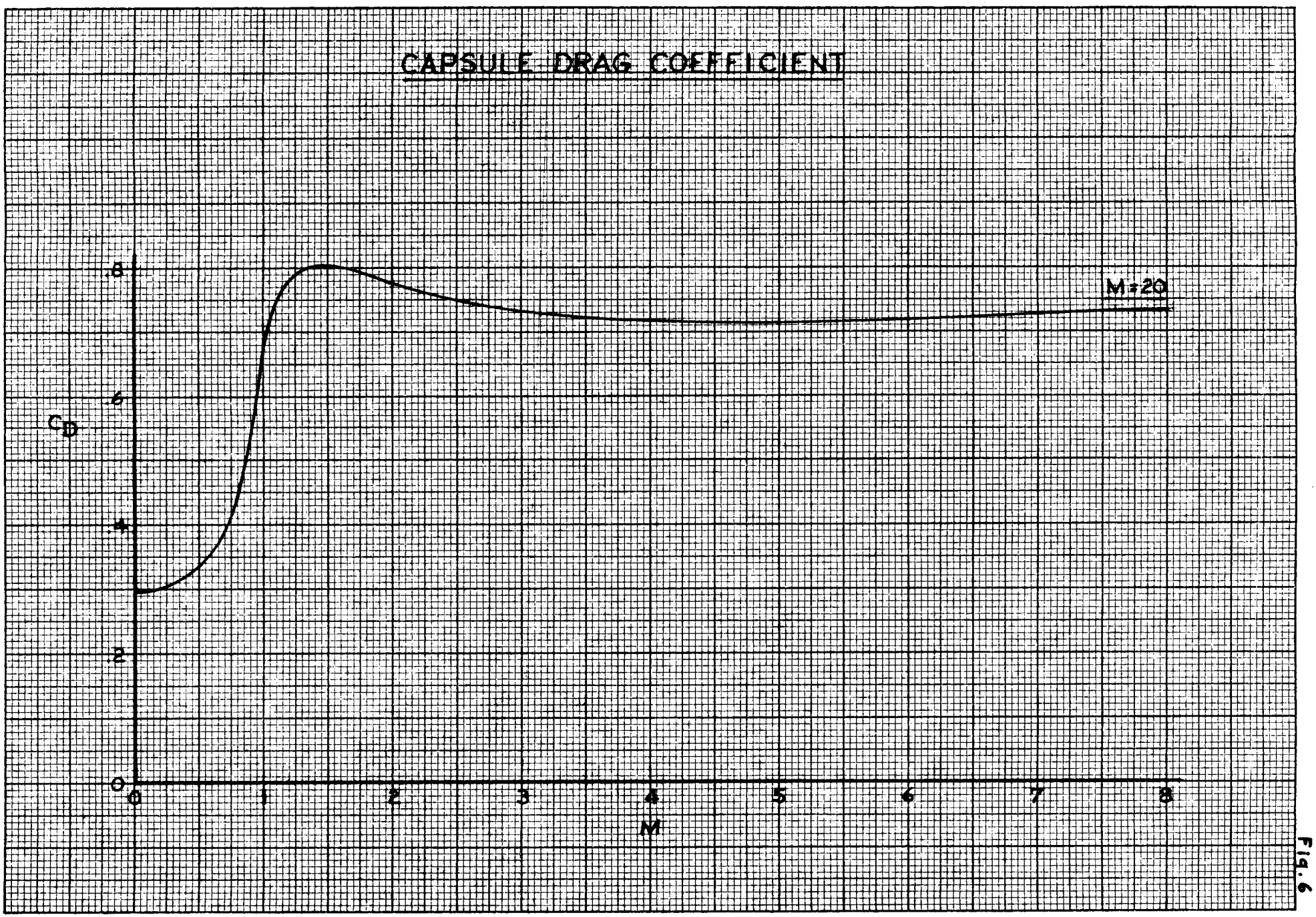

Fig. 6

Ford Motor Company

AERONUTRONIC DIVISION

Intra-Company Communication

30 October 1961

TO: J. Kemmerly

FROM: A. A. Gammal

SUBJECT: Mariner B Capsule Entry Trajectories

REF.: (1) Gammal, A. A., Mariner B Capsule Entry Trajectories, 10/24/61.
(2) Blifford, I. H., Mariner B Capsule Study, 9/28/61.

cc: R. Auelmann
M. Boobar
R. Foster
S. Lampert
F. Losee
R. Nagorski
T. Neumann
J. Oslake
D. Rodriguez
L. Stimpson

The Atmospheres B, C, and E considered in the study described in Reference 1 were said, in that reference, to have been chosen from among the five of Reference 2 on the assumption that B, C, and E "would impose the most stringent requirements upon the capsule" This assumption, itself, tacitly assumed that Atmospheres A and D of Reference 2 indicate a surface density of much less probability than those indicated by Atmospheres B, C, and E

If all five atmospheres are assumed equally probable, the atmosphere which imposes the most stringent requirement relative to subsonic flight duration (picture-taking time available) is Atmosphere D. For the 47-inch capsule, considering variable drag coefficient (Figure 6 of Ref. 1), Atmosphere D yields a subsonic flight duration of only 29 seconds as against 74 seconds, the minimum yielded by the atmospheres considered in Reference 1. Impact velocity increases to 648 ft/sec from a maximum of 456 ft/sec. Altitude at which the Mach number is one decreases to 21,900 ft from 38,500 ft, thereby aggravating the problem of deploying a parachute, should one be used.

Abdon A. Gammal

AAG:cyl

APPENDIX D

STABILITY ANALYSIS

Ford Motor Company

AERONUTRONIC DIVISION

Intra-Company Communication

24 October 1961

TO: D. Rodriguez

FROM: L. D. Stimpson

SUBJECT: Mariner B Capsule Aerodynamic Coefficients

REF.: Memorandum AD-017, October 17, 1961

cc: R. Auelmann
M. Caldwell
R. Foster
A. Gammal
J. Housego
J. Kemmerly
S. Lampert
T. Neumann

Aerodynamic coefficient data have been derived for the latest Mariner B capsule described in the above reference for a range of Mach numbers and angles-of-attack. Principle use was made of the Hyper-Environmental Test System (HETS) wind-tunnel data given in Aeronutronic Publication Nos. U-816 and U-826, and by Newtonian theory for hypersonic flow with a complete range of angles-of-attack, courtesy of R. V. Warden. Comparison with the aerodynamic data previously known for a sphere and flat plate, enabled some modification of the HETS (15° aft cone body) data to adequately represent the Mariner B capsule (10° aft cone and a blunter nose) for the stability investigation. Although some reference has been made to classified NASA reports for direction, it has been ascertained that the data presented here is unclassified.

The HETS data provided an immediate source of aerodynamic coefficient data over wide ranges of both M and α, not easily found from other sources. However, reference to Publication No. U-826 indicated that a subsonic drag coefficient of only about one-tenth existed; and reference to Newtonian theory indicated an axial force coefficient of about one-half existed at hypersonic velocities. Since the point-mass trajectory studies demonstrated a need for an m/C_DA of the order of unity; which, with a weight of about 300 lbs, requires a capsule base diameter of about forty inches, using $C_D = 1$. The HETS average C_D is more like 0.3 which would almost double the diameter to eighty inches and prohibitively increase the structural weight. With the aid of the NASA TM X-467 and TM X-507 reports, it is seen that blunting the body will increase the hypersonic axial coefficient to about 3/4 for the latest design. Blunting any further undoubtably will aggravate the stability problem at subsonic velocities.

Figure 1 shows the estimated axial force coefficient as a function of Mach number, falling between the HETS data and the sphere drag (Charters and Thomas, J.A.S., pp. 468-476, October 1945 and Hodges, J.A.S., pp. 755-758, October 1957). Figure 2 indicates the manner in which the axial coefficient varies with angle-of-attack. The subsonic behavior was given in U-826 up to about 25°, being extrapolated to a $C_A = -1.5$ at $\alpha = 180^{\circ}$ ($f_A = -1.5/0.3 = -5$, negative because of a 180° rotation of the axis. C_D for a flat plate $\simeq 2$: Goldstein, Modern Developments in Fluid Dynamics, Vol. 1, pg. 37). The hypersonic behavior of the

177

axial coefficient with α is given by Newtonian theory, with the base pressure included in an approximate fashion.

Figure 3 shows the normal force coefficient dependence upon Mach number (lift at $\alpha = 0$). The HETS data are from U-826 (subsonic) and from Newtonian theory (hypersonic), being faired through an expected maximum around M = 1. The Mariner data were extrapolated from this and consideration for the blunter nose, resulting in lower lift at small α. Correlation with pitch moment data tends to substantiate the choice shown.

The digital computer program, for a symmetrical spinning body entering the Martian atmosphere, utilizes the body axis system of axial and normal forces. It develops the pitching moment through multiplication of the normal force by the lever arm between the c.g. & the center-of-pressure. The c.g. has been estimated at about 45% of the length, from the nose. Figure 4 shows the estimated c.p. shift with Mach number for the Mariner vehicle; it doesn't shift much with α except close to 180°.

The analog computer will use only a one degree-of-freedom (non-spinning) system, i.e., angle-of-attack; thus requiring only pitch moment data. This is obtained by multiplication of normal force data in Figure 3 by c.g.-c.p. data in Figure 4. The pitch moment coefficient data are presented in Figure 5 and compared to both HETS and sphere data. The HETS moment data were increased by a ratio of Mariner to HETS c.g.-c.p., where the HETS c.g. is at the 50% point. The sphere c.g. was assumed at the 30% point for comparison, which would be quite difficult to achieve.

The dependence of normal force and pitching moment upon α is seen to be nearly sinusoidal in Figure 6 (sine dependence is correct for the sphere moment). For the small angle linear theory, $f(\alpha)$ becomes simply α, which is seen to be fairly adequate up to 20 or 30 degrees. The HETS normal force dependence falls below the pitching moment (Newtonian theory), however the upper sine-like curve is suggested for both normal force and pitching moment on the Mariner vehicle, since the normal force was already reduced in Figure 3 (blunter shape consideration).

Figure 7 is an estimate of the pitch rate damping coefficient as a function of Mach number, where $\dot{\theta}$ will be approximated by $\dot{\alpha}$ in the analog solution. Figures 8 and 9 are regraphs of the normal and axial forces as two-parameter families of M and α for convenience of digital input. The abrupt change from subsonic to supersonic behavior has been smoothed in Figure 9.

For purposes of stability investigation, emphasis is placed upon accurate representations at low Mach numbers with small angles-of-attack. Only approximate representation is necessary at the higher Mach numbers and large α; similarly for pitch rate damping since it is an integrated effect and is relatively small compared to the exponentially increasing atmospheric density and dynamic pressure variation.

L. D. Stimpson

LDS:cyl

K+E 10 X 10 TO THE ½ INCH 359-11
KEUFFEL & ESSER CO. MADE IN U.S.A.

FIGURE 1 AXIAL FORCE VS MACH NUMBER

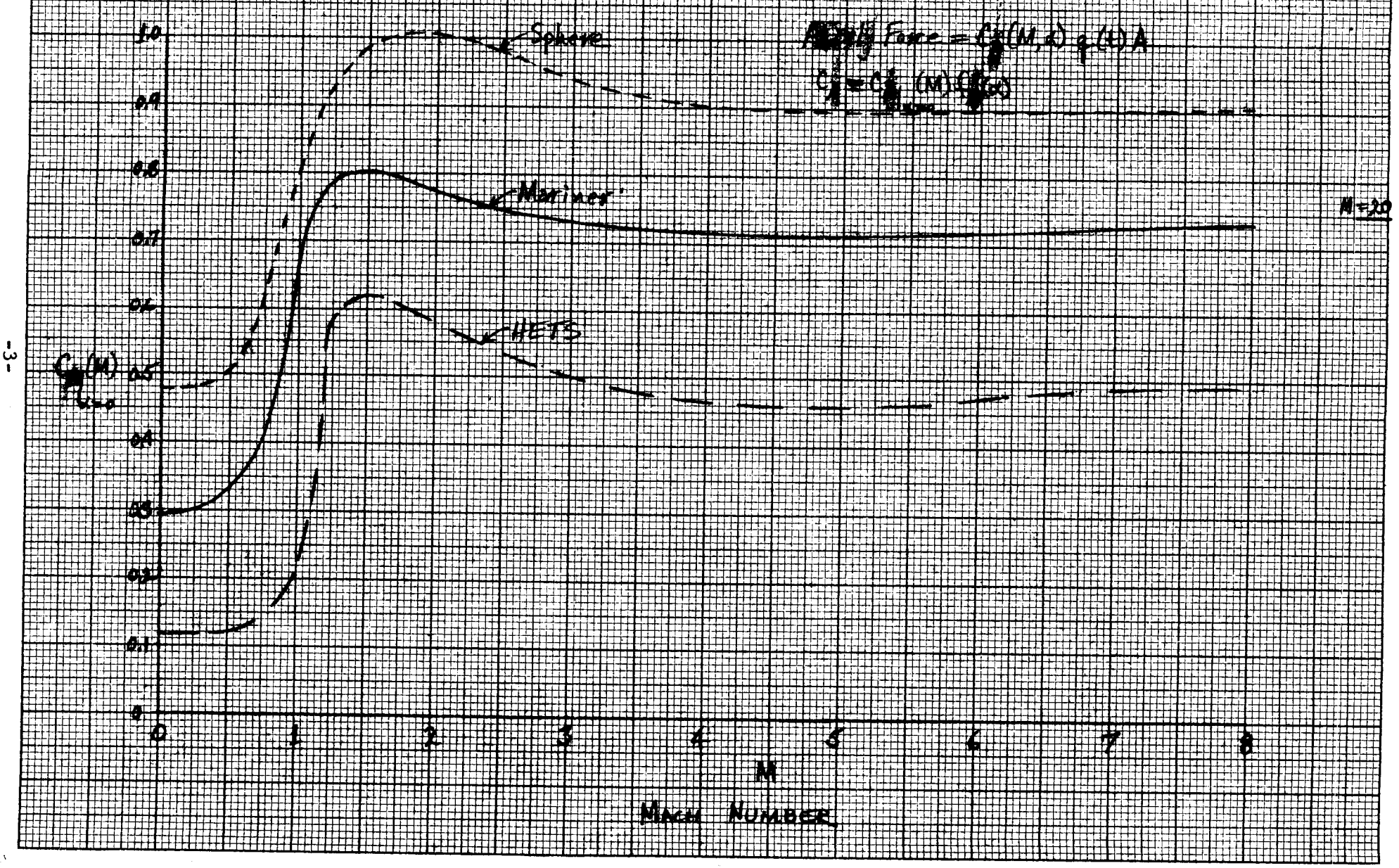

K+E 10 X 10 TO THE ½ INCH 359-11
KEUFFEL & ESSER CO. MADE IN U.S.A.

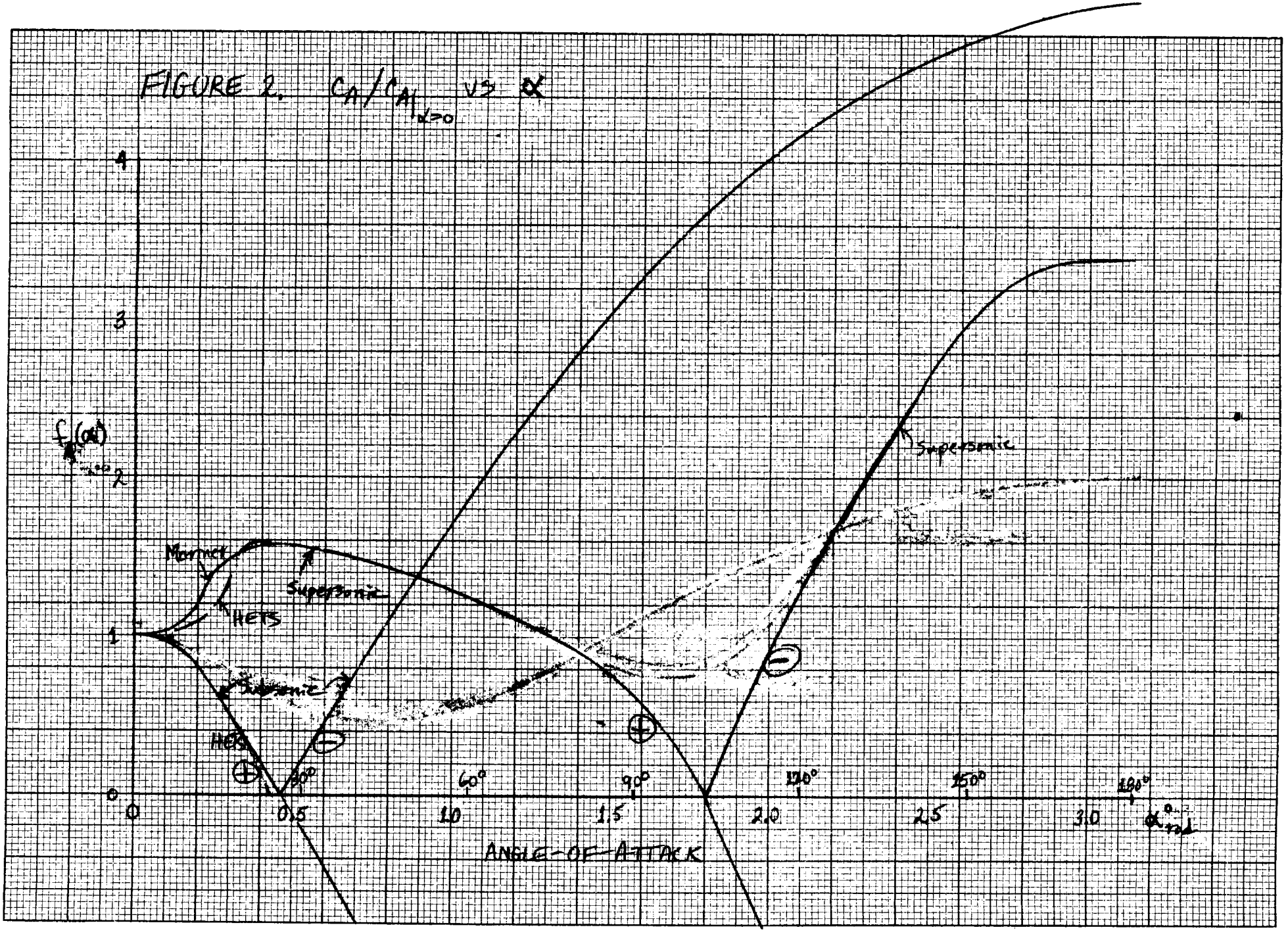

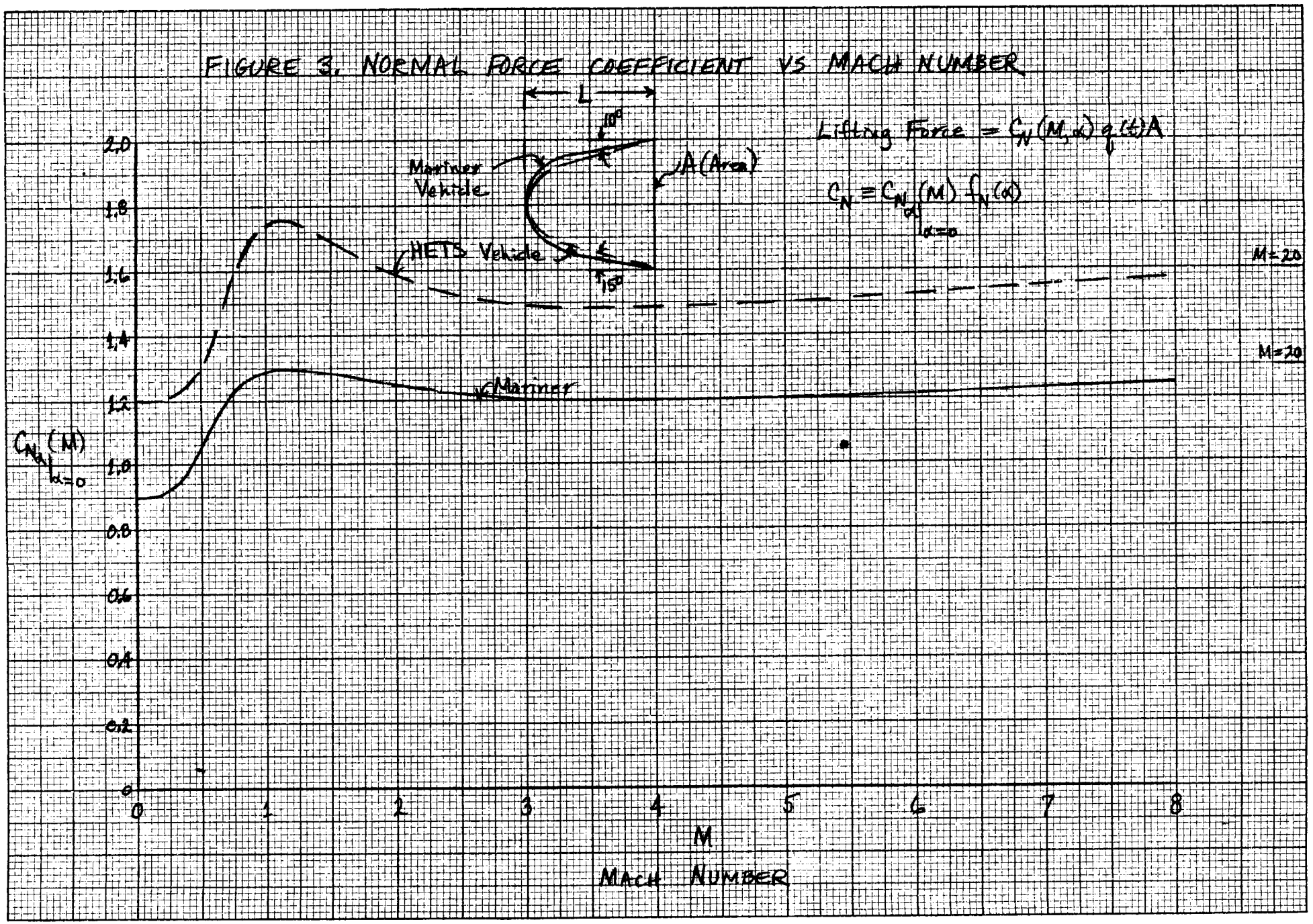
FIGURE 3. NORMAL FORCE COEFFICIENT VS MACH NUMBER
L
10°
Mariner Vehicle
A (Area)
HETS Vehicle
15°
Lifting Force = $C_N(M,\alpha)\, q(t) A$
$C_N = C_{N_\alpha}(M)\, f_N(\alpha)$
M=20
M=10
Mariner
$C_{N_\alpha}(M)\big|_{\alpha=0}$
2.0
1.8
1.6
1.4
1.2
1.0
0.8
0.6
0.4
0.2
0
0
1
2
3
4
5
6
7
8
M
MACH NUMBER

K+E 10 X 10 TO THE ½ INCH 359-11
KEUFFEL & ESSER CO. MADE IN U.S.A.

FIGURE 4. CENTER-OF-PRESSURE VS MACH NUMBER

FIGURE 5. PITCH MOMENT COEFFICIENT VS. MACH NUMBER

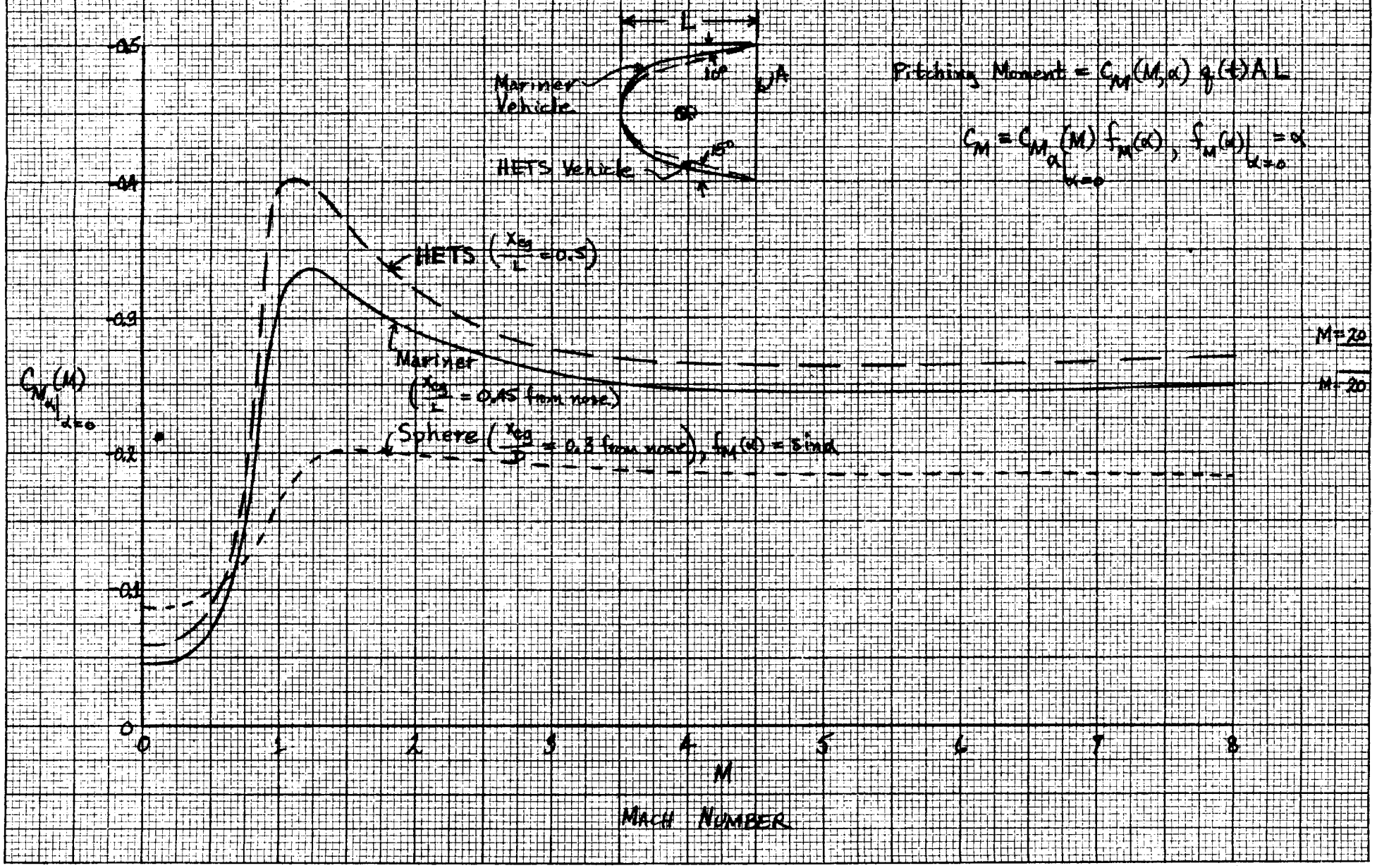

FIGURE 6. $C_N/C_{N_\alpha}\big|_{\alpha=0}$ AND $C_M/C_{M_\alpha}\big|_{\alpha=0}$ VS α

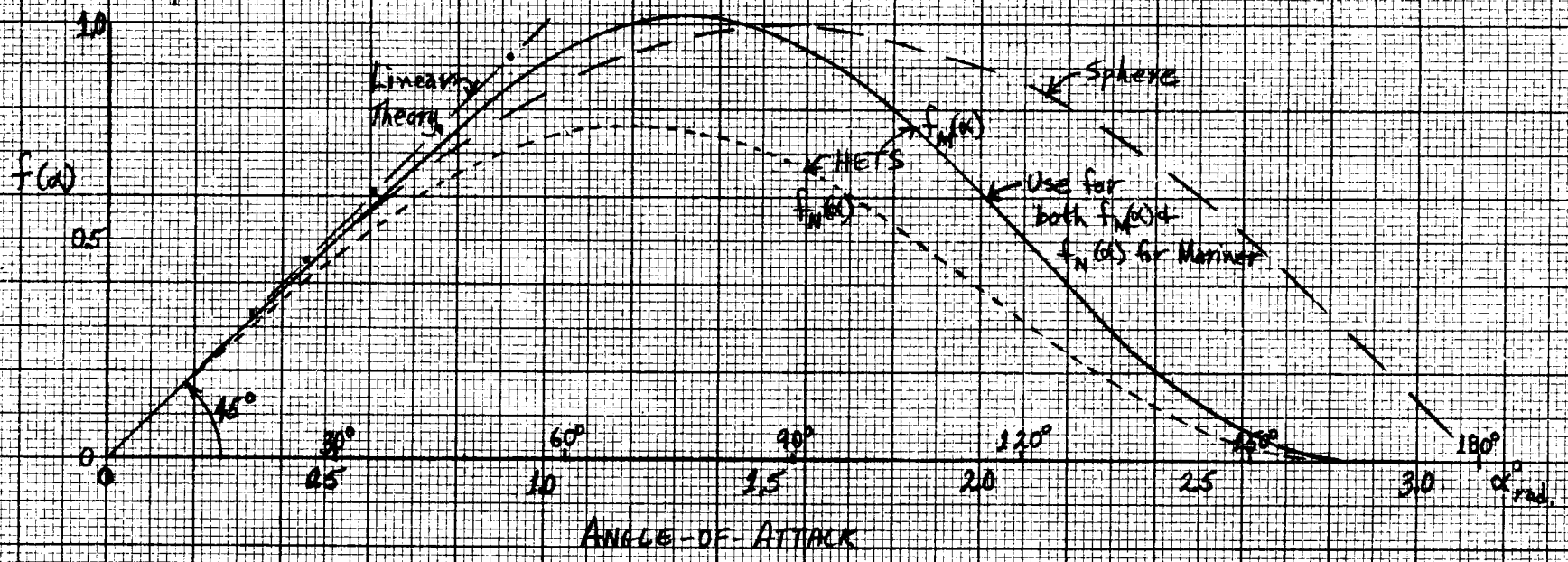

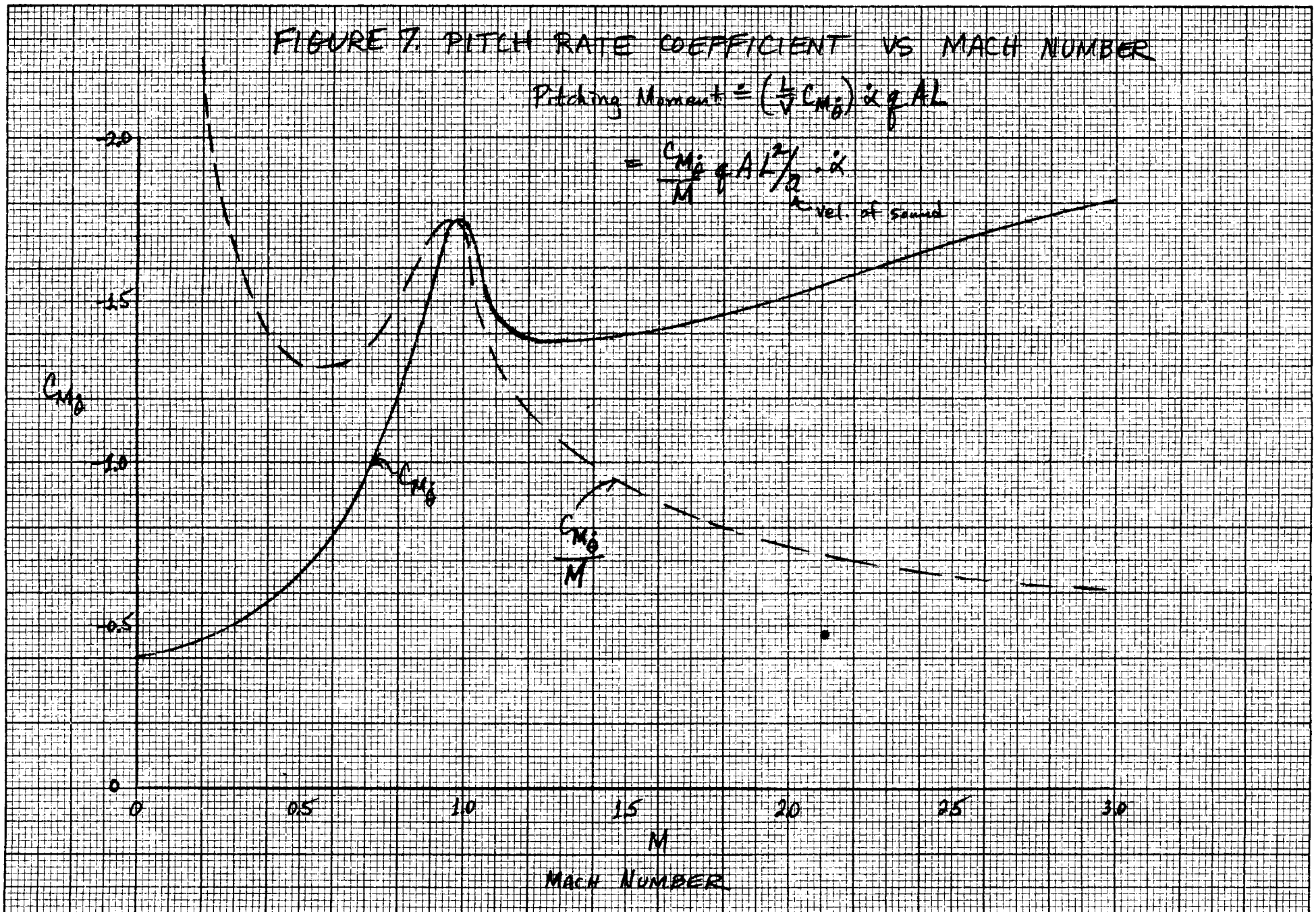
FIGURE 7. PITCH RATE COEFFICIENT VS MACH NUMBER
Pitching Moment $\doteq \left(\frac{1}{V} C_{M_{\dot\theta}}\right) \dot\alpha \, q A L$
$= \frac{C_{M_{\dot\theta}}}{M} q A L^2/2 \cdot \dot\alpha$
vel. of sound
C_{M_θ}
$C_{M_{\dot\theta}}$
$\frac{C_{M_{\dot\theta}}}{M}$
-2.0
-1.5
-1.0
-0.5
0
0
0.5
1.0
1.5
2.0
2.5
3.0
M
MACH NUMBER

K+E 10 X 10 TO THE ½ INCH 359-11L
KEUFFEL & ESSER CO. MADE IN U.S.A.

FIGURE 8. NORMAL FORCE COEFFICIENT VS. M AND α

FIGURE 9. AXIAL FORCE COEFFICIENT VS M & α

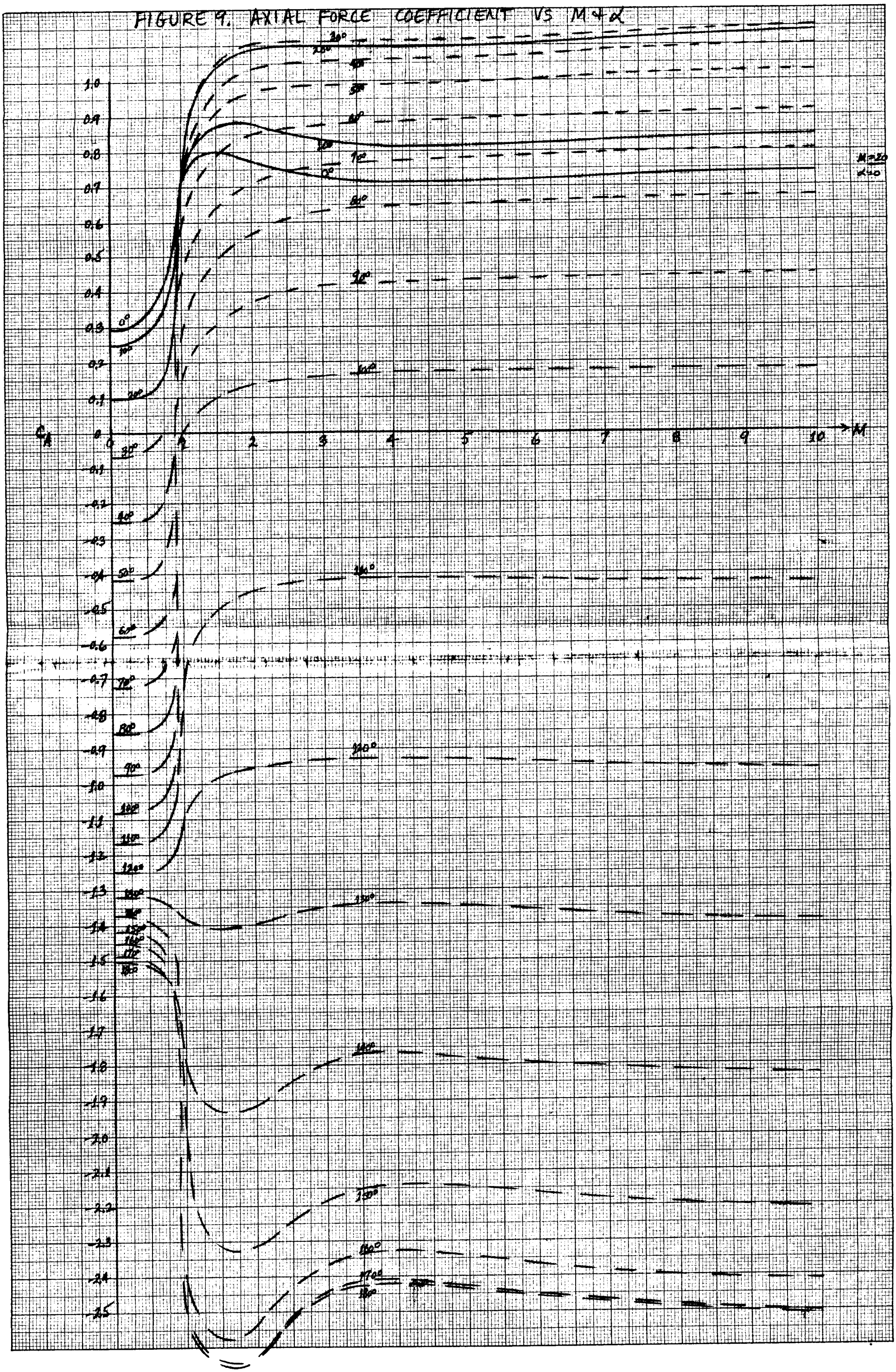

Ford Motor Company AERONUTRONIC DIVISION

Intra-Company Communication

15 November 1961

TO: J. Kemmerly (2)

FROM: D. Rodriguez

SUBJECT: Mariner B Mars Atmospheric Entry - Dynamic Stability

cc: R. Auelmann
A. Gammal
S. Lampert
T. Neumann
L. Stimpson

The angle of attack convergence of the Mariner B capsule during Mars atmospheric entry has been examined. The maximum angles of attack experienced by the vehicle during the periods of peak heating and peak deceleration are of concern from the points of view of heat shield and structural design. The angle of attack history is also of interest in view of the possible influence of the oscillatory motion of the vehicle on experimental mission feasibility or requirements during the descent.

The angle of attack history was computed on the Aeronutronic IBM 709 digital computer. An approximate 3-degree of freedom rotational motion program was employed for the stability calculations. This program computes the rotational or angular (pitch and yaw) motion of a body traversing a point mass trajectory. The dynamic pressure-, Mach number-, velocity-, and altitude-time histories are provided by the output of a separately computed point mass trajectory. The approximation inherent in the uncoupling of the point mass and rotational motion equations (implied in the previously indicated computation scheme) should be acceptable where only the angle of attack envelope is sought as an indication of vehicle stability, and precise calculation of the influence of vehicle attitude history on the point mass trajectory is not of interest. This argument is reinforced by the unavoidable presence at this time and at this point of the study of a number of rather uncertain aspects in the input quantities for the computation, and also by the consideration that only a preliminary assessment of the dynamic stability of the vehicle during Mars entry is desired here. A spherical non-rotating model of the planet Mars was considered adequate for these purposes. Gas dynamic coefficient data for the Mariner B capsule was developed as a function of Mach number and of angle of attack*. This development is presented in the memo "Mariner B Capsule Aerodynamic Coefficients", by L. D. Stimpson.

---

* The capsule is considered to have an axis of nominal rotational symmetry (also the nominal spin axis) which is, of course, the geometrical reference for specifying angle of attack.

Computations have been made using Atmosphere model E* for a trajectory entry angle of 90° (vertical descent), an initial angle of attack of 90°, a representative entry velocity of 22,000 fps, and a spin rate of 10 rpm. The following parametric variations were introduced.

(a) The estimated damping coefficient was reduced by a factor of ten in an attempt to indicate the possible influence of uncertainties in the estimated damping on the assessment of vehicle dynamic stability.

(b) A case was run with the damping set equal to zero in order to establish a reference for assessing the sensitivity of the dynamic behavior to the effects of damping.

(c) The spin rate was increased to 100 rpm to indicate the effects of high spin rates on angle of attack convergence during entry.

(d) An angle of attack history was run for a higher entry velocity of 26,000 fps.

(e) To indicate the effect of changes in the atmosphere model, the model characterized by the lowest dynamic pressures associated with the point mass trajectory at higher altitudes (above say 150,000 ft**) was selected--since no point mass trajectory was available for Atmosphere C with an entry velocity of 22,000 fps, the computations were made for the case of an entry velocity of 26,000 fps.

(f) The initial angle of attack was increased to 135°.

(g) Finally, computations were made for an entry angle of 20°, varying the damping.

In all cases a roll moment of inertia of 15 slug ft^2 and a pitch moment of inertia of 10 slug ft^2 with a 47 in. base diameter were used. The computations were started at about 800,000 ft. Point mass trajectories based on a mass-drag parameter $m/C_DA = 1$ were used. Since the terminal dynamic pressure is dependent only on the vehicle weight (Mars weight) to drag parameter, the essential influence of variable drag effects is merely to change the subsonic flight time. The results are presented in the form of total angle of attack envelopes vs. altitude.

---

* Atmosphere model E was chosen mainly on the basis of the available selection of point mass trajectories.

** The gas dynamic pitching moment, largely responsible for angle of attack convergence prior to peak heating and peak dynamic pressure, is proportional to dynamic pressure, q. The effect of damping is also proportional to q; everything else being the same (including descent time).

D. Rodriguez

MARINER B – MARS ATMOSPHERE ENTRY – ANGLE OF ATTACK ENVELOPE

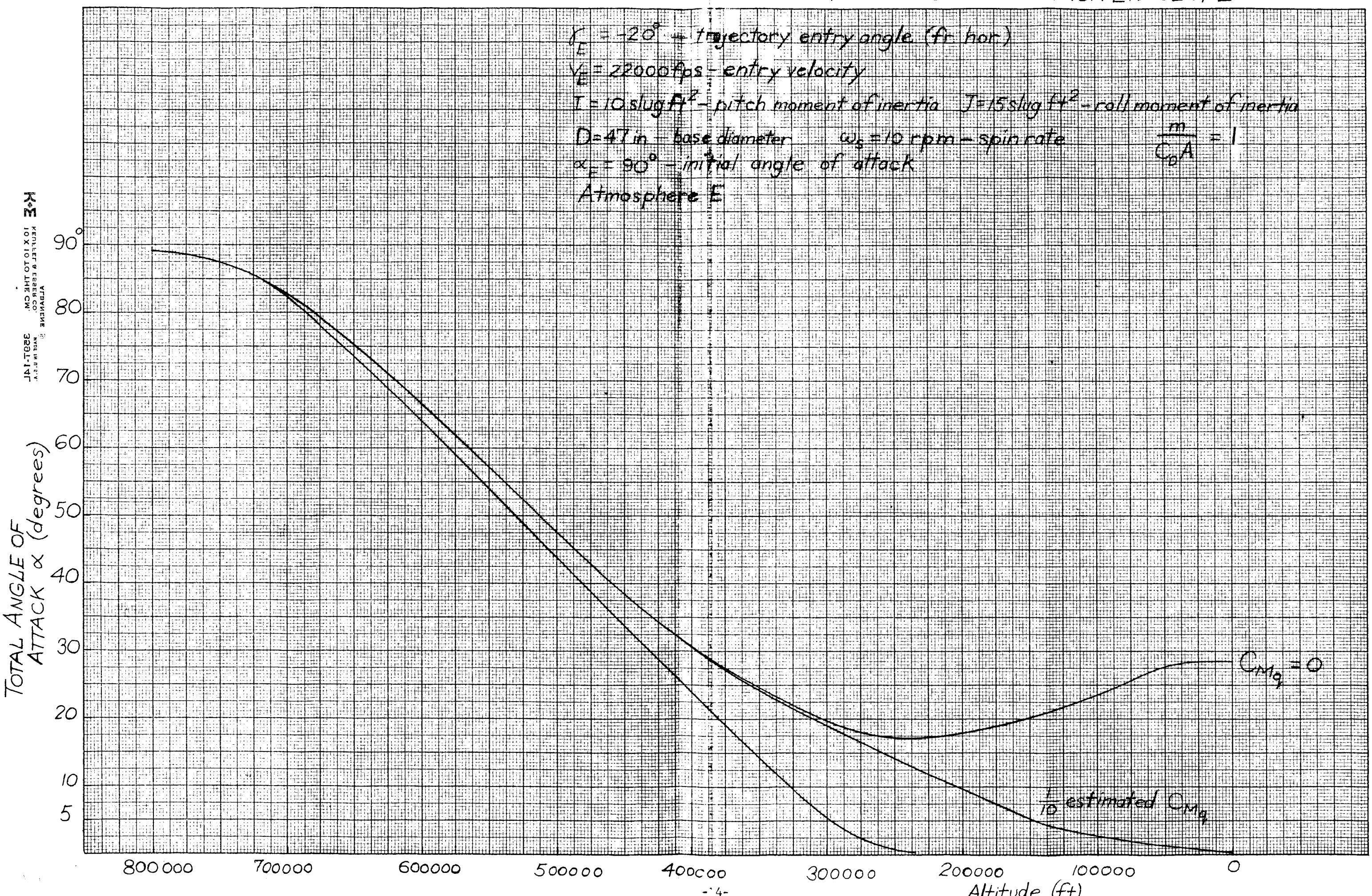

D. Rodriguez

MARINER B – MARS ATMOSPHERE ENTRY – ANGLE OF ATTACK ENVELOPE

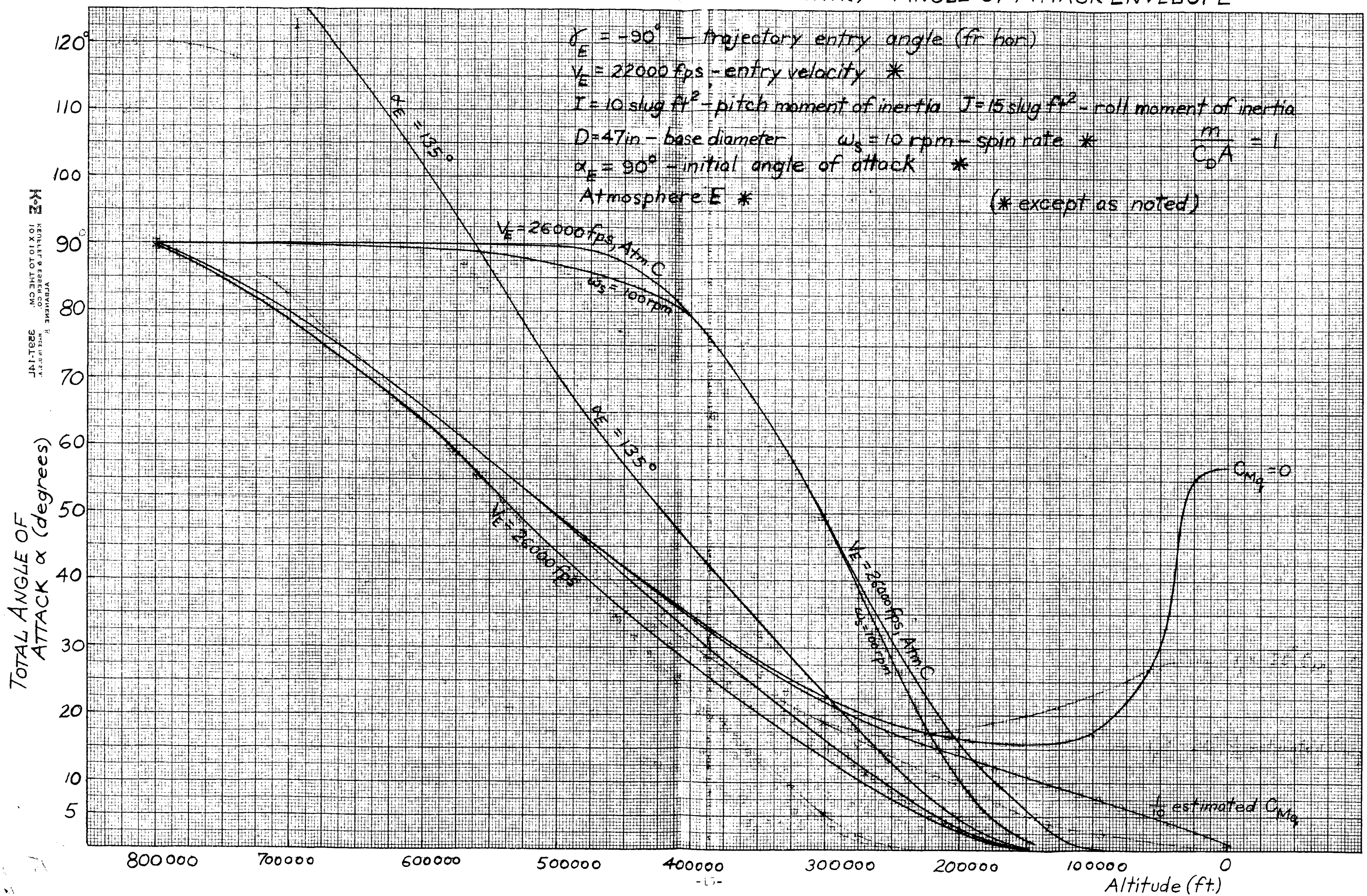

APPENDIX E

CAPSULE HEATING AND HEAT PROTECTION

Publication No. U-1461

SPACE SYSTEMS OPERATIONS

TECHNICAL NOTE

SOME AEROTHERMODYNAMIC CONSIDERATIONS FOR MARTIAN ENTRY AND HEAT SHIELD DESIGN

Prepared by: M. G. Boobar and R. M. Foster
Aerospace Mechanics Department

1 November 1961

AERONUTRONIC
A DIVISION OF Ford Motor Company
FORD ROAD / NEWPORT BEACH, CALIFORNIA

TABLE OF CONTENTS

SECTION		PAGE NO.
1	GENERAL CONSIDERATIONS	1
2	ENTRY HEATING	2
	2.1 Convective Heating	2
	2.2 Real Gas Effects	5
	2.3 Radiative Heat Transfer	7
	2.4 Effect of Environmental Uncertainties . . .	9
	2.5 Summary Comparisons and Design Criteria . .	11
3	HEAT SHIELD	
	3.1 Heat Protection System Selection	13
	3.2 Ablation Heat Shield	15
	REFERENCES	17

ABSTRACT

A study has been made of some of the aerothermodynamic considerations associated with entry into the Martian atmosphere and the heat shield requirements for such entries.

Previous investigators have concentrated on the determination of convective heat transfer rates. However, real gas effects, including their influence on radiant heat transfer and the characteristics of the plasma sheath, generally have been ignored. This investigation shows that radiation can contritube significantly to the total heating at the stagnation point for high angle, high velocity entry trajectories because of the CN which may be formed in the shock layer. A Mollier diagram and equilibrium concentrations of CN for an N_2-CO_2 system which typifies the reported Martian atmosphere are presented.

Convective and radiant heating rates for different entry velocities and angles are compared. Stagnation point electron densities and collision frequency values for the plasma sheath also are reported. After an analysis of the effects of uncertainties in the atmospheric properties (e.g., density gradients, composition, etc.) on entry heating, the requirements and criteria for the selection of a heat protection system are discussed. The study concludes with a preliminary heat shield design for a capsule capable of entering the Martian atmosphere.

SECTION 1

GENERAL CONSIDERATIONS

The design of a heat protection system for entry into the Martian atmosphere at first glance might appear to be a fairly routine task. Inasmuch as the surface density is reported to be an order of magnitude lower than that of the earth, the heat fluxes should be lower. Also the apparently inert atmosphere, alleged to consist mostly of nitrogen, should present a minimum of "real gas" problems.

A second and more careful look, however, discloses a number of factors which complicate the aerothermodynamic analysis. These include the real gas effects arising from the interaction of the nitrogen and carbon dioxide in the Martian atmosphere and their influence on radiative heat transfer and the transmission characteristics of the plasma sheath. The ultimate selection and design of the heat protection system will be influenced by these considerations plus those constraints imposed by uncertainties in the initial conditions and the atmospheric constants. These uncertainties include such inputs as the entry angle, entry velocity, density and density gradient of the atmosphere as a function of altitude, and the composition of the atmosphere; factors which usually are known with reasonable certainty for terrestrial reentry.

SECTION 2

ENTRY HEATING

The instantaneous entry heating rate is comprised of the net convective flux, $\dot{q}_c$, plus the net radiative flux, $\dot{q}_r$. The total heat input per unit area, Q, over a given trajectory is equal to:

$$Q = \int_0^t (\dot{q}_c + \dot{q}_r)\, dt$$

2.1 CONVECTIVE HEATING

Applying the theory of Lees[1], it can be shown that at the stagnation point:

$$\dot{q}_{cs} = 1.9 \times 10^{-8} \frac{\rho_\infty^{\frac{1}{2}} V_\infty^3}{R_N^{\frac{1}{2}}} \left[1 - 1.395 \frac{2 g_c J h_w}{V_E^2} \right]$$

where ρ_∞ = free stream density, slugs/ft^3

V_∞ = free stream velocity, ft/sec

V_E = entry velocity, ft/sec

R_N = noise radius, ft

g_c = universal gravitation constant, 32.2 ft/sec^2

J = mechanical equivalent of heat, 778 ft lbs/BTU

h_w = instantaneous wall enthalpy of the gas, BTU/lb

The turbulent heat transfer rates, $\dot{q}_{c_t}$, at the point of maximum heating ($P/P_s = 0.6$) has been shown to be[2]:

$$\dot{q}_{c_t} = 1.54 \times 10^{-7} \frac{\rho_\infty^{0.8} V_\infty^{3.19}}{R_N^{0.2}} \left[1 - \frac{1.705\ 2g_c\ J\ h_w}{V_E^2} \right]$$

and

$$\frac{h_{w_s} \neq 0}{h_{w_t} \neq 0} = \frac{1 - \dfrac{1.395\ 2g_c\ J\ h_w}{V_E}}{1 - \dfrac{1.705\ 2g_c\ J\ h_w}{V_E^2}}$$

The convective heating on the skirt at the sphere-cone intersection can be computed as follows:

$$\dot{q}_{skirt} = k\ \dot{q}_{max}$$

The variation in k as a function of the cone half-angle is as follows:

θ	$k_{laminar}$	$k_{turbulent}$
10°	0.18	0.40
15°	0.23	0.45
20°	0.28	0.54

In order to establish the most critical convective heating trajectory, it is necessary to determine the combination of entry conditions that produce the most adverse entry environment. If the preceeding convective heating equations are combined with equations describing the motion of the vehicle, the heat rate and total heating can be expressed in terms of the entry conditions, the ballistic parameter and the atmospheric constants. Since the entry angles of interest in this study were greater than 10°, the vehicle trajectory is adequately described by the analyses of Reference 3. The combination

of the heating and motion equations results in the following cold wall heating equations[4-6]. It should be noted that at the lower entry angles, the assumption of a constant entry angle implicit in the trajectory analysis is in error, and the parametric expressions underestimate the actual heating.

$$\dot{q}_s = 7.2 \times 10^{-9} \left[\frac{\beta \ (m/C_D A) \ \sin \theta_E}{R_N} \right]^{\frac{1}{2}} V_E^{\ 3}$$

where $\dot{q}_s$ = maximum stagnation heat flux, BTU/ft^2 sec

β = atmospheric density gradient, ft^{-1}

$m/C_D A$ = ballistic coefficient, slugs/ft^2

V_E = entry velocity, ft/sec

θ_E = entry angle

R_N = nose radius

When

$$\frac{\rho_o}{\beta \ (m/C_D A) \ \sin \theta_E} > 6$$

where ρ_o = sea level density, slugs/ft^3

$$Q_{total\ stag} = 3.6 \times 10^{-8} \left[\frac{(m/C_D A)}{R_N \beta \sin \theta_E} \right]^{\frac{1}{2}} V_E^{\ 2}$$

Similarly,

$$\dot{q}_{turb\ max} = 2.5 \times 10^{-7} \frac{\left[\beta \ (m/C_D A) \ \sin \theta_E \right]^{0.8}}{R_N^{\ 0.2}} V_E^{\ 3}$$

and

$$Q_{total\ turb} = 1 \times 10^{-6} \frac{(m/C_D A)^{0.8}}{(R_N \beta \sin \theta_E)^{0.2}} V_E^{\ 2}$$

Therefore

$$\frac{\dot{q}_s}{q_{t_{max}}} = \frac{3 \times 10^{-2}}{(R_N \beta \sin\theta_E \; m/C_D A)^{0.3}}$$

and

$$\frac{Q_{stag}}{Q_{turb\ max}} = \frac{3.6 \times 10^{-2}}{\left[R_N \beta \sin\theta_E \; (m/C_D A)\right]^{0.3}}$$

These relationships were applied to calculate the instantaneous and integrated convective heat fluxes. Figures 1a, 1b, and 1c show the instantaneous heat fluxes for the following typical trajectory conditions:

$m/C_D A = 1$

$R_N = 1$ ft

$\beta = 0.17 \times 10^{-4}$ ft^{-1} (Atm. E) and 0.324×10^{-4} ft^{-1} (Atm. C)

$V_E = 22{,}000$ ft/sec and 26,000 ft/sec

$\theta = 90^\circ$ and 20°

2.2 REAL GAS EFFECTS

Real gas effects must be considered in the aerothermodynamic analysis of Martian entry inasmuch as they significantly influence the radiant transport and communications during the entry period.

a. Mollier Diagram

Inasmuch as the real gas temperature is a parameter common to radiation, electron density, and collision frequency computations, the first step was to generate a Mollier diagram. An "average" Martian atmosphere consisting of 1.9% CO_2 and 98.1% N_2 by volume was selected as the basis for the chart and the resulting P-H-T-S equilibria conditions for this atmosphere are shown in Figure 2. The effect of varying the composition of the atmosphere was investigated at two pressures for one temperature. The results were as follows:

Species		Pressure	Temperature	Enthalpy	Entropy
CO_2 (%)	N_2 (%)	(atm.)	(°K)	(BTU/lb)	(cal/gm °K)
0.7	99.3	1	4500	2367	2.42
1.9	98.1	1	4500	2389	2.44
7.2	92.8	1	4500	2482	2.48
0.7	99.3	10	4500	2318	2.25
1.9	98.1	10	4500	2335	2.27
7.2	92.8	10	4500	2395	2.31

The data were obtained by employing the Aeronutronic IBM-709 Free Energy Method Program for equilibrium compositions. Eqilibrium data[7] for nitrogen are superimposed on the chart for comparative purposes.

b. Entry Communications Parameters

The computation of the entry communications parameters under quasi-steady state conditions (i.e., electron densities and collision frequencies) requires a knowledge of the boundary layer and shock layer temperatures, pressures, and species concentrations. Given a trajectory, the real gas temperatures and pressures at the stagnation point can be obtained readily with the aid of a Mollier diagram. This has been done for a typical trajectory and the results are shown in Figure 3. Temperature and pressure distributions at the skirt and in the wake are shape dependant and ultimately require the development of a flow field. The angle of attack, if any, the oscillation frequency and amplitude must be considered. The effort indicated was beyond the scope of this preliminary study.

The other parameter required for computing electron densities are the species concentrations. The computer program, which obtained the thermodynamic input data, also printed out the equilibrium concentrations of over 20 species for each temperature-pressure input point. The time available did not permit these data to be graphed. However, inspection of the data indicated the presence of significant concentrations of carbon vapor and NO. These species have relatively low ionization potentials as compared to the bulk of the gas (which consists primarily of N_2 and N) and would contribute significantly to the electron density concentrations at "low" temperatures. On the other hand, because of the relatively "high" temperatures ($\gtrsim 4500°$ K) and the limited time available, an "average" ionization potential of 14 e.v. was selected rather than to examine the contribution of each species separately. Thus, the lower limit

on the equilibrium, stagnation point electron densities was obtained, using the methods described in References 8 and 9 for the trajectory employed in Figure 3. The data are plotted as a function of time and altitude in Figure 4. The electron densities encountered for this and other trajectories ($\theta_E = 20^o$ and 90°, and V_E = 22,000 and 26,000 ft/sec) indicate a probable transmission blackout (based on stagnation conditions) from altitudes above 800,000 ft to below 150,000 ft. It should be noted that conditions on the skirt and rear probably will not be as severe.

2.3 RADIATIVE HEAT TRANSFER

The computation of the radiative heat transfer includes the consideration of a number of real gas effects. However, because of the nature of the results and their implications, radiative heat transfer will be treated separately.

The radiation heat input to a vehicle from the gas cap can be defined as:

$$\dot{q}_r = \alpha \epsilon_g \sigma T^4$$

where α = absorptivity of the surface

ϵ_g = effective emissivity of the gas cap

σ = Stefan-Boltzman constant

T = temperature of the gas

The effective emissivity of the gas cap, ϵ_g, represents the summation of the emissivity of all the significant species contributing to the radiation at the temperatures encountered ($\epsilon_g - \sum_i \epsilon_i$). Thus, the species resulting from the interaction of CO_2 and N_2 were examined for their radiative contribution. Typical of the 24 species were: (a) O_2(S-R) and NO_β and $_\alpha$ of the broad band system, (b) CN red and violet, N_2 second positive, N_2 first positive, N_2^+ first negative, CO, NO vibration-rotation and CO_2 of the semi-sharp band systems, and (c) O, N, NO, A, O_2, N_2, N^+, O^+ of the Kramers class. Carbon was not considered.

Over the range of temperatures and pressures of interest the radiation contributed by CN red and violet was dominant. The emissivity per unit length (ϵ_i/ℓ) for each species from one side of an optically thin plane, as well as the coefficient for each species, have been given by Kivel and Bailey.[10] Thus for CN

$$(\epsilon/\ell)_{red} = X_{CN}\ (P/T)\ 1.365 \times 10^2 \left[\frac{5 \times 10^2}{\ell^{13000/T}\ (T \times 10^{-4})^4}\right]$$

and

$$(\epsilon/\ell)_{violet} = X_{CN}\ (P/T)\ 1.365 \times 10^2 \left[\frac{1 \times 10^4}{\ell^{36000/T}\ (T \times 10^{-4})^4}\right]$$

where X_{CN} = mol fraction of CN in gas

P = stagnation pressure, atm.

T = temperature, K^o

The equilibrium concentrations of CN for the system 1.9% CO_2-98.1% N_2 as a function of temperature and pressure have been taken from the computer runs and are shown in Figure 5.

Figure 6 shows how (ϵ/ℓ) varies as a function of time for entry into such an atmosphere at V_E = 22,000 ft/sec and $\theta_E = 90^o$. Also shown for comparative purposes, are the equivalent (ϵ/ℓ) values for entry into an "air" atmosphere and a single point for a 7.2% CO_2 atmosphere. The (ϵ/ℓ) values for the Martian atmosphere are an order of magnitude, or more, higher for the Martian atmosphere than they would be for air due to the formation of CN behind the shock. This analysis is borne out by shock tube results[11] which demonstrate experimentally that the presence of CN can raise the radiant intensity of hot nitrogen (6100° K) by approximately an order of magnitude.

The thickness of the gas cap, ℓ, at the stagnation point has been shown by Li and Geiger[12] to be:

$$\ell = \frac{(\rho_\infty/\rho_s)\ R_N \left[1 - \sqrt{(\rho_\infty/\rho_s)(2 - \rho_\infty/\rho_s)}\right]}{(1 - \rho_\infty/\rho_s)^2}$$

where ρ_∞ = free stream density

ρ_s = stagnation point density

R_N = nose radius, cm

For the nose radii, temperatures and pressures encountered in this study it was assumed that there was no self absorption. There are a number of other factors which affect radiation. These include the

geometry of the vehicle; the fact that ϵ_g cannot exceed 1.0, no matter how thick the gas cap; and the fact that the radiant energy cannot exceed the stagnation energy.

Non-equilibrium conditions can increase the radiant heat transfer rates over those at equilibrium by as much as an order of magnitude.[13] Non-equilibrium conditions are more likely to occur at low densities (high altitudes) when the collision frequencies are low (e.g., slip and free molecular flow regimes). The maximum stagnation pressures encountered in Martian entry are one to two orders of magnitude lower than those normally achieved by an ICBM and, hence, so are the collision frequencies. The area of non-equilibrium radiation and its effect on heat transfer requires further study.

In summary, although the radiation heat transfer rates reported in this study are based on the analytical techniques available at present, there are many uncertainties (beyond those which will be discussed in the following section) regarding the precise magnitudes. Furthermore, test data at the conditions of interest also is meager. However, this study does point out that the potential for a large radiative heat flux contribution does exist at high angle entries into the Martian atmosphere. This flux is due primarily to the pressure of CN, a high-temperature reaction product of CO_2 and N_2. Figure 7 shows the comparative stagnation point radiative and convective heat fluxes for 90° entry at 22,000 and 26,000 fps in the two atmospheres for a one ft nose radius. It should be noted that doubling the nose radius decreases the convective flux by a factor equal to $\sqrt{2}$ and doubles the radiative flux.

2.4 EFFECT OF ENVIRONMENTAL UNCERTAINTIES

There is an uncertainty factor of two in the values of β (density gradient) reported for the Martian atmosphere. The lowest β atmosphere (Atmosphere E) was employed for the heat transfer calculations. β for Atmosphere C is approximately equal to twice β_E ($\beta_C = 2\beta_E$). The effect of this uncertainty on entry heating may be evaluated approximately, as follows:

a. <u>Laminar, Stagnation Point Heating</u>

$$\dot{q}_s \sim \sqrt{\beta}$$

or

$$\dot{q}_{atm\ C}/\dot{q}_{atm\ E} \simeq 1.41$$

and $$Q_{total} \sim 1/\sqrt{\beta}$$

or $$Q_{atm\ C}/Q_{atm\ E} \simeq 0.707$$

b. Turbulent Heating at $P/P_s = 0.6$

$$\dot{q}_t \sim \beta^{0.8}$$

or $$\dot{q}_{atm\ C}/q_{atm\ E} \simeq 1.74$$

and $$Q_{total} \sim 1/\beta^{0.2}$$

or $$Q_{atm\ C}/Q_{atm\ E} \simeq 0.87$$

c. Altitude of Maximum Convective Heating

$$y_{\dot{q}_{max}} \sim \frac{1}{\beta} \ln \frac{1}{\beta}$$

or $$y_{\dot{q}_{mac\ C}}/y_{\dot{q}_{max\ E}} \simeq 0.724$$

where $$y_{\dot{q}_{max\ stag}} \neq y_{\dot{q}_{max\ turb}}$$

d. Radiative Heating

The radiative pulse is a complex function of many variables including the density, CN concentration, and temperature. The form of the equation is not readily reducible to function of β. A comparison at peak dynamic pressure is presented in the next section.

In summary, our computations are based on Atmosphere E, which is representative of the lower limit in β. An increase in β (e.g., atomsphere C) would lead to higher peak heat fluxes but lower total heating loads. Numerical comparisons are presented in Section 2.5.

2.5 SUMMARY COMPARISONS AND DESIGN CRITERIA

Table I summarizes the pertinent aerothermodynamic entry parameters for extremes in entry velocity, entry angle, atmospheric density and density gradients.

As was expected, low angle entry yields lower peak fluxes but higher total convection loads. The predicted heating relationships between Atmosphere C and E were borne out by the machine computations. The instantaneous radiative heat pulse, $\dot{q}_r$, follows the same trend as $\dot{q}_c$ with increased velocity and β. The maximum radiative pulse lags the maximum stagnation point convective pulse in time; and is the reason for tabulating the radiative pulse at maximum dynamic pressure. However, it should be noted that the radiative pulse at maximum dynamic pressure, although close to the maximum, does not necessarily represent $\dot{q}_{r,max}$. At low angle entry, the radiative pulse is small and becomes insignificant when compared to the total integrated pulse. At high angle entry, the maximum radiative pulse may exceed the maximum convective pulse by a factor of two, or more. Fortunately, the effective time duration of this pulse is short and varies inversely with the magnitude. Again it would be noted that although there may be considerable uncertainty as to the precise values of the radiative contribution, the potential radiative heat transfer contribution for high angle Martian entry is significant. This factor previously has been overlooked, by most workers. It is also worth noting that although the convective flux varies inversely with the square root of the nose radius, the radiative flux is nearly proportional to R_N. Future studies to optimize the heat shield weight should consider possible tradeoffs in this area.

With regard to design criteria for the heat protection system, the uncertainties in entry velocity, entry angle and the Martian atmosphere dictate that the shield be designed for the most adverse conditions. At the stagnation point a total heating load in the order of 9000 BTU/ft^2 must be accommodated ($R_N \sim 2$ ft; $V_E < 26{,}000$ fps; $\theta_E > 20^o$). The materials selected for the nose cap should be capable of withstanding instantaneous (maxima) convective fluxes in the order of 500 BTU/ft^2 sec (laminar or turbulent) and radiative fluxes in the order of 3500 BTU/ft^2 sec ($V_E = 26{,}000$; $\theta_E = 90^o$; $R_N \sim 2$ ft; Atmosphere C). These fluxes will not necessarily occur at the same time. Flight Reynolds numbers in the order of one million appear possible for the trajectories and configurations selected, and thus, turbulent heating must be considered. The maximum total flux, Q, at the point of maximum turbulent heating ($\sim 45^o$) will be 8000 BTU/ft^2 and the maximum convective load turbulent on the skirt will be 2800 BTU/ft^2 ($V_E < 26{,}000$; $\theta_E > 20^o$; Atmosphere E).

It should be noted that for purposes of this preliminary analysis, radiative heating beyond the 45° station is assumed negligible because of the expansion of the gas and its consequent drop in temperature. It also should be noted that the ablation rates will not be uniform because of the uneven heat loads and, hence, the effect of the potential changes in the shape on the aerodynamic coefficients must be evaluated.

SECTION 3

HEAT SHIELD

3.1 HEAT PROTECTION SYSTEM SELECTION

The general categories of heat protection systems within the present state of the art which are suitable as heat shields for ballistic entry into the Martian atmosphere may be described as heat sinks, radiators and ablators.

Heak sinks and most radiator materials are limited by their physical properties (e.g., melting point, specific heat, thermal conductivity, etc.) as to the magnitude and duration of the thermal pulse ($\dot{q}$) which they can accommodate. Because of the inherent uncertainties in the entry heat fluxes and loads described previously, the conventional metal heat sink must be rejected immediately because of its relatively low heat capacity ($\lesssim$1000 BTU/lb for beryllium) and its inability to accept the potentially high combined radiative and convective fluxes (even with such excellent conductor materials as copper). Essentially these same objections, plus others including "low" equilibrium temperatures, uncertainties in surface emissivity and absorptivity coefficients, and the usual gamut of mechanical behavior, stress, attachment, support, fabrication, and handling problems, can be raised against the selection of a "simple", metallic, equilibrium temperature radiator. This, however, does not preclude consideration of a composite radiator--heat sink-ablator, such as pyrographite, from future studies.

Ablation materials, on the other hand, have demonstrated the capability to accommodate the long-time duration, low-$\dot{q}$ pulses associated with shallow-angle entry on Mercury type trajectories and the high-$\dot{q}$, short-time pulses of ICBM reentry missions. Thus, ablation appears to be well within the state of the art required to satisfy the

heat shield requirements for the Martian entry trajectories of interest and the matter of an ablating heat shield was pursued further.

The choice in ablation materials lay between the reinforced thermosetting plastics which pyrolize and form a carbonaceous char upon heating (e.g., phenolics and epoxies) and the thermoplastics which depolymerize, liquify and/or vaporize on heating without forming a char on the surface (e.g., Teflon, nylon, polyethylene). The prime advantage of the latter is in that some thermoplastics like Teflon retain their dielectric properties upon heating and therefore also function as antenna windows. However, with the high electron densities encountered, transmission through the plasma sheath during entry is questionable. The thermosetting materials form a conductive char and lose this transmission capability. On the other hand, this char permits the attainment of much higher surface temperatures than is possible with the thermoplastic materials. These higher surface temperatures result in reduced convective heat transfer to the surface and increased reradiation rates.

The potentially high radiation fluxes associated with the high angle entry angles present a new problem area. In a convective heating environment, ablators function as heat shields by (a) exhibiting an endothermic heat of reaction on decomposition which acts to absorb that heat which is transmitted to the surface, (b) emitting or transpiring gaseous (and liquid) products of decomposition into the boundary layer to "block" or reduce the convective heat transfer rate, and (c) operating at a sufficiently high surface temperature to reradiate significant quantities of energy and to reduce the driving potential (e.g., ΔT) of the transport process. The relative importance of each of these mechanisms is dependent upon the material. (Because of their low conductivities, most ablators generally do not have any appreciable "heat sink" capacity in the high flux-short time trajectories.) In a radiative heat transfer the mechanisms and hence desired properties include (a) high endothermicity, (b) low absorbtivity surface, (c) high temperature, high emissivity surface backed by low conductivity material. In the case of ablators, a portion of the incident radiant energy to the surface also may be "blocked" if the nature of the ablation products is such that they are at least partially opaque to the emitted wavelengths, thereby reflecting or absorbing some of the energy destined for the surface.

Understanding of the behavior of plastics in a radiation environment is meager. Resins which char, or which exhibit any tendency to char upon pyrolysis, can not be counted upon to reflect the incident radiative energy. However, thermosetting materials which carbonize may be relied upon to re-radiate a significant portion of the incident flow. The endothermicity of the ablation process is an interent property of the material whereas, theoretically, the potential opacity of thermosetting decomposition products is higher than those of thermoplastic materials.

3.2 ABLATION HEAT SHIELD

In analyzing the heat shield requirements, the shield was divided into three zones. These were the stagnation point region, the 45° station or zone of maximum turbulent heat transfer, and the skirt. The weights needed for each zone in the critical convective and radiative heating environments were calculated separately. The final shield design, although not necessarily an optimum one, will adequately protect the capsule should it enter the Martian atmosphere at an angle between 20° and 90° at a velocity of less than 26,000 ft/sec with a $m/C_DA \ll 1$. Also considered, for comparative purposes, were the heat shields which would be required if the entrance angle were known, a priori.

The ablation and insulation requirements were determined separately. For convective heating, the mass ablated was obtained by dividing the total cold wall convective heat input, Q_c, by the total effective heat of ablation, Q^*. For the radiative flux, Q_r, the effective endothermicity of phenolic-nylon was estimated to be 1500 BTU/lb. For structural and attachment purposes, it was assumed that there must be at least 0.1 inches of virgin ablation material at the point of maximum deceleration. The thickness of insulation was determined by the mass of insulation required to prevent the inside wall temperature from exceeding 300° F when the vehicle had decelerated to Mach 1.

The properties of the several materials considered are given in Table II. Both phenolic-nylon (P-N) and polyethylene gave lower shield weights than Teflon. P-N finally was chosen over polyethylene because its higher turbulent Q^*, higher surface temperature for reradiation, and the potential "blocking" of the radiative pulse by its decomposition products. Because of the uncertainties regarding the magnitude of the radiative heating it was decided that an additional factor of safety could be achieved at the stagnation point and at the 45° station if P-N also was employed as the insulation backing for 90° entry. At the skirt, the weight could be reduced by resorting to a composite heat shield. Thus, the P-N ablator was backed by Johns-Manville Min-K 2000 insulation, the latter being representative of a class of high temperature, high compressive strength, low density insulation materials.

The shield weights, as a function of body station, for 20° and 90° entry angles and the two extremes in atmospheric density gradients are compared in Table III. Case D selects the worst features of each of the previous cases to determine the weight of a shield required to survive any entry between 20° to 90° at velocities below 26,000 fps ($m/C_DA \ll 1$).

At this point, a brief comment on refractory heat shield materials is in order. One of the best of these materials is pyrographite. For the parameters considered in this study, pyrographite will behave more as a radiator than as an ablator or heat sink. A very approximate calculation indicated that a composite nose-cap consisting of a pyrographite radiator and a high temperature, high compressive strength insulator would weigh approximately 4 lb/ft^2 as compared to 7.5 lbs/ft^2 for P-N. A number of potential problems are associated with such a system; the most significant probably lie in the areas of thermal stress, attachment, support, fabrication and handling. Although a pyrographite radiator appears promising as a heat shield material, a detailed study would be required to properly evaluate its ultimate feasibility. On the other hand, there are a number of other unresolved problems concerning Martian entry which also require additional research and development. They include a closer look at the radiation phenomena, preferably backed up by an experimental program wherein chemical and environmental simulation could be achieved in an arc plasma facility. If the final heat shield selected was ablator, the materials should be subjected to high vacua and ultraviolet radiation environments for extended periods to evaluate possible degradation effects during the long transit period.

REFERENCES

1. Lees, Lester, "Laminar Heat Transfer Over Blunt-Nosed Bodies at Hypersonic Flight Speeds", Jet Propulsion, 26, 4 (April 1956), 259-69.

2. Sibulkin, Merwin, "Estimation of Turbulent Heat Transfer At The Sonic Point of a Blunt-Nosed Body", Jet Propulsion, 28, 8 (August 1958), 548-554.

3. Allen, J. Julian and Eggers, A. J., Jr., A Study of the Motion and Aerodynamic Heating of Missiles Entering the Earth's Atmosphere At High Supersonic Speeds, NACA TN 4047, October 1957.

4. Chapman, D. R., An Approximate Analytical Method for Studying Entry Into Planetary Atmospheres, NACA TN 4276, May 1958.

5. Roberts, Leonard, An Analysis of Nose Ablation for Ballistic Vehicles, NASA TN D-254, April 1960.

6. Brunner, M. J., "Analysis of the Aerodynamic Heating for a Re-Entrant Space Vehicle", Journal of Heat Transfer (August 1959), 223.

7. Treanor, C. E. and Logan, J. G., Jr., Thermodynamic Properties of Nitrogen from 2000° to 8000° K, Cornell Aeronautical Laboratories, Buffalo, New York, Report No. BE-1007-A-5, January 1957.

8. Boobar, M. G., Determination of Electron Densities and Collision Frequencies in the Shock Layer, General Electric Company, MSVD, Advanced Engineering Memo. No. 3, March 6, 1958.

9. Friel, P. J. and Boobar, M. G., The Electron Densities and Electrical Conductivity of Gases with Ionization Potentials Between 3 and 15 Electron Volts, General Electric Company, MSVD, Aerosphysics Engineering T.M. No. 150, January 1960.

10. Kivel, B. and Bailey, K., Tables of Radiation From High Temperature Air, Avco Report 21, December 1957.

11. Allen, R. A., et al., Radiation From Hot Nitrogen, Avco Research Report 102, April 1961.

12. Li, T. Y. and Geiger, R. E., "Stagnation Point of a Blunt Body in Hypersonic Flow", J. Aero. Sci., 24, 1 (January 1957).

13. Camm, J. C., et al., Absolute Intensity of Non-Equilibrium Radiation In Air and Stagnation Heating at High Altitude, Avco Laboratory Report 93, December 1953.

TABLE I

SUMMARY OF AEROTHERMODYNAMIC PARAMETERS

Atm	m/C_DA	V_E (fps)	θ_E (°)	Time (sec)	Alti. (k-ft)	P_{stag} (atm)	H_{stag} BTU/lb	T_{stag} (°K)	$q_{c_s}(R_N)^{\frac{1}{2}}$ BTU/ft$^{3/2}$sec	Ne^- e^-/cm^3	col./sec	$Q_{c_{total}}(R_N)^{\frac{1}{2}}$ BTU/ft$^{3/2}$
					AT MAXIMUM CONVECTIVE STAGNATION POINT HEATING							
E	1	22,000	20	114	326	0.189	7450	6050	135	2×10^{14}	1×10^{9}	8500
			90	35.5	230	0.99	6500	6300	280	3×10^{14}	6×10^{10}	4000
E	1	26,000	20	100.5	325	0.255	10000	6400	215	6×10^{14}	2×10^{9}	12250
			90	30.1	224	1.42	9750	7100	490	8×10^{14}	8×10^{10}	5500
C		26,000	90	32.9	143	2.55	10200	7400	700	3×10^{14}	1×10^{11}	3900
									q_r/R_N BTU/ft^{3}sec	$Q_{r_{total}}/R_N$ BTU/ft^3	Stag. Point $Q_c + Q_r@R_N=25.5''$ BTU/ft^2
					STAGNATION POINT RADIATIVE HEAT FLUX AT MAXIMUM DYNAMIC PRESSURE							
E	1	22,000	20	133	265	0.302	4050	4950	8	nil	5850	
			90	38.9	167	1.44	3960	5700	240	1420	5740	
E	1	26,000	20	120.5	262	0.36	4760	5200	23	nil	8400	
			90	32.6	174	2.02	6100	6400	625	2500 est.	9100	
C	1	26,000	90	34.9	105	4.1	4470	6200	1630	2900	8820	

TABLE II

MATERIAL PROPERTIES

	ρ lb/ft^3	C_p BTU/lb ^oF	K BTU/sec ft ^oF	T_D* ^oF	T_s** (^oF)	Q* (BTU/lb)	
						Laminar	Turb
Teflon	135	0.25	4.0×10^{-5}	1180	1180	3000	1500
Polyethylene	59	0.55	5.4×10^{-5}	775	775	4000	2500
Phenolic-Nylon	75	0.3	8.3×10^{-5}	1400	3000-4000	4000	4000
Pyrographite	137	0.3	5×10^{-5}	6600	--	--	--
Min-K 2000	20	0.2	1×10^{-5}	--	--	--	--

* T_D = decomposition temperature

** T_s = surface temperature

TABLE III

SUMMARY OF HEAT SHIELD THICKNESSES AND WEIGHT REQUIREMENTS

	Q_c BTU/ft^2	Q_R BTU/ft^2	Q_{total} BTU/ft^2	Ablation Thickness	Insulation Thickness	Total Weight lb/ft^2
CASE A - $\theta_E = 90^\circ$; V_E = 26,000 fps; $m/C_DA = 1$; Atmosphere C; R_N = 25.5 inches						
Stagnation Point	2670	6150	8820	← 1.2 inches P-N →		7.5
45° Station	3800	4100*		← 1.0 inches P-N →		6.25
Skirt	1520	nil	1520	0.15" P-N	0.3" Min-K	1.5
CASE B - $\theta_E = 90^\circ$; V_E = 26,000 fps; $m/C_DA = 1$; Atmosphere E						
Stagnation Point	3760	5300	9060	← 1.1 inches P-N →		6.9
45° Station	4350	3500*		← 1.0 inches P-N →		6.25
Skirt	1750	nil	1750	0.17" P-N	0.3" Min-K	1.6
CASE C - $\theta_E = 20^\circ$; V_E = 26,000 fps; $m/C_DA = 1$; Atmosphere E; R_N = 25.5 inches						
Stagnation Point	8400	nil	8400	0.34" P-N	0.8" P-N / 0.4" Min-K	7.5 / 2.8
45° Station (turb)	7000	nil	7000	0.28	0.7" P-N / 0.4" Min-K	6.25 / 2.5
Skirt (turb)	2800	nil	2800	0.2	0.4" Min-K	2.0
CASE D - $\theta_E = 20^\circ$ to 90°; V_E = 26,000 fps; $m/C_DA = 1$; Atmospheres C and E; R_N = 25.5"						
Stagnation Point	--	--	--	← 1.2 inches P-N →		7.5
45° Station	--	--	--	← 1.0 inches P-N →		6.25
Skirt	--	--	--	0.2	0.4" Min-K	2.0

* Estimated at 2/3 Q_R at stagnation point.

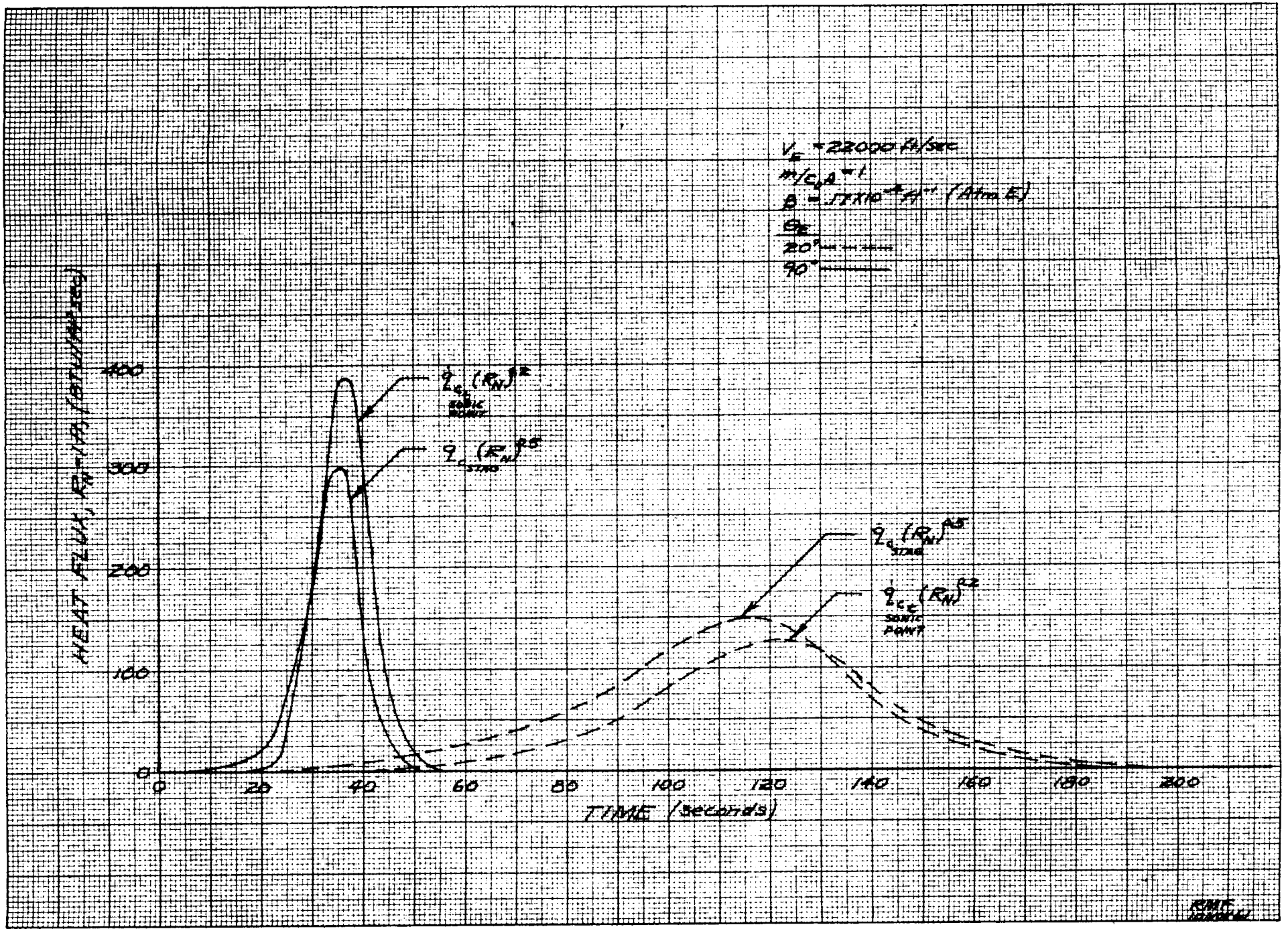

FIGURE 1a MARINER-B CAPSULE ENTRY CONVECTIVE HEAT FLUX

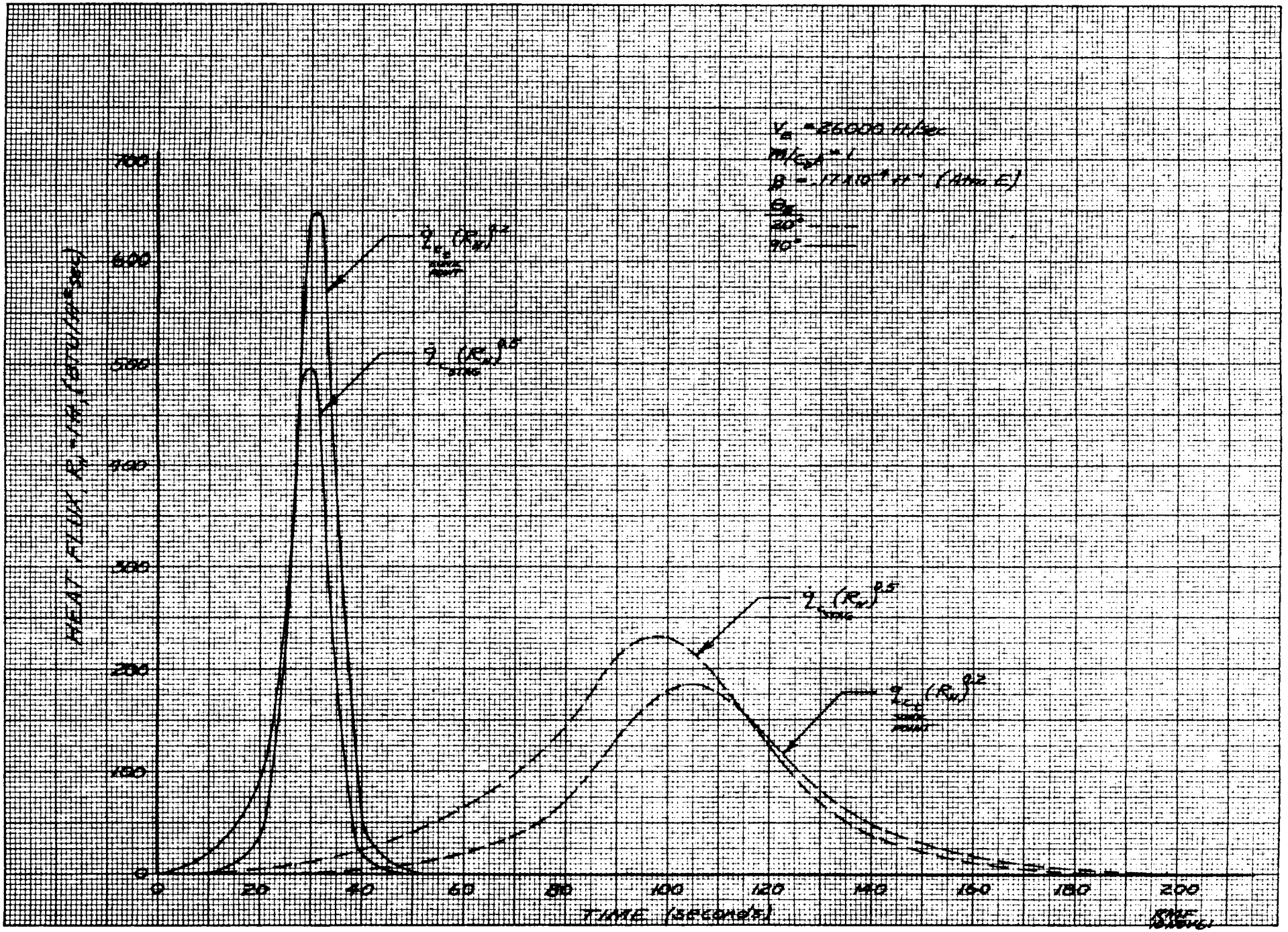

FIGURE 16 MARINER-B CAPSULE ENTRY CONVECTIVE HEAT FLUX

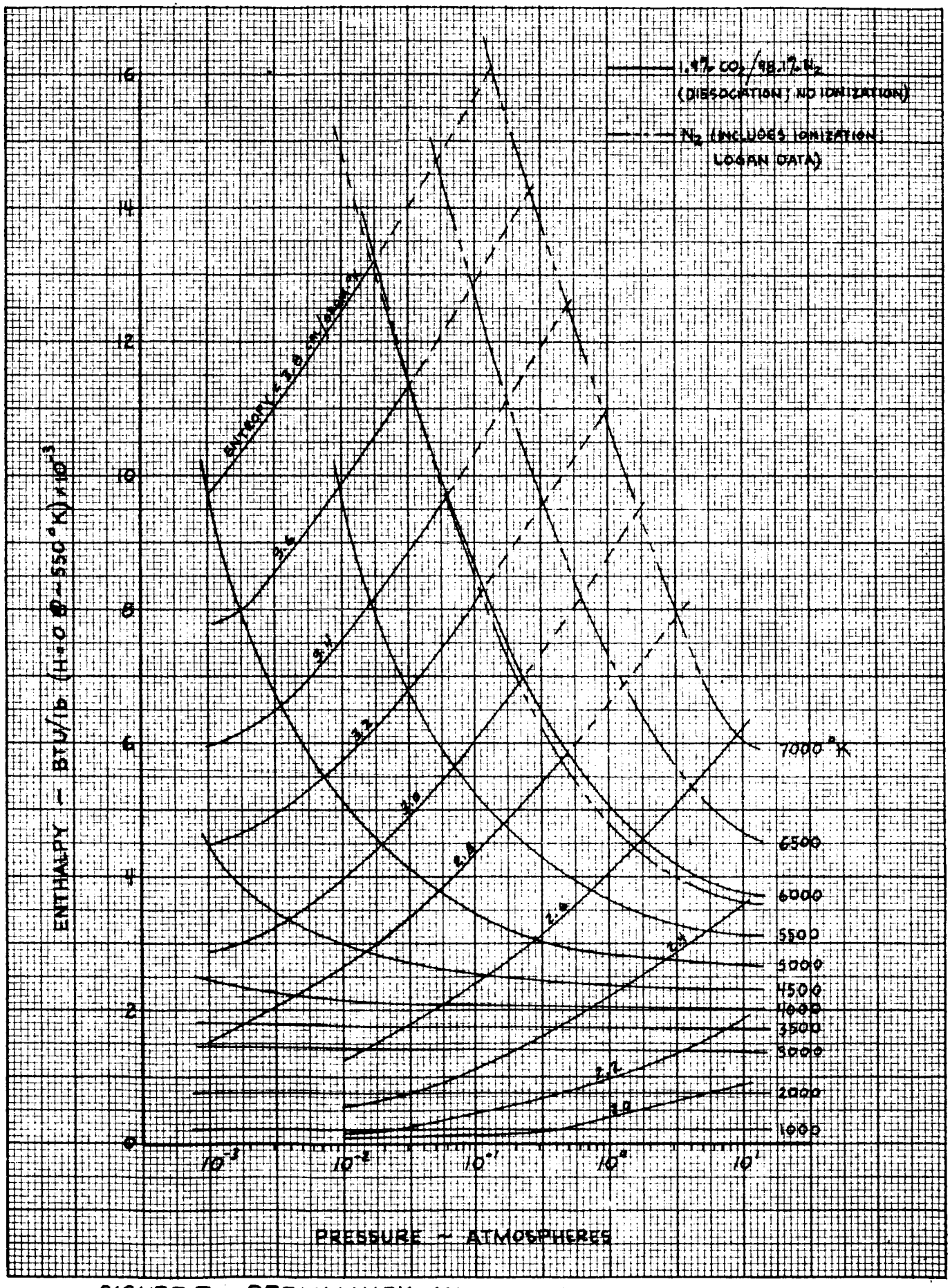

FIGURE 2 PRELIMINARY MOLLIER DIAGRAM FOR MARTIAN ATMOSPHERE

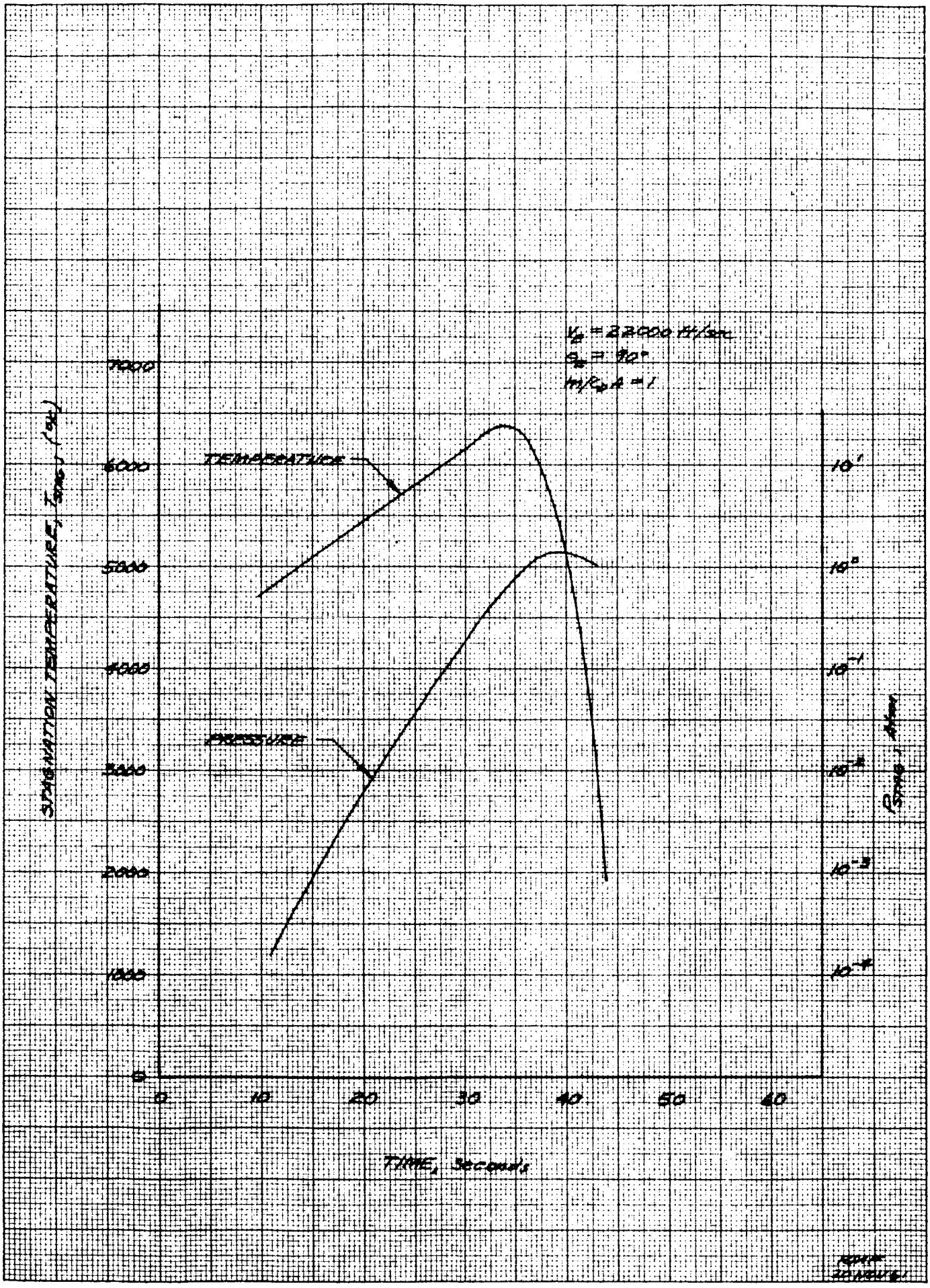

FIGURE 3 MARS ENTRY - PRESSURE AND TEMPERATURE AT THE STAGNATION POINT

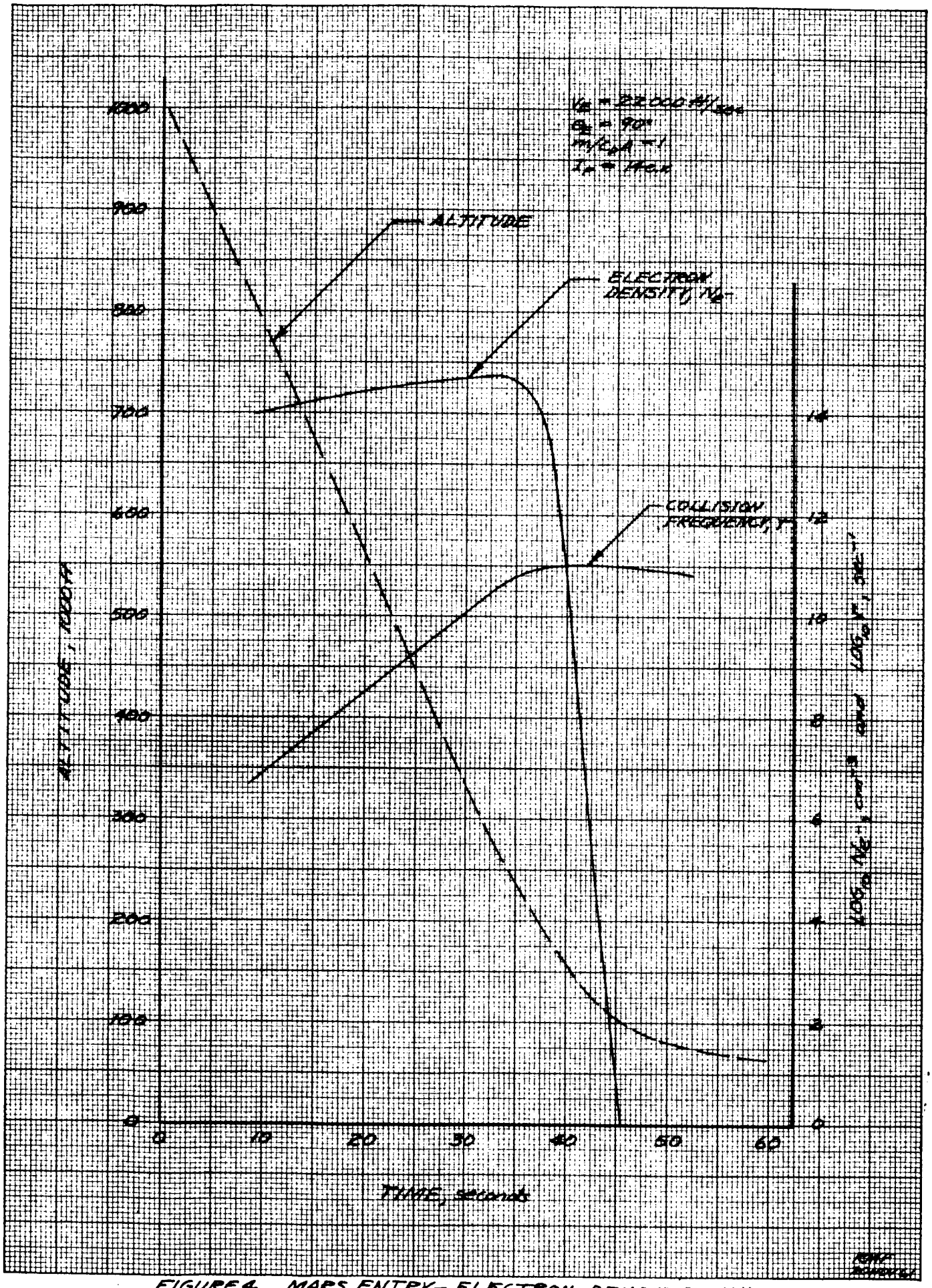

FIGURE 4 MARS ENTRY – ELECTRON DENSITIES AND COLLISION FREQUENCIES AT THE STAGNATION POINT

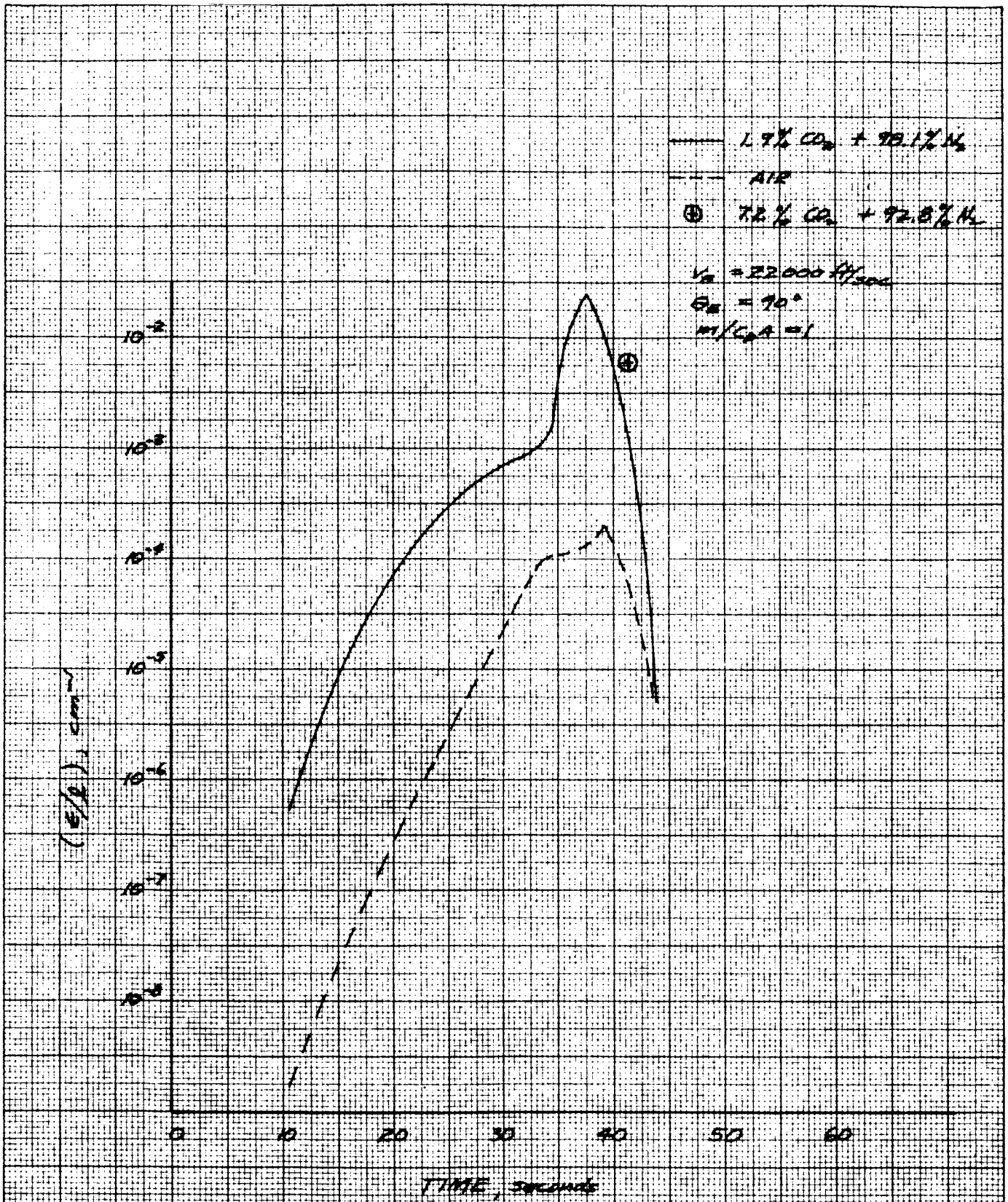

FIGURE 6. MARS ENTRY – GAS EMISSIVITY AT THE STAGNATION POINT

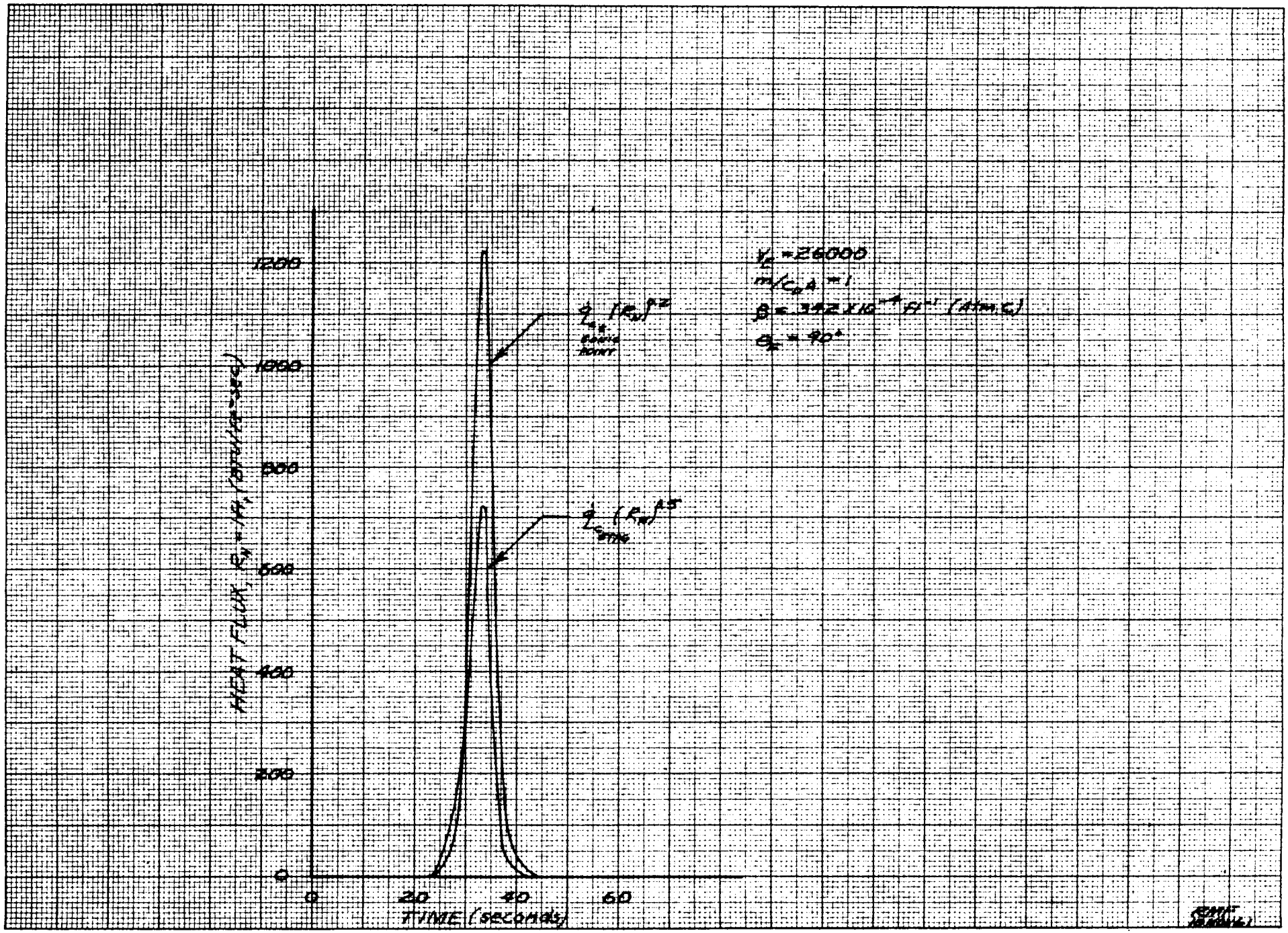

FIGURE 1c MARINER-B CAPSULE ENTRY CONVECTIVE HEAT FLUX

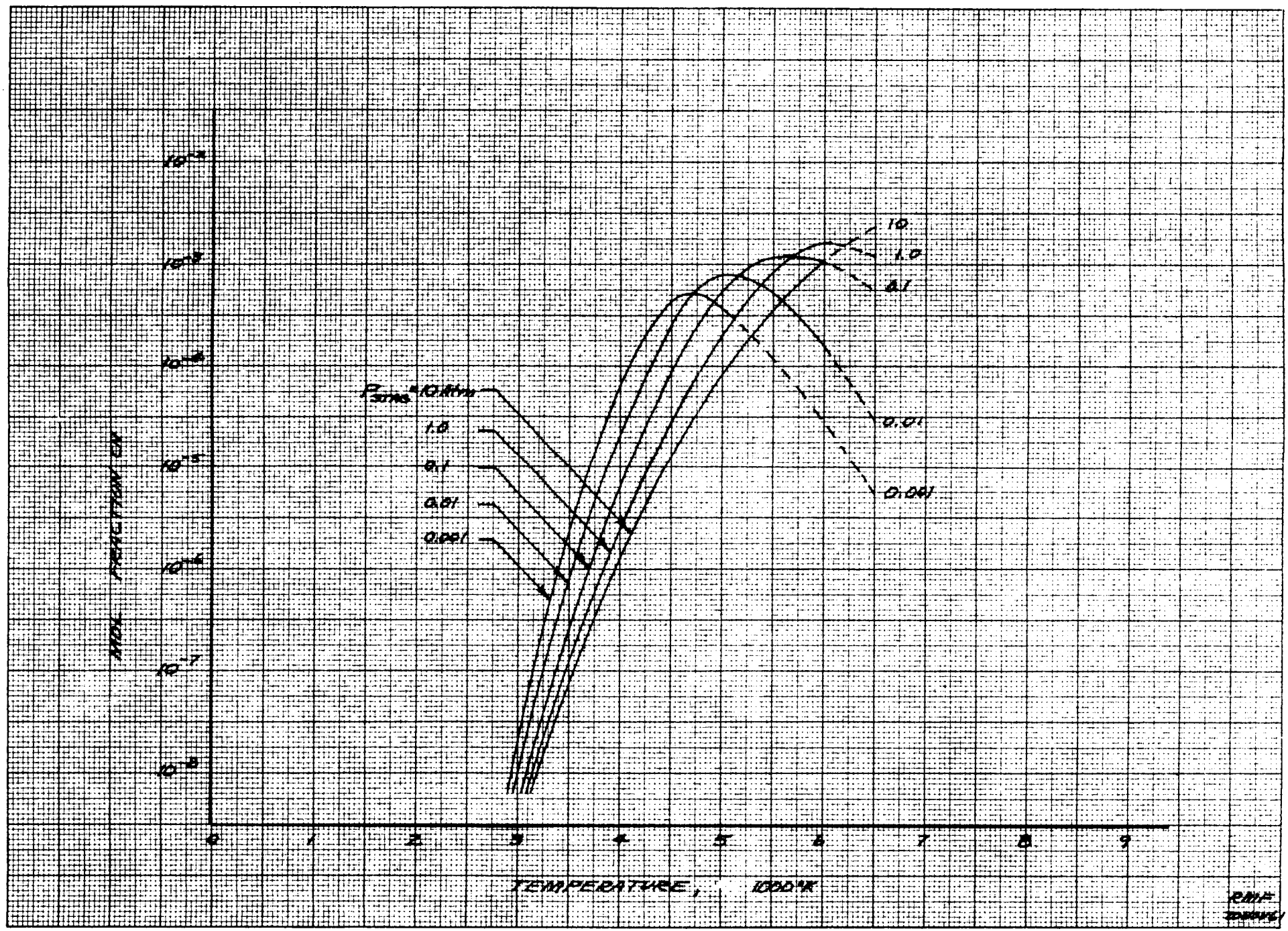

FIGURE 5 MARS ENTRY - MOL FRACTION OF CN AT THE STAGNATION POINT

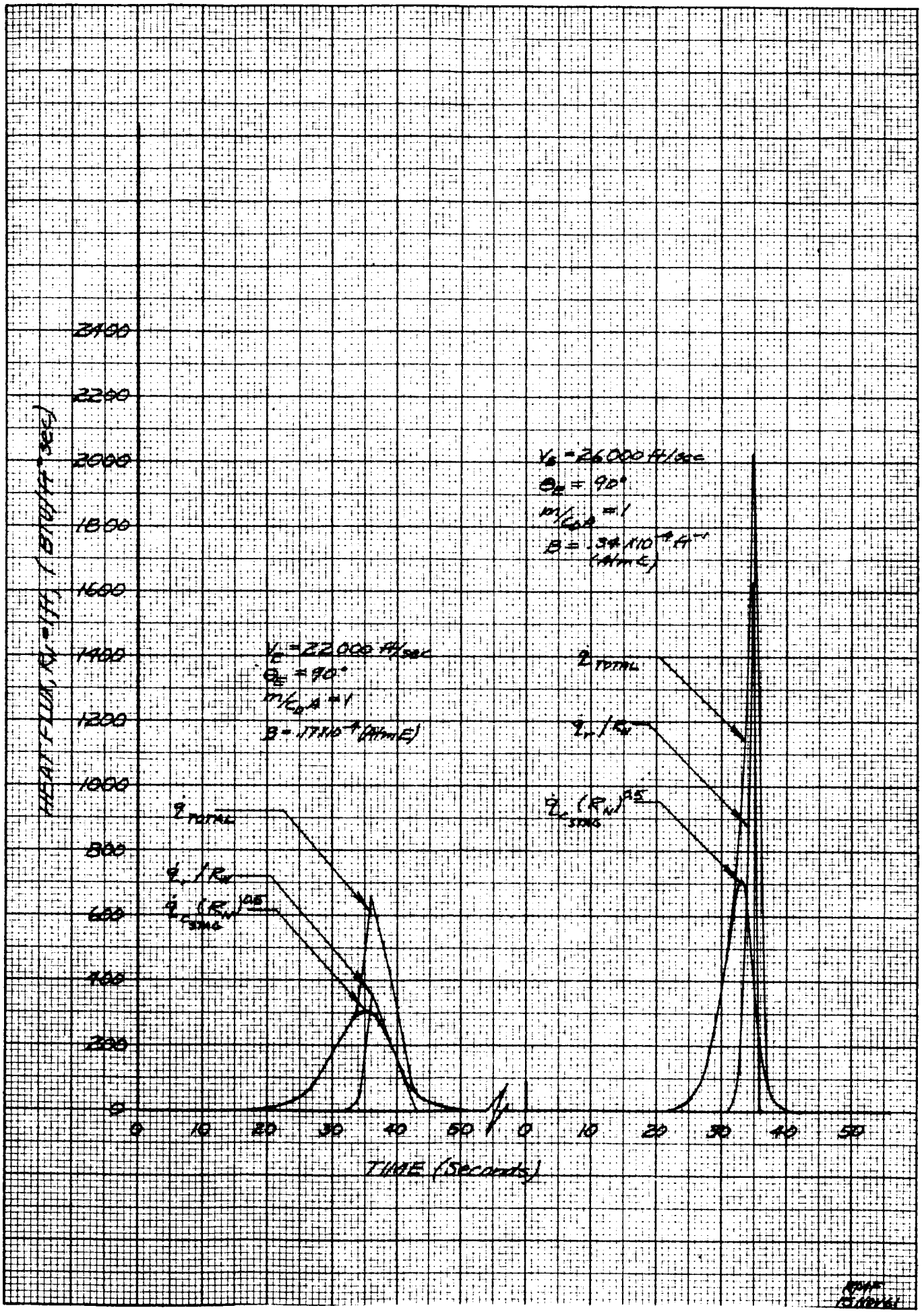

FIGURE 7 COMPARISON OF LAMINAR, RADIATION, AND TOTAL HEAT FLUXES AT THE STAGNATION POINT

Ford Motor Company

AERONUTRONIC DIVISION

Intra-Company Communication

27 October 1961

TO: Mariner B Distribution

FROM: M. G. Boobar and R. M. Foster

SUBJECT: Mariner B Entry Heat Protection System

The heat shield requirements and cold wall heat loads for the configuration released by T. W. Neumann, 10/17/61, AD-017, are as follows:

Station	Total Heat Load
Stagnation Point	9000 BTU/ft
45° Station	8000
10° skirt	2800

The loads encompass the following entry conditions:

$V_E \cong 26{,}000$ fps
$\theta_E = 20^{\circ}$ to 90°
$m/C_DA = 1$ slug/ft^2
Atmosphere - E and C

Nose cap material should be capable of accommodating instantaneous convective heat fluxes (maxima) in the order of 500 BTU/ft^2 sec and radiative fluxes of 3500 BTU/ft^2 sec. These fluxes can, but need not necessarily, occur at the same time.

For a phenolic-nylon (PN) ablator and J-M/MIN-K 2000 back-up insulation on the skirt, the thicknesses and weights required to maintain an inside wall temperature of -300°F at the time the vehicle has decelerated to Mach 1 are as follows:

Stations	Ablation Thickness	Insulation Thickness	Total Weight
Stagnation Point	← 1.1 inches PN →		7 lbs-PN/ft^2
45° Station	← 1.1 inches PN →		7 lbs-PN/ft^2
10° skirt	0.2 inches PN	0.7 inch MIN-K 2000	2.5 lbs/ft^2

/cyl

R.M. Foster

177

Ford Motor Company

AERONUTRONIC DIVISION

Intra-Company Communication

3 November 1961

TO: Mariner B Distribution

FROM: M. G. Boobar and R. M. Foster

SUBJECT: Mariner B Entry Heat Protection System

In reference to our memo of 27 October 1961, there have been some questions about how the shield might look. Below is a schematic representation (not to scale) to show how the installation and the phenolic nylon portions might be fared. Please note changes in thicknesses of P-N and Min-K 2000 (ρ Min-K = 20 lbs/ft^3 and ρ P-N = 75 lbs/ft^3).

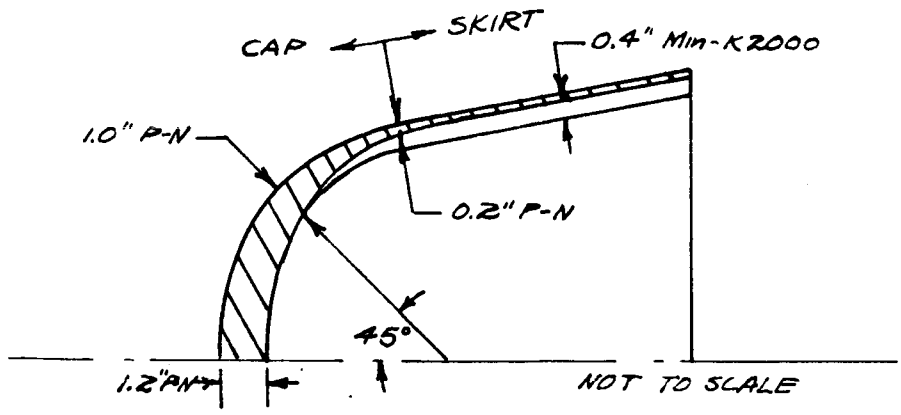

R. Foster

APPENDIX F

COMMUNICATIONS SYSTEM

Ford Motor Company AERONUTRONIC DIVISION

Intra-Company Communication

TO: File

2 November 1961

FROM: J. Kemmerly (based on rough notes submitted by P. Bower and J. Oslake on October 24, 1961)

Subject: MARINER B CAPSULE-TO-BUS COMMUNICATIONS SYSTEM

Summary

Two electronic systems are described which would implement the two missions presently envisaged. Primary emphasis is placed upon the photographic mission since it produces the most stringent requirements. The system analysis indicates that either mission could be implemented to a large extent with presently available, proven equipment. A set of three 100-watt transmitters on the capsule would be adequate for the photographic mission (no parachute), while a 2-watt telemetry transmitter would be capable of handling all other scientific and engineering data. For the impact-survival mission, a 10-watt transmitter is indicated. The weight, size, and power supply requirements, listed in Tables 3.1 and 3.2, do not appear to be excessive.

2-1 Capsule-Spacecraft Communications

The relationship between the parameters involved in capsule-to spacecraft communication can be expressed by the following:

$$P_D = R_B + S_o/N_o + N_o + L_s + M + L_p - (G_T + G_R) + L_m \quad \text{dbw}$$

where

P_D = Transmitted power associated with data, dbw.

R_B = 10 log r_b, r_b = transmitted bit rate, b/s.

S_o/N_o = Received signal power per bit to noise power per cps, db.

N_o = Noise power per cps, dbw/cps

L_s = Transmission loss (free space) between two isotropic antennas, db.

L_p = Polarization loss, db

G_T = Transmitting antenna gain, db

G_R = Receiving antenna gain, db

M = System margin, db

L_m = Miscellaneous system losses, db.

It is assumed that not all the available transmitter power will be in the modulation. That is, there will be some signal power loss in the demodulation process. It has been assumed that this will be a 3 db loss, or $P_T = 2\ P_D$ (P_T = available transmitter power).

The value of S_o/N_o may be obtained from Ref. 10 where S_o/N_o is plotted versus bit error probability for various modulation schemes. If it is assumed that the desirable word error probability for 3-bit words is $P_e = 10^{-2}$, then the bit error probability desired is one in 302 or 3.3×10^{-3}. Coherent PSK theoretically would require an S_o/N_o of 5.6 db for this probability. Non-coherent PSK would require 3 db more, or 8.6 db. It has been assumed in this study that a PCM/PSK/PM modulation scheme would be utilized. PCM is certainly desirable from the data accuracy standpoint. PSK is desirable, particularly bi-phase $\pm 90^o$, be cause with coherent detection, error rates are reduced to the lowest level theoretically possible[10] by this method. PM, with phase-lock reception, is apparently desirable because of enhanced receiver capture capabilities. However, the latter would have to be investigated to determine its validity in the case of the wide-band TV data transmission system. Subcarriers are used in order to avoid the loss of near-dc frequencies. The value assumed to be required for S_o/N_o is 8 db, which is 2.4 db greater than that theoretically required and takes into account practical limitations.

The transmission loss between isotropic antennas is given by

$$L_s = 20 \log R(\text{n.mi.}) + 20 \log f\ (\text{mc}) + 38 \text{ db.}$$

where

R = Communications range.

f = Operating frequency.

A typical case, in terms of capsule-to-space-vehicle communications range, would be 6000 n. mi. for post-entry transmissions. Since most transmissions will be made shortly prior to and after entry on the photographic mission, this is the range which will be used for that case. On the impact-survival mission the maximum communications range may be considerable longer, like 10,000-20,000 n. mi. This latter is due to travel of the spacecraft away from Mars. The operating frequency need not be definitely established at this time. However, due to the considerable amount of presently available equipment in the 215-265 megacycle telemetry band, a frequency of 250 mc. was assumed in defining the present system. The advantage in going to a higher frequency would be a resultant smaller transmitting antenna on the capsule. The disadvantage is that for the same receiving antenna beam-width there is a reduction in received power with increased operating frequency. The effective area of the receiving antenna is

$$A_e = g_r \frac{\lambda^2}{4\pi}$$

where

g_r = Receiving antenna gain.

λ = wavelength.

If λ is reduced (higher frequency), then g_r must be increased to keep the received power the same. But the only way to increase g_r is to decrease the antenna beamwidth (increase directivity), and this has presumably been established by the capsule-spacecraft geometrical relationships (see Section 4.4). Then the transmission loss for f = 250 mc and R = 6000 nautical miles is

$$L_s = 76 + 48 + 38 = 162 \text{ db.}$$

The overall receiving system noise figure is given by:[11]

$$f = f_a + f_r - 1$$

where

f_a = Antenna noise figure (radiation from Mars, etc.)

f_r = Receiver noise figure.

A conservative estimate of f_a is 2, and a receiver noise figure of 2 should be achievable. Then, f = 2 + 2 - 1 = 3, or in decibels F = 5 db. The effective noise temperature would be about 900°K. The noise power per cps of bandwidth would then be

$$N_o = 10 \log k T_o + NF$$

$$= -204 + 5 = -199 \text{ db}\mho$$

where

k = Boltzman's constant

T_o = 290°K

NF = System noise figure.

The transmitting and receiving antenna gains have been lumped together and a value of 10 db. will be assumed for the total. This seems to be achievable without too much difficulty. Circular polarization on the spacecraft can also be obtained and is very necessary since the received field may be of any polarity due to the unpredictable motion of the capsule. Circularly polarized energy may be radiated from the capsule in certain directions but will not be counted upon in this analysis. Therefore, a polarization loss of 3 db will be assumed.

A number of decibels must be assigned to miscellaneous system losses - losses in connections, multiplexers, etc. These are assumed to be less than 3 db in total.

The previous discussion is summarized below in Table 2-1. The aim in choosing values has been to assume not the worst case but the near-worst case. The impact-survival case is discussed later.

TABLE 2-1 COMMUNICATION PARAMETERS

Parameter	Assumed Value	Range
S_o/N_o	8 db	6 to 12 db
N_o	-199 dbw	-196 to -204 dbw
L_S	162 db	158 to 164 db
L_p	3 db	0 to 3 db
$G_T + G_R$	10 db	8 to 14 db
L_m	3 db	1 to 4 db

Then

$$P_D = R_B + M - 33 \text{ dbw.}$$

or

$$P_T = 2\,P_D$$

$$= R_B + M - 30 \text{ dbw.}$$

This equation is plotted in Figure 2-1. It indicates that, with the assumptions previously made, a 100-watt transmitter will transmit 20 kilobits/sec. with a margin of 7 db.

The bit rate for the photographic, or TV, data is given by

$$H = n_1 n_2 \log_2 N_G \frac{\text{bits}}{\text{picture}} \times \frac{1}{\tau_p} \frac{\text{picture}}{\text{sec}} = Q_B \frac{\text{bits}}{\text{picture}} \times \frac{n_p \text{ pictures}}{T \text{ sec}}$$

KEUFFEL & ESSER CO. MADE IN U.S.A.
2 X 3 CYCLES

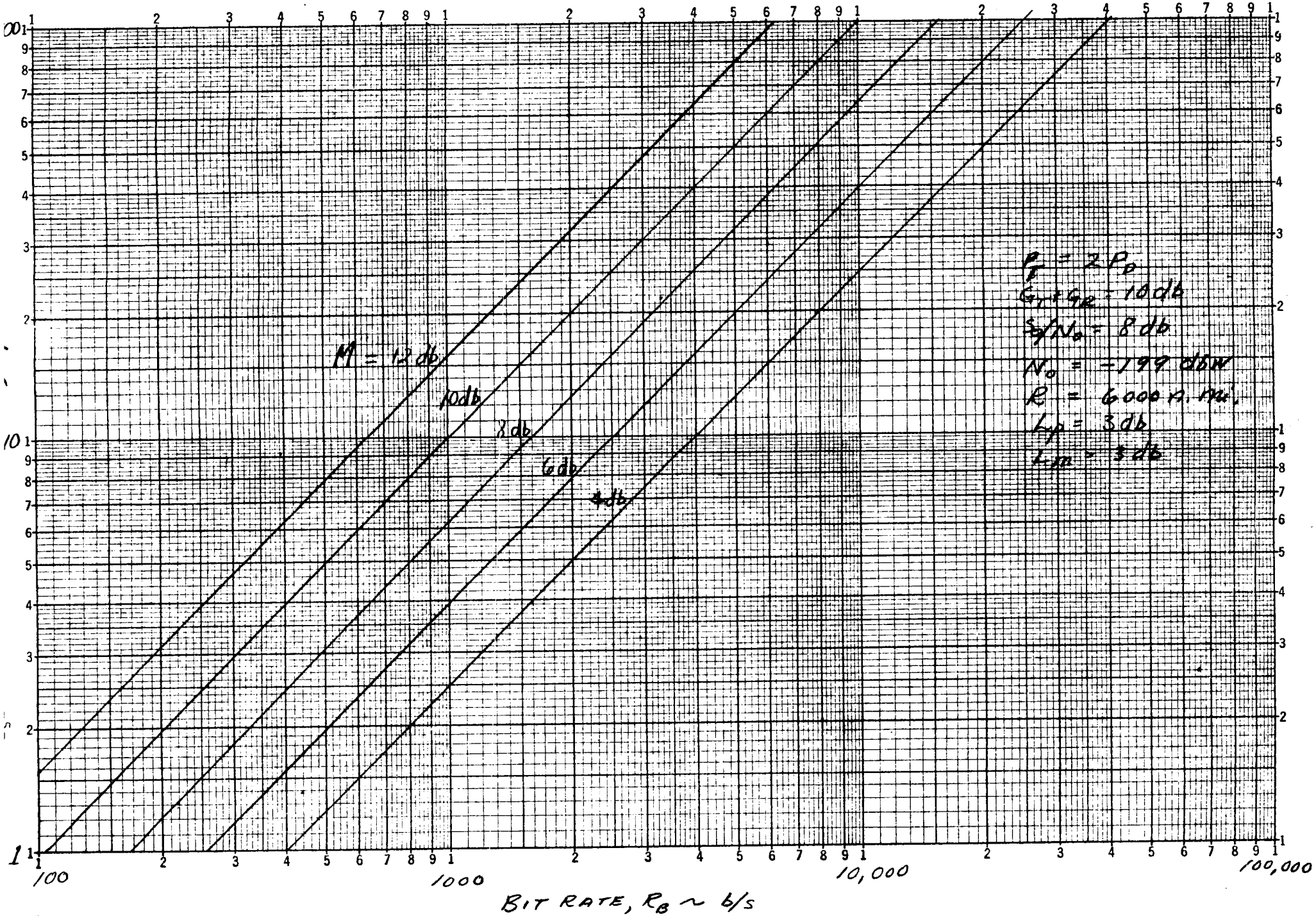

FIG. 2-1 TRANSMITTER POWER REQUIREMENTS

where

H	=	data rate, bits/sec
n_1, n_2	=	number of picture elements in each direction
N_G	=	number of gray levels
τ_p	=	readout time for each picture
Q_B	=	total number of bits per picture
N_p	=	total number of pictures transmitted
T	=	total photo transmission time

This relationship is illustrated in Figure 2-2 which assumes an insignificant amount of time will be required to erase and expose (less than a second). The total picture-taking time available will depend upon the density of the Martian atmosphere, the entry angle and entry velocity and (assuming no parachute) may vary from 70 seconds to 5 minutes at the extremes. A nominal range of 2-4 minutes was assumed for the determination of the bit rate and spacecraft storage capacity.

The photographic data transmission system (which will provide tri-color pictures) has been separated into three separate transmitting and receiving subsystems, one for each camera. This will greatly enhance reliability and will allow lower transmitter power. The following discussion will apply to a single subsystem. If one assumes a 200-line resolution, then a bit rate of 20 kilobits/sec will provide about 18 pictures in 2 minutes. The first picture would be taken at 40-60,000 feet.

The narrow-band telemetry system would require a data rate of 100-200 b/s. According to Figure 2-1, a 2-watt transmitter would transmit 200 b/s with a margin of 10 db. This assumes that both the wide-band TV system and the narrow-band telemetry system utilize the same antenna system.

For the impact-survival mission the data rate will probably be less than 100 b/s after impact and the communications range may be as great as 20,000 nautical miles. Then $L_S + 48 + 86 + 38 = 172$ db, or 10 db more than the previous case. A 10-watt transmitter would provide a 10 db margin in this case.

TABLE 2-2 COMMUNICATION PARAMETERS

	Bit Rate	P_T	M
TV	20,000 b/s	100 W	7 db
Telemetry	100-200 b/s	2	10
Impact-Survival	100 b/s	10	10

K+E 10 X 10 TO THE ½ INCH 359-11
KEUFFEL & ESSER CO. MADE IN U.S.A.

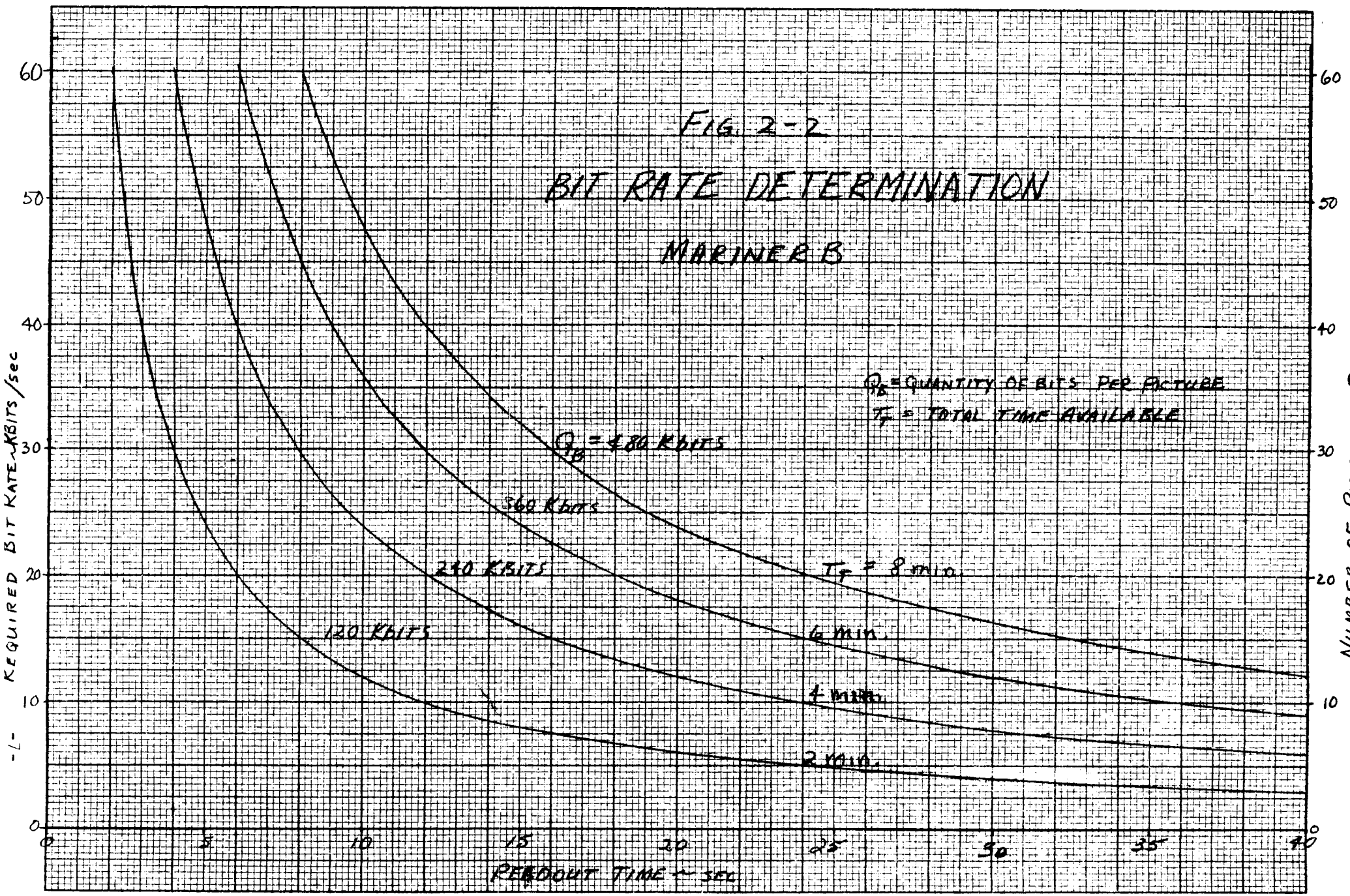

3-1 Mariner - B Capsule Electronic System

The electronic requirements for this picture-taking mission may be satisfied by implementing the functional block diagrams shown in Figures 3-1 and 3-2 for the capsule and spacecraft, respectively. The video data are transmitted to the spacecraft and stored on magnetic tape for eventual re-transmission to Earth.

The television cameras all employ a one-half inch-diameter vidicon, standard 8 mm camera optics, & transistorized signal and control circuitry. Analog video data from each camera is converted into a binary PCM train of pulses in separate television encoders. To facilitate transmission of the low-frequency components of the video signal the PCM output of the encoder modulates a subcarrier which in turn modulates each television transmitter. A separate power amplifier is provided in each channel to produce the desired RF power. The three RF signals and a separate telemetry signal are fed into a quadruplexer and then to a common antenna on the capsule. Composition of the data word with picture elements and synchronization bits is described fully in a separate memo.

The narrow-band telemetry channel handles scientific and diagnostic data at relatively low information rates; 100-200 bits per second compared with approximately 20,000 bits per second in each television channel. An encoder takes analog voltages from various sensors and transducers, including a radar altimeter, and converts these to digital data which in turn are sampled periodically and incorporated into a standard word format for modulation of a subcarrier oscillator. The subcarrier phase modulates a small solid-state transmitter which produces approximately 2 watts of RF power.

The function of the event controller is to program the sequence of events as shown diagrammatically in Figure 3-3. The television synchronizer and telemetry synchronizer which control the timing of repetitive or periodic events may also be considered as subordinate parts of the programmer. The programmer accepts three input signals which form the basis for all other events. These input signals are as follows in chronological order:

a) A "start" signal from spacecraft which occurs before separation and initiates a timer that controls the ignition of the main rocket

b) A "go" signal from the capsule separation mechanism which starts several timers

c) An "enable" signal from an accelerometer aboard the capsule which signifies the occurrence of a significant penetration into the Martian atmosphere.

The latter signal becomes the reference point in time for all subsequent events.

FIG. 3-1 MARINER-B CAPSULE ELECTRONICS

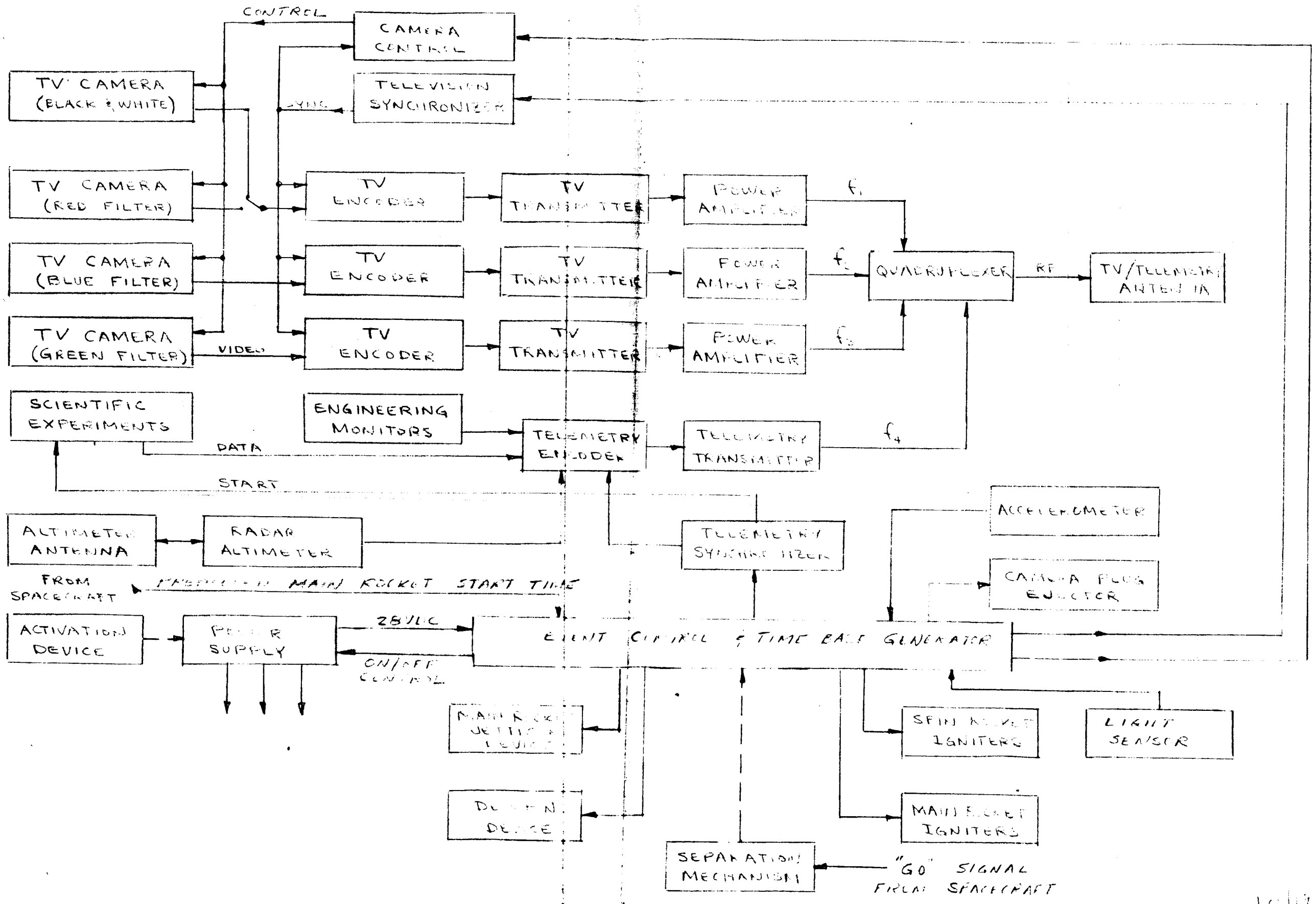

10/17/6

FIG. 3-2 MARINER-B SPACECRAFT ELECTRONICS

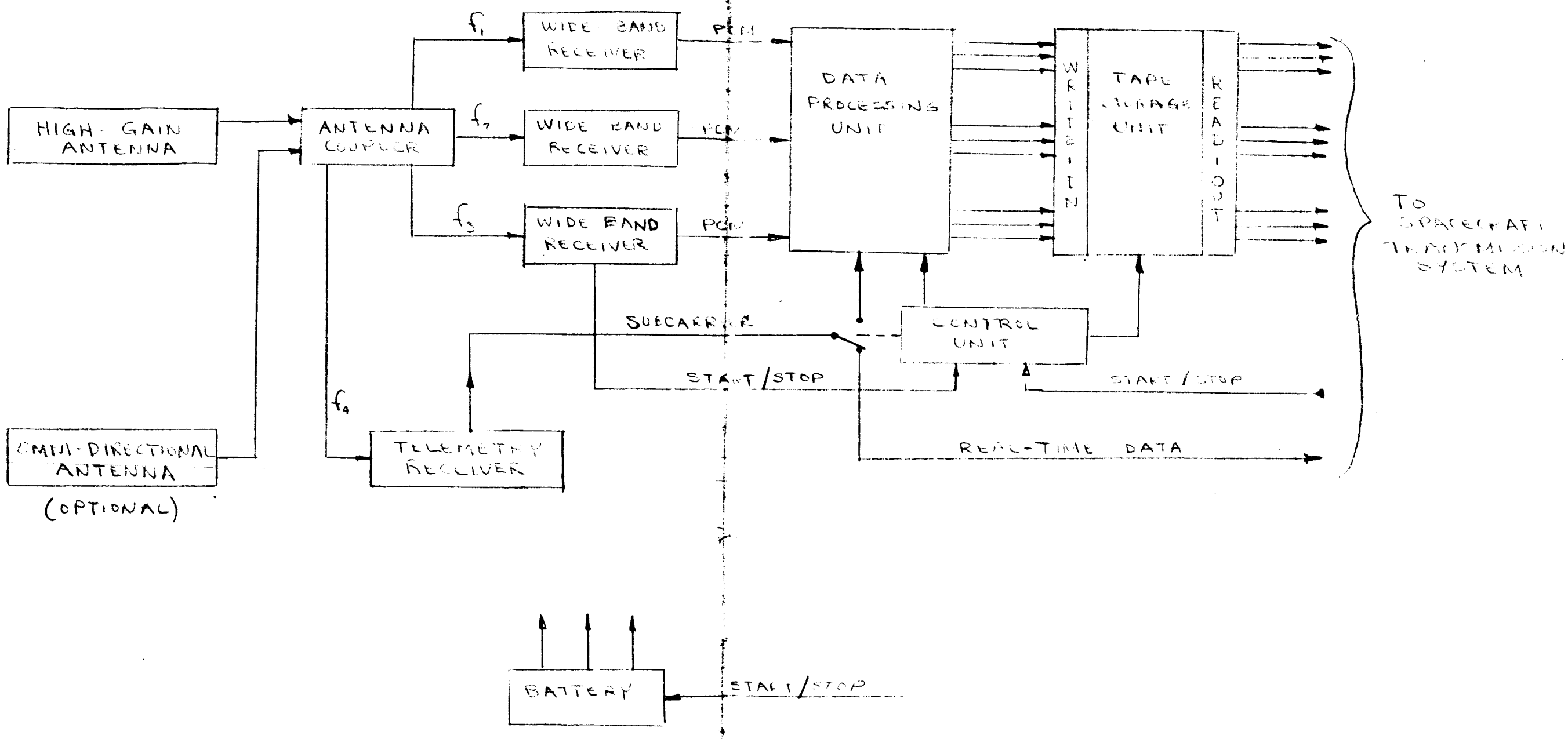

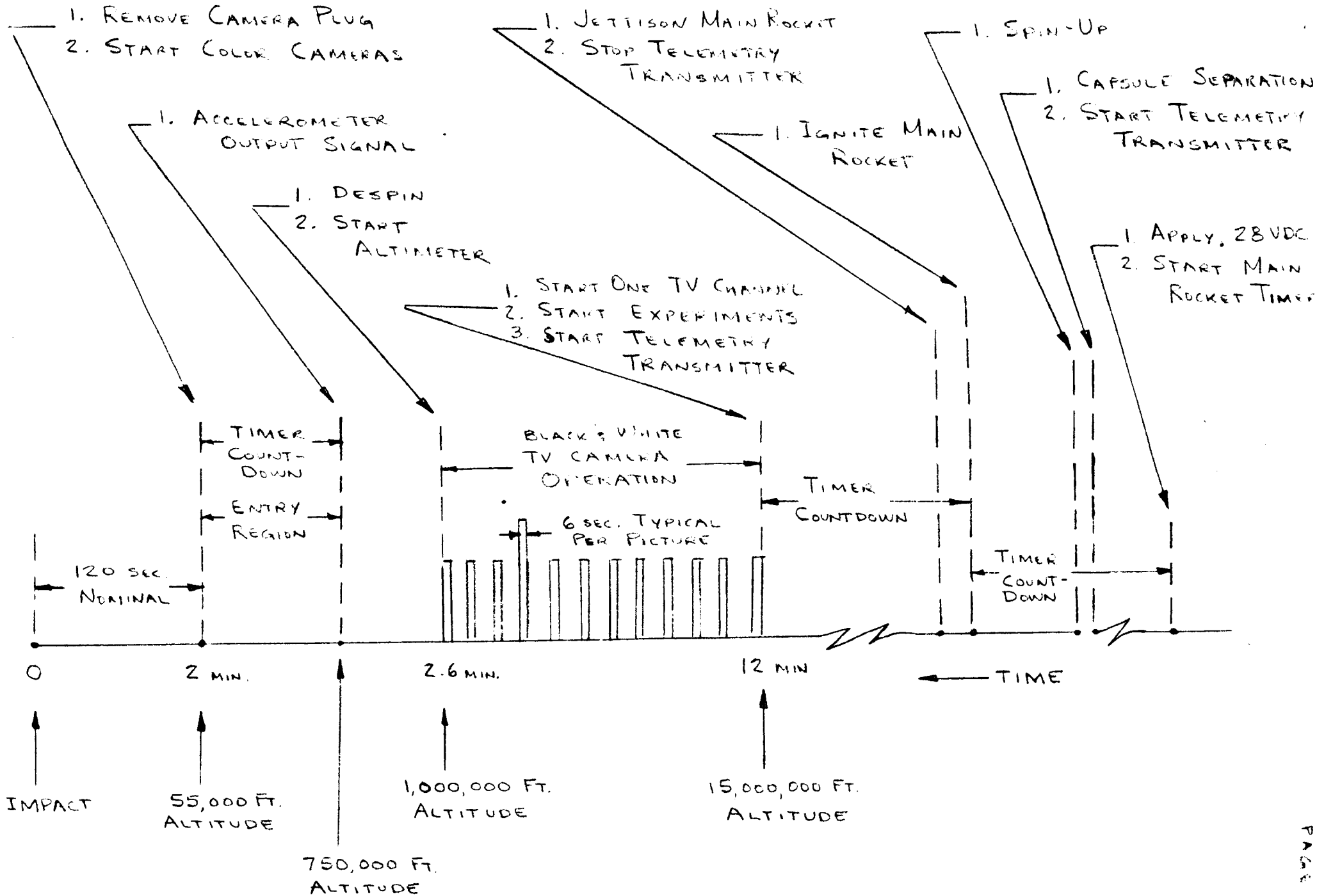

FIG. 3-3 SEQUENCE OF EVENTS FOR TV MISSION

The electronic equipment required aboard the spacecraft may be deduced from the functional block diagram of Figure 3-2. A high-gain (10 db) antenna is continually servoed toward the center of Mars using a platform or control signals presumed to be available aboard the spacecraft. An optional omni-directional antenna can be provided to insure reception of diagnostic telemetry data in the event of a failure in the primary communication path. Separate wide-band PM receivers are provided for each of the three television channels, and a narrow-band receiver handles the telemetry data.

The output of the narrow-band telemetry receiver is the data subcarrier which can be sent directly to the spacecraft transmission system for broadcast to earth in real-time. Although this data is available at a low enough information rate for direct re-transmissions, it can be demodulated and stored along with the video data if desired.

Start/stop cues for the data storage unit are provided from one of the wide-band receivers. This is necessary when the video data is not being transmitted continuously; i.e., for burst transmissions as during the period when black and white television pictures are being taken. Otherwise, the magnetic tape unit would have to run continuously and require excessively long reels of tape.

The method of data storage on magnetic tape is PCM recording. It has the advantage of employing saturated recording techniques so that amplitude variations and non-linearities are not important. The data processing unit receives the demodulated PCM output from the wide-band receivers and divides each serial train of pulses into three parallel output channels. The tape storage unit therefore accepts the PCM video data, on nine separate tracks simultaneously. The major advantage of this technique is that it greatly simplifies the record drive mechanisms because of the reduction in the ratio of write-in speed-to-readout speed. A secondary advantage is the lesser amount of magnetic tape required. Readout of video data into the spacecraft transmission system is accomplished upon command therefrom. The tape storage unit is described in a separate memo.

Size and weight data and power requirements for the electronic equipment aboard the capsule and spacecraft are given in Table 3-1.

TABLE 3-1

SIZE, WEIGHT AND POWER REQUIREMENTS FOR B1

CAPSULE EQUIPMENT

Unit	Quantity	Equipment	Unit Weight	Input Power	Buy or Make
TV Camera	4	8" x 2 1/2" dia	6 lb	15 W	Buy
Vidicon Electronics	4	3 3/4" x 5" x 7"	6 lb	15 W	Buy
TV Transmitter	3	6.5" x 3.8" x 2.0"	2.0	36	Buy
Power Amplifier	3	8.5" x 6.3" x 3.6"	5.9	23	Buy
Quadruplexer	1	9.3" x 6.0" x 6.0"	4	-	Buy
TV/TM Antenna	1	24" x 5" x 5"	1.5	-	Make
Telemetry Transmitter	1	22 cu in	1.3	23	Make
Event Control & TB Gen.	1	400cu in	6	8	Make
Telemetry Synchronizor	1	80 cu in	2	2	Make
Television Synchronizer	1	40 cu in	1.3	1	Make
Camera Control	1	20 cu in	0.6	0.5	Make
TV Encoder	3	8 cu in	0.3	0.5	Make
TM Encoder	1	70 cu in	2.6	4	Make
Accelerometor	1	1/2" x 5/8" dia	0.2	0.2	Buy
Light Sensor	1	5 cu in	0.5	1	Buy
Altimeter Antennas	2	8" x 2" x 3"	1	-	Make
Radar Altimeter	1	160 cu in	4	20	Buy
Scientific Instruments	See separate memo by I. H. Blifford				
Power Supply	See separate memo by V. H. Henderson				

SPACECRAFT EQUIPMENT

Unit	Quantity	Size	Unit Weight	Input Power	Buy or Make
High Gain Antenna	1	4' x 15" dia	5	-	Make
Broad Beam Antenna	1	12" x 1/2" dia	1	-	Make
RF Coupler/Multiplexer	1	500 cu in	5	-	Buy
Wide Bond Receiver	3	24 cu in	1.7	5.8	Buy
Data Processing & Storage	1	200 cu in	7	2	Buy
Telemetry Receiver	1	24 cu in	1.7	5.8	Buy
Battery	1	N/A	N/A	-	Buy

3.2 Mariner-B1 Impact-Capsule Electronic System

The electronic requirements for this capsule-landing mission may be satisfied by implementing the functional block diagrams shown in Figure 3-4 and 3-5 for the capsule and spacecraft, respectively. The emphasis is on those scientific experiments which are initiated at or after impact. However, since a parachute is deployed to lessen the impact shock, a relatively slow descent will be made. It therefore is anticipated that even more secondary experimentation will be attempted prior to impact than in the photo mission.

There will be three distinct phases of data collection and/or data transmission during this mission. These are:

(1) After separation and before chute deployment

(2) After chute deployment and before impact

(3) After impact

Based upon the preceding discussion, it is possible to estimate the probable range of data gathering rates during each of the four phases. The values might be as follows:

(1) Before chute deployment	-	2 to	20 bits/sec
(2) After chute deployment	-	20 to	200 bits/sec
(3) Impact to Blackout	-	10 to	100 bits/sec
(4) After Blackout	-	2 to	20 bits/sec

If the survival capsule consists of two concentric spheres as in the Ranger Program, then the inner sphere will be free to rotate and align its center of gravity axis perpendicular to the surface of Mars after impact. This feature permits the placement of an antenna within the inner sphere, so that the principal radiation will always be normal to the surface of Mars. Only one antenna and one transmitter would be required in this case.

The electronic equipment required in the spacecraft for the impact mission is relatively simple and straight-forward as seen in Figure 3-5. The antenna system and RF portion are similar, if not identical, with the counterparts in the Photo mission. The only innovation is the diversity combiner in the data receiver which continuously samples the incoming signals from the capsule and applies the strongest one to the PM detecting circuitry in the receiver.

FIG. 3-4 MARINER - B1 CAPSULE ELECTRONICS

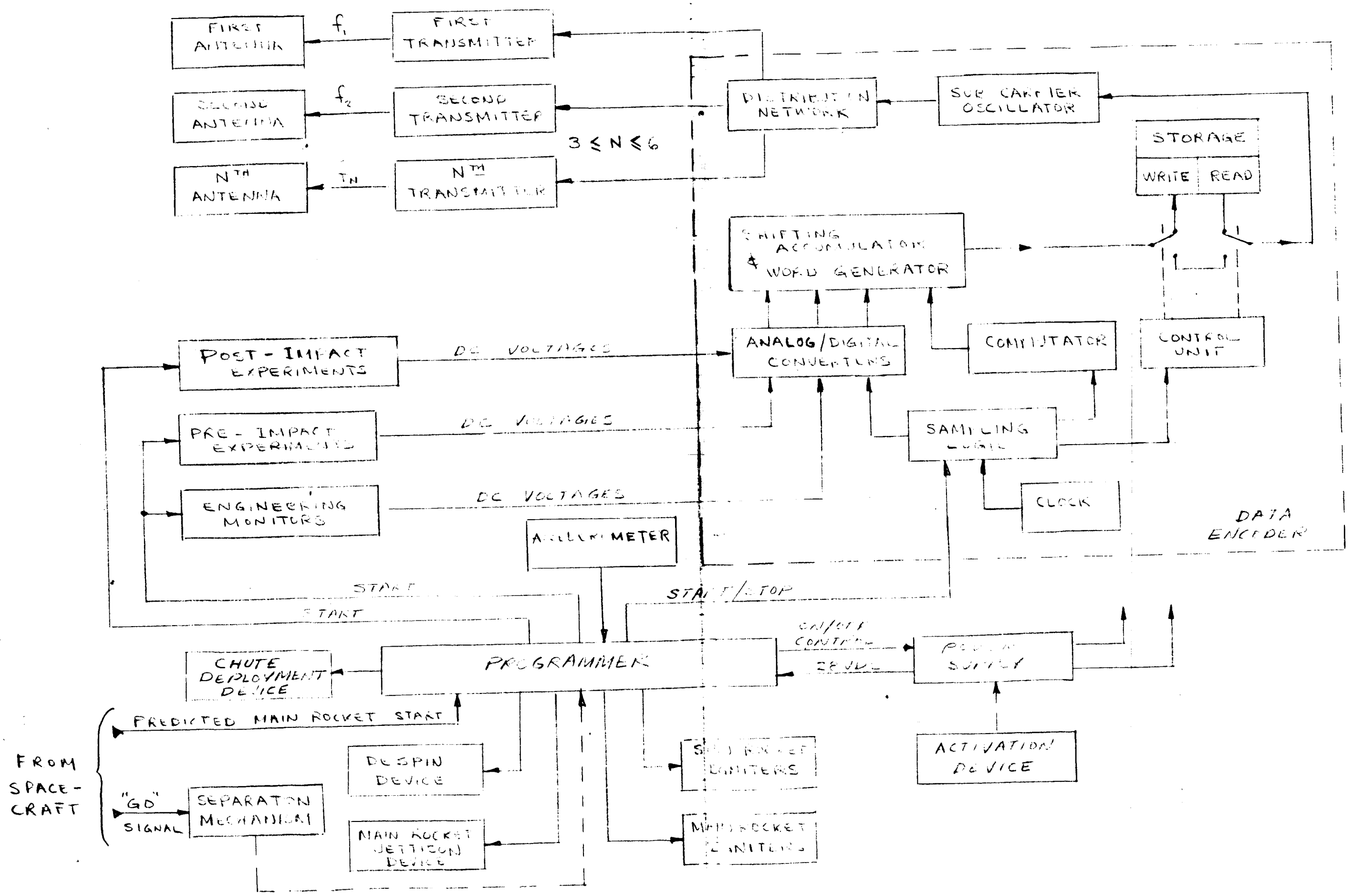

10/11/61

FIG. 3-5 MARINER - B SPACECRAFT ELECTRONICS

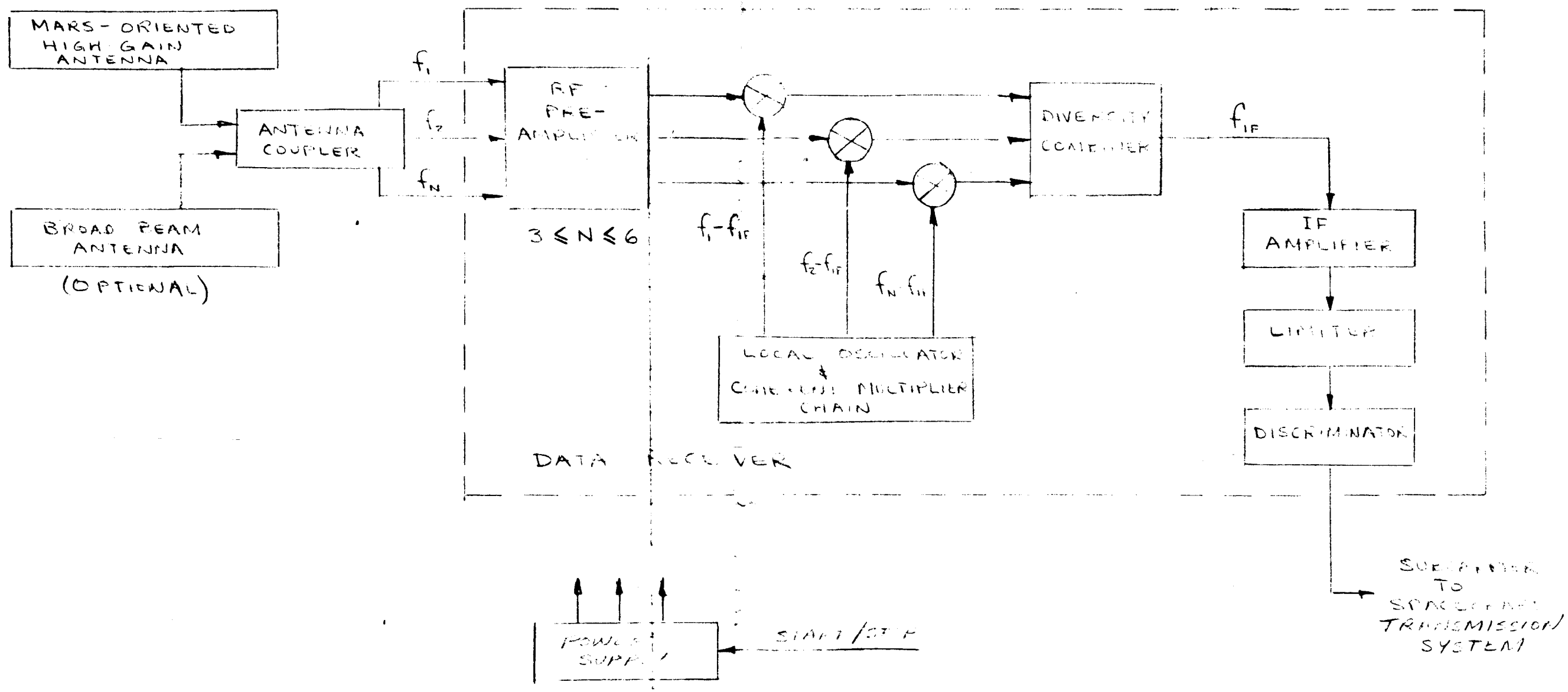

10/11/61

The sequence and timing of events during the mission are shown diagrammatically in Figure 3-6. The similarity with the photo mission is apparent and no explanation is necessary.

Size and weight data and power requirements for the electronic equipment aboard the capsule and spacecraft are given in Table 3-2.

4.1 Camera Equipment

Vidicon camera characteristics are given in Table 4-1.

A block diagram of the camera system is shown in Figure 4-1. Magnetic deflection coils are driven by transistor amplifiers. Other circuitry includes a focus current regulator for maintaining constant current in the focusing coil, a dc-dc converter to provide vidicon operating voltages, and a blanking amplifier for eliminating the electron beam during deflection retrace time. The video signals from the vidicon are amplified by a preamplifier mounted on the vidicon yoke, which in turn feeds a transistorized dc video amplifier. This amplifier is preceded by a clamp circuit to restore the DC component.

Figure 4-2 contains a photograph of a slow-scan television system built by Hallamore Electronics Corp. for space applications.

The average expected scene brightness impinging on the photoconductor through the lens is 0.001 ft-candle-seconds, with maximum dark of 0.0001 and a dynamic range of 100. Typical vidicons will provide an image bright enough to provide a good picture on a television screen when 0.03 ft-candle-seconds is incident on the photo conductive surface (Ref. 8).

The storage capabilities of the typical vidicon's photo conductive surface allow short exposures to be made and scanned over a frame time of from 2 to 15 seconds without serious image decay. Special types (Westinghouse, for example) can retain the image for over 30 seconds.

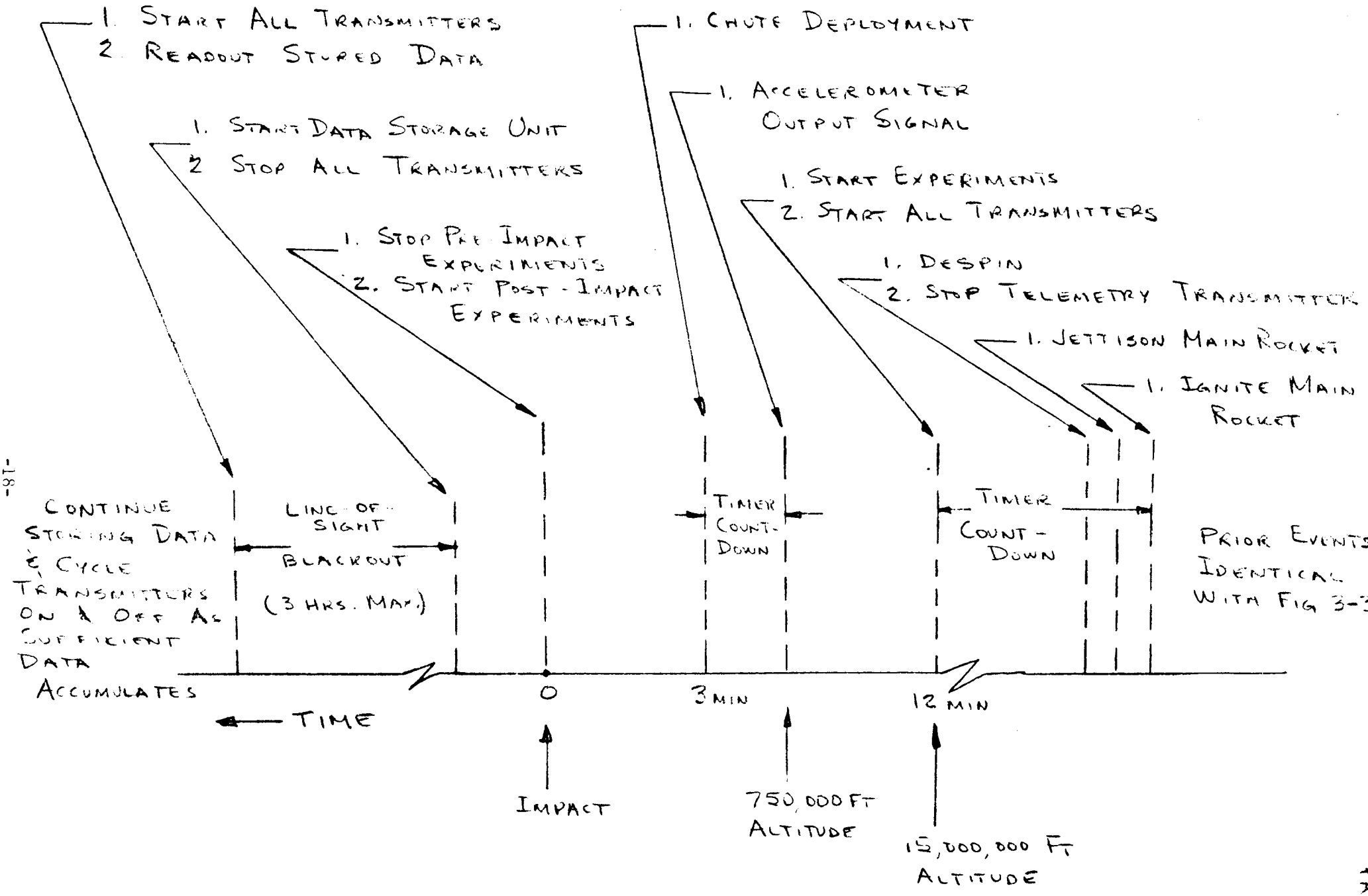

FIG. 3-6 SEQUENCE OF EVENTS FOR IMPACT MISSION

TABLE 3-2

SIZE, WEIGHT AND POWER REQUIREMENTS FOR B2

CAPSULE EQUIPMENT

Unit	Qty	Size	Unit Weight	Input Power	Buy or Make
Antenna	N	24" x 5" x 5"	1.5	---	Make
Transmitter	N	22 cu. in.	1.3	23 W	Make
Data Encoder	1	300 cu. in.	12	15	Make
Programmer	1	250 cu. in.	3	2	Make
Scientific Instruments	See separate memo by J. H. Blifford				
Power Supply	See separate memo by V. H. Henderson				

SPACECRAFT EQUIPMENT

Unit	Qty	Size	Unit Weight	Input Power	Buy or Make
High-Gain Antenna	1	4' x 15" dia.	5	---	Make
Broad-Beam Antenna	1	12" x ½" dia.	1	---	Make
RF Coupler/Multiplexer	1	500 cu. in.	5	---	Buy
Data Receiver	1	60 cu. in.	4	15	Buy
Battery	1	N/A	N/A	---	Buy

TABLE 4-1

TELEVISION CAMERA CHARACTERISTICS

Recommended Exposure	0.1 Ft-candle-seconds
Shutter Speed	1/1000 Sec.
Electrical Characteristics	
Vidicon Tube Diameter	1 inch
Intrinsic Resolution	200 x 200 image points
Gray Shades Reproduced	8
Residual Image After Erase	Negligible*
Horizontal Period	30 milliseconds
Vertical Period	6 Seconds
Horizontal Sweep Rate	33-1/3 cycles/sec.
Frame Rate	1/6 cycles/sec.
Input Power Source	27.5 VDC ± 10%
Power Consumption	15 watts
Physical Characteristics	
Vidicon Unit	8" L x 2-1/2" Dia.
Vidicon Electronics	3-3/4 x 5" x 7"
Total Weight	6 Pounds

*Residual image after one readout depends on beam current. Several additional fast frame-scans results in virtually complete erasure.

Ruggedized vidicons of both the one-inch and the one-half-inch size have been constructed, the latter being able to withstand a shock of 100-g and 25-g (rms) random noise vibration (Ref. 7) The vidicon is not affected adversely by cosmic radiation, but temperature extremes will reduce sensitivity and result in a poorer signal-to-noise ratio. The "stickiness" or lag decreases at low temperatures thereby increasing the time required to erase any residual image from an exposed picture after the initial readout.

AERONUTRONIC—DEVELOPMENT SKETCH

	NAME	DATE			REMARKS:
PREPARED BY			TEMPORARY		
CHECKED BY			PERMANENT		
APPROVED BY			PROJECT		

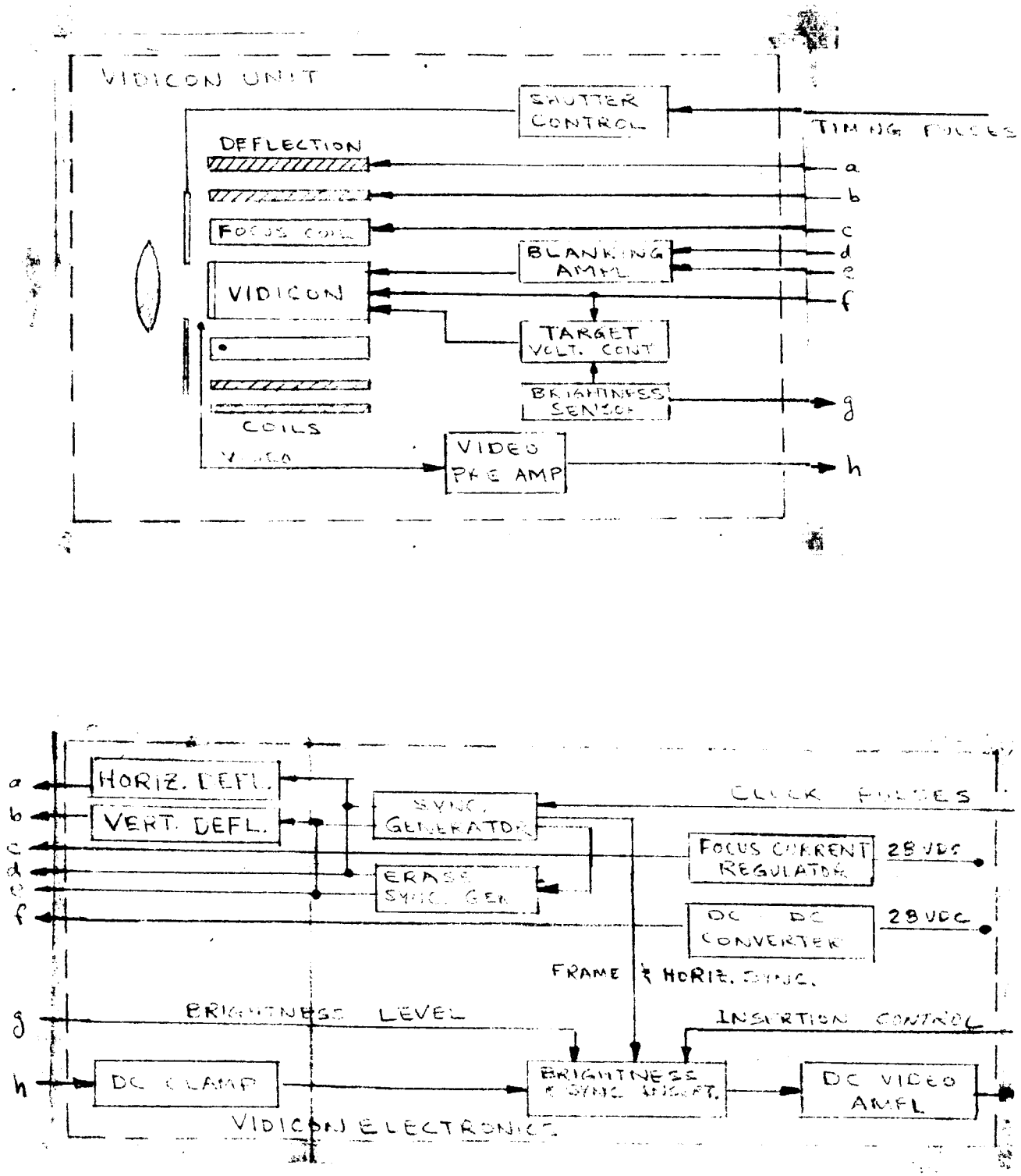

FIG 4-1 Television Camera Equipment

AERONUTRONIC—DEVELOPMENT SKETCH

	NAME	DATE			REMARKS:
PREPARED BY:			TEMPORARY		
CHECKED BY:			PERMANENT		
APPROVED BY:			PROJECT		

PACK OF PALL MALLS

VIDICON ELECTRONICS

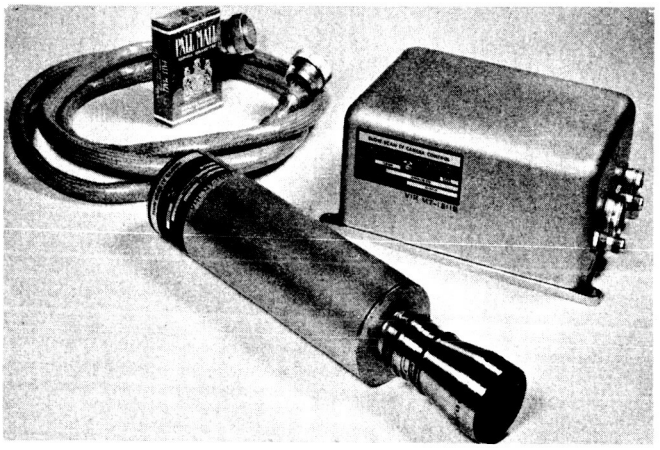

VIDICON UNIT

Hallamore Model HE 431A

FIG. 4-2 Photograph of Space Television Camera

Gen Adm
Feb 60 **ARD-7027**

REFERENCES

1. Carbrey, R.L., "VIDEO TRANSMISSION OVER TELEPHONE CABLE PAIRS BY PULSE CODE MODULATION", Proc. IRE , Vol. 48, No. 9, September, 1960, p 1546.

2. Weimer, P.K, et all, "A DEVELOPMENTAL TRICOLOR VIDICON HAVING A MULTIPLE-ELECTRODE TARGET," IRE Transactions on Electron Devices, July, 1960, p. 147

3. Fink, D.G., "TELEVISION ENGINEERING HANDBOOK," McGraw-Hill, 1957

4. Intra-Company Memorandum, I. H. Blifford, dated October 11, 1961

5. Intra-Company Memorandum, AL-127, R. R. Auelmann, dated August 23, 1961.

6. Intra-Company Memorandum, AL-126, R. R. Auelmann, dated August 22, 1961.

7. Ritter, M., and Mesner, M. H., "IMAGE SENSORS AND SPACE ENVIRONMENT", Journal of the SMPTE, Vol. 69, No. 1, January 1960, p. 18.

8. Mesner, M.H., and Staniszewski, J. R., "TELEVISION CAMERAS FOR SPACE EXPLORATION" Astronautics, May 1960, p. 36

9. Intra-Company Memorandum, I. H. Blifford, dated October 18, 1961.

10. "THEORETICAL COMPARISON OF BINARY DATA TRANSMISSION SYSTEMS," Cornell Aeronautical Lab Report No. CA-1172-S-1, May 1958.

11. Norton, K. A., "TRANSMISSION LOSS IN RADIO PROPAGATION" Proc. of the IRE, January 1953.

12. Intra-Company Memorandum AD-017, T. W. Neumann, October 17, 1961.

13. Intra-Company Memorandum, M. G. Boobar, October 17, 1961.

14. S. Feldman, "NUMERICAL COMPARISON BETWEEN EXACT AND APPROXIMATE THEORIES OF HYPERSONIC INVISCID FLOW PAST SLENDER BLUNT-NOSED BODIES," ARS Journal, May 1960.

15. Scharfman and Morita, "VOLTAGE BREAKDOWN OF ANTENNAS AT HIGH ALTITUDES," SRI Technical Report No. 69.

Ford Motor Company

AERONUTRONIC DIVISION

Intra-Company Communication

SUBJECT: Plasma Sheath Attenuation - Mariner B

DATE: October 20, 1961

FROM: P. B. Bower

CC: J. Jansen
J. Kemmerly
F. Losee
J. Oslake

TO: John Housego

References:

1. Intra-Company Memorandum AD-017, T. W. Neumann, October 17, 1961

2. Intra-Company Memorandum, M. G. Boobar, October 17, 1961

3. S. Feldman "Numerical Comparison Between Exact and Approximate Theories of Hypersonic Inviscid Flow Past Slender Blunt-Nosed Bodies," ARS Journal, May, 1960

According to Reference 3, the features of the inviscid flow surrounding the viscous wake of a short blunt body are not too different from the gas flow far away from the nose of a slender blunt body. To estimate the temperatures and pressures about the wake of the Mariner B capsule (Reference 1) in the Martian atmosphere, the following approximations will be made:

1. While the magnitudes will be different, the relative variation of temperature and pressure about the capsule will not be greatly different than for air.

2. The ratios of stagnation temperature and pressure to the temperatures and pressures in other points in the flow field remain the same (extrapolation).

On the basis of these approximations and the use of data from Reference 2 and 3, one can arrive at an estimate of flow field parameters about the aft end of the capsule. This is desirable since the present concept includes an antenna on the aft end of the capsule for transmission of the television and telemetry data.

The attached figure presents peak temperatures and associated pressures for a transmission path perpendicularly outward from the capsule axis at the aft end (for the trajectory of Reference 2). It is estimated that the peak temperature shown (3600° K) will yield an electron concentration on the order of 10^6 e/cc. This would in turn mean a plasma frequency on the order of 10^8 rad/sec which is too low to result in a calculable signal attenuation for a transmission frequency of 250 mc.

It is obvious from Reference 2 that a radar altimeter would be useless between the altitudes of 800,000 and 150,000 feet since it would require transmission (and reception) in a forward direction where high electron concentrations exist.

PBB

P. B. Bower

PBB/sj

K+E KEUFFEL & ESSER CO. MADE IN U.S.A.

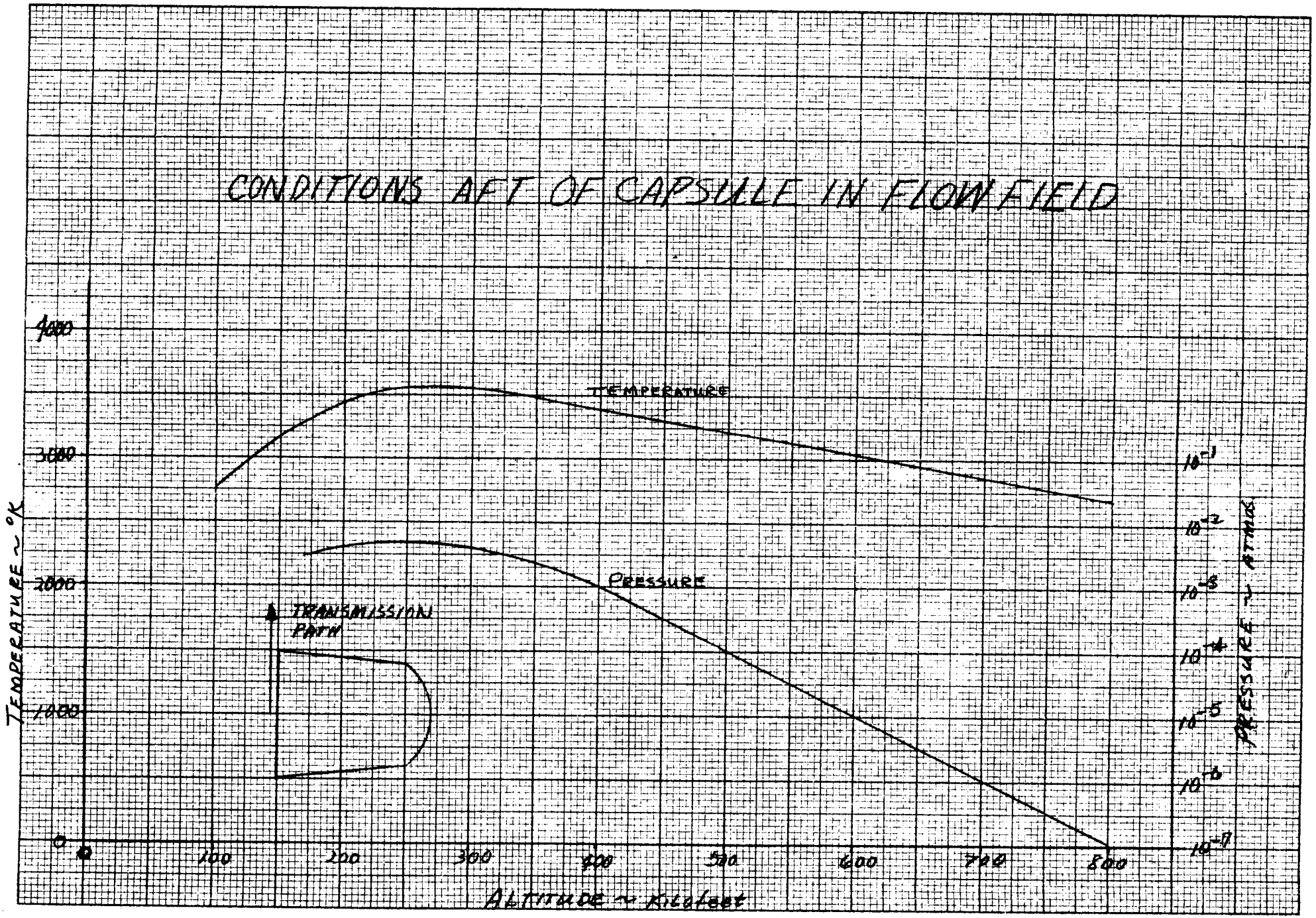

Intra-Company Communication

2 November 1961

To: J. E. Kemmerly

From: P. B. Bower

Subject: TRANSMITTING AND RECEIVING ANTENNAS FOR CAPSULE-TO-SPACECRAFT COMMUNICATIONS: MARINER B CAPSULE

Transmitting Antennas

The design of the capsule antenna system for the capsule-to-spacecraft data link will depend upon the capsule trajectory to a large extent. One possible trajectory indicates a pattern which provides coverage at $\theta = 0^\circ - 10^\circ$ and $\theta = 80^\circ - 90^\circ$ (see Figure 4-14). Another trajectory would require a pattern which provides coverage from $\theta = 0^\circ$ to $\theta = 60^\circ$. In either case, the pattern shape is dictated by the capsule-spacecraft relationship and must be nearly symmetrical about the capsule axis (since the capsule will probably be spinning).

These two patterns will be called Cases 1 and 2 respectively, or

Case	Coverage
1	$\theta = 0^\circ - 10^\circ$, $\theta = 80^\circ - 90^\circ$
2	$\theta = 0^\circ - 60^\circ$

For Case 1, the size of the capsule and the operating frequency indicate a combination of types of antennas might be desirable. It appears that an annular slot plus crossed, rectangular slots mounted in the aft end might give the desired coverage (see Figure 4-15). There would be circularly polarized radiation in the aft direction ($\theta = 0^\circ - 30^\circ$, approximately), and linearly polarized radiation off the side ($\theta = 70^\circ - 110^\circ$, approximately).

For Case 2, the crossed, rectangular slots alone would probably provide the desired coverage, as shown in Figure 4-16.

For the altimeter antenna, it appears that two circumferential slots mounted near the nose of the capsule would provide satisfactory radiation if fed in opposite phase (see Figure 4-17).

Table 4-4 indicates approximate sizes and weights.

TABLE 4-4 ANTENNA DATA

	Size	Weight
Case 1		
Annular Slot	25" dia., 2" x 5"	3 lb.
Rectangular Slot (ea.)	12" x 2" x 5"	1 lb.
Case 2		
Rectangular Slot (ea.)	24" x 5" x 5"	1.5 lb.
Altimeter Antenna(ea.)	8" x 2" x 3"	1 lb.

Receiving Antenna

As has been indicated, it is imperative that the primary receiving antenna aboard the spacecraft be circularly polarized. Transmissions from the capsule may be of linear polarization and it would be difficult or impossible to design a linearly-polarized receiving antenna which would successfully couple the radiated field after atmospheric entry. The orientation of the electric field vector at the spacecraft during that period would be nearly impossible to predict.

It is during the time shortly prior to and after entry that a relatively high-gain on the spacecraft is desirable. This may be accomplished by mounting a helical antenna on the Mars-oriented boom aboard the spacecraft (assuming such a boom exists). The beam-width of this antenna would be controlled by size limitations, since (see Figure 5-1) the geometrical relationship would yield a relatively small beam-width. A 50° beam helical antenna would be approximately four feet long and fifteen inches in diameter, with a two-foot-by-two-foot ground plane. It would be collapsible.

Telemetry data transmitted from the capsule immediately after ejection and during the earlier stages of the flight could be received by means of a simple whip antenna aboard the spacecraft. The orientation of the electric field vector at the spacecraft should be predictable during this period, and a high gain antenna is not required. The telemetry receiver could be connected to both the high-gain antenna(through a multiplexer) and the low-gain antenna.

P. B. Bower

Distribution

J. J. Oslake
M. Caldwell
J. A. Jansen
W. Lemm
T. W. Newmann
F. A. Losee

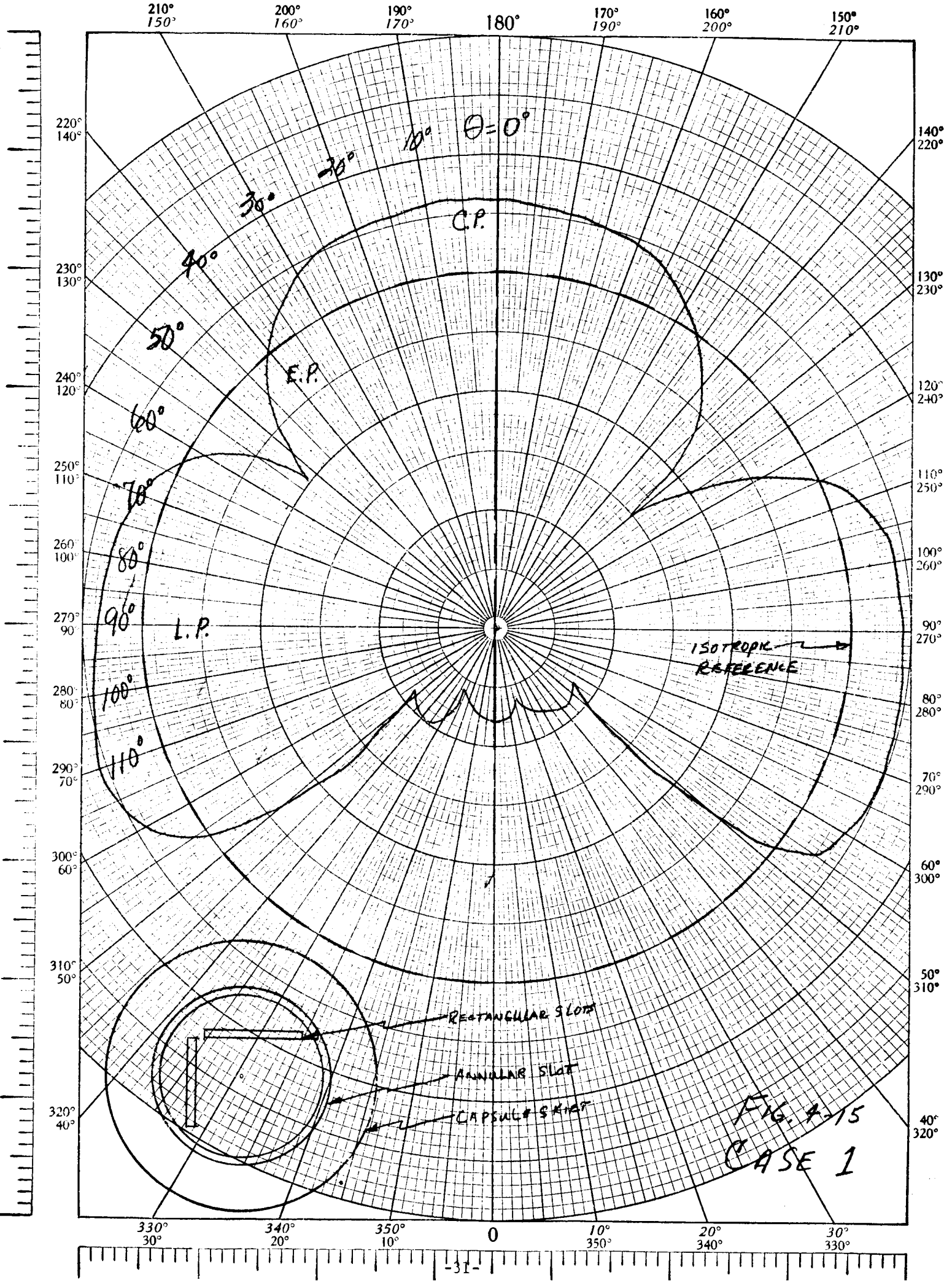
θ=0°
10°
20°
30°
40°
50°
60°
70°
80°
90°
100°
110°
C.P.
E.P.
L.P.
ISOTROPIC REFERENCE
RECTANGULAR SLOT
ANNULAR SLOT
CAPSULE SKIRT
FIG. 4-15
CASE 1
210° 150°
200° 160°
190° 170°
180°
170° 190°
160° 200°
150° 210°
220° 140°
230° 130°
240° 120°
250° 110°
260° 100°
270° 90°
280° 80°
290° 70°
300° 60°
310° 50°
320° 40°
140° 220°
130° 230°
120° 240°
110° 250°
100° 260°
90° 270°
80° 280°
70° 290°
60° 300°
50° 310°
40° 320°
330° 30°
340° 20°
350° 10°
0
10° 350°
20° 340°
30° 330°

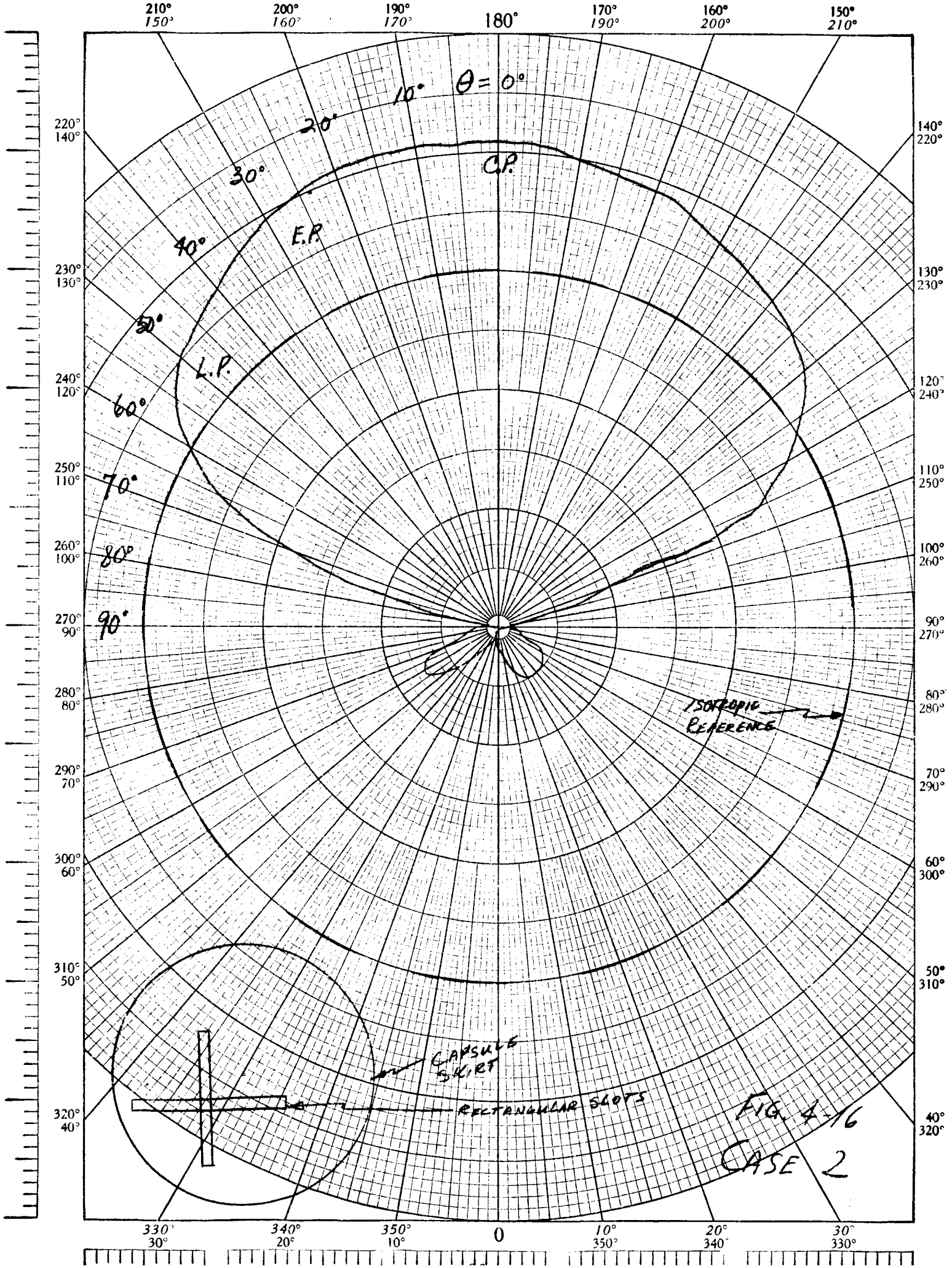
θ = 0°
10°
20°
30°
40°
50°
60°
70°
80°
90°
C.P.
E.P.
L.P.
ISOTROPIC REFERENCE
CAPSULE SKIRT
RECTANGULAR SLOTS
FIG. 4-16
CASE 2
180°
0
KEUFFEL & ESSER CO.

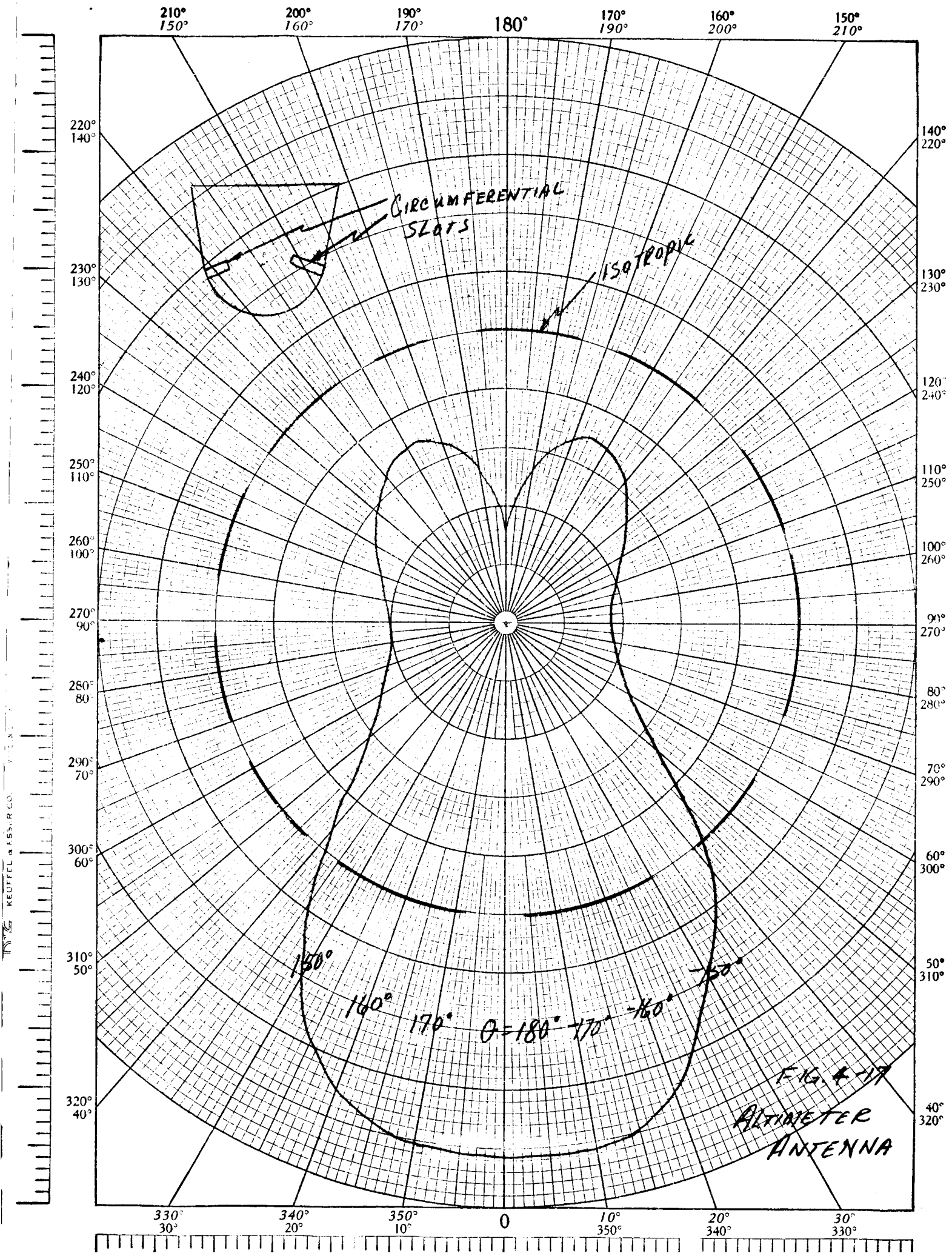
210° 150°
200° 160°
190° 170°
180°
170° 190°
160° 200°
150° 210°
220° 140°
230° 130°
240° 120°
250° 110°
260° 100°
270° 90°
280° 80°
290° 70°
300° 60°
310° 50°
320° 40°
140° 220°
130° 230°
120° 240°
110° 250°
100° 260°
90° 270°
80° 280°
70° 290°
60° 300°
50° 310°
40° 320°
330° 30°
340° 20°
350° 10°
0
10° 350°
20° 340°
30° 330°
CIRCUMFERENTIAL SLOTS
ISOTROPIC
150°
160°
170°
θ=180°
-170°
-160°
-150°
FIG. 4-17
ALTIMETER ANTENNA

AERONUTRONIC—DEVELOPMENT SKETCH

	NAME	DATE			REMARKS:
PREPARED BY:			TEMPORARY		
CHECKED BY			PERMANENT		
APPROVED BY			PROJECT		

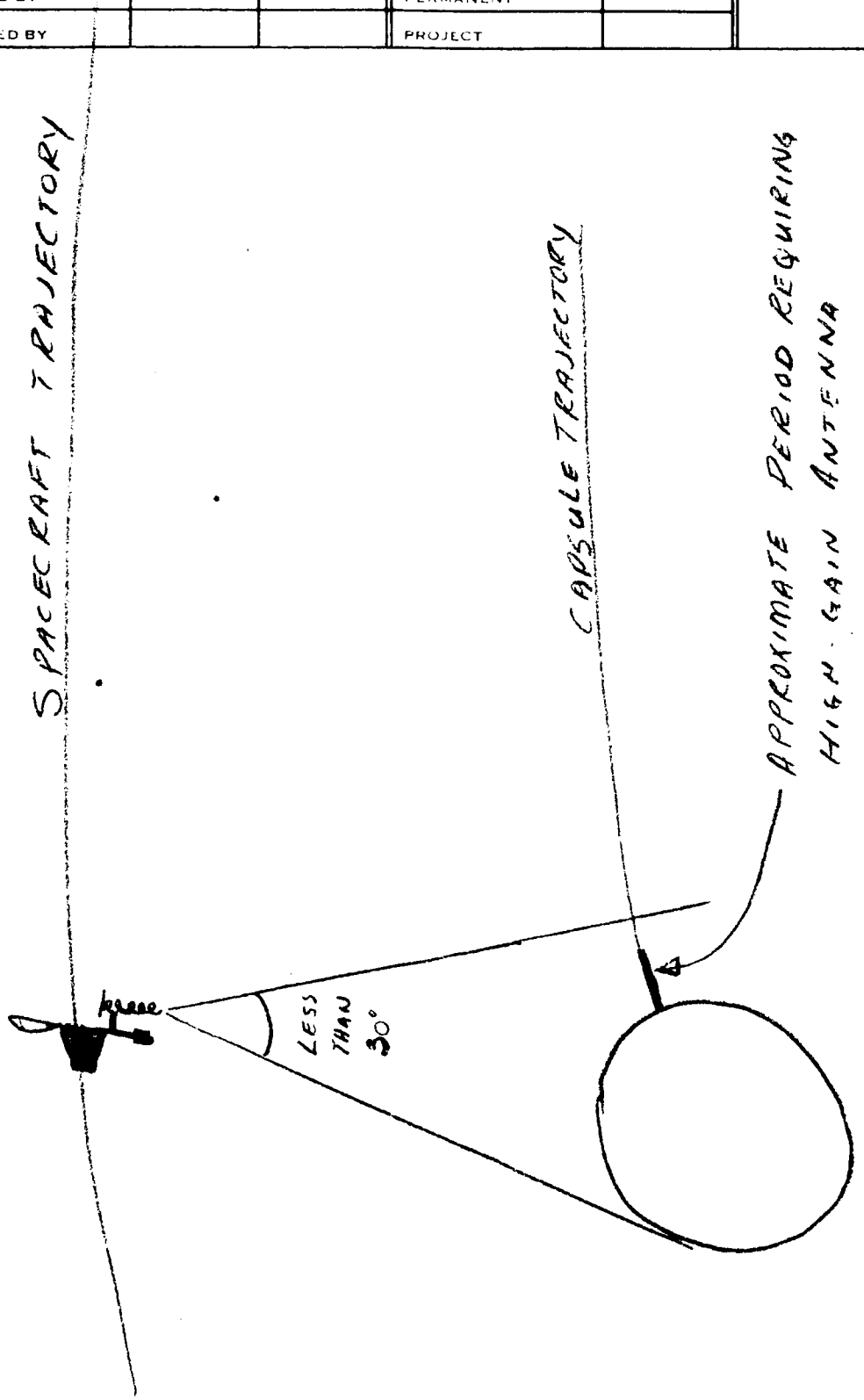

Gen Adm
Feb 60 **ARD-7027**

FIG. ~~5.7~~ 5.1 GEOMETRY

Ford Motor Company — AERONUTRONIC DIVISION

Intra-Company Communication

SUBJECT: Antenna Breakdown - Mariner B

DATE: October 20, 1961

FROM: P. B. Bower

CC: J. Kemmerly
F. Losee
J. Oslake
File

TO: John Housego

---

1. SUMMARY

Two antenna configurations are being considered for the capsule - slot and monopole. The slot is favored, however, since crossed slots mounted in the aft end of the capsule will provide circular polarization in the region of interest.

The attached curves present antenna breakdown power versus altitude for the two antenna types. For the case of a pair of crossed slots, of course, the slot curve indicates breakdown power per slot. The total transmitter power would then be twice this amount. Then, for the pair of crossed slots, a 300-watt transmitter could be turned on at any point below about 120,000 feet.

2. CALCULATIONS

Monopole Antenna

An earth-type atmosphere was assumed, which may be slightly pessimistic for our purpose. Data from SRI Technical Report No. 69, "Voltage Breakdown of Antennas at High Altitudes" by Scharfman and Morita, was used in computing the curves. They have experimentally obtained a curve of E_e/p versus pr, where p is the pressure in mm-Hg, r is the monopole radius in cm, and

$$E_e = \frac{E}{\sqrt{1 + \frac{\omega^2}{\nu^2}}} \text{ v/cm}$$

E = Field intensity, v/cm

ω = Radiated frequency, rad/sec

ν = Collision frequency, rad/sec

The field intensity about a quarter-wave monopole is strongest at the tip. The field at the tip is

$$E_t = \frac{91\ I}{r} \text{ v/cm}$$

I = Current at input terminals, amp.

r = Radius of monopole, cm

177

For a resonant monopole the input resistance is 37 ohms, so that for the input average power

$$P = \tfrac{1}{2} I^2 R = \tfrac{1}{2} \cdot 37 \cdot I^2$$

$$= 18.5 \; I^2$$

$$= 18.5 \left(\frac{E_t \; r}{91}\right)^2$$

$$= 2.24 \times 10^{-3} \; r^2 \; E_t^{\,2}$$

and

$$E_t^{\,2} = \left(1 + \frac{\omega^2}{\nu^2}\right) E_e^{\,2}$$

to initiate breakdown.

Slot Antenna

Scharfman and Morita have also obtained (experimentally) a curve of E_e/p versus pb for a slot antenna, where b is the slot width in cm. For the slot, the aperture dimensions which are $\lambda/2$ by 0.01λ, the field intensity at aperture is

$$E_s = \frac{31.6}{b} \sqrt{P} \quad \text{v/cm}$$

$$= \frac{31.6}{2.24} \sqrt{P} = 14.1 \sqrt{P} \quad (f = 250 \text{ mc}).$$

then

$$P = \text{Transmitted power, watts}$$

$$= \frac{E_s^{\,2}}{200}$$

But

$$E_s^{\,2} = \left(1 + \frac{\omega^2}{\nu^2}\right) p^2 \left[E_e/p\right]^2$$

Therefore

$$P = \frac{\left(1 + \frac{\omega^2}{\nu^2}\right) p^2 \left[E_e/p\right]^2}{200} \text{ watts}$$

for antenna breakdown.

PBB

Paul B. Bower

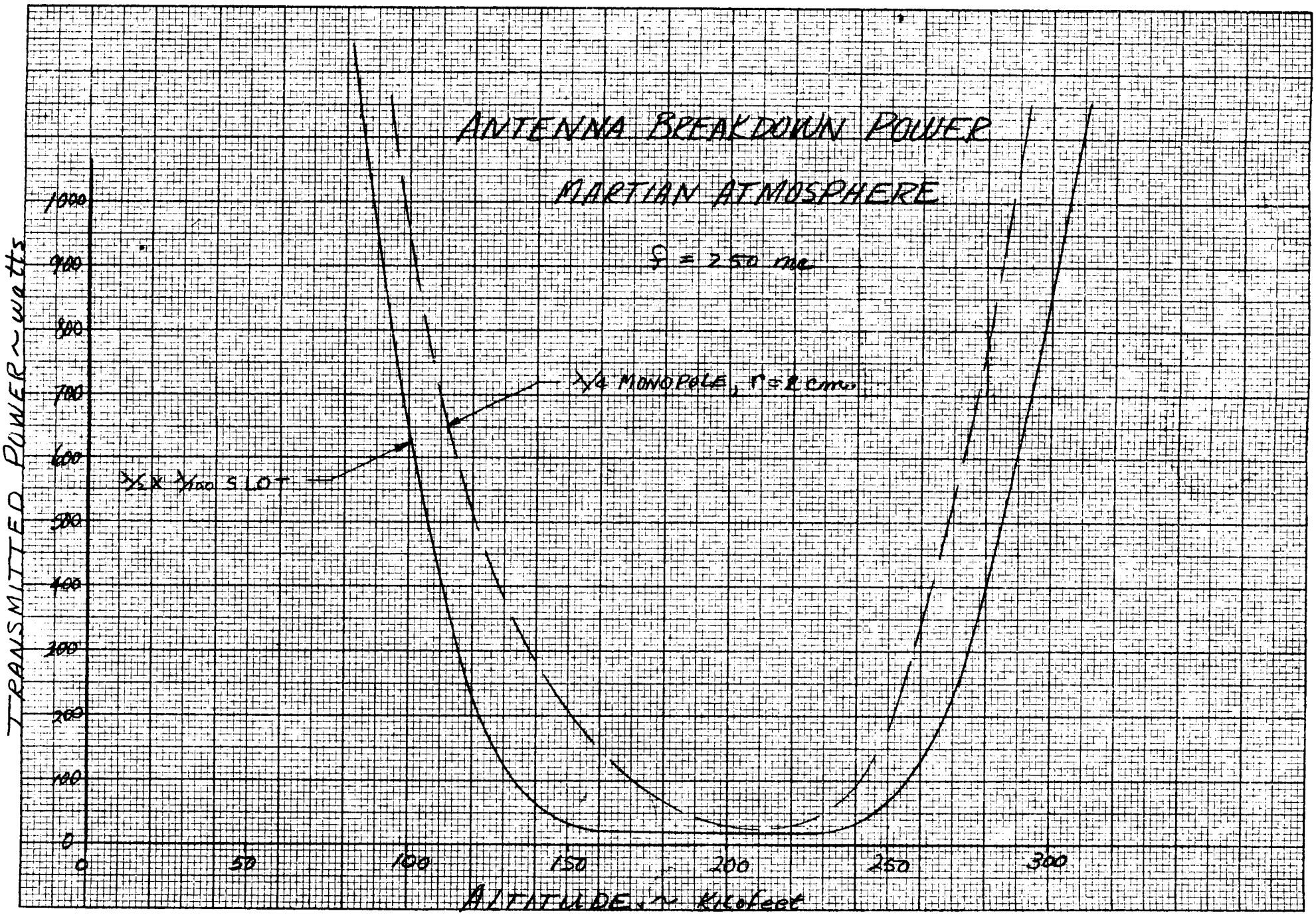
ANTENNA BREAKDOWN POWER
MARTIAN ATMOSPHERE
f = 250 mc
λ/4 MONOPOLE, r = 2 cm
λ/2 X λ/100 SLOT
TRANSMITTED POWER ~ watts
1000
900
800
700
600
500
400
300
200
100
0
0
50
100
150
200
250
300
ALTITUDE ~ Kilofeet

Ford Motor Company, AERONUTRONIC DIVISION

Intra-Company Communication

November 6, 1961

To: J. E. Kemmerly

From: G. J. Pastor

Subject: MARINER B STUDY

In accordance with your request, please find attached description of the Mariner B Capsule Data Handling Equipment.

GJP/pl/clm

177 A

4.2 DATA HANDLING SYSTEM

The purpose of the data handling system is to accept data from information sources such as TV camera, sensors, etc., and to convert these raw output signals into uniform pulse code modulated video signals suitable for transmission to the spacecraft for storage and retrnsmission to earth.

It is convenient to divide the necessary equipment into two categories:

1) Data Links

2) Timing System and Programming

The former performs basically data sampling and encoding functions, while the latter provides all necessary timing and programming functions for both data links, data sources and other devices.

In the following description, it will be assumed that all required timing signals are available from the Programmer. Thereby, the timing requirements will be developed for each unit and the Programmer design presented in a more logical manner.

4.2.1 Data Links

The information emanating from the capsule sensors can be conveniently divided into two groups:

1) Wide band information, such as TV.

2) Narrow band information, such as experiments, capsule performance, equipment performance, etc.

Since the first group requires considerably more power than the second for any desired accuracy and S/N margin, it is logical to employ two different telemetry systems. A wide band (WB) and a narrow band (NB) system is proposed such that power consumption can be maintained at a minimum, by employing the WB telemetry only during brief transmission periods.

Television (WB) Telemetry

System reliability and mission success confidence level consideration require complete redundancy in processing the three (red, blue and green filter) TV camera outputs. Since the redundant design includes three subcarriers, each encoder (video section) of the WB telemeter may be simultaneously operating and only one needs to be described. The black and white TV camera can time share one of the three encoders since it ceases operation prior to the beginning of the color picture taking.

The TV camera output signal is assumed to represent a TV frame with 200 x 200 resolution (40,000 samples) at eight (8) gray levels. It is further assumed that the scan time for a single frame is approximately 5-6 seconds, while erase time is negligible.

Since the camera control and WB telemetry timing is synchronized by the same programmer, the following message structure is proposed:

1 Telemetry Word	= 211 Words = 633 Bits = Bits data + 33 bits TM frame sync.
1 Television (TV) frame	= 200 TM frames = 42,200 words = 126,000 bits
TM Frame Sync.	= 33 bit Barker Code = 11 TM words
TV Frame Sync.	= 33 bit Barker Code, complement of the TM frame sync. = 11 TM words

These time units are shown pictorially in Fig. 4-4. The operating concept is as follows (See Fig. 4-5):

1) Upon command from the programmer, a pre-exposure transmission is initiated before each picture. This consists of transmitting a programmer generated train of alternating ones and zeros interrupted after each 600 bits by a 33 bit Barker code word. This is the equivalent of one TM frame. The alternating ones and zeros provide quick bit sync acquisition in the spacecraft. The TM frame sync code represents approximately 5% of frame energy and, therefore, transmission of a few (N) TM frames will provide TM frame lock-on in the spacecraft. (The number N will depend on the S/N ratios, detector thresholds and on the desired error probability). During the Nth frame an erase command is given to the camera, and during the Nth frame sync period (TV frame sync) the shutter is opened by the programmer. Note that the different TV frame sync word will serve, when detected in the spacecraft, as an enable to start recording the forthcoming data.

2) After the shutter has closed, (end of TV frame sync) the Video signal from the camera is sampled and held at the word rate (which is one third of the bit rate). Each held sample then is encoded into a three bit word in the encoder. At the end of each TM frame the encoder will generate the RM frame sync code word. At the end of the transmission, (one complete TV frame), the inverted code word will be generated similarly to the pre-exposive operation. This will serve as a stop recording command in the spacecraft.

Assuming a bit rate of 25,000 bits per second the complete frame transmission time is approximately 5.06 seconds.

Adding a parity bit to each word would increase the power requirement by 25%; consequently is not considered. If improved error probability will be required, parity bits after some groups of data words will be provided as a compromise.

AERONUTRONIC—DEVELOPMENT SKETCH

	NAME	DATE			REMARKS:
PREPARED BY:			TEMPORARY		
CHECKED BY:			PERMANENT		
APPROVED BY:			PROJECT		

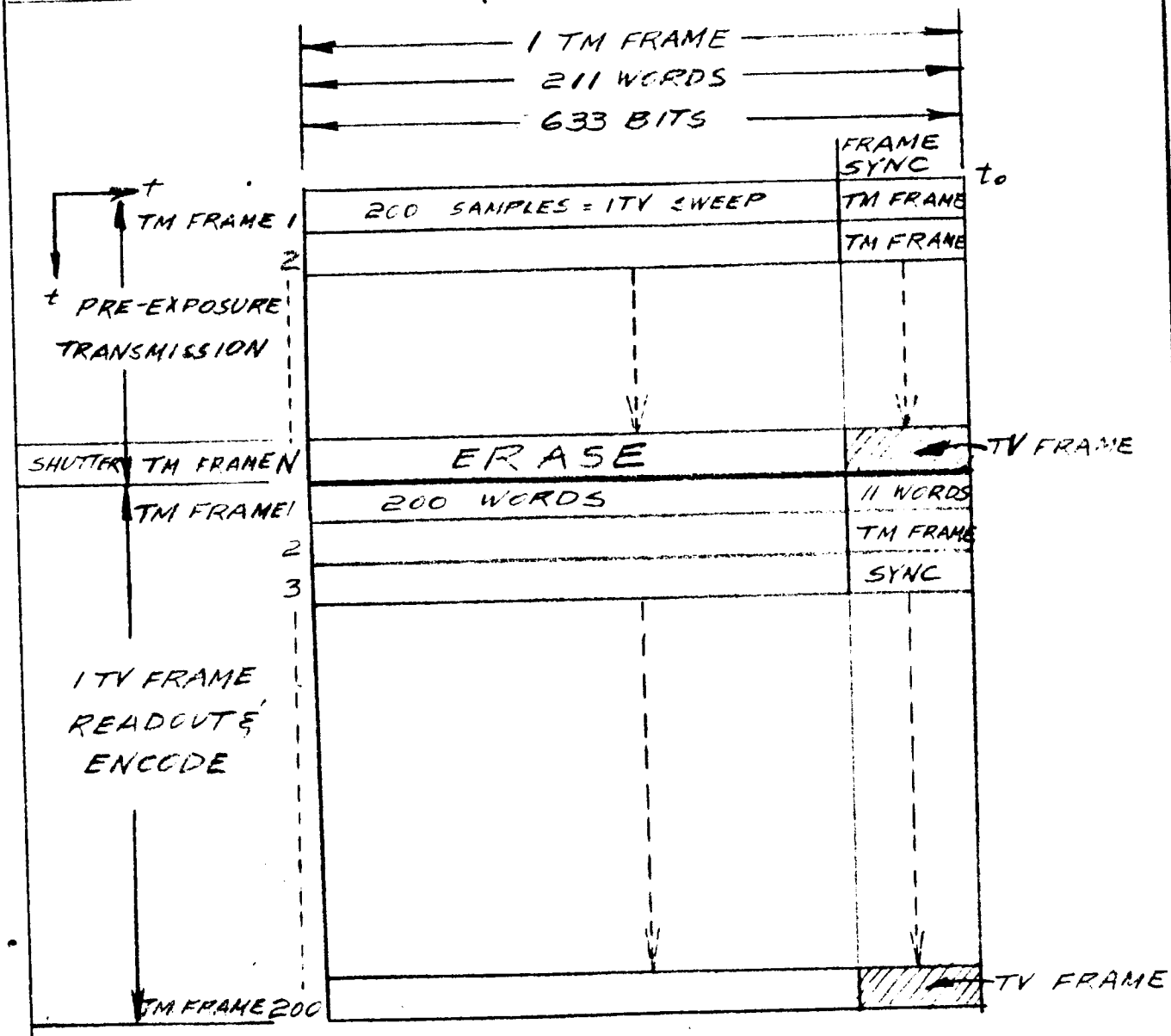

FIG 4-4 MESSAGE STRUCTURE TV (WB) TELEMETRY

GEN. ADM. ARD7027
DEC. 59

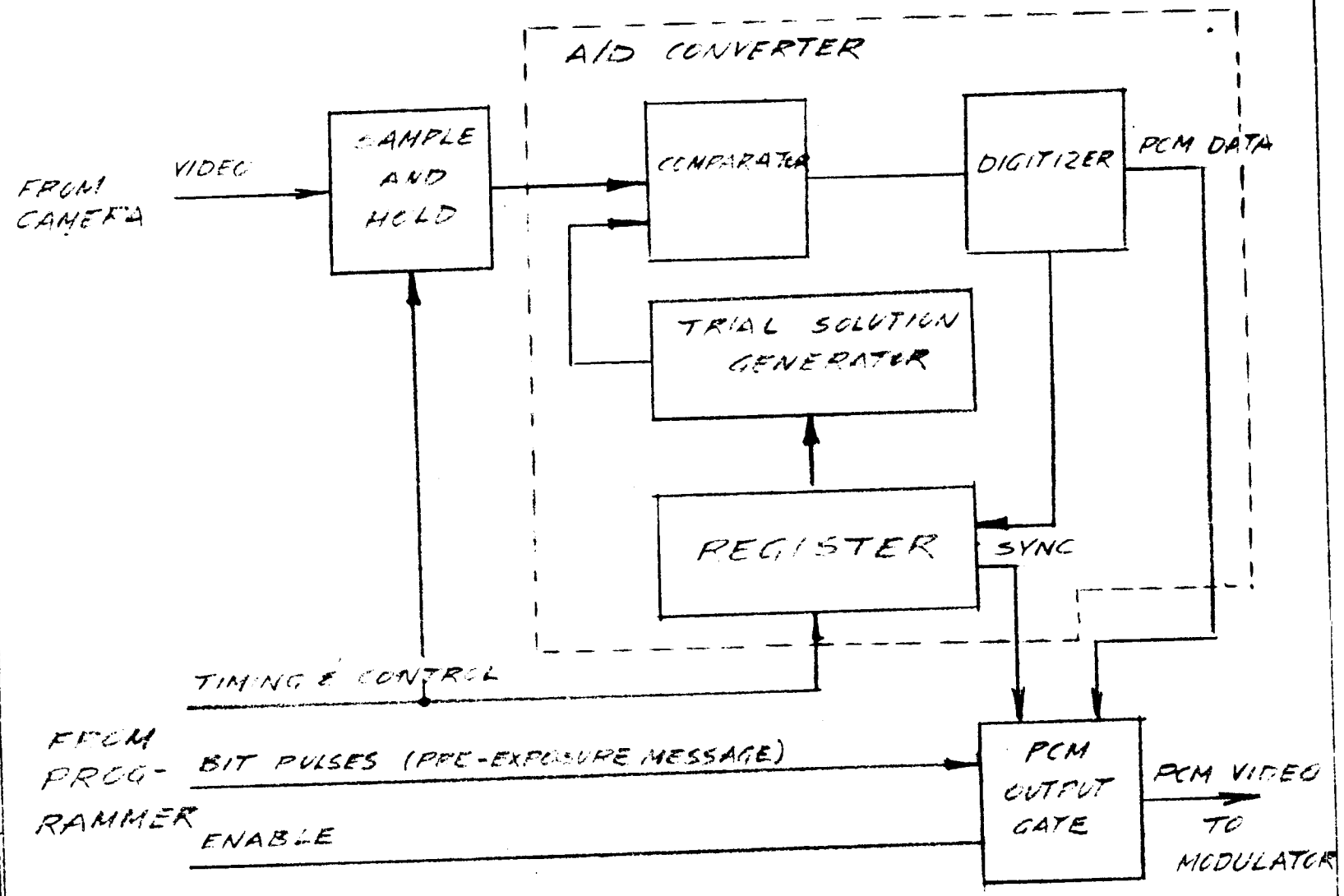

FIG. 4-5 BLOCK DIAGRAM —V (W.B) ENCODER

AERONUTRONIC—DEVELOPMENT SKETCH

	NAME	DATE	REMARKS:
PREPARED BY:			TEMPORARY
CHECKED BY:			PERMANENT
APPROVED BY:			PROJECT

GEN. ADM. AR07027 DEC. 59

The required equipment is quite simple. It consists of a sample and hold circuit and a three bit A/D converter. For the A/D converter the digital feedback type, serial, half-range trial solution generating circuits are recommended. This device provides easily sync code generation by parallel to serial conversion during the sync word periods.

The pertinent physical characteristics of a single WB encoder are as follows:

Weight	5 oz.
Volume	8 cu. in.
Power Requirement	400 milliwatts

Diagnostic and Experimental (NB) Telemetry

The NB telemetry is to provide information about the performance of the capsule, its instrumentation, the data obtained in the scientific experiments and the performance of the TV camera - WB telemetry subsystems.

In order to perform these tasks it will be turned on prior to separation from the spacecraft.

A typical vehicle-borne PCM telemeter that will provide sufficient channel and information capacity is briefly described in the following:

The system parameters are as follows:

Bit rate	100 bits per second
Word length	6 bits including parity
Frame length	16 words = 96 bits
Primary Channels	14 + 2 per frame sync.
Subcommutation sequence	8 frames

Resulting Typical Information Capacity

Type of Channel	Sampling Rate
1 Supercommutated primary	4 samples/sec
6 Direct primary	1 sample/sec
31 Subcommutated information channel within 4 primary	1/8 sample/sec

The totaled information capacity is approximately 14 samples per second excluding sync.

The typical message structure is shown in Fig. 4-6. The operation of the NB telemetry is typical. (See Fig. 4-7). The programmer generates 6 bit pulses, 16 word pulses, 8 frame pulses and all necessary control signals.

The frame pulses operate the sub-multiplexers whose outputs feed the analog primary multiplexer.

AERONUTRONIC—DEVELOPMENT SKETCH

	NAME	DATE			REMARKS:
PREPARED BY:			TEMPORARY		
CHECKED BY:			PERMANENT		
APPROVED BY:			PROJECT		

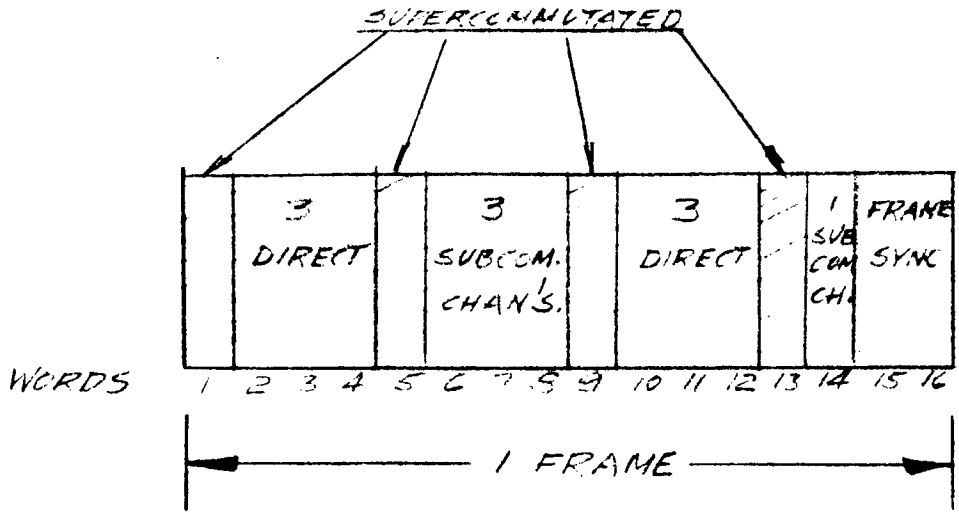

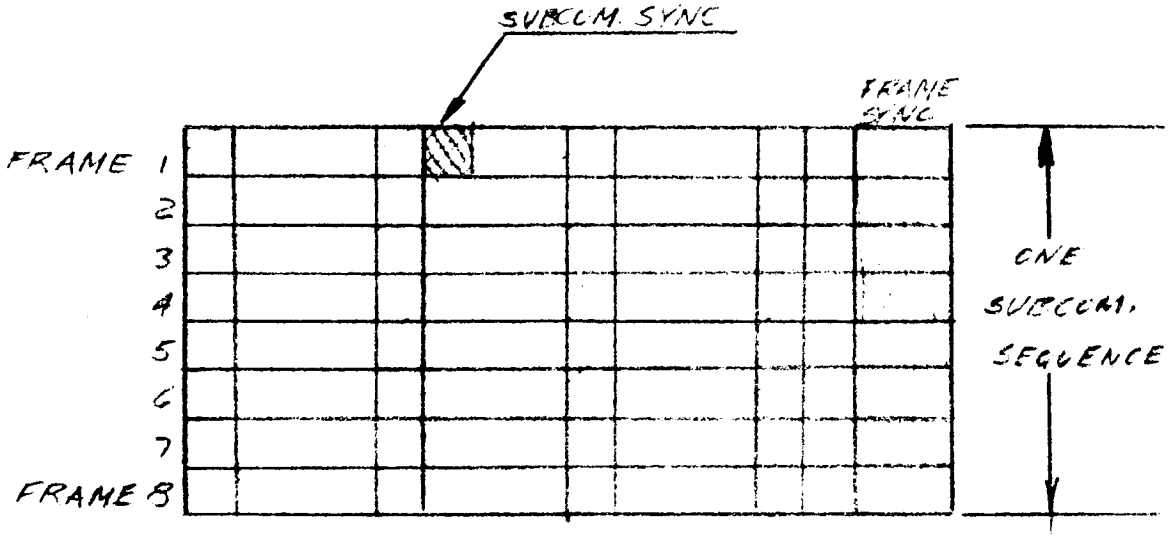

FIG 4-6 MESSAGE STRUCTURE
NARROW BAND TELEMETRY

GEN. ADM. ARD7027
DEC. 59

AERONUTRONIC—DEVELOPMENT SKETCH

	NAME	DATE			REMARKS:
PREPARED BY:			TEMPORARY		
CHECKED BY:			PERMANENT		
APPROVED BY:			PROJECT		

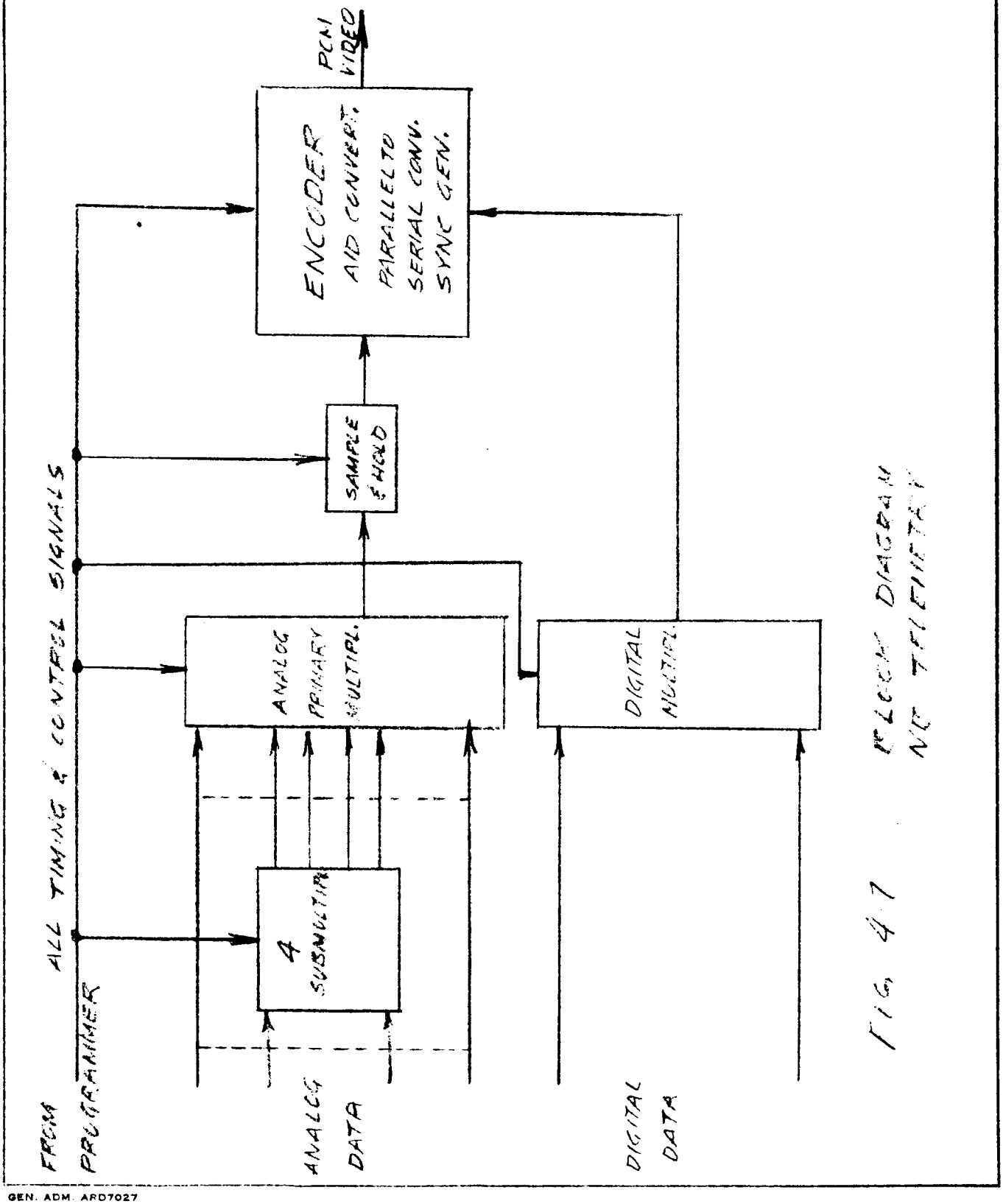

FIG. 4.7 BLOCK DIAGRAM
NC TELEMETRY

GEN. ADM. ARD7027
DEC. 59

The word and bit pulses enable the analog or digital multiplexer. The former provides a single time division multiplexed signal of PAM samples. The latter provides sequenced, interlaced parallel readout pulses corresponding to all digital sources.

The PAM pulse train is re-sampled and held constant for encoding, while the digital multiplexer output is inserted in parallel into the encoder register. The encoder may be similar in design to the one discussed for the WB telemetry. In that case it also provides sync word generation and parallel-to-serial conversion.

The estimated physical characteristics of the Narrow band telemetry (excluding the programmer) are as follows:

Weight	2 lbs.
Volume	50 cu. in.
Power Consumption	3 watts

In the above description, no allowance is made for signal conditioning equipment prior to entering the NB telemetry unit. These may include special amplifiers, storage registers, etc. at an estimated:

Volume	20 cu. in.
Weight	10 oz.
Power Consumption	750 milliwatts

4.2.4 Timing System and Programming

Three of the major capsule subsystems; the camera, wide band television and narrow band telemetry usually contain their own timing and programming circuits. In this application, however, the operation of these subunits must be so closely integrated not only among themselves but with other switching functions that a central timing and programming system is envisioned.

The central timing and programming system will have only switching type inputs from either the spacecraft or some event detecting transducers such as the g-switch and accelerometer. The outputs are two kinds: turn on-turn off, type switching commands and logic-generated timing and enable signals.

A possible sequence of events pertinent to the operation of the central timing and programming system is shown in Fig. 3-3. (See page F-11)

Four major subunits of the central timing and programming system will perform all of these functions. A description of these subunits follows (see Fig. 4-8):

- Events and Time Base Generation

The events control and time base generator consists of two types of devices; electromechanical switches and timers, and electronic oscillators and counters.

AERONUTRONIC—DEVELOPMENT SKETCH

	NAME	DATE			REMARKS:
PREPARED BY			TEMPORARY		
CHECKED BY			PERMANENT		
APPROVED BY			PROJECT		

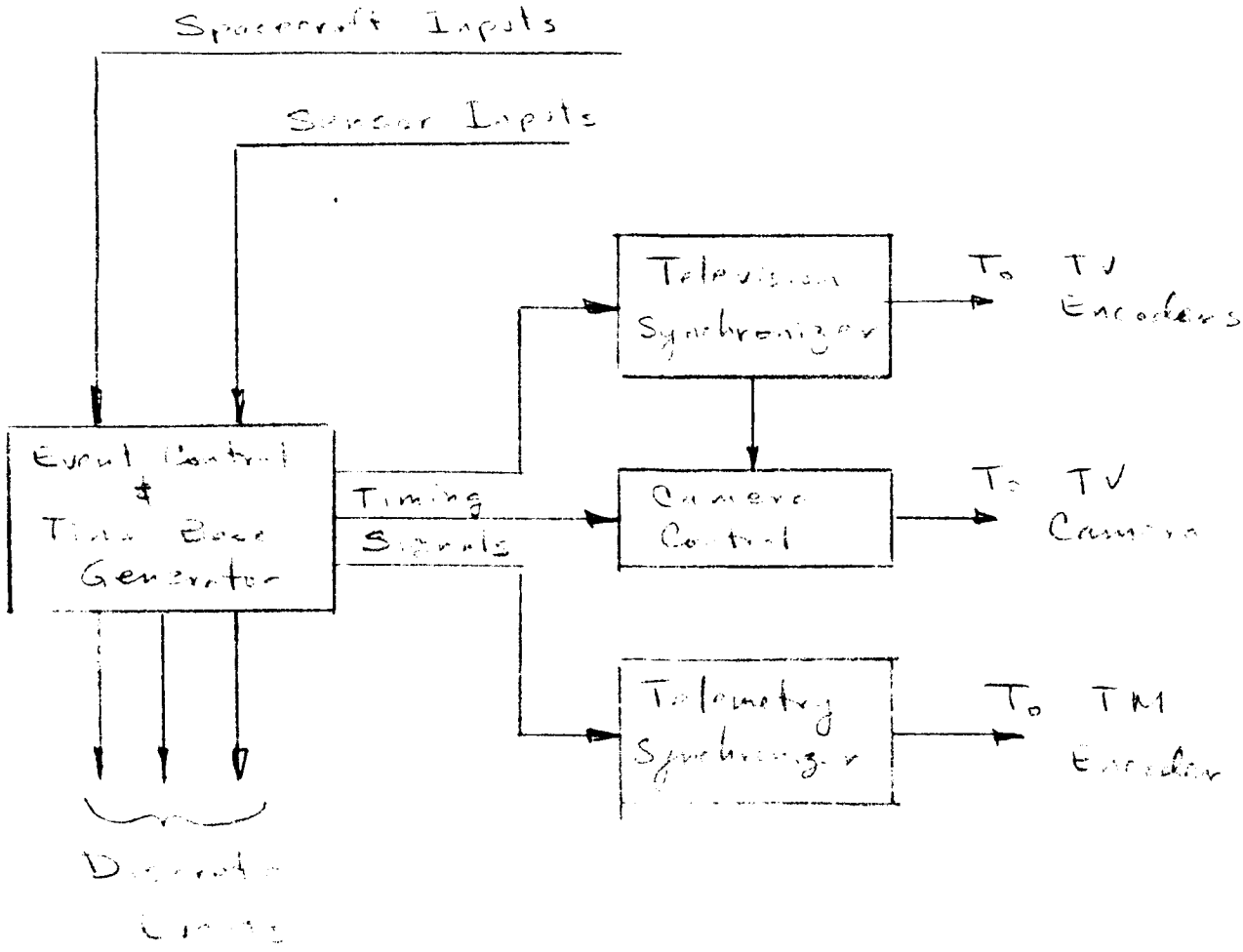

Fig 4-8 Central Timing & Programming System

All basic event controls and time intervals are generated to operate the rest of the instrumentation through the camera control unit and telemetry and television synchronizers.

The estimated physical characteristics of this subsystem are as follows:

Volume	400 cu. in.
Weight	6 lbs.
Power Consumption	8 watts

Camera Control

The camera control unit receives various timing signals from clock pulse counters in the time base generator and from these it generates the following signals by logical gating:

a) Word and TV frame clock pulses for the camera sync generator.
b) TM frame sync pulse for insertion control.
c) TM frame pulses for erasure control.
d) TV frame sync pulse for shutter control.

These signals are in agreement with Fig. 4-4 where the general timing of camera operation is shown.

Since it is assumed that all three subcarriers are operated simultaneously, the same outputs operate all three cameras synchronously. The estimated physical characteristics of the camera control programmer are as follows:

Volume	20 cu. in.
Weight	10 oz.
Power Consumption	500 milliwatts

Television Control

The television synchronizer contains the usual circuit elements of a PCM telemetry programmer. From the clock pulse counters, outputs in the Time Base Generator sequenced bit, word and TM frame pulses are derived through rectangular matrices. The bit pulses operate the A/D converter and in conjunction with selected word and frame pulses provide both TM and TV frame sync code word generation. From the word counter the sample and hold command pulse is derived, while the bit counter with some logical gating provides the alternating ones and zeros of the pre-exposure message.

Note that the TM frame sync pulses are the same as the insertion control pulse for the camera; similar parallelism applies to the TV frame sync pulse and shutter control.

The estimated characteristics are as follows:

Volume	40 cu. in.
Weight	20 oz.
Power Consumption	1 watt

Telemetry Control

The elements of the NB telemetry synchronizer are very similar to those of the television synchronizer. Here again rectangular matrices provide the sequenced bit, word, frame and subcommutation frame pulses.

The selected word pulses operate the analog primary multiplexer, while the frame pulses turn on the submultiplexer.

Selected bit and word pulses provide readout from several digital data sources in the digital multiplexer.

Sample and hold and A/D converting operations are only required during the analog-source-sampling portion of the frame. During the digital source words the bit and word pulses operate the Encoder register as a shift register for parallel-to-serial conversion.

Sync code words are generated in a similar fashion from the selected bit, word and frame pulses.

The physical characteristics are estimated as follows:

Volume	80 cu. in.
Weight	2 lbs.
Power Consumption	2 watts

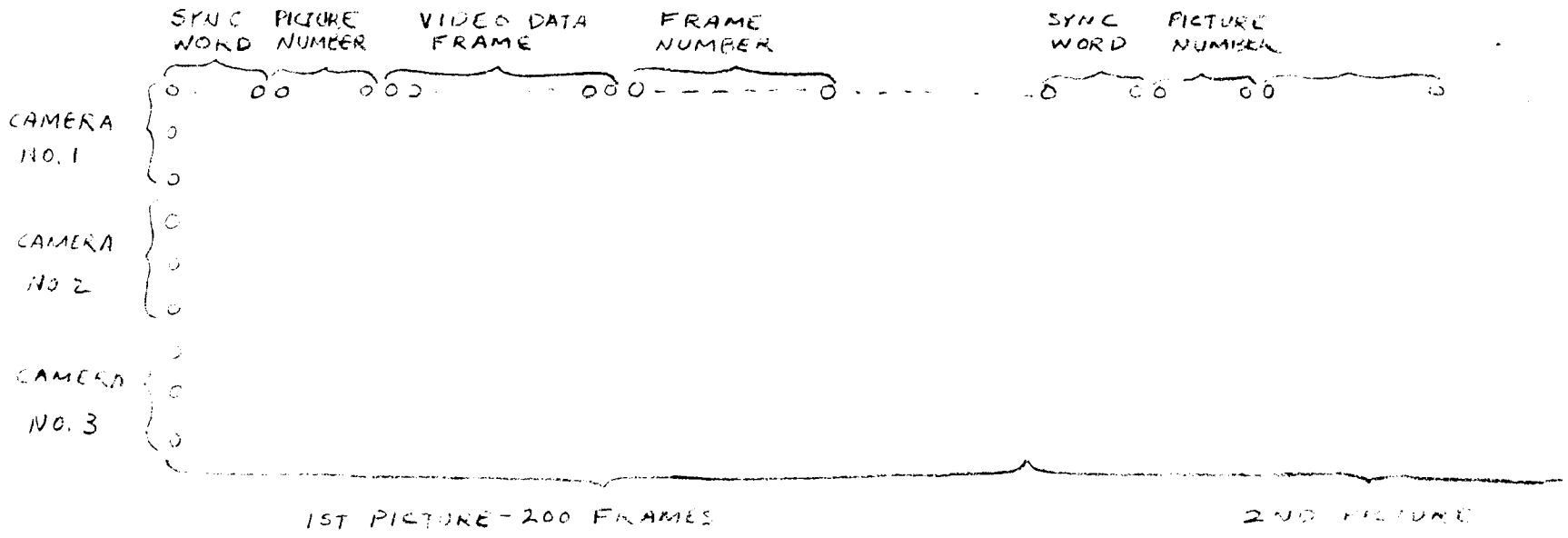

FIG. E-4 STORAGE TAPE FORMAT

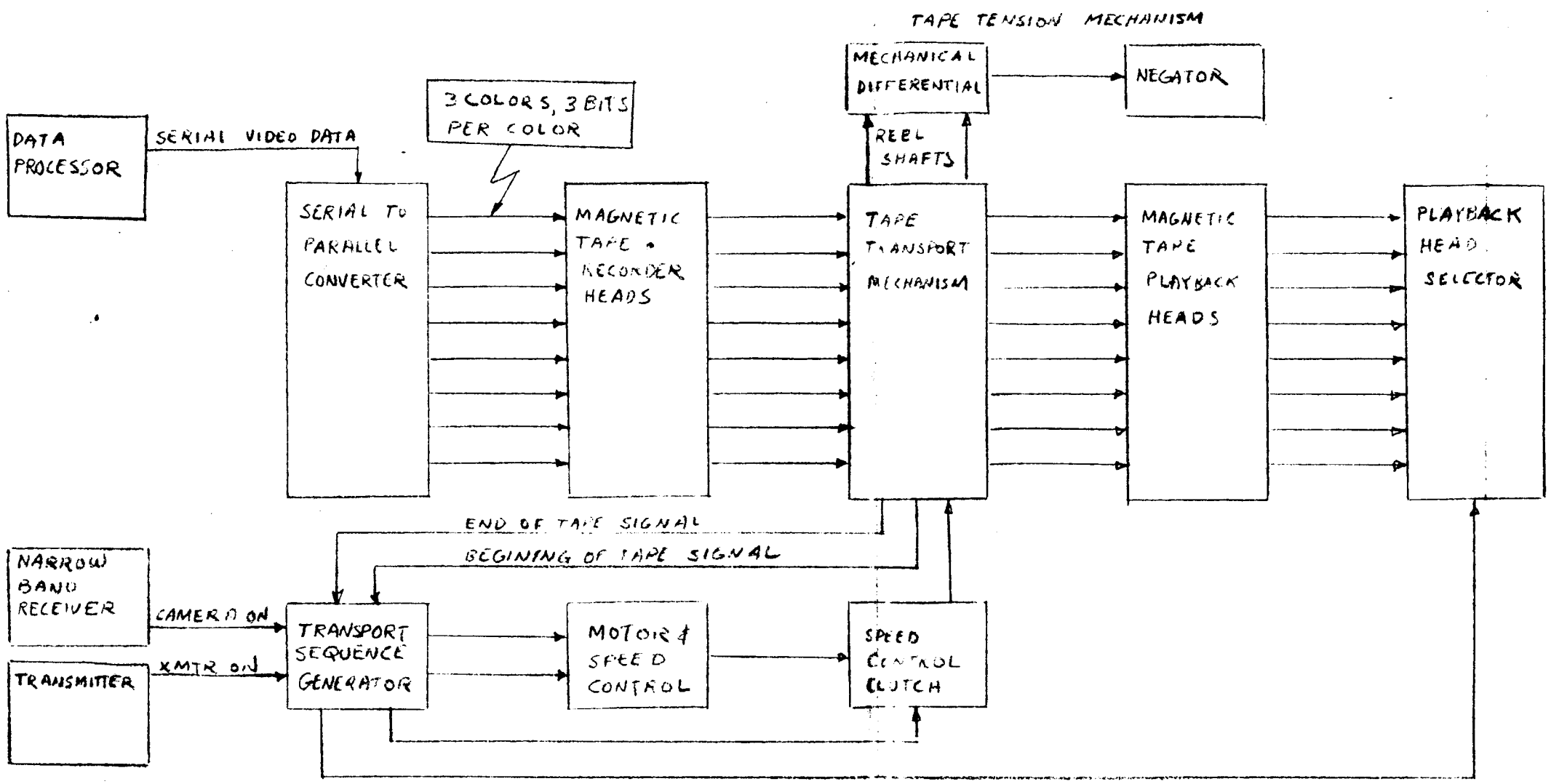

FIG. 5-5 TAPE STORAGE SYSTEM

1)	Number of pictures	10 black and white 30 color
2)	Bits per picture (including sync)	1.3×10^5 black and white 4×10^5 color
3)	Scan Time	6 sec./picture
4)	Playback rate	100 bits per second
5)	Recording Time	2 minute black and white 1 minute gap 2 to 4 minutes color

These requirements lead to the specifications listed in Table 5-2.

Table 5-2

Tape Storage Specifications

Number of Recording Tracks	9
Bit rate per head	7400 bits per second
Packing Density	200 bits per inch
Tape length (40 pictures) (10% for 1 start-stop gap)	800 feet
Recording Velocity	37 inches per sec.
Playback Velocity	0.5 inch per sec.
Power	2 amp. at 28V
Weight	10 pounds
Size	7 in. OD, 10 in. long
Playback Time	4 hours
Start or Stop Time	3 seconds

Currently under development at Consolidated Electrodynamics Corporation, Pasadena, California, is a satellite magnetic tape recorder/reproducer with specifications very close to our requirements. It is representative of the state-of-the-art of aerospace magnetic tape equipment.

The following specifications have been published by the manufacturer:

Size	200 cubic inches (reduceable to 100 cubic in.)
Weight	6 lbs. or less
Tape Speed	1 ips record 18 ips reproduce
Wow & Flutter	1.5% peak-peak 1 to 300 ips
Design Life	4000 hours
Frequency Response	1 K and 25 KC
Tape Capacity	750 ft.
Tape Width	1/4 or 1/2
Start Time	2 Seconds
Power Consumption	28 VDC supply
Record	0.27 watts
Reproduce	0.54 watts

DEG/pl

Ford Motor Company — AERONUTRONIC DIVISION

Intra-Company Communication

October 17, 1961

TO: Distribution

cc: S. Lampert
D. Rodriguez
L. Stimpson

FROM: M. G. Boobar

SUBJECT: Mariner B Capsule Study - Communications Blackout During Entry

---

Attached are two figures showing the stagnation point temperatures, pressures, electron densities and collision frequencies, as a function of time and altitude, for a capsule entering the Martian atmosphere (Atmosphere E) at an initial velocity of 22,000 ft/sec, $\theta_E = 90$ and $m/C_DA = 1$.

The high electron densities ($\sim 10^{14}$) indicate a probable transmission blackout, based on stagnation point conditions, from altitudes of over 800,000 feet to below 150,000 feet. A cursury examination of the 20° entry angle trajectory and both 20° and 90° angle trajectories at $V_E = 26{,}000$ ft/sec indicates that the same conditions will prevail.

Conditions at the skirt (side) and rear will not be as severe. The degree of improvement is difficult to "guestimate" without the development of some sort of flow-fields. Time limitations on this study obviously do not permit this sort of development. However, an "eyeball approximation" will be attempted if and when our Mollier diagram is completed.

M G Boobar

/cyl

Two Attachments

Distribution:

J. Arsenault
R. Auelmann
T. Bergstrahl
I. Blifford
M. Boobar
P. Bower
M. Caldwell
E. Durand
R. Foster
A. Gammal
J. Hanrahan
K. Harder
V. Henderson
J. Housego
J. Jansen
J. Kemmerly
W. Lemm
F. Losee
R. Morrow
G. Miczaika
R. Nagorski
T. Neumann
E. Onstead
J. Oslake

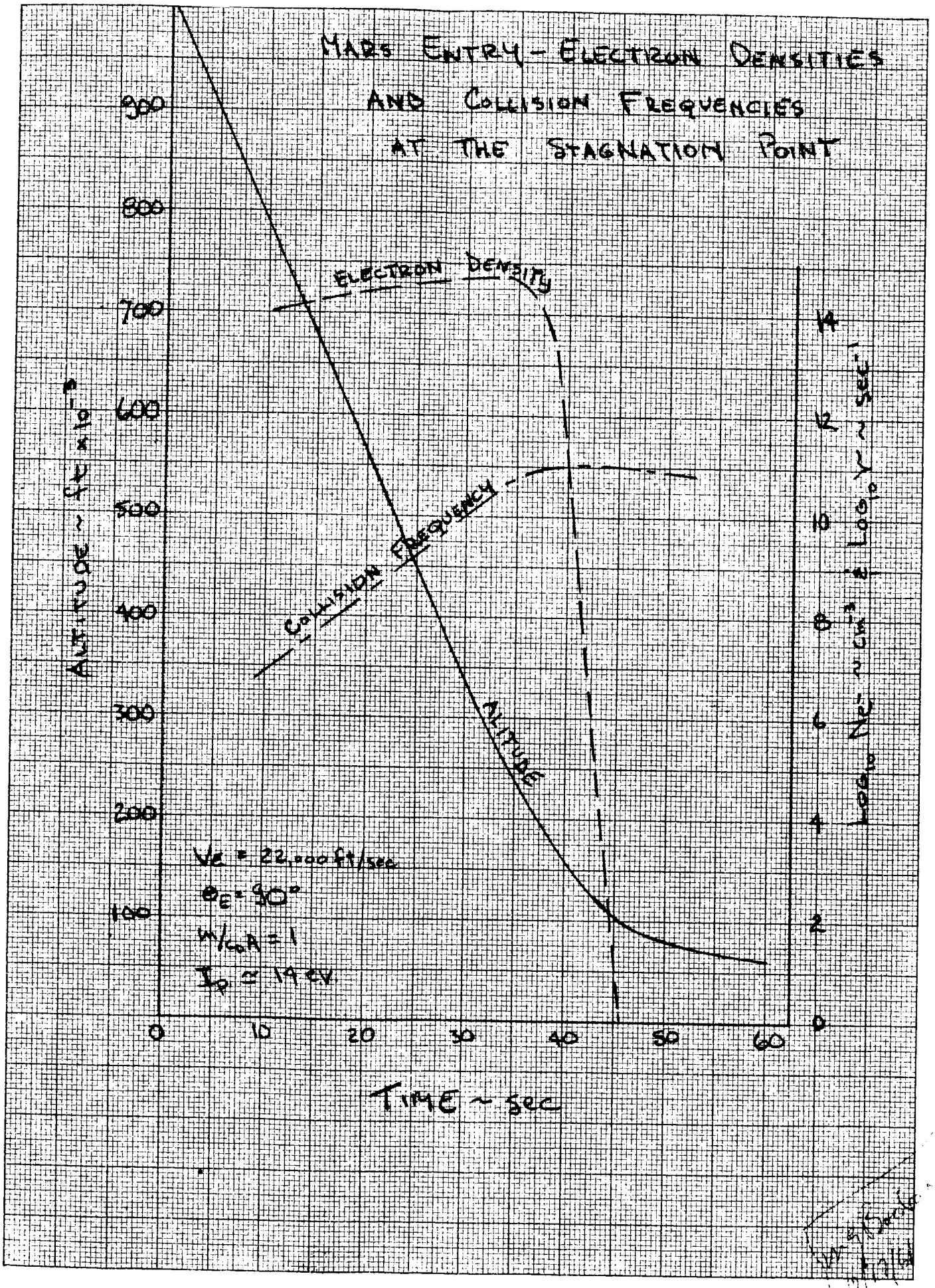
MARS ENTRY - ELECTRON DENSITIES
AND COLLISION FREQUENCIES
AT THE STAGNATION POINT
ELECTRON DENSITY
COLLISION FREQUENCY
ALTITUDE
ALTITUDE ~ ft x 10^-3
900
800
700
600
500
400
300
200
100
0
10
20
30
40
50
60
TIME ~ sec
14
12
10
8
6
4
2
0
LOG10 Ne- ~ cm^-3 & LOG10 ν ~ sec^-1
Ve = 22,000 ft/sec
θE = 90°
m/CoA = 1
Ip ≃ 14 eV

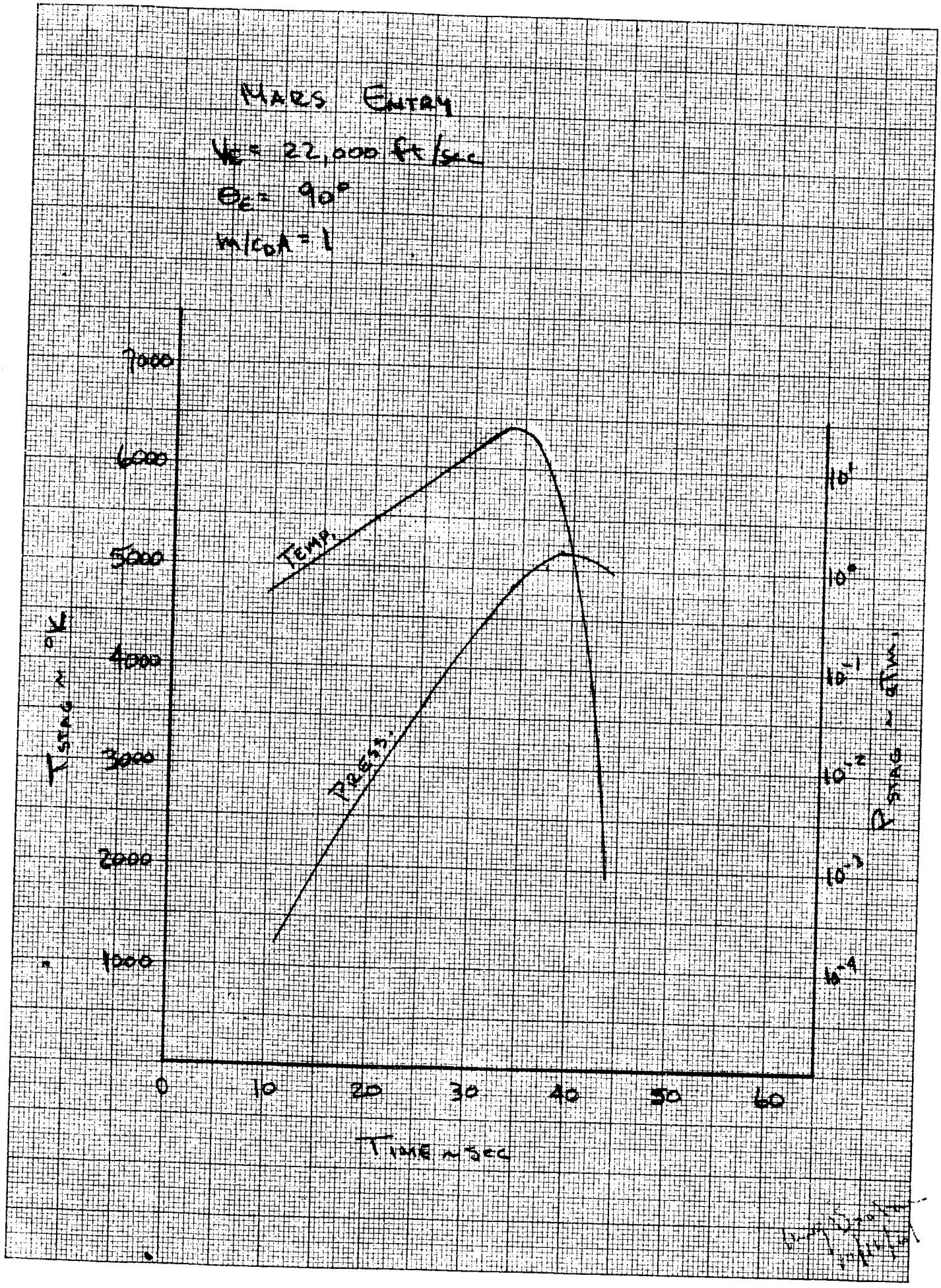
MARS ENTRY
V_E = 22,000 ft/sec
θ_E = 90°
m/C_DA = 1
7000
6000
5000
4000
3000
2000
1000
T_{STAG} ~ °K
TEMP.
PRESS.
10^1
10^0
10^{-1}
10^{-2}
10^{-3}
10^{-4}
P_{STAG} ~ atm
0
10
20
30
40
50
60
TIME ~ sec

Ford Motor Company, AERONUTRONIC DIVISION

Intra-Company Communication

30 October 1961

TO: Mariner B Distribution List

FROM: E.W. Onstead and J.L. Arsenault

SUBJECT: Maximum and Minimum Capsule Transmitting Angles and Distances

This memo provides the preliminary values of the maximum and minimum capsule transmitting angles in order that the power requirements of the capsule may be defined. The capsule transmitting angle (α) is defined as the angle between the capsule-bus line of sight and the capsule areo-centric (Martian) vertical. As a result of this definition, the maximum α for a given set of initial conditions will always occur at impact.

This preliminary investigation was carried out for the range of bus minimum altitudes (h), capsule impact parameters (S), and initial velocities (V_1) of interest. The values of these quantities are tabulated below:

S (km)	h (km)	$V_1 = V_a$ (km/sec)
2×10^3	6×10^3	4
4×10^3	8×10^3	5
0	10×10^3	6

These particular values of S, h, and V_1 were dictated by launch date, geocentric energy, and the photographic mission constraint that $\Lambda_s = \pm 30°$ during the vertical descent portion of the capsule.

Figure 4, which is a plot of the trueanomaly difference (true anomaly at impact of the capsule minus the true anomaly at "impact" of the bus) versus bus minimum altitude for different values of capsule impact parameters and asymptotic velocities, indicates that the conditions giving rise to the maximum capsule transmitting angle are S = 0, V_1 = 4 km/sec, and h = 6×10^3 km. Likewise, the conditions giving rise to the minimum capsule transmitting angle are S = 4×10^3 km, V_1 = 6 km/sec and h = 10×10^3 km. These angles are evaluated to be as follows: $\alpha_{MAX} = 73.6°$ and $\alpha_{MIN} = 5°$. These angles and their corresponding communication distances are tabulated in Figure 2.

EVALUATION OF $\Delta\nu$ AND α

The capsule trajectory and bus trajectory have three things in common: radius at "infinity" (r_1), velocity at "infinity" (V_1), and, for our investigation, the elapsed time on each trajectory is the same. (See Figure 1) The elapsed time is the amount of time required for the capsule to impact on the surface of Mars. This elapsed time is very nearly equal to elapsed time to perigee. Since the capsule trajectory is a hyperbolic trajectory, Lambert's equation as expressed by Eq. (1) provides an accurate means for computing this time. Lambert's equation is written as:

$$t = \sqrt{\frac{a^3}{\mu_M}}\left[-(\alpha - \sinh\alpha) + (\beta - \sinh\beta)\right] \qquad (1)$$

where: $$\sinh\frac{\alpha}{2} = \frac{1}{2}\sqrt{\frac{r_1 + r_2 + c}{a}},$$

AND

$$\cosh\frac{\alpha}{2} = \frac{1}{2}\sqrt{\frac{r_1 + r_2 - c}{a}}$$

The quantities r_1 & r_2 are any two radii. The quantity C is the chord length between these two radii.

In order to find the true anomaly of the bus at capsule impact, it is to be noted that the total travel time of both vehicles is very nearly equal and quite large (on the order of 70,000 sec). Therefore, we need only use one trajectory, the capsule trajectory in this case, and perturb it at perigee to find the variation in trip time to infinity (r_1). This time variation multiplied by the mean motion (n), yields a ΔM (change in the mean anomaly) which is added to the mean anomaly of the bus at "impact" (M_{IC}). In essence, it is being implied that the Δt between the two orbits to perigee is approximately equal to the Δt or ΔM by which the bus must lead or lag the capsules at impact; that is, $M_{IB} = M_{IC} \pm \Delta M$ which in turn yields a value for ν_{IB} (true anomaly at impact of the bus).

The actual method of computing $\Delta\nu$ and α is as follows:

I. Differentiate (1) under the constraint that r_1 and a are constants.

$$\Delta t = \sqrt{\frac{a^3}{\mu}}\left[-\frac{\partial\alpha}{\partial\Pi_2}\Delta\Pi_2 - \frac{\partial\alpha}{\partial c}\Delta c + \cosh\alpha\frac{\partial\alpha}{\partial\Pi_2}\Delta\Pi_2 + \cosh\alpha\frac{\partial\alpha}{\partial c}\Delta c\right.$$

$$\left. + \frac{\partial\beta}{\partial\Pi_2}\Delta\Pi_2 + \frac{\partial\beta}{\partial c}\Delta c - \cosh\beta\frac{\partial\beta}{\partial\Pi_2}\Delta\Pi_2 - \cosh\beta\frac{\partial\beta}{\partial c}\Delta c\right]$$

where

$$\frac{\partial\alpha}{\partial\Pi_2} = 2\frac{\partial\frac{\alpha}{2}}{\partial\Pi_2} = \left(4a\sinh\frac{\alpha}{2}\cosh\frac{\alpha}{2}\right)^{-1}$$

$$\frac{\partial\alpha}{\partial c} = 2\frac{\partial\frac{\alpha}{2}}{\partial c} = \left(4a\sinh\frac{\alpha}{2}\cosh\frac{\alpha}{2}\right)^{-1}$$

$$\frac{\partial\beta}{\partial\Pi_2} = 2\frac{\partial\frac{\beta}{2}}{\partial\Pi_2} = \left(4a\sinh\frac{\beta}{2}\cosh\frac{\beta}{2}\right)^{-1}$$

$$\frac{\partial\beta}{\partial c} = 2\frac{\partial\frac{\beta}{2}}{\partial c} = -\left(4a\sinh\frac{\beta}{2}\cosh\frac{\beta}{2}\right)^{-1}$$

Note: Second order effects may be neglected here as the second differential was found to be identically zero. Therefore:

$$\Delta t = \sqrt{\frac{a^3}{\mu}}\left[\frac{\cosh\alpha - 1}{2a\sinh\alpha}(\Delta\Pi_2 + \Delta c) - \frac{\cosh\beta - 1}{2a\sinh\beta}(\Delta\Pi_2 - \Delta c)\right]$$

However:

$$\Delta c \ll \Delta\Pi_2 \quad \text{AND} \quad c \approx \Pi_1$$

This yields:

$$\sinh\frac{\alpha}{2} = \frac{1}{2}\sqrt{\frac{2\Pi_1 + \Pi_2}{a}}, \quad \sinh\frac{\beta}{2} = \frac{1}{2}\sqrt{\frac{\Pi_2}{a}}$$

$$\Delta M = \frac{\Delta t}{\sqrt{\frac{a^3}{\mu}}} = n\Delta t = \left[\frac{\cosh\alpha - 1}{2a\sinh\alpha} - \frac{\cosh\beta - 1}{2a\sinh\beta}\right]\Delta r_2 \quad (3)$$

where Δr_2 for this investigation is the difference between the capsule and bus perigee distances, r_2 is the perigee distance of the reference orbit (capsule trajectory), a is the semi-major axis of the reference orbit also.

II. Utilizing equation (2) and other known quantities, $\Delta\nu$ may be calculated.

$$\Delta\nu = (\nu_{1B} - \nu_{IB}) - (\nu_{1C} - \nu_{IC})$$

III. From the geometry of the situation, Figure (3), ρ and α may be calculated.

$$r_{IB} = \frac{p_B}{1 + e_B \cos \nu_{IB}}$$

$$\rho = \sqrt{r_{IB}^2 + r_M^2 - 2 r_{IB} r_M \cos \Delta\nu}$$

$$\cos\alpha = \frac{r_{IB}\cos\Delta\nu - r_M}{\rho}$$

IV. For rectilinear hyperbolas (S = 0) β goes to zero. This implies that we are interested in the limit of equation (3) as β approaches zero.

$$\Delta t_{\text{RECT. HYP.}} = \lim_{\beta\to 0}\{n\Delta t\} = \lim_{\beta\to 0}\left\{\left[\frac{\cosh\alpha - 1}{2a\sinh\alpha} - \frac{\cosh\beta - 1}{2a\sinh\beta}\right]\Delta r_2\right\}$$

$$= \frac{\cosh\alpha - 1}{2a\sinh\alpha}\Delta r_2 - \lim_{\beta\to 0}\left\{\frac{\sinh\beta}{2a\cosh\beta}\right\}\Delta r_2$$

$$= \frac{\cosh\alpha - 1}{2a\sinh\alpha}\Delta r_2$$

61

From this point on, Steps I, II, and III are again utilized to evaluate the parameters of interest:

S KM	V KM/SEC	h KM	α DEGREES	ρ KM
0	4	6×10^3	73.5° *	10.45×10^3
0	6	10^4	24.2	*** 14.44×10^3
2×10^3	4	6×10^3	55.0	8.35×10^3
4×10^3	6	10^4	5.0 **	10.20×10^3

* MAXIMUM α

** MINIMUM α

*** MAXIMUM ρ

FIGURE 2 SUMMARY OF SIGNIFICANT PARAMETERS AND THEIR VALUES.

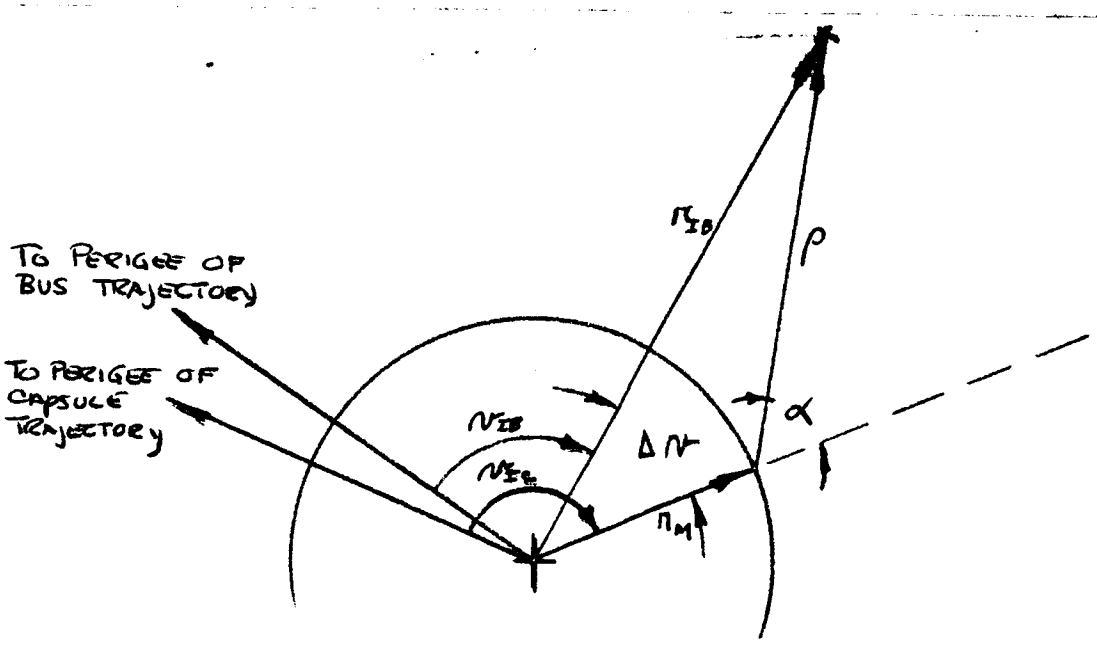

FIGURE 3 GEOMETRY AT TIME OF IMPACT.

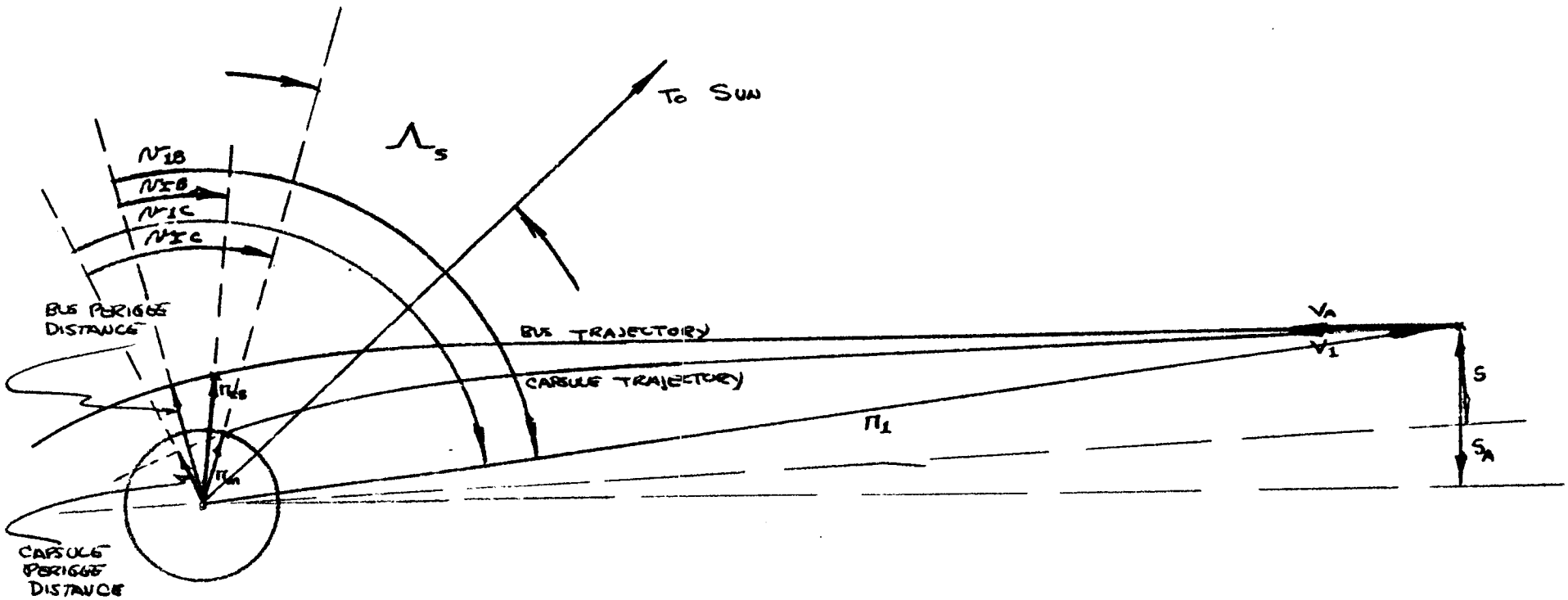

FIGURE 1 GEOMETRICAL DESCRIPTION OF CAPSULE-BUS MISSION FROM TIME OF SEPARATION (1) to TIME OF IMPACT (I) WITH APPROPRIATE NOMENCLATURE.

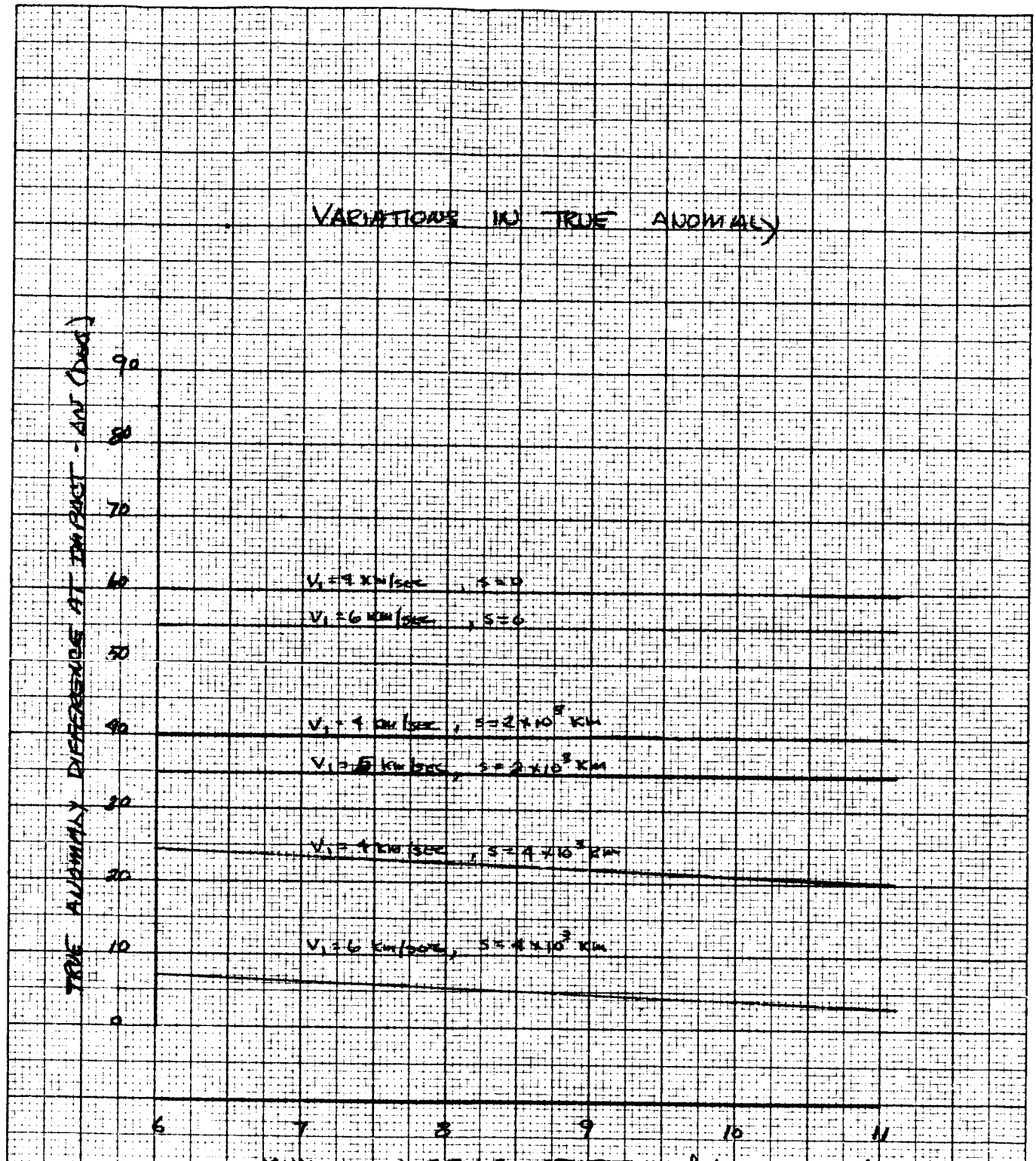
VARIATIONS IN TRUE ANOMALY
TRUE ANOMALY DIFFERENCE AT IMPACT - Δν (DEG)
90
80
70
60
50
40
30
20
10
0
V₁ = 7 km/sec , s = 0
V₁ = 6 km/sec , s = 0
V₁ = 7 km/sec , s = 2×10³ km
V₁ = 6 km/sec , s = 2×10³ km
V₁ = 7 km/sec , s = 4×10³ km
V₁ = 6 km/sec , s = 4×10³ km
6
7
8
9
10
11
MINIMUM ALTITUDE OF BUS ~ h (KILOMETERS)

FIGURE 4

GLOSSARY OF TERMS

Symbol	Definition	Units
S_A	Impact parameter of bus orbit	
S	Impact parameter of capsule orbit	km.
h	Minimum altitude of bus orbit	km.
V_1	Velocity of capsule at $r = r_1$	km/sec
V_A	Velocity of bus at $r = r_1$	km/sec
r_1	Initial radius of both bus and capsule	320,000 km
r_M	Radius of Mars and impact radius of capsule orbit	3,310 km
r_{IB}	"Impact" radius of bus orbit	km.
ρ	Communication distance	km.
ν_{IB}	True anomaly of bus at "impact"	degrees
ν_{IC}	True anomaly of capsule at impact	degrees
ν_{1B}	True anomaly of bus at $r = r_1$	degrees
ν_{1C}	True anomaly of capsule at $r = r_1$	degrees
α	Capsule transmitting angle	degrees
a	Semi-major axis of capsule trajectory	km.
μ_M	Gravitational constant of Mars $\times r_M^2$	km^3/sec^2
n	Mean motion	rad/sec
M	Mean anomaly	rad
e_B	Eccentricity of bus orbit	
p_B	$a_B(e_B^2 - 1)$	km.
a_B	Semi-major axis of bus orbit	km.
Δr	Angle between bus radius vector and capsule radius vector	degrees

Ford Motor Company

AERONUTRONIC DIVISION

Intra-Company Communication

November 6, 1961

TO: J. E. Kemmerly

FROM: W. Garrigus

SUBJECT: Notes on Mariner B Transmitter and Receiver

Attached please find the rough draft of the description of the 250 Mc transmitters and 250 Mc phase clock receivers for the Mariner B.

Attach
WG/pl

177

3.1 RECEIVER SYSTEM

The receiver system for the Mariner B-1 spacecraft sub-system communications system receives the signals transmitted by the capsule. For purposes of this section, two separate receiver types will be discussed; namely a wide band and a narrow band. However, there might be certain savings of primarily power, size, and weight to combine certain portions of these two types receivers. The desirable improvement in reliability by redundancy of completely individual receivers might make separate receivers more desirable. The final trade off of reliability versus primary power size and weight of the overall spacecraft would result in the final decision of completely separate receivers or partially combined functions of the two receiver types.

Aeronutronic has a welded module laboratory and is engaged in constructing sub-assemblies using this technique. The estimates of size and weight for this section are based on using the welded module technique where applicable and on using a cast module construction as mentioned in Section 4.3 where applicable. Receivers thus constructed can be used on the Mariner B-1 spacecraft with flight assurance.

The calculations in other sections of this proposal for required performance plus margins considered necessary indicate phase modulation techniques be used. The receivers described here, therefore, are designed to demodulate RF carriers that have been phase modulated. The resulting demodulated subcarriers have been phase modulated and these receivers are provided with circuits capable of converting these subcarrier signals into the desired PAM, PCM, etc. outputs to be used by the data processing circuits described in Section 3.3 of this study.

3.1.1 Wide Band Receiver

This receiver is a double superhetrodyne receiver and has sub-carrier demodulation circuits. It consists of an RF preselector, RF amplifier, first mixer and associated multipliers, etc., first IF amplifiers, second mixer and associated oscillator, second IF amplifiers, phase lock detector and associated oscillator, and subcarrier phase lock type disciminator circuits. The block diagram of this receiver is shown in Fig. 3.1.1-1.

The RF preselectors provide a reasonable image and IF rejection such as 40-60 db. as well as match the input to the RF amplifier and the RF amplifier to the first mixer. The RF amplifier may be a low noise traveling wave tube, an all ceramic-metal type (GE 7077 series) or a new low noise transistor (available by 1964.) The mixer will be a UHF diode mixer. The multiplier chain used to perform the L.O. function in this mixer will be composed of the required transistors (e.g. 2N708) and varactors (e.g. Microamp Associates MA4356E) used as amplifiers, buffers and multipliers. The first IF amplifier (e.g. 30 Mc) may include three to five transistor (e.g. 2N501) stage. The second mixer will have an oscillator injection derived from a transistor crystal oscillator and buffer stage. The second IF amplifier (e.g. 455Kc) will consist of three or four transistorized amplifier stages. The phase lock detector consists of phase detector with two input signals--one signal from a crystal oscillator (e.g. 455Kc) buffer amplifier and one signal the output of the second IF amplifier. The output of the phase detector is filtered and used to control the oscillator which drives the multiplier string, thus closing the phase lock loop, and the output is also the sub-carrier phase lock discriminator.

The phase lock discriminator is composed of the proper standard IRIG sub-carrier channel filter, a limiter amplifier, a phase detector, fed

TABLE I

SECTION 3.1.1

	PACKAGE	DC POWER (INPUT-WATTS)	VOLUME (CUBIC INCHES)	WEIGHT
1)	RF Preselector, Mixer, First IF, VCO & Multipliers	2.5	9.0	10.0 Oz.
2)	2nd Mixer, Second IF Amp, VCO & Buffer, Phase Comp.	1.5	8.0	9 Oz.
3)	Ref. Osc., Buffer Amp., Lim. Amp, Loop Amp, VCO, etc.	1.8	7.0	8 Oz.
4)	One Receiver	5.8 Watts x 3	24 Cu. In. x 3	27 Oz. x 3
5)	Three Receivers	17.4 Watts	72 Cu. In.	81 Oz.
6)	One Receiver Three Outputs	14.9 Watts	63 Cu. In.	71 Oz.

by the sub-carrier signal and a VCO (operating at the chosen standard IRIG sub-carrier frequency), a loop filter, loop amplifier, proper output filter, and output amplifier having the proper signal level to drive the data processing equipment.

As described elsewhere in this study, it may be desirable to have three separate wide band RF channels. If separate receivers are used for each of these channels they will each be as described--each being tuned to separate RF carriers. If one receiver fails, then the two remaining receivers will still send signals. As shown in Table 3.1.1-I this required more size, weight, and primary power. If a substantial saving in size, etc. is desired, one receiver with separate detectors can be used as shown in Table 3.1.1-I.

The block diagram of such a receiver is shown in Fig. 3.1.1-2. This receiver uses common RF first IF, and first mixer oscillator-multiplier by having the RF,and first IF bandpass characteristics wide enough to pass all three signals without relative phase shift between them.

3.1.2 Narrow Band Receiver

The narrow band receiver handles the telemetry signals employed on the mission. It is probable that this receiver could be one more receiver much the same as the ones described in Sec. 3.1.1 with the required changes in filtering to handle the required telemetry signals. By using the same basic receiver, a considerable saving of time and money could be realized.

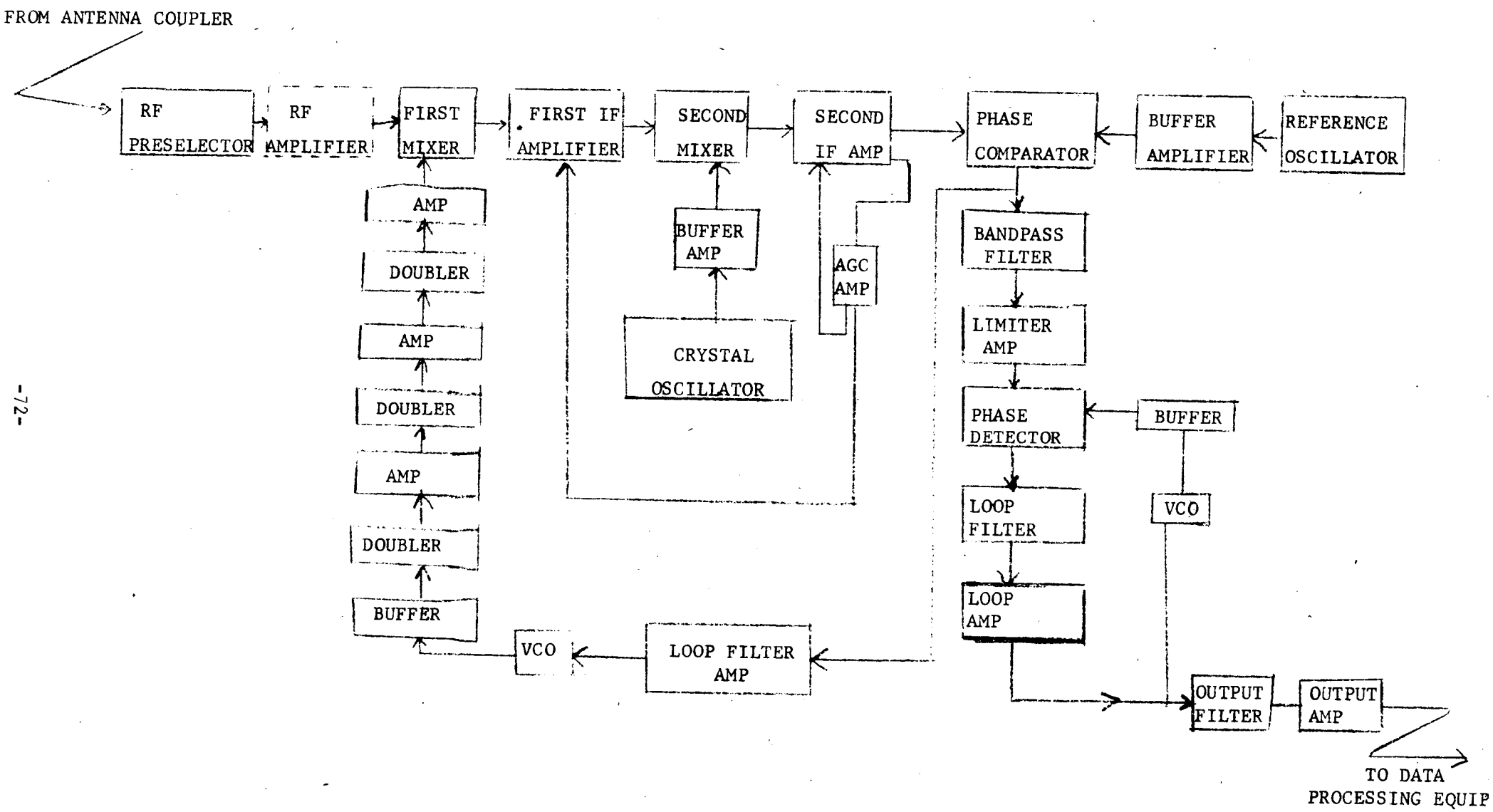

FIG. 3.1.1-1 BLOCK DIAGRAM OF WIDE BAND PHASE MODULATION RECEIVER

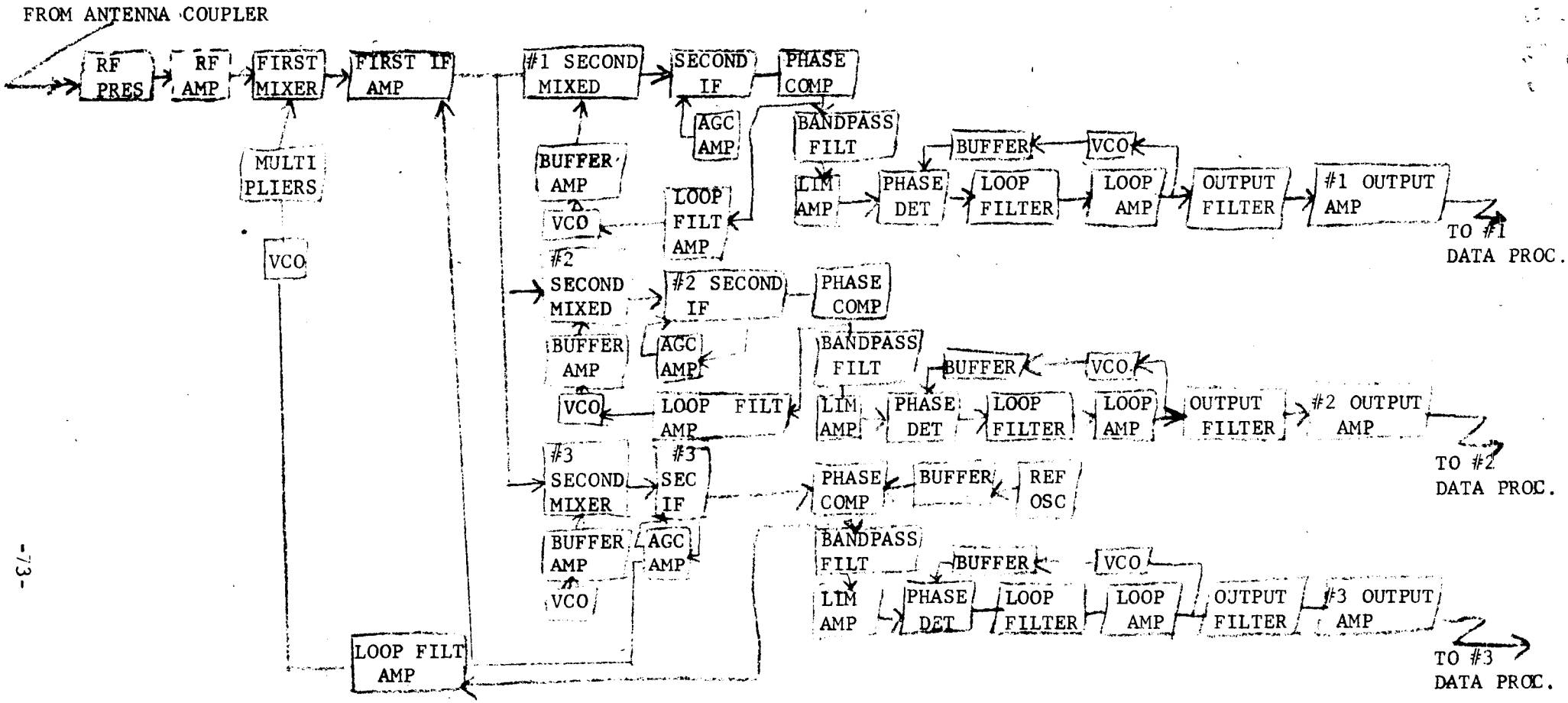

Fig. 3.1.1-2 BLOCK DIAGRAM ALTERNATE RECEIVER SYSTEM

4.3 TRANSMITTER SYSTEM

The transmitter system for the Mariner B-1 communication system must be discussed in terms of flexibility. Aeronutronic is presently delivering a 960 Mc 50 MW transmitter to JPL for the Capsule for the present Ranger program. Aeronutronic is presently developing a 5 watt transmitter for 960 Mc use for a follow on program for the Ranger program.

These transmitters are all semiconductor transmitters packaged to withstand 3000 g shock by using a cast modular construction. They are very small, light-weight units cast of aluminum and gold plated. Some cavities have been made of magnesium and then plated. By using the basic circuitry of lower frequency stages low power transmitters for the Mariner B-1 could be constructed with very little engineering effort as the circuitry and layout could be very similar to the units now being employed for the Ranger RA-3, 4, and 5 and follow on programs. Valuable phase modulation experience and phase stability experience has been gained during the design of these transmitters.

For the purpose of this study powers of 2 watts, 10 watts, 100 watts, 200 watts, 500 watts will be discussed. They will have phase modulated sub-carriers and phase modulated RF carriers.

4.3.1 Modulation

The transmitters discussed in this section are all phase modulated to be compatible with the phase detector receivers discussed in Section 31 of this study. The actual degree of modulation and rate of modulation will depend on trade-off of many factors e.g. battery power, weight, size, pictures desired for time allowable, etc. Figure 4.3.1-1 shows the probable modulation block diagram.

The present Ranger unit uses a Dorsett Laboratories Model O-8 for the voltage controlled oscillator. This unit is an FM unit and would have to be modified to operate PM. Depending on the required data bandwidth various IRIG channels can be used and various VCO's can be selected. The VCO output is then amplified by a linear transistor amplifier (such as a 2N736), the transistor type being selected depending on the required amount of modulation.

The output of the transistor amplifier feeds a varactor which is connected to the tuned circuit of the Class C amplifier. A typical varactor would be a Pacific Semiconductor Type PC 117-14 but the actual type would be selected on the basis of the required modulation etc.

The amplifier and multiplier stages following the modulation stage must be designed to be phase stable with respect to electrical levels and environmental changes. This has been accomplished on the transmitters now being used in the Ranger capsule program.

4.3.2 The Wide-Band Transmitter Exciter

This exciter will be used to drive the Power Amplifier and depending on the power amplifier input requirements the output of this exciter will be designed to provide the required drive power.

It is estimated that the output of the wide band transmitter exciter will be 2 to 10 watts depending on the power level required by the power amplifier. Figure 4.3.2-1 shows a block diagram of such a transmitter. The dotted stage would be used only if the required output is about 10 watts. The crystal oscillator and the buffer amplifier could use type 2N915 transistors and the next two amplifier stages could use type 2N1709 transistors. The power amplifier (dotted) might use a pair of type TA 2084 transistors. A typical schematic diagram is shown in Figure 4.3.2-2.

The estimated power requirements, weight, and volume are shown in Table 1 (Section 4.3.2).

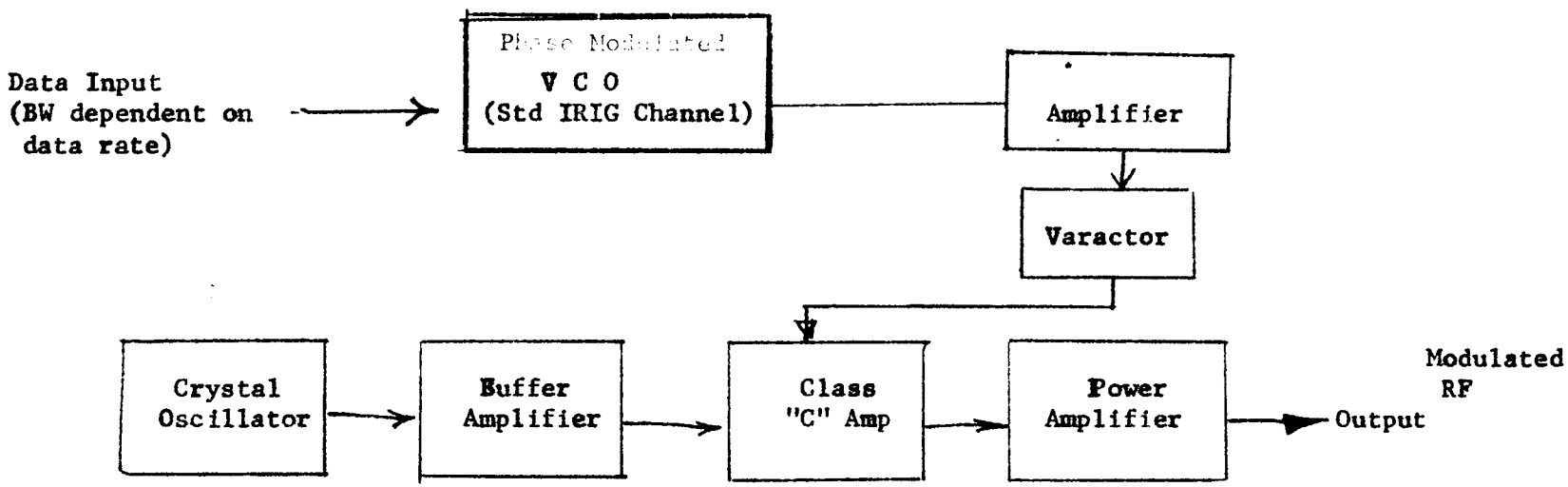

Figure 4.3.1-1 Block Diagram of Transmitter Modulator

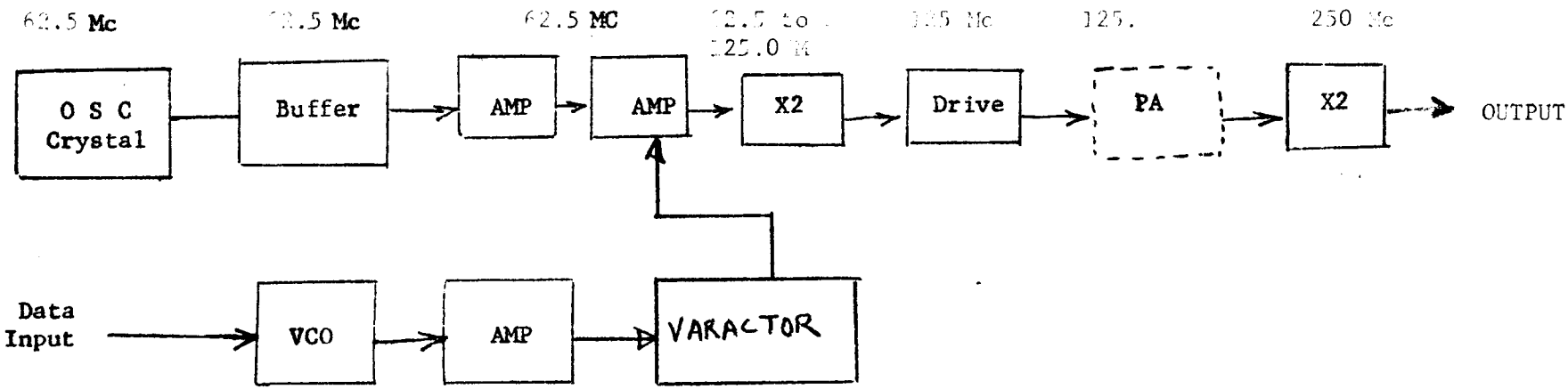

Figure 4.3.2-1 Block Diagram of Wide Band Transmitter Exciter

4.3.3 Power Amplifier

The present semiconductor art considering 1964 era does not indicate practical amplifiers operating at 250 Mc having power outputs of 100 to 500 watts. The power amplifiers that appear to offer the most promising results will be the ceramic metal tubes such as the RCA type 7457 and type 7650. RCA has used a ceramic pin in the center of the 7457 tube to make it strong enough to survive severe shock. Aeronutronic is testing this tube and the G.E. type Z 2869 which is a tube capable of supplying about 5 watts of RF power.

The Power Amplifier for this program would actually consist of two amplifier stages as well as the self-contained power supply. The power supply would be integral to the PA package to reduce the problems of high voltage connectors, etc. Figure 4.3.3-1 shows a block diagram of one possible configuration. In RF work where high powers are involved it is desirable to divide the lower level high gain stages from the high power stages thus the power amplifier actually has one driver stage as well as the output stage. The driver would consist of an all metal-ceramic tube such as a type 7457 or similar tube supplying 30-80 watts of power to drive the power amplifier stage. The power amplifier would consist of one all ceramic-metal tube such as a type 7650 or similar type having an output of 200 to 600 watts. This tube line up will adequately provide this power range when the proper supply voltages are applied and proper drive levels are set up. The level control shown samples the RF output level and if for some reason the antenna system does not present the proper load to the power amplifier, the level control will reduce the driver level to prevent arc-over of the power amplifier circuits. This would allow the transmitter to operate at reduced levels, thus hoping to get some signal transmitted. A typical circuit diagram is shown in Figure 4.3.3-2. A typical dc to dc converter circuit as shown in this circuit will provide 80-90% efficiency. Size, weight, and power are shown in Table 1 Section 4.3.2.

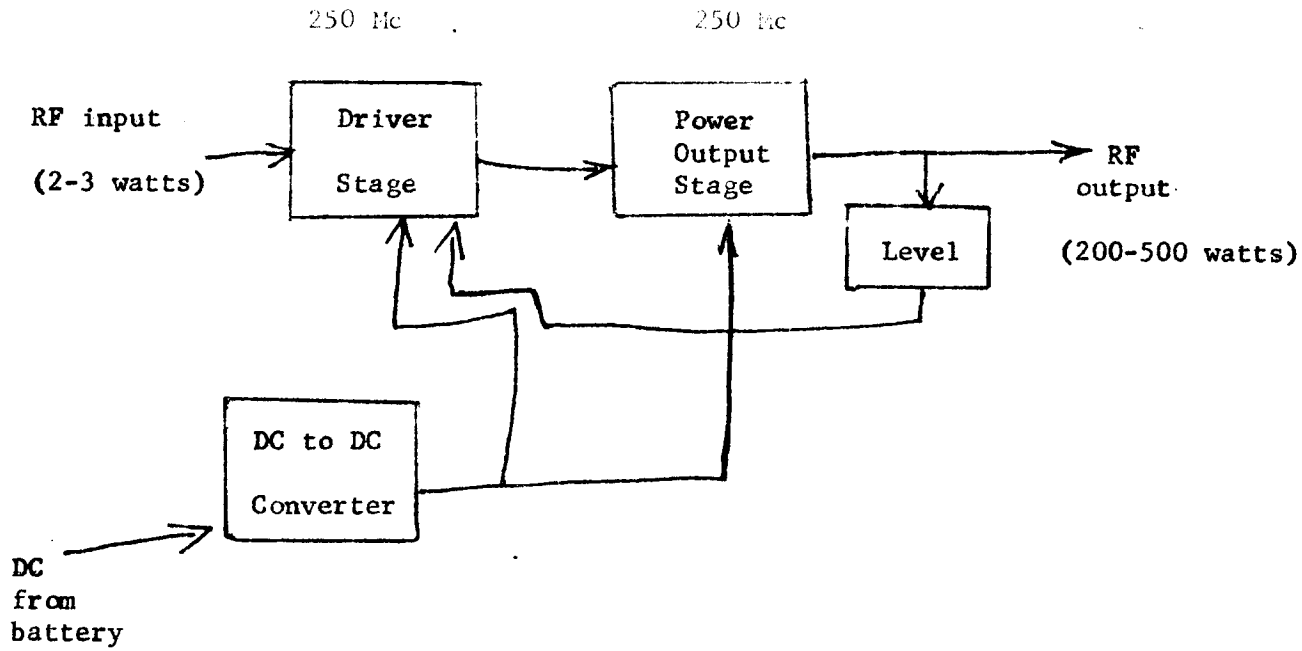

Figure 4.3.3-1 Block Diagram Power Amplifier

4.3.4 Narrow Band Transmitter

This transmitter will take the basic general block diagram as already shown and discussed in Section 4.3.2 as the Wide Band transmitter exciter. The only change would be the phase modulation would be less. The size and weight would be the same relative size. It might prove of great benefit to use the same transmitter to reduce design costs, etc.

TABLE 1 SECTION 4.3.2

SUMMARY OF 250 Mc TRANSMITTER CHARACTERISTICS FOR MARINER B-1

Package	DC Power (Input-Watts)	Volume (Cubic Inches)	Weight
Complete 2 watt transmitter	14.1	30	32 Oz.
Complete 10 watt transmitter	57.4	40	45 Oz.
Complete 100 watt power amplifier and dc-dc converter	223 (45% eff)	120	7 lb.
Complete 200 watt driver, power amplifier and dc-dc converter	550 (36% eff)	180	10 lb.
Complete 500 watt driver, power amplifier & dc-dc converter	1220 (41% eff)	250	14 lb.

APPENDIX G

CAPSULE MISSIONS AND MISSION EXPERIMENTATION

Ford Motor Company

AERONUTRONIC DIVISION

Intra-Company Communication

24 October 1961

SUBJECT: MARINER B CAPSULE STUDY - CAMERA SUBSYSTEMS

FROM: ERIC DURAND TO: JOHN HOUSEGO

GENERAL OBJECTIVES

The general objective of the camera subsystem is to obtain as many pictures of Mars as possible, covering a wide range of fields of view and resolution. The greatest interest would be in pictures of the entire visible illuminated disc, but the interest in smaller areas at higher resolution is also very high. A secondary objective is to obtain part or all of these pictures in color.

SPECIFIC OBJECTIVES

In order to be compatible with the requirements for simplicity and reliability, the principal specific objective has been established to obtain the best possible pictorial coverage in color, starting as soon as the heat shield can be ejected after reentry, and continuing down to impact. Again, for simplicity and reliability, no parachute is proposed, so that no picture-taking or data transmission can occur after impact.

An addition tentative objective has also been included, to take monochrome pictures of large areas prior to reentry. Equipment for this purpose would be included if further study verified the preliminary conclusions as to its feasibility and simplicity.

DESCRIPTION

a. Primary Subsystem

The primary subsystem provides post-reentry 3-color and monochrome pictures from an altitude of about 12 Km down nearly to impact. It consists of three completely independent vidicon cameras with appropriate color filters, each with its own electronics and data transmission equipments. The only items common to the three are the programming control, a multiplexer, and the transmitting antenna. Video data from the cameras are encoded and transmitted by a PCM/PSK/FM telemeter to the bus, where they are received through a common antenna and separate receivers, and recorded on three channels of a magnetic tape recorder for subsequent retransmission to earth at a reduced bit rate.

177

Figure 1 is a block diagram of the camera subsystem and includes the secondary pre-reentry camera. The principal parameters of both parts of the subsystem are given in Table 1.

It would be very simple to use common sweeps, amplifiers, etc., for the three cameras. However, while this scheme would give improved reliability for obtaining a complete set of color pictures, it gives a reduced reliability of obtaining at least one or two. Table 2 shows the relative probabilities for various cases assuming a 90% reliability of the separate (or single) channel, and 100% reliability of the common elements.

TABLE 2

PROBABILITIES OF SUCCESSFUL OPERATION

SUCCESS ACHIEVED	SEPARATE CHANNELS	COMMON CHANNEL
All three pictures	.729	.9
At least two out of three	.972	--
At least one out of three	.999	--
None	.001	.1

It is certainly far more important to get some kind of pictures than to get a full color set, and the probability of achieving this is greatly increased in the separate-channel arrangement.

A second advantage of the separate-channel arrangement is that it permits the use of up to 600 watts total transmitted power using off-the-shelf transmitters, which are currently available up to 200 watts. Alternately, the 200 watt transmitter can be operated at reduced power to enhance reliability.

The three cameras are mounted in a cluster in the nose, looking axially downward. They are exposed to view by the process of nose-cone separation, and immediately start taking pictures. At first, all three cameras operate in synchronism, with a short exposure (0.01 to 0.001 second) followed by a 6- second readout, the vidicons being of the storage type. At lower altitudes, however, the percentage change in altitude between successive frames increases rapidly, and it may be desirable to shift the "phases" of the cameras relative to each other, thereby getting effectively a three-fold increase in picture-taking rate, sequentially red, green, and blue, at the expense of not being able any longer to superimpose these into a single color picture. Table 3 gives the planned picture sequence for both the pre-reentry and the post-reentry subsystems.

MARINER-B CAPSULE ELECTRONICS

(MISSION Nº 1)

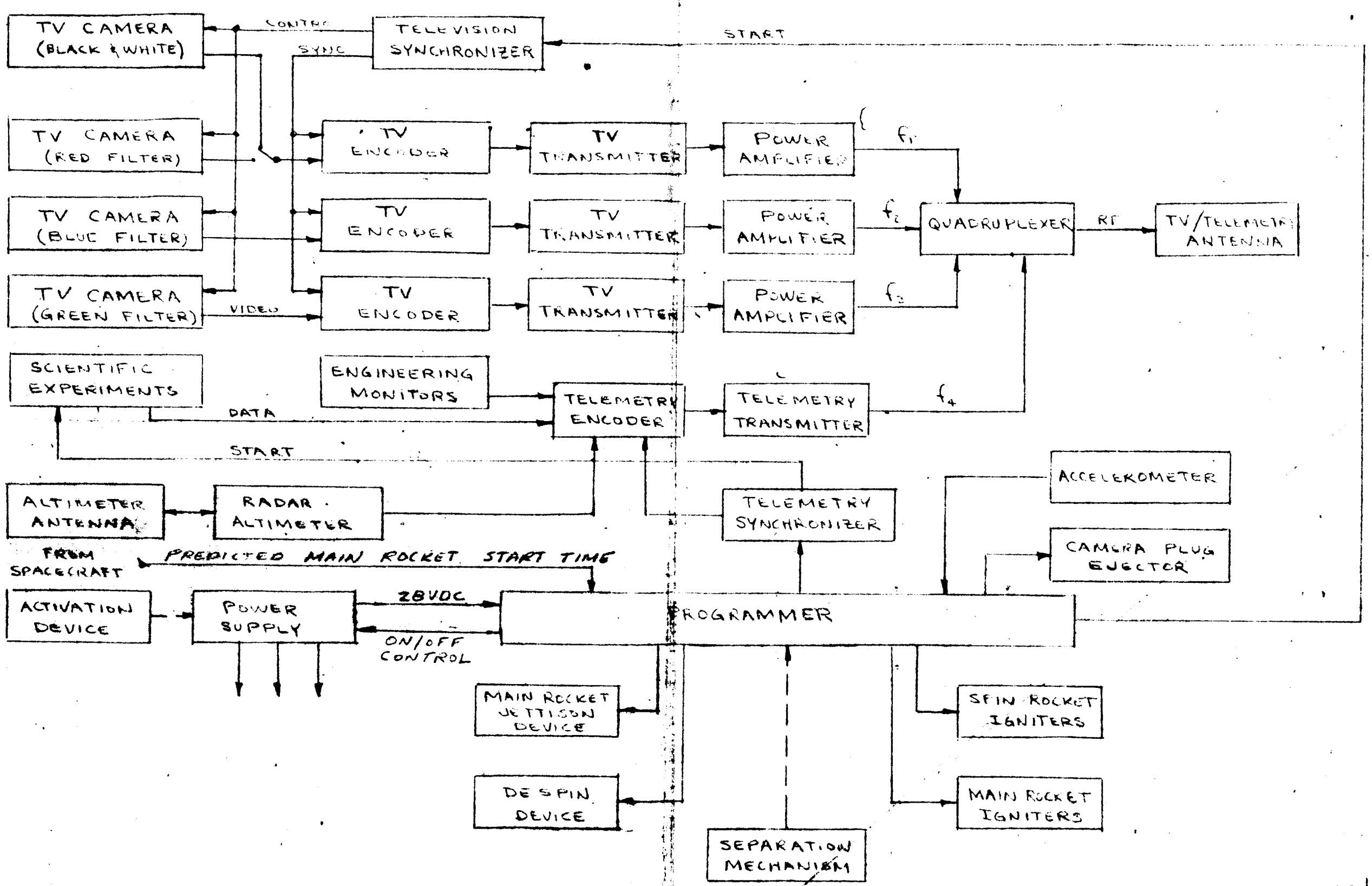

10/19/61

TABLE 1

CAMERA SUBSYSTEM PARAMETERS

TYPE	VIDICON
Camera dimension	8" long x 2-1/2" dia
Control unit dimension	3-3/4" x 5" x 7"
Total weight	6 lb
Resolution	200 x 200 TV lines
Gray scale	8 level
Format (square)	0.44" x 0.44"
Frame Rate	1/6 per sec
Data transmission	Coded digital
Data rate	30,000 bits/sec

	PRE-REENTRY	POST REENTRY
Type	B & W	Color
Number	1	3
Tube Type	WX4530	WX4530(2) 7351(1)
Operating Altitudes	33,000-175 Km	15-0 Km
Lens	50 mm F/1.4	12.5 mm F/1.4
Angular resolution	1 mr	4 mr
Field Covered	7300 - 40 Km	15 - 1 Km
Ground resolution	37 - 0.2 Km	75 - 5 m/rad
Exposure	1/1000 sec	1/200 sec
Pictures obtained, BW	28	--
Color	--	18

TABLE 3a

PRE-REENTRY PICTURE SEQUENCE*
50 mm Lens - 0.44 inch field

RANGE 1. Power shut-down between pictures, timed to give 20% reduction in field of view from picture to picture.

ALTITUDE	TIME TO REENTRY	FIELD COVERED	TV RESOLUTION
33,000 Km	4310 sec.	7400	37 Km
26,400	3420	5900	30
21,000	2730	4700	24
16,800	2180	3780	19
13,400	1740	3000	15
10,700	1380	2400	12
8,570	1100	1910	9.5
6,850	880	1530	7.7
5,490	700	1230	6.2
4,390	550	980	4.9
3,500	435	780	3.9
2,700	351	600	3.0
2,160	260	480	2.4
1,730	203	385	1.9
1,380	158	308	1.5
1,100	121	245	1.2
880	92	195	975 meters
700	69	155	775

RANGE 2. Power on continuously. One picture per 6 seconds. Nominal reentry at 175 Km.

ALTITUDE	TIME TO REENTRY	FIELD COVERED	TV RESOLUTION
631 Km	60	140 Km	700 meters
585	54	130	650
540	48	120	600
494	42	110	550
449	36	100	500
403	30	90	450
357	24	80	400
312	18	70	350
266	12	60	300
221	6	50	250

* Based on constant approach velocity of 7.62 Km/sec. Actual sequence would be slightly modified because of increasing speed and non-vertical descent.

TABLE 3b

POST REENTRY PICTURE SEQUENCE
12.5 mm lens - 0.44 inch field

ALTITUDE	TIME TO IMPACT	FIELD	RESOLUTION
50 K feet	112 sec	14.2 Km	71 meters
45.0	106	12.8	64
41.0	100	11.6	58
37.0	94	10.5	53
34.0	88	9.7	49
31.5	82	9.0	45
28.5	76	8.1	42
26.0	70	7.4	37
24.0	64	6.8	34
21.0	58	6.0	30
18.7	52	5.3	27
16.6	46	4.7	24
14.4	40	4.1	21
12.2	34	3.5	18
10.1	28	2.9	15
8.0	22	2.3	12
5.8	16	1.6	8
3.6	10	1.0	5

b. Secondary Subsystem

As was mentioned earlier, it is most desirable to be able to get the "big picture" view of Mars as well as the finer details obtainable after reentry. A camera on the bus can easily observe the entire disc, but its distance of closest approach of 8000 Km (with a probable tolerance of ±5000 Km) does not permit covering the intermediate level of detail between this and the coverage of the primary cameras. The secondary subsystem serves to bridge this gap. Since it can operate, if desired, as soon as the capsule separates from the bus, it can also perform the same picture taking role as the bus, and can either replace a bus camera, or back it up.

The principal problems of a pre-reentry camera subsystem relate to attitude control and orientation. A simple scheme is proposed to circumvent these problems. In this scheme, the capsule is allowed to retain the orientation with which it separates from the capsule, which is roughly 90° from the then-existing capsule-Mars line. The capsule is partially despinned, leaving an angular rotation of about 10 rpm, which is fast enough to hold the orientation and yet slow enough to permit motion-stoppage during the exposure. Therefore neither attitude control, reorientation, nor image motion compensation is required.

To minimize the coverage gap between the pre-reentry and post-reentry cameras, the former should use a long-focus lens and the latter a wide-angle lens. The maximum allowable focal length for the pre-reentry camera is determined by image motion effects. Thus, for the assumed spin rate of 1 radian per second and an exposure time of 0.001 second, the displacement during exposure at right angle to the spin axis is 1 milliradian. Since proposed vidicon system has 200 TV lines, a smearing of one line-spacing occurs for a field of view of 200 mr or about 12°. The diagonal of the image on the vidicon is 0.62 inch, so that the longest-focus lens that can be used for one-line smearing is 3.1 inches. If the vidicon is oriented so that smearing occurs along (or perpendicular) to a scanning line, whose length is 0.44 in., the focal length must be reduced to 2.2 inches. There are many high-speed 50 mm and 58 mm lenses commercially available.

Wide-angle lenses are used for the post-reentry camera. A good choice would be a 12.5 mm F/1.5 lens designed for 16 mm movie camera use. This lens has a field of view of 50° across the frame and 67° across the diagonal.

VIDICON SELECTION

A number of vidicons of several different manufacturers have the right general characteristics for the present application. Table 4 lists the more prominent candidates for the job. Of these, only the ones labeled "Slow Scan" and "Storage Type" are explicitly designed for short exposures and delayed readout, but contacts with manufacturer's representatives indicate that all of the others will hold their signal for 5 to 10 seconds. Machlett Laboratories, Inc. actually tested the ML522B and the 7351 under conditions similar to those described here and found them to perform satisfactorily.

As a preliminary choice, the Westinghouse WX4530 has been selected for the blue and yellow cameras and the pre-reentry camera, and the Machlett 7351 for the red camera. All of these and other tubes should be studied and operated experimentally however, before final selection. In particular, it may be better to use a fourth WX4530 for the red camera to get good geometric matching for color. Also, the new RCA 1/2-inch tubes, which can stand up to 2000 g shock, may prove suitable, providing a somewhat smaller camera.

All tubes appear to be amply sensitive, and should give good signal-to noise ratios with a mean illumination of 10^{-3} foot-candle-seconds on the faceplate.

EXPOSURE AND LENS APERTURE

The question of the surface brightness of Mars is covered in a separate memo*, which shows that an F/10 lens will give an illuminance of 180 foot candles, so that the shutter time of one millisecond required for the pre-reentry camera gives a total exposure of 0.18 foot-candle-second.

* Blifford, I. H., "Mariner B Capsule Study - Surface Brightness of Mars," October 2, 1961.

As mentioned earlier, the vidicons being used have adequate signal-to-noise ratios for exposure of 10^{-3} fcs, so that there is a factor of 18 margin for the F/1.0 system. This would be used up as follows:

1. Reduce exposure time to 1/2000 sec if a suitable shutter can be found of adequate reliability.

2. Use an F/1.4 lens.

3. Increase exposure light level to 4.5×10^{-3} fcs to provide better signal-to-noise ratio and allow for transmission losses in the system.

b. Post Reentry

For the post-reentry cameras, the effective speeds (for the 7351 vidicon spectral response) will be reduced by about 10x, 5x, and 3x, respectively, by the red, green, and blue filters. However, at this time, there should be very little angular motion, and the exposure times can be increased by at least a factor 10. Consequently, an F/1.4 (or F/2.0) lens can be used with, say, a 1/200 sec exposure to provide ample illumination.

TABLE 4

VIDICONS

MANUFACTURER	TYPE	SIZE	SENSITIVITY[1]	SPECTRAL PEAK[2]	REMARKS
RCA	C73496	1/2"	3000	4500Å	Ultra-rugged
RCA	C74053	1/2"	2000	4500Å	Ultra-rugged
RCA	7263A	1"	1300	4500 Å	Rugged
Westinghouse	WX4350	1"	1300	4500 Å	Slow Scan
Westinghouse	WX4384	1"	1300	4500 Å	Slow Scan
Machlett	ML522B	1"	115	4050	UV Sensitive
Machlett	7351	1"	1300	6400	See Text
GEC	1326	1"	NA	NA	Storage Type

NA: Information not available.

Note 1: Microamperes per lumen of 2870°K color temperature lamp.

Note 2: Peak for source of uniform spectral output. All 4500Å tubes have S-18 surfaces which peak at 5500Å for 2870°K tungsten lamps and have 40-50% response at 6000Å. The ML522B has a sharp cut-off at 5500Å and the 7351 is sharply peaked in the red.

Intra-Company Communication

AL-137A

Revised 10/11/61

To: J. E. Kemmerly

From: J. A. Jansen

Subject: ALTIMETER, ACCELEROMETERS AND GYRO - MARINER B CAPSULE

The purpose of this memo is to describe the size, weight, power dissipation and operational characteristics of the altimeter, accelerometers and gyro for the contemplated Mariner B capsule. Tables 1, 2 and 3 summarize the characteristics of these instruments; the memo concludes with a tentative sequence of events pertinent to them.

Accelerometers

The functions of the accelerometers are as follows:

1. To monitor capsule "retro" from spacecraft
2. To monitor spin-up and de-spin
3. To sense incipient drag so that events timed from initial entry may be triggered
4. To measure capsule acceleration during entry as a means of determining atmospheric density vs. altitude
5. To provide acceleration data to the parachute deployment system.

Two accelerometers and a g-switch are proposed for the capsule, placed as sketched in Figure 1. One accelerometer measures longitudinal acceleration for functions 1, 4 and 5 above and as a backup for function 3. The other accelerometer is placed to measure the square of spin rate for function 2. This accelerometer will also measure accelerations associated with malfunctions of spin-up, retro or entry.

The function of the g-switch is to detect centrifugal force due to aerodynamic righting of the capsule during the initial phase of entry. As indicated in Figure 1, the acceleration a_Z at the g-switch location is

$$a_Z = \dot{v}_z - r(\omega_x^2 + \omega_y^2) \qquad (1)$$

If $\dot{v}_z$ is assumed near zero during initial righting of the vehicle, and the threshold level is assumed to be ¼ g, the rate $\sqrt{\omega_x^2+\omega_y^2}$ required to yield threshold acceleration at ½ foot from the c.g. is

$$\sqrt{\omega_x^2+\omega_y^2} = \sqrt{\frac{\frac{1}{4}\ 32.2\ \mathrm{ft/sec^2}}{\frac{1}{2}\ \mathrm{foot}}} \approx 4\ \frac{\mathrm{rad}}{\mathrm{sec}} \approx \frac{2}{3}\ \frac{\mathrm{rev}}{\mathrm{sec}} \qquad (2)$$

It is expected that the rates encountered during righting will exceed this value. If the centrifugal force doesn't trigger the g-switch, the subsequent $\dot{v}_z$ deceleration will; in addition, the z-axis accelerometer will be used as a backup threshold detector.

Gyro

The function of the gyro is to measure the initial entry angle to permit integration of the acceleration for determination of the entry trajectory. Characteristics of a suitable gyro are indicated in Table 2.

Altimeter

The functions of the altimeter are:

1. To provide data for relating all other measurements to altitude.

2. To serve as an input to the chute deployment system.

3. To provide final-value altitude and altitude rate data for the acceleration integrations.

A pulsed altimeter operating at a frequency around 100 mc is proposed. This comparatively low frequency yields the following advantages:

1. **permits all-transistor design, reducing weight, volume and power requirements;**

2. **produces for a given antenna size a large beamwidth to give adequate ground coverage for large variations in capsule attitude;**

3. **reduces attenuation through the heat shield, the atmosphere, and clouds.**

Characteristics of a suitable altimeter are indicated in Table 3.

Sequence of Events

The sequence of events pertinent to the accelerometer-gyro-altimeter measurements is as follows based on "retro" thrust of the capsule rather than the spacecraft:

1. The capsule separates from the spacecraft (t_0).

2. The timer switches power onto the accelerometer package.

3. Spin-up and "retro" acceleration are measured and telemetered to the spacecraft.

4. Accelerometer power is switched off; this is perhaps minutes after separation.

5. At about ... hours, the timer switches on the accelerometer power and initiates de-spin; accelerometer outputs are telemetered to the spacecraft. Accelerometer power is then switched off.

6. At about ... hours, the timer arms the g-switch circuit.

7. Aerodynamic rotation of the capsule throws the g-switch which:

   a. initiates altimeter operation,

   b. applies power to the accelerometers and the gyro pickoffs,

   c. spins up and uncages the gyro,

   d. provides a new "zero-time" origin for events to be timed from entry.

8. Altitude, acceleration and gyro angle data is telemetered and also fed to the chute deployment system.

9. When the chute-deployment criterion is met, the exterior structure of the capsule including heat shield and extra-atmospheric instrumentation is jettisoned; altitude, acceleration, and gyro data continues to be telemetered.

10. The signal which initiates camera operation switches power off the accelerometers and the gyro.

11. Altitude data continues to be telemetered until the minimum operational altitude of the altimeter is reached.

J. A. Jansen

JAJ:clm

Attachments (3)

Distribution

R. R. Auelmann
T. A. Bergstrahl
T. F. Blifford
M. G. Boobar
P. B. Bower
M. Caldwell
D. M. Conrad
F. G. Denison
R. M. Foster
A. A. Gammal
K. C. Harder
W. W. Hawley
V. H. Henderson
S. Lampert
W. T. Lemm
F. A. Losee
G. R. Miczaika
R. P. Nagorski
R. F. Nease
T. W. Neumann
J. J. Oslake
D. Rodriquez
W. H. Schilling
I. F. Sobczak
D. Stimpson

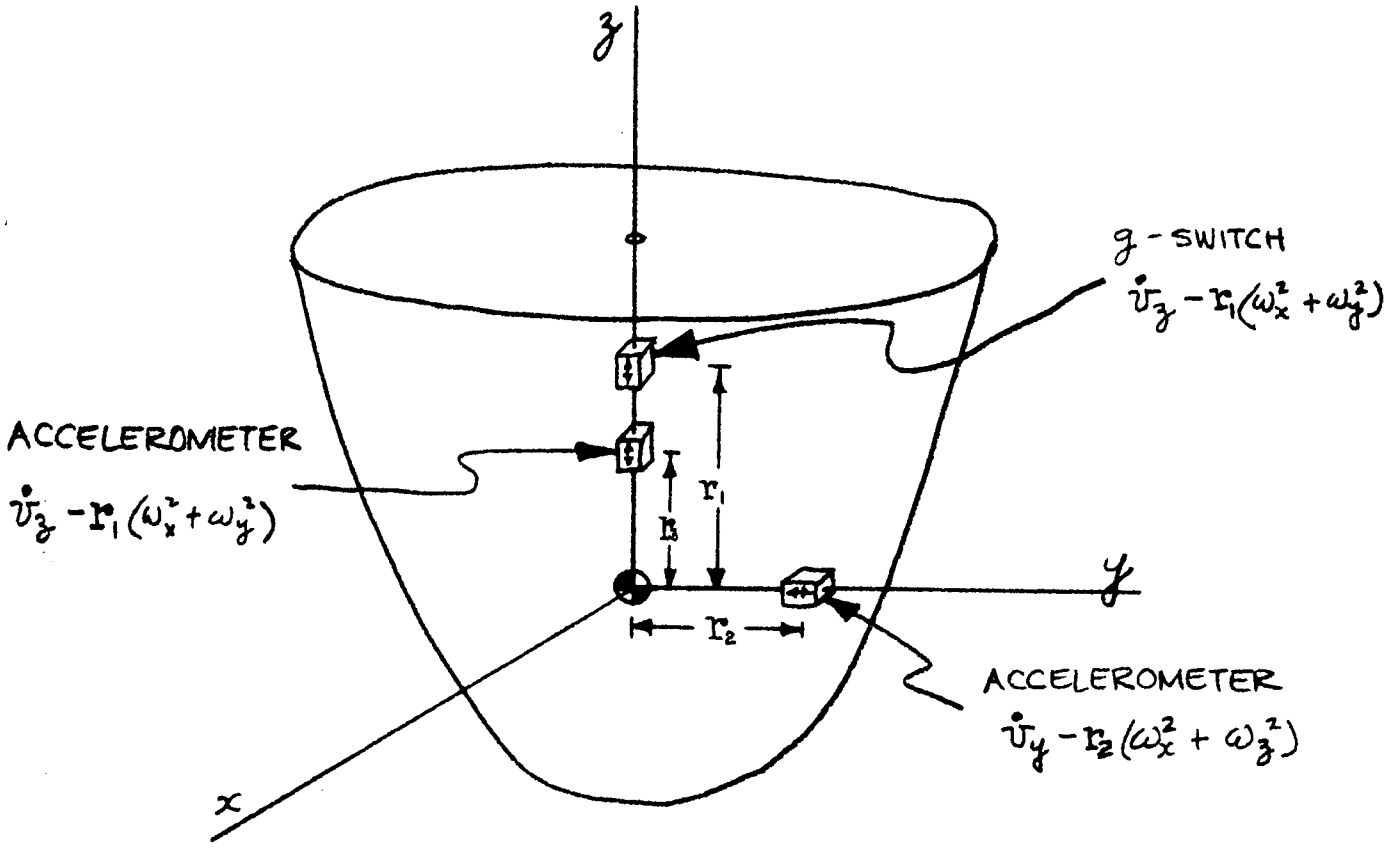

FIGURE 1
ORIENTATION OF ACCELEROMETERS
AND G-SWITCH

Type of sensing element	Silicon strain-gage bridge
Power dissipation	0.2 watts
Full scale output	0.250 volts
Minimum allowable load resistance	2000 ohms
Accuracy	Sensitivity: 2% F.S. Zero shift: 1½% F.S.
Size	5/8" dia. x 1/2" long
Weight	0.2 lb.
Possible vendor	Fairchild Controls

TABLE 1. REPRESENTATIVE CHARACTERISTICS OF SUITABLE ACCELEROMETERS

Type of wheel drive	Spring plus sustainer motor
Wheel speed	24,000 RPM
Motor power	3 to 4 watts
Pickoffs	Potentiometers or digital commutators
Size	2¼" dia. x 3½" long
Weight	1-3/4 lb.
Max. drift rate	1 deg/min
Operating time	3 min. max. (determined by trajectory)
Possible vendors	U. S. Time, Greenleaf

Table 2

Representative Characteristics of a Free Gyro

Suitable for the Mariner B Capsule

MAXIMUM ALTITUDE	150 000 FT
MINIMUM ALTITUDE	3000 FT
MAXIMUM DESCENT RATE	11 000 FT/SEC
FREQUENCY	100 MC
PEAK RADIATED POWER	10 TO 100 WATTS
PRF	500 PER SEC
DATA RATE	100 CPS
ACCURACY	1%
SIZE	4" x 5" x 8"
WEIGHT	4 LB
POWER DISSIPATION	20 WATTS

TABLE 3
ALTIMETER CHARACTERISTICS

3.0 CAPSULE MISSIONS

The most obvious missions for a Mars capsule are those designed to increase our knowledge of the physical characteristics of the body, surface and atmosphere of the planet. Present knowledge is to a large extent limited to a few facts which can be derived from dynamics and from telescopic observations of the surface and atmosphere. The accuracy with which the basic data are known is generally insufficient to assure a successful mission. It is important that atmospheric parameters be measured within the atmosphere and that surface structure be determined with resolution on a scale comparable to the vehicle dimensions. Pictorial records (Vidicon pictures) would serve some of the above purposes as well as providing a degree of public interest difficult to obtain in any other way. Mars is the only planet for which enough information is available to be able to postulate life forms such as exist on earth. While conditions are comparable to those in the terrestrial stratosphere, the possibility of detecting life is sufficiently good that such an experiment should have high priority for inclusion in the capsule design.

Apart from vehicle operation and communications, the experiments necessary for future missions are very much the same as the purely scientific measurements. This is true particularly for the atmosphere and to some extent for surface studies. The state variables of temperature, pressure and density are undoubtedly of first importance and should be measured for all altitudes and the surface. The chemical composition and electrical properties are perhaps next in desirability.

Experiments designed to provide knowledge of the surface composition and physical properties have quite similar objectives. Obtaining photographs is an obvious first step since by comparing lunar and terrestrial geology much can be learned about the structure of the planet and condition of the surface. From the landed capsule it should be possible to use instrumentation similar to that to be employed for similar operations on the moon. These include various bore-hole measurements which are in general miniaturized versions of standard instruments. Seismometers and devices for remote chemical analysis by various spectrographic and nuclear methods could be used provided that the weight capability exists.

Biological investigations designed to detect the existence of life forms are likely to be complicated because of the difficulty of identification. Various nutrients could be innoculated with samples of soil or earth and some method for detecting changes could be used to indicate growth. On the other hand there are few criteria for selection of the nutrient media and perhaps other methods such as a search for protein may be possible. In its Research Laboratories, Aeronutronic Division of Ford Motor Company has under investigation a detector for protein which operates on a photometric principle. Although the effort is in quite preliminary stages the results have been encouraging and work is proceding under a contract to NASA.

In general it is probably reasonable to look to the devices presently being developed for analyzing the lunar surface even though many

of the instruments which have potential utility are still insufficiently far along in design to be able to obtain a good idea of size, weight, power, etc. An additional requirement which the capsule must satisfy in order to provide useful measurements, besides the obvious temperature and vibration isolation, is penetration of the capsule skin by probes. For virtually all measurements with the landed capsule, orientation with respect to the Mars vertical will be necessary.

4.2 MAJOR EXPERIMENTS

For convenience the experiments have been divided into three groups; atmospheric, geophysical and surface measurements. Of course no such listing can be complete since the entire field is evolving rapidly. It is probably safe to say that every one of the devices suggested here is individually capable of being packaged to operate in the Mars capsule. How many instruments or what priority is to be assigned to certain experiments is a complicated matter than can be decided only more or less subjectively and in the light of results of development programs now in progress. Based on statements by various authorities probably the atmospheric measurements should be made first. The instrumentation is already available in miniaturized form for terrestrial atmospheric investigations and a high degree of reliability can be expected. The atmosphere of Mars is probably not so different from that of the terrestrial stratosphere that great modifications will be necessary. Other measurements which are essentially geophysical are similar to those made by rockets launched from the surface of the earth to investigate the upper atmosphere and differ mainly in the reversed order of taking data. Some of these measurements could be taken from the bus and significant results achieved. For example the magnetic field, radiation and Schumann U-V experiments are in this category and the problem becomes one of adapting existing instrumentation to the planetary probe.

A third class of experiments can be performed only from the launched capsule. In the main they will be similar to those planned for lunar surface studies. However since most of the instrumentation is still in the developmental stage it is hard to predict which will be most practical for planetary exploration.

LIST OF MAJOR EXPERIMENTS

TELEVISION

LIFE DETECTION

ATMOSPHERE

1. State variables
2. ρ, V, T
3. Ionization
4. Dust
5. Composition
6. Wind Velocity

GEOPHYSICAL

1. Magnetic Field
2. Radiation
3. Plasma and Ionosphere Transmission
4. Schumann U-V
5. Micrometeorites

SURFACE MEASUREMENTS

1. Seismic
2. Bore Hole Survey
3. Chemical Analysis

4.3 PRELIMINARY SUGGESTIONS FOR CAPSULE EXPERIMENTS

4.3.1 Photographic Reconnaissance

Probably television (Vidicon) photographs should have first consideration for a major capsule mission. Therefore this particular experiment is discussed in some detail. It has been pointed out that temporal resolution may be important in the case of a planet like Mars where obscurations due to atmospheric conditions are observed. By analogy with terrestrial conditions atmospheric processes may be expected to have characteristic time scales.

From the earth, the resolution of features on the Martian surface will be about 300-400 km or with balloon-borne equipment 30-40 km. It appears that with the above spatial resolution atmospheric phenomena with time scales of the order of days can be observed from the earth or from balloons, on a scale of hours. From a previous discussion it seems that it may be possible to obtain 200 line TV pictures of the surface which will have resolution of the order of 10-100 ft. In other words, it is quite feasible to take photographs in proximity to Mars that will give resolution of the surface vastly improved over that of terrestrial photographs of the Moon. Even in the event of obscuration of the surface by clouds such photographs should provide considerable information about atmospheric processes. The basic limitation will no doubt be due to restricted data transmission capability.

---

(1) Studies of the Physical Properties of the Moon and Planets, RM-2817-JPL, June 30, 1961.

4.3.2 Life Detection Capsule

It is suggested that a second major capsule design be devoted to an experiment to detect life forms. At the present time it is felt that it would be premature to attempt to describe specific means for accomplishing this objective. As mentioned above the photometric protein detector has shown some promise in the laboratory. In operation the device would require obtaining a sample of the soil or perhaps the atmosphere. This sample would then be put into a dye solution and the "J band" which is formed in the presence of protein detected photometrically and the information transmitted as a "yes or no" answer. Other types of detectors are likely to be at least as complicated and therefore more or less sophisticated.

4.3.3 General Experiments

Magnetometer

The measurement of the magnetic field of Mars would be of great interest and it seems reasonable to expect that the instrumentation will be available. Such devices have been developed for lunar and space application. In view of the present lack of knowledge a simple rotating coil device similar to that used on Pioneer would be useful. More sophisticated instruments such as the rubidium vapor magnetometer may also fall within the weight and size capability.

Plasma Studies

Another closely connected experiment of interest is the measurement of accelerated protons and electrons in the magnetic field of Mars

(if a field exists). This can be done by a plasma probe similar to that being developed by Rossi at MIT. If Mars has these "Van Allen Belts" Geiger and scintillation counters developed for rockets and satellites would provide relatively simple sensors and logic circuitry.

Ionospheric Studies

If Mars has an ionosphere probably radio probes can be used in which signals of varying frequency are transmitted either from above or below and the returning echo measured. Other probe-type measurements have been made in the terrestrial ionosphere employing ion collectors and impedance probes which utilize the detuning effect on a matched antenna.

Optical Measurements

In the near infrared, emissions on the dark side of Mars would be important. On the light side it should be possible to measure (a) molecules having IR absorption spectra, (b) character of the reflecting layer and, (c) temperature at the reflecting layer. Such experiments would employ IR detectors sensitive in the wavelength range of interest and probably would consist of thermocouple elements with appropriate filters.

Another useful wavelength region is the far ultraviolet. Using relatively simple photoelectric detectors it should be possible to determine some of the constituent gases, and in particular hydrogen and oxygen which exhibit resonance scattering in the 1300 Å region. Also telemetering monochromators and retarding potential analyzers have been designed for rocket use and may be useful if the required data rate is low[2].

---

(2) Report on Conf. on Planetary Atmospheres, Space Science Board NAS, Arcadia, California, June 24, 1960.

Atmosphere

The most important quantities to measure first are the surface pressure, composition and temperature. This could be done by pressure and temperature gauges much as in terrestrial upper air soundings since the range of variables is probably not so great as to require radically different instrumentation. Somewhat more advanced experiments could employ mass spectrometers, ion probes and perhaps even a gas chromatographic device. The vertical gradient of the above quantities would be of the greatest interest and it is difficult to see how it can be obtained except with a probe to the surface. It may be mentioned here that the reduction in velocity which would be obtained with a parachute would be an advantage from the standpoint of obtaining representative samples.

In connection with studies using far U-V absorption it is also possible to carry along a source such as a small hydrogen arc. This would be used in conjunction with photon counters having spectral responses adjusted to coincide with the appropriate absorption bands. The same detectors would of course function with the sun as a source but within the atmosphere the auxiliary source would probably be necessary.

By selecting the proper frequencies it is probable that radio transmitters within the capsule could measure the heights of clouds as well as the degree of ionization in the upper atmosphere.

A more or less conventional spectrometer can be incorporated into the capsule and measurements of the night and twilight airglow could give valuable information regarding recombination processes in the high atmosphere. In addition, direct measurement of the density of such ions

as N_2^+ and O_2^+ can be made.

Horizontal Wind Velocity

Dr. Y. Mintz, a RAND consultant, has proposed that the drift of the descending capsule be used to measure the horizontal wind speed. He proposes to use successive photographs taken from the slowly descending capsule.

Surface Wind Velocity

There are meteorological reasons to anticipate rather high surface winds on Mars and the suggestion has been made that strong convection similar to that observed in the Himalayan Plateau exists. Therefore wind velocity measurements would be extremely interesting. If at all possible, a landed capsule should include an anemometer, perhaps of the hot wire type.

Dust Clouds

One of the prominent observational features of Mars is the presence of dust clouds which tend further to support the existence of a high altitude desert climatic regime. It may be possible to use the velocity of the descending capsule to provide information about the dust concentration by recording impacts with a sensitive microphone such as employed for micrometeorite detection. The sensitivity has been given as 5×10^{-4} to 5×10^{-3} gm cm sec^{-1}. For a 10 micron particle and velocity of fall of 500 ft sec^{-1} the momentum will be approximately

$$\frac{4}{3}\pi \; r^3 \rho \; v \simeq \frac{4}{3}\pi (10\times10^{-4})^3 \times 5 \times 5\times10^2 \times 30$$

$$\simeq 3 \times 10^{-4} \text{ gm cm sec}^{-1}.$$

Therefore particles of the order of 10-100 microns should be detectible by this method.

Neutron Elastic Scattering

It appears that considerable success has been obtained experimentally by the use of a neutron scattering technique. The prompt gammas produced in the inelastic scattering process are detected with a scintillation spectrometer and by utilizing fast gating circuits the response to the activation gamma rays is suppressed. Experiments with piles of silica sand doped with certain trace elements have demonstrated the feasibility of a remote semi-quantitative analysis of such material. The application to planetary surveys is obvious. In the case of Mars a search for oxygen would be especially interesting, since there is some reason to believe that the surface materials are completely oxidized. A light weight scintillation spectrometer has been designed for the Ranger experiment and the construction of an accelerator is presently underway.

The above suggestions for experiments to be conducted with a Mars probe are felt to be representative of present expert opinion on the subject. It is not clear that there is as yet a real measure of agreement as to specific measurements to be made.

---

1 "Remote Analysis of Surfaces by Neutron Gamma-Ray Inelastic Scattering Technique", G. H. Schrader and R. J. Skimmer, J. Geophys. Res. 66, p. 1951 (1961).

4.4 DESCRIPTION OF EXPERIMENTS

In the following table an attempt has been made to list representative experiments along with information which is important for design purposes. The state of the art in this area is advancing rapidly and present efforts to develop instruments for lunar exploration should provide a number of devices suitable for the Mars capsule. For this reason most of the numbers given should be considered only as best guesses although in some cases they may be based on existing designs.

TABLE I

Experiment	Device	Weight (Lb)	Size (In^3)	Power Watt	Output	Capsule Requirements
PHOTOGRAPHS	Vidivon TV					
LIFE DETECTION						
ATMOSPHERE						
1. Temperature	Bolometer, Resistance Thermometer	0.1	10	0.1	d.c.	Penetration, Altitude Meas.
2. Density	Accelerometer	1	100			Velocity Meas.
3. Pressure	Pirani Gauge, Ion Gauge	0.5	50	0.1		Penetration, Altitude Meas.
4. Ionization	Retarding Potential Plasma Probe					Penetration, Altitude Meas.
5. Dust	Microphone	3-6	50	1		Penetration, Velocity Meas.
6. Composition	Mass Spectrometer, U-V Spectrometer	1	50-100	1		Penetration, Orientation, Velocity
7. Wind Velocity	Hot Wire Anemometer	1	50-100	1		
GEOPHYSICAL						
1. Magnetic Field	Fluxgate Magnetometer	5	150	2	1-5 -	Position
	Search Coil Mag.	1	50	<0.1	2-5 cps	
2. High Energy Particles	Geiger Counter	0.1	10	0.1		Position
	Scintillation Counter	3	100	1		
3. Plasma	Ion Probe	3	200			Altitude
4. Solar U-V in Schumann Region	Photon Counter	0.5	100	1		Altitude
5. Ionosphere Transmission	Transmitter	0.5	30	5		Altitude
6. Cosmic Rays	C-R Telescope	5	200	2		
7. Micrometeorites	Microphone	3-6	50	1		Velocity
SURFACE MEASUREMENTS						
1. Seismic	Seismometer Active Passive					
2. Bore Hole	Drill, Shaped Charge					Orientation
3. Bore Hole Survey Sound Speed Temperature Thermal Diffusivity Density Hardness Magnetic Susceptibility Electrical Resistivity						Penetration, Orientation
4. Chemical Analysis Neutron Activation Neutron Inelastic Scattering	Neutron Source, Accelerator and Scintillation Spectrometer	20	1000	5-10		
Spectroscopy	X-Ray Diffractometer Mass Spectrometer Absorption Spectrograph					
Radioactivity Gas Chromatography	Scintillation Spectrometer					

4.5 MISSIONS

There are two basic types of capsule missions and both seem feasible for Mariner-B. An impacting capsule making a relatively hard landing can be employed for a parachute deployed to slow down the descending capsule and provide a soft landing. These missions differ in that they may place constraints on the type and accuracy of an experiment, or seriously affect data transmission.

Experience with the Ranger and Surveyor programs will be exceedingly valuable and will no doubt determine to a large extent the planetary investigations. In Table 4.5 the experiments previously described are arranged in accordance with the impacting or landing concepts in a rather arbitrary manner based mainly on the feasibility of making the measurements at high velocity. Specific instruments such as seismometers are suitable for a landing at relatively high velocity while more sophisticated devices for determining surface properties will almost certainly require soft landing. For atmospheric measurements low velocities are desirable because of slow response times of the instruments and the advantages of making a fairly large number of measurements as a function of altitude. There may be in addition transmission difficulties due to the short times available. In many cases recording and retransmission after landing may be necessary. The geophysical measurements are nearly all presently accomplished at high velocity and except for high data rates are adaptable to an impacting payload carrier.

With the exception of the Vidicon Camera and Life Detection experiments no specific capsule designs are proposed. It is felt that an objective choice is neither possible nor desirable at this time. As a practical matter the selection of specific experiments will have to be made mainly on the basis of available space and weight as well as on data rate and bandwidth considerations.

TABLE 4.5

CAPSULE MISSIONS

IMPACT	LANDING
Photo Reconnaissance	Life Detection
Atmosphere	Atmosphere
Density	Temperature
Pressure	Pressure
Ionization	Ionization
Dust	Composition
Mass	Wind Velocity
Geophysical	Surface Measurements
Magnetic Field	Seismic
Radiation	Bore Hole Surveys
Plasma	Chemical Analysis
Solar U-V	Activation
Ionospheric Transmission	Chromotography
Cosmic Rays	
Micrometeorites	
Surface Measurements	
Seismic	
Chemical Analysis	
Radioactivity	
Spectroscopy	

Ford Motor Company AERONUTRONIC DIVISION

Intra-Company Communication

SUBJECT: MARINER B ATMOSPHERIC MEASUREMENTS November 15, 1961

FROM: Irving H. Blifford TO: T. A. Bergstralh
J. E. Kemmerly
R. F. Nease

From both the scientific and practical standpoints it would be highly desirable to obtain information regarding the atmosphere of Mars. The problems of making such measurements are similar to those encountered in conducting rocket-borne experiments on the earth. Therefore it should be possible to use much the same instrumentation with relatively little modification at least in principle. In such measurements the atmosphere is assumed to obey the equation of state for an ideal gas,

$$P = \rho \frac{R}{M} T \quad .$$

With this equation and the barometric equation

$$\rho = -\frac{1}{g} \frac{dp}{dh}$$

if either the pressure, density, or temperature is known as a function of altitude this quantity is sufficient to allow calculations of the other two. However, to derive the temperature a knowledge of the average molecular weight is required. This latter can be estimated for the earth's atmosphere but for any degree of certainty should be determined by independent measurement for Mars. Unfortunately the direct measurement of temperature is not simple and on the earth has been performed by using the relationship between the speed of sound and the temperature. In this case grenades are exploded at high altitude and the sound speed measured by ground stations. This is not feasible on Mars at least within the restraints imposed by the present Mariner B capsule. Of course if parachute deployment is feasible measurements of temperature and pressure in the lower atmosphere can be made with equipment similar to the balloon-sonde devices presently used for synoptic meteorology. However the only case considered here is that of entering without velocity reduction excepting that due to drag in the atmosphere. Actually the problem of making the above measurements is very similar to that encountered using high altitude rockets to study the earth's atmosphere.

TABLE I

ROCKET METHODS FOR DETERMINING ATMOSPHERIC STRUCTURE

Basic Measurement	Method of Measurement	Theory	Final Atmospheric Quantities		Altitude Range (km)	Non-Instrumental Sources of Error
			Primary	Secondary		
Pressure on side of rocket	Pressure gages	Ambient pressure ring exists on flying rocket	Pressure	Density Temperature	30-120	Wind; yaw; outgassing
Pressure on nose cone of rocket	Pressure gages	Taylor-Maccoll; Stone	Pressure	Density Temperature	30-120	Wind; yaw; outgassing
Pressure at nose tip of rocket	Pressure gages	Rayleigh pitot-tube formula	Density	Pressure Temperature	> 30	Wing; yaw; outgassing
Pressure at nose tip and on nose cone	Alphatrons	Taylor-Maccoll; Stone; Kopal	Temperature	Pressure Density	30-120	Wind; outgassing
Absorption of solar X-rays in atmosphere	Photon counters	X-ray absorption function of intervening air mass	Air mass	Density		
Partial densities of atmospheric constituents	RF mass spectrometer	Sum of partial densities equals total density	Density	Pressure Temperature	> 95	Outgassing
Ratio of argon to nitrogen	RF mass spectrometer	Variation of A/N_2 gives measure of diffusive separation	Estimate of mixing		> 95	Outgassing
Absorption of solar ultraviolet light in atmosphere	Spectrograph	Solar ultraviolet heats atmosphere	Daily temperature variation		20-70	
Pressure modulations on rolling rocket	Pressure gages	Modulation proportional to density	Density		> 30	Wind; yaw; outgassing
Pressure modulations; trajectory and missile attitude	Pressure gages; Magnetometer; cameras; radar	Displacement of relative wind gives atmospheric wind	Wind		> 30	

In Table I a recent compilation of methods for determining atmospheric structure is given.[1] On Mars the range of measurement will be extended to considerably higher altitudes since above about 10 km the Martian atmosphere is probably more dense than that of the earth. However the estimates are subject to such large errors that it is difficult to provide a picture of the structure versus altitude that will allow very precise instrument design. Perhaps the best that can be done under the circumstances is to plan to use the more or less standard rocket devices and record pressure and density as a function of altitude. It should be noted at this point that independent measures of the altitude, roll rate and aspect are highly desirable but will not be discussed here since they are more properly part of the vehicle instrumentation.

It will be noted also that generally the minimum altitude of measurement is indicated as 20-30 km which, according to best available estimates may be from 0-50 km on Mars. Below these altitudes fairly crude pressure sensors such as bellows type gauges can be employed. It is clear also that an opening to the atmosphere must be provided although typical sensors need not project beyond the capsule skin. A hole about a centimeter in diameter is roughly what is required. A single instrument or perhaps two gauges could be employed, such as a bellows gauge and Pirani vacuum gauge or a composite device such as the Havens gauge which has an a-c output and is sensitive over the range of 10^3-10^{-3} mm Hg. The lower limit of vacuum pressures measureable in a rocket is controlled by outgassing of the vehicle surface and in practice seems to be near 10^{-5} mm Hg. Although after several months in space outgassing may not be serious in the present case it is probably desirable to concentrate on the relatively low vacuum conditions obtaining in the atmosphere near the planet. The above devices can be small and light in weight and should not occupy more than a few cubic inches and weigh roughly 1-2 lbs including circuitry. Since there will be about 5 minutes available after reentry ($\sim$ 200,000 ft) to the surface the data sampling rate does not have to be high. Data every 10,000 ft would be sufficient from the scientific standpoint but in practice it is of course desirable to take as nearly continuous a set of readings as possible.

Atmospheric composition can be studied best using the mass spectrometer. It is sueful only at altitudes where the mean free path in the gas becomes comparable to the dimensions of the tube and on earth this is above about 100,000 ft. On Mars then measurements could be taken only above 200-300,000 ft and therefore before reentry. This may lead to difficulties because of the high velocity since pumping effects are observed which alter the relative ion concentrations. However qualitative information about the masses of the atmospheric constituents at least should be obtainable. On the other hand the device is relatively complex and a typical

---

1 Ratcliffe, "Physics of the Upper Atmosphere", Academic Press, 1960.

unit[2] weighs about 40 lb and requires about 1.4 ft^3. Power consumption is also fairly high with the above system employing 15 telemetry channels.

The instrument which has been used widely is the Bennett r-f mass spectrometer. This instrument employs a series of charged grids in place of the usual magnet for deflection of the ions. It is understood however that recent progress has been made in the design of magnetic instruments and that the weight factor is not significant although there are advantages in the form of reduced complexity and increased reliability. In any event this instrument should give the molecular composition of the high atmosphere from which the chemical composition can be deduced.

In actual practice contamination by the vehicle is a problem and some what elaborate precautions are observed. These include evacuation of the instrument, break-off seals which are actuated at the time of measurement, and positive rocket motor shut-offs to eliminate the exhaust gases.

In accordance with our recent discussions the following brief discussions of magnetic and radiation detectors is included.

Magnetic Instrumentation

Because of its simplicity a magnetometer could be a considered for the capsule. Because the field of a dipole decreases with the radius cubed it is perhaps most reasonable to think of this measurement as a bus experiment. However there is no question but that additional information particularly if the field is weak, can be obtained right down to the surface. The device itself is exceedingly simple[3] and consists of a coil of fine wire wound on a high permeability core. The coil is fixed with respect to the rocket and is connected to a high gain amplifier. The rotation of the vehicle provides a voltage proportional to the field strength modulated of course at a few cps. The output can be sampled at a fairly low rate because of the expected slow change in field strength, probably even for the case of sizeable local anomalies at the surface. Such a rotating coil magnetometer would weigh less than 1 lb including batteries. The sensitivity can be of the order of 10^{-5} gauss or about as low as feasible for a rocket-borne device. Of course the interplanetary field is of intense interest which will no doubt make this experiment a serious candidate for the bus. Local fields generated by the vehicle are generally static and experience with Pioneer V showed that these fields were unimportant. Of course this measurement requires that the surrounding shell be non-magnetic.

---

2 Townsend, RSI, 23 538 (1952).

3 Sannett, J. Geophys. Res. 65 55 (1960).

Van Allen Radiation

If Mars has a magnetic field of sufficient strength, belts of charged particles may encircle the planet in an analogous manner to the Van Allen belts surrounding the earth. In any case a simple radiation detector similar to the one used by Van Allen in early satellite and rocket experiments would not be difficult to install. In view of its simplicity and the largely unknown character of the phenomena to be encountered it is also a good candidate for the bus instrumentation. Whether there is some advantage to having it within the capsule is somewhat problematic. Basically the device would employ one or perhaps two small halogen-quenched Geiger counters as sensors. No access to the exterior of the vehicle is required although a minimum of dense material immediately surrounding the detectors is desirable. Additional circuitry required is a high voltage ($\sim$ 700 volts) supply and counting (scaling) circuits capable of handling $\sim$50,000 random impulses per second. The sampling rate need not be high since the counting rates should not change rapidly with altitude. This experiment at least in theory, should provide some measurement of the natural radioactivity of the body of the planet. Again the variation with altitude is relatively small and a fly-by trajectory may be the best method of making the measurement.

The weight, space and power requirements are minimal and the instrumentation can be designed to weigh less than a pound. A volume of say 50 in^3 should contain the detectors and electronics. As in the case of the magnetic measurements the extension of the experiment to interplanetary space is of interest and provides an additional reason for incorporating it into the bus payload.

APPENDIX H

CAPSULE STRUCTURE; WEIGHT, POWER, AND PROPULSION REQUIREMENTS

AD-017

Ford Motor Company

AERONUTRONIC DIVISION

Intra-Company Communication

October 17, 1961

SUBJECT: MARINER B CAPSULE STUDY CAPSULE ENVELOPE

FROM: T. W. Neumann

EXT: 1686

REFERENCE: Memorandum AD 014
October 9, 1961

TO:

J. Arsenault
T. Bergstrahl
M. Boobar
M. Caldwell
R. Foster
J. Hanrahan
V. Henderson
J. Jansen
S. Lampert
F. Losee
G. Miczaika
E. Onstead
D. Rodriquez
R. Auelmann
I. Blifford
P. Bower
E. Durand
A. Gammal
K. Harder
J. Housego
J. Kemmerly
W. Lemm
R. Morrow
R. Nagorski
J. Oslake
L. Stimpson

In referenced memorandum, values of $m/C_DA = 1.0$ and $C_D = 1.0$ were assumed in order to select a capsule envelope for preliminary evaluation. Subsequent investigation on the sphere cone selected has shown that average drag coefficients of .4 are more accurate than the 1.0 value selected. Using a drag coefficient of .4 and the original proportions, produced a capsule of prohibitive size. As a result, some investigation was made into various capsule shapes using the following constraints:

1. Drag coefficient to be as large as possible.

2. Nose radius of sufficient size to allow packaging of equipment for maximum static margin.

3. Nose shape such that heat shield weights did not become prohibitive.

The envelope selected, and some aerodynamic data are presented in NASA TMX-507 entitled "Free Flight Measurements of Drag and Static Stability for a Blunt Nosed 10° Half Angle Cone at Mach Number of 15.0". The proportions of the envelope are shown below:

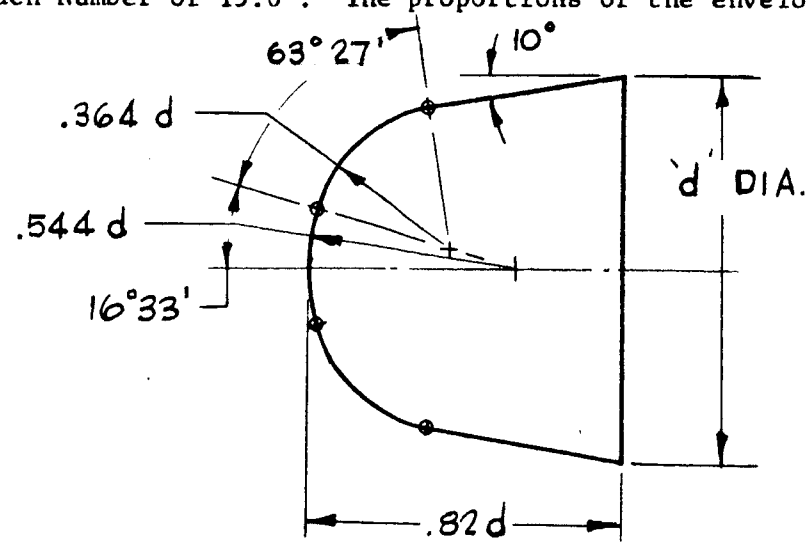

The average drag coefficient for this envelope was conservatively estimated to be $C_D = .65$ thus:

$$\frac{m}{C_D A} = 1.0 = \frac{7.77}{.65A}$$

$$A = 11.85 \text{ ft}^2$$

The base diameter (d) was calculated from:

$$d = 2\sqrt{\frac{A}{\pi}} = 2\sqrt{\frac{11.85}{\pi}}$$

$$d = 3.880 \text{ ft} = 46.6 \text{ in.}$$

∴ Use base diameter of 47.0 inches

The outline shape of the proposed capsule is shown below.

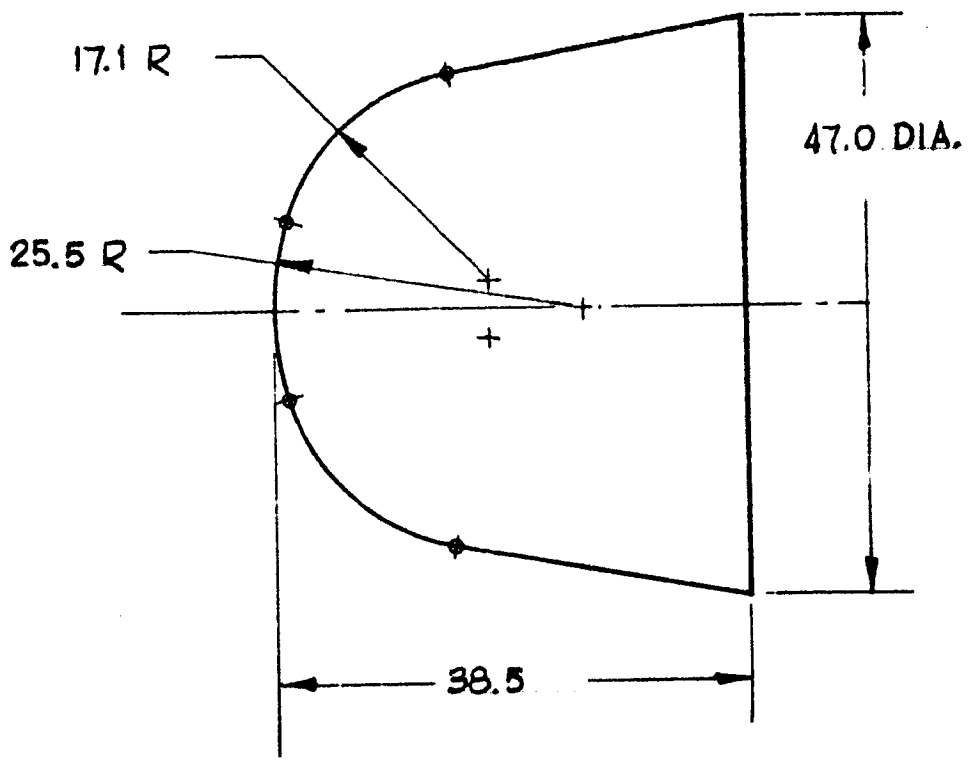

AD - 018

Ford Motor Company

AERONUTRONIC DIVISION

Intra-Company Communication

October 25, 1961

SUBJECT: MARINER B CAPSULE DESIGN

TO: T. W. Neumann

COPIES TO: J. Housego
J. Kemmerley

FROM: M. Caldwell

REFERENCE:
1. J. Housego Memorandum "Mariner B Capsule Study" dated 27 September 1961
2. Memorandum AD-017 "Mariner Capsule Envelope Study" dated 17 October 1961

An inboard profile drawing of one configuration of Mars entry vehicle is shown in Figure 1. The primary mission of the configuration shown is to photograph the surface of Mars and transmit the data to the flyby spacecraft. A secondary function of this configuration is to perform engineering and scientific experiments of interest. The nature of these experiments are dependent upon the size, weight and operational complexity of equipment required to accomplish them. This mission profile corresponds to Capsule Type I as outlined in Reference 1. The majority of effort expended during this study has been directed toward accomplishment of the primary function of the mission. Data received from Irving Blifford in his memo "Mariner B Capsule Study", dated 18 October 1961 indicated that the sizes and weights of equipment required to perform the desired secondary experiments were small. Any follow on effort should be directed toward refining capsule weights in order to include as many of the secondary experiments as possible.

Time has not permitted more than a cursory investigation of Capsule Type II (Mars Impact Vehicle) as outlined in Reference 1. However the differences between the capsule required for an impact mission and the capsule delineated in this memorandum will be covered in a separate memorandum.

The external envelope of the capsule shown in Figure 1 is described in Reference 2. The size and shape of the capsule were based upon the concept that proper selection of body envelope could produce aerodynamic properties which favorably influence the entire mission profile. For instance, the drag coefficient and base area of the envelope shown in Reference 2 was chosen so that the time between capsule velocity of Mach 1.0 and ground impact is sufficient for recording and transmitting all photographic data without the use of a secondary deceleration system. The shape also provided useful volume well forward in the capsule. The heavier equipment was placed in the nose of the capsule and the resultant center of gravity location provided a subsonic static stability margin of approximately 7% (supersonically considerably more).

177

The cameras are mounted inside of the heat shield and their lenses are not uncovered until the capsule has decelerated to less than Mach 2. In the configuration shown, a spring loaded plug in the heat shield is released and ejected, thus exposing the camera lenses. Other methods of exposing the lenses are certainly feasible, and should be carefully evaluated. For this study however, it was felt that the method used offered the advantage of simplicity andoperational reliability over other methods.

The equipment components are located and identified in Figure 1. Without careful design the equipment could be exposed to rather high temperatures during the entry phase of the mission. However, conductive heating from the shield can be minimized by careful selection of materials for the structural components. Radiative heating can be controlled by suitable radiation shield insulation and by proper selection of manufacturing techniques and materials. The radial location of the equipment can be adjusted as required to provide the most ideal balance of pitch and roll moments of inertia.

The nature and function of the major structural components can be described as follows:

1. A cylindrical column supports the heat shield and mounts to the equipment disk. Its major function is to transmit loads from the equipment deck into the heat shield during capsule ejection and entry.

2. A circular disk is used to mount all equipment and experimental components. It is used to transmit all component inertia loads into the heat shield support column or the mounting cone. It serves also as a load transfer member for transverse loads on the heat shield .

3. A stiffened cone extends from the equipment disk to the aft and outer periphery of the capsule. It is used to transfer all capsule loads to the spacecraft during boost and guidance phases. It also transfers capsule spin loads to the equipment disk and heat shield.

A summary of the major components, their weight and mass, center of gravity location, and moment of inertia properites is shown in Table I. The dimensional nomenclature used in Table I is explained below.

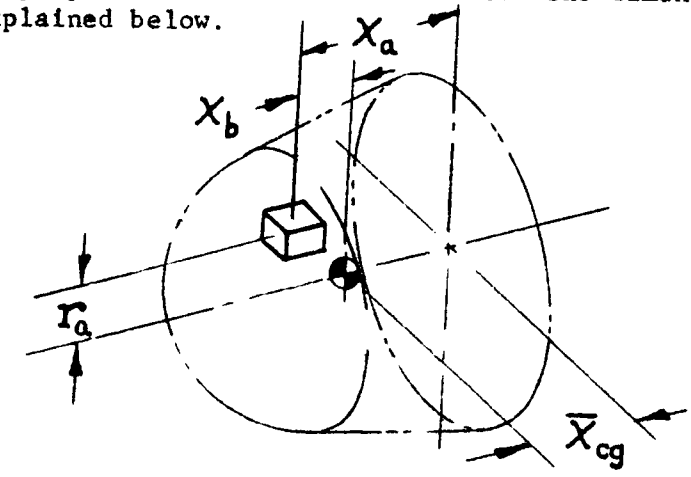

TABLE I

MARS ENTRY CAPSULE MASS PROPERTIES

ITEM	WEIGHT	X_a	WX_a	X_b	WX_b^2	I_{CG}	r_a	Wr_a^2	J_{CG}
Heat Shield Nose	81.2	28.00	2270	5.70	2635	2.91	0	0	6.98
Heat Shield Body	59.8	10.25	613	-12.05	8690	3.47	0	0	6.08
Aft Closure & Antenna	5.0	5.00	25	-17.30	1495	---	0	0	---
Support Structure	5.0	18.00	90	- 4.30	92	---	0	0	---
Color Cameras	24.0	30.00	720	7.70	1423	----	0	0	---
TV Synchronizer	2.0	24.00	48	1.70	6	---	11.8	279	---
TV Encoder	6.0	26.40	158	4.10	101	---	5.0	150	---
TV Transmitter	6.0	25.40	152	3.10	58	---	7.4	329	---
Power Amplifier	17.7	24.80	439	2.50	111	---	10.0	1770	---
Quadruplexer	4.0	19.00	76	- 3.30	44	---	14.0	784	---
Telemetry						---			---
Transmitter	1.3	25.20	33	2.90	11	---	14.0	255	---
Telemetry						---			---
Encoder	2.0	24.40	49	2.10	9	---	11.2	251	---
Telemetry						---			---
Synchronizer	2.0	26.40	53	4.10	34	---	11.2	251	---
Radar Altimeter	15.0	27.00	405	4.70	332	---	9.2	1270	---
Programmer	2.0	24.40	49	2.10	9	---	8.8	154	---
Power Supply	30.0	28.00	840	5.70	975	---	7.4	1636	---
Retro Rocket Case	14.0	13.60	191	- 8.70	1060	---	0.0	0	---
Miscellaneous	2.0	0.0	0	-22.30	992	---	0.0	0	---
	279.0		6211		18077	6.38		7129	13.04

Mass = 8.68 slugs

$$\overline{X}_{cg} = \frac{6211}{279} = 22.3 \text{ in.}$$

$$\frac{\ell - \bar{X}_{cg}}{\ell} = 42\%$$

$$I_P = \sum WX_b^{\,2}/g + \sum I_{CG}$$

$$= \frac{18077}{(144)(32.2)} + 6.38 = 3.89 + 6.38$$

$$I_P = 10.27 \text{ slug-ft}^2$$

$$J_r = \sum Wr_a^{\,2}/g + \sum J_{CG}$$

$$= \frac{7129}{(144)(32.2)} + 13.04 = 1.53 + 13.04$$

$$Jr = 14.57 \text{ slug-ft}^2$$

The values shown in Table 1 above represent the mass configuration of the capsule at the completion of retro rocket ignition. Values of interest for the capsule as mounted on the flyby spacecraft are as follows:

Weight	=	299.0 pounds
Mass	=	9.29 slugs
$\bar{X}_{cg}$	=	21.6 inches
$\frac{\ell - \bar{X}}{\ell}$	=	44.0%
I_P	=	10.57 slug-ft^2
J_R	=	14.60 slug-ft^2

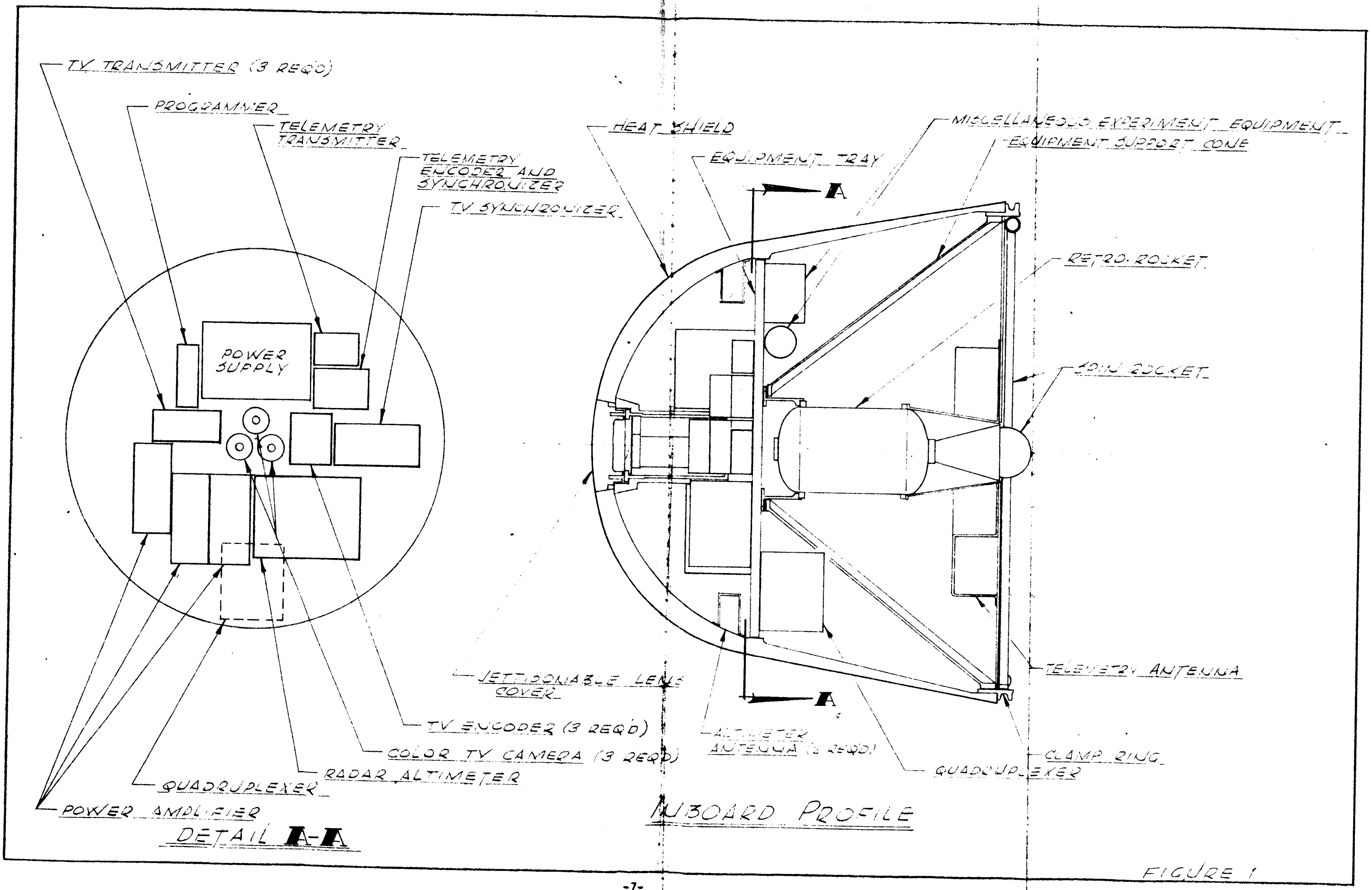
TV TRANSMITTER (3 REQ'D)
PROGRAMMER
TELEMETRY TRANSMITTER
TELEMETRY ENCODER AND SYNCHRONIZER
TV SYNCHRONIZER
POWER SUPPLY
QUADRUPLEXER
POWER AMPLIFIER
DETAIL A-A
TV ENCODER (3 REQ'D)
COLOR TV CAMERA (3 REQ'D)
RADAR ALTIMETER
JETTISONABLE LENS COVER
HEAT SHIELD
EQUIPMENT TRAY
MISCELLANEOUS EXPERIMENT EQUIPMENT
EQUIPMENT SUPPORT CONE
A
RETRO. ROCKET
SPIN ROCKET
TELEMETRY ANTENNA
ALTIMETER ANTENNA (3 REQ'D)
QUADRUPLEXER
CLAMP RING
INBOARD PROFILE

FIGURE 1

Ford Motor Company

AD - 021
AERONUTRONIC DIVISION

Intra-Company Communication

October 26, 1961

SUBJECT: MARINER B CAPSULE STUDY - MARS IMPACT CONFIGURATION (CAPSULE TYPE II)

TO: T. Neumann COPIES: J. Housego, J. Kemmerley

FROM: M. Caldwell

EXT: 1669

REF:
1. AL 126 "Preliminary Parachute Requirements for the Mariner Capsule" dated 22 August 1961
2. AL 127 "Preliminary Impact Limiter Requirements for the Mariner Capsule" dated 23 August 1961

Primary effort has been directed toward a preliminary configuration of Capsule Type I, which has a mission of Mars surface photography and pre-impact experimentation. Even though little thought has been given to an impact vehicle, some general consideration of design philosophy is in order at this time.

Dissipation and/or absorption of the impact energy requires the incorporation of some type of impact cushion. An alternative to absorbing the energy on impact is to decelerate the capsule, in the Mars atmosphere, to a velocity that almost negates the impact forces. A thorough study of the parameters involved should be made before firm configurations are established. Studies made in conjunction with the Ranger Program for a lunar impact vehicle have indicated that end grain balsa wood provides a most ideal absorber.

Preliminary calculations on an impact capsule identical in shape to the Capsule Type I indicated that the drag produced by the entry body alone did not decelerate the mass to an acceptable level for impact absorption. Reference 1 indicated that balloon deceleration devices were efficient and stable, and that impact velocities of the order of 50 fps were easily achieved.

Preliminary calculations outlined in Reference 2 indicated that if a secondary deceleration device was employed and an impact velocity of 50 fps attained, end grain balsa in thickness of the order of 3 inches provided adequate impact protection.

The equipment to be included in this mission has not been selected. However, the variations in impact angle, horizontal velocity component, and terrain that may occur will probably require the use of some type of erection device subsequent to impact. A large diameter thin disk offers the advantage of passive once it has been ejected from the impact wreckage. The use of a decelerating balloon or parachute reduces the requirement for forward placement of equipment since lower

static stability margins can be tolerated.

The functional requirements for separation from the flyby spacecraft, spin-up, retro thrust, de-spin, and Mars atmosphere entry remain the same as for Capsule Type I. The configuration of the two capsules, however, may differ widely. The cursory data outlined in this memorandum has been considered in the very preliminary capsule configuration shown in the inboard profile of Figure 1.

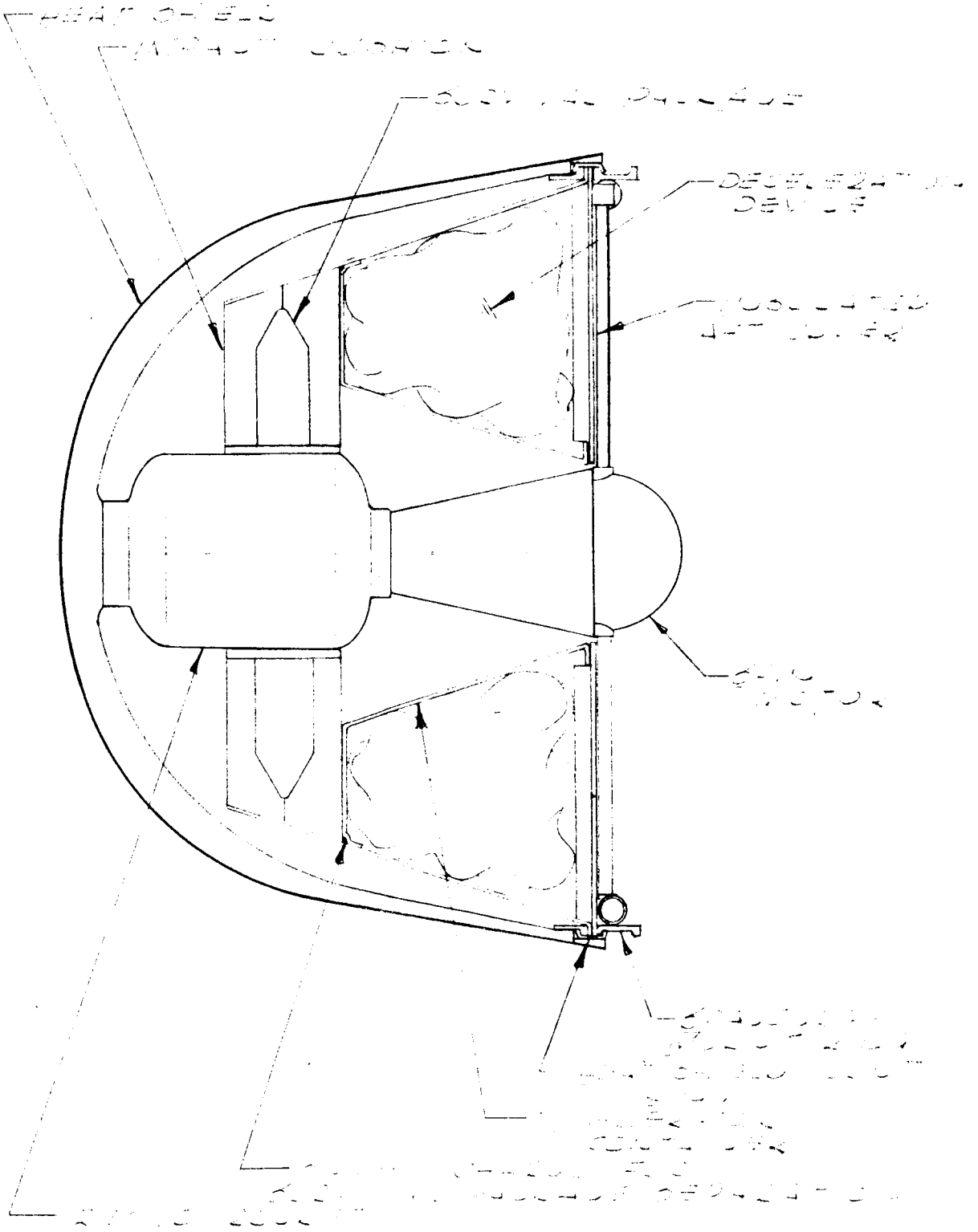

Ford Motor Company

AERONUTRONIC DIVISION

Intra-Company Communication

AL-161

11 December 1961

To: Distribution

From: W. T. Lemm

Subject: AL-144, "Mariner B - Capsule Propulsion System Requirements", 10/24/61

Listed below are revisions to the subject memorandum.

1. Item 4, page 2 should read

   "It will be assumed that motor hardware can be developed in which the hardware will not exceed 15 percent of the total propulsion system weight. On this basis the hardware will weigh 4.5 pounds $(31.54 \times \frac{.15}{.85})$." The previous estimate, 3.02 pounds, is overly optimistic.

2. Item 6, page 3, correct the given burn time to read 10 seconds.

W. T. Lemm

W. T. Lemm

WTL:clm

Distribution

R. R. Auelmann	T. A. Bergstrahl
I. F. Blifford	M. G. Boobar
P. B. Bower	M. Caldwell
D. M. Conrad	F. G. Denison
R. M. Foster	A. A. Gammas
K. C. Harder	W. W. Hawley
V. H. Henderson	J. Housego
J. A. Jansen	J. E. Kemmerly
S. Lampert	F. A. Losee
G. R. Miczaika	R.P. Nagorski
R. F. Nease	T. W. Neumann
J. J. Oslake	D. Rodriquez
W. H. Schilling	D. Stimpson

Intra-Company Communication

AL-144

24 October 1961

To: J. E. Kemmerly

From: W. T. Lemm

Subject: MARINER B - CAPSULE PROPULSION SYSTEM REQUIREMENTS

A. The following determines the amount of rocket propellant required to produce a 300 pound capsule velocity change of 300 to 1000 feet per second. Ref: Rocket Propulsion Elements - G. P. Sutton

1. The instantaneous mass m of the capsule can be expressed as a function of the initial mass m_o of capsule (including propulsion fuel) and the instantaneous time t.

$$m = m_o - \frac{m_p}{t_p} t \; :$$

m_p = initial propellant mass
t_p = propellant burning time

$$m = m_o \left(1 - \frac{m_p}{m_o} \frac{t}{t_p}\right) \; :$$

W_o = initial capsule weight
W_e = final vehicle weight

$$= m_o \left(1 - \xi \frac{t}{t_p}\right) \; : \qquad \xi = \frac{W_o - W_e}{W_e}$$

$$= m_o \left(1 - \frac{\lambda - 1}{\lambda} \frac{t}{t_p}\right) \; : \qquad \lambda = \frac{W_o}{W_e} = \frac{m_o}{m_o - m_p}$$

2. Since there will be no gravitational or aerodynamic drag, the equation of motion for the capsule may be written

$$\frac{dv}{dt} = \frac{\frac{c\xi}{t_p}}{1 - \frac{\xi t}{t_p}}$$

c = effective gas velocity

177A

Integrating: The cut off velocity at the end of burning becomes

$$v_p = -c\ln\ (1 - \xi) + v_o :$$ v_o = initial velocity assumed to be 0.

$$v_p = \bar{c}\ln \frac{m_o}{m_o - m_p} = \bar{c}lu\ \lambda$$ $\bar{c}$ = average effective gas velocity

$$v_p = gI_{sp} \ln \frac{m_o}{m_o - p}$$ $\bar{c} = gI_{sp_{eff}}$

3. Determining the propellant weight m_p

$$\ln \frac{m_o}{m_o - m_p} = \frac{v}{gI_{sp}}$$

$v(max)$ = 1000 ft/sec
I_{sp} = 280 sec
Hercules propellant

$$= \frac{1000}{32.2 \times 280} = .111$$

$$\frac{m_o}{m_o - m_p} = \epsilon^{\frac{v}{gI_{sp}}} = \epsilon^{.111} = 1.1175$$

$$m_o = 1.1175\ m_o - 1.1175\ m_p$$ m_o = 300 lbs

$$m_p = \frac{.1175}{1.1175}\ m_o = 31.543 \text{ lbs}$$

4. Estimating the weight of propulsion hardware:
The Ranger retro-propulsion system criteria indicates that 8-3/4% of the total propulsion system is hardware.

Therefore, the hardware weight is 3.02 lbs = $31.54 \times \frac{8.75}{91.25}$

5. It is suggested the total weight of the propulsion systems required to produce capsule velocities ranging from 300 ft/sec to 1000 ft/sec are of interest. The attached Figure 1 illustrates this variation for a solid propellant having an I_{sp} of 280 seconds.
6. Estimating the size of the propellant grain:

Given: Burning time = 10 seconds

W_p (wt. of propellant) = 31.5 lbs.

I_{sp} specific impulse = 280 sec

r_b (burning rate) = .61 inch per sec

ρ (density) = 0.064 lbs/in^3

$$\text{The thrust F (lbs)} = \frac{W_p \times I_{sp}}{t_b} = \frac{31.5 \times 280}{10} = 880$$

say $\cong$ 900 lbs

Grain length L (inches) = $r_b \times t_b$ = 0.61 x 20 = 12.2 inches

$$\text{Area of burning} = \frac{W_p}{L\rho_b} = \frac{31.5 \text{ lbs} \quad \text{in}^3}{12.2 \text{ inch} \times 0.064 \text{ lbs.}}$$

= 40.3 square inches

Grain diam. = 7.16 inches

B. The following considerations determine the amount of propellant required for capsule spin stabilization.

Given: Capsule weight = 300 lbs.

Spin velocity = 300 RPM $\cong$ 31.42 rad/sec

1. Since spin up is to be accomplished in 1 second

$\ddot{\theta}$ = 31.42 rad/sec^2

2. Capsule polar moment of inertia (given) = 15 slug ft^2
3. The torque required

$$M = I\ddot{\theta} = 15 \frac{\text{lb}}{\text{ft}} \text{ sec}^2 \text{ ft}^2 \times 31.42 \text{ rad/sec}^2$$

= 472 ft lb

= 5.68 x 10^3 inch lb

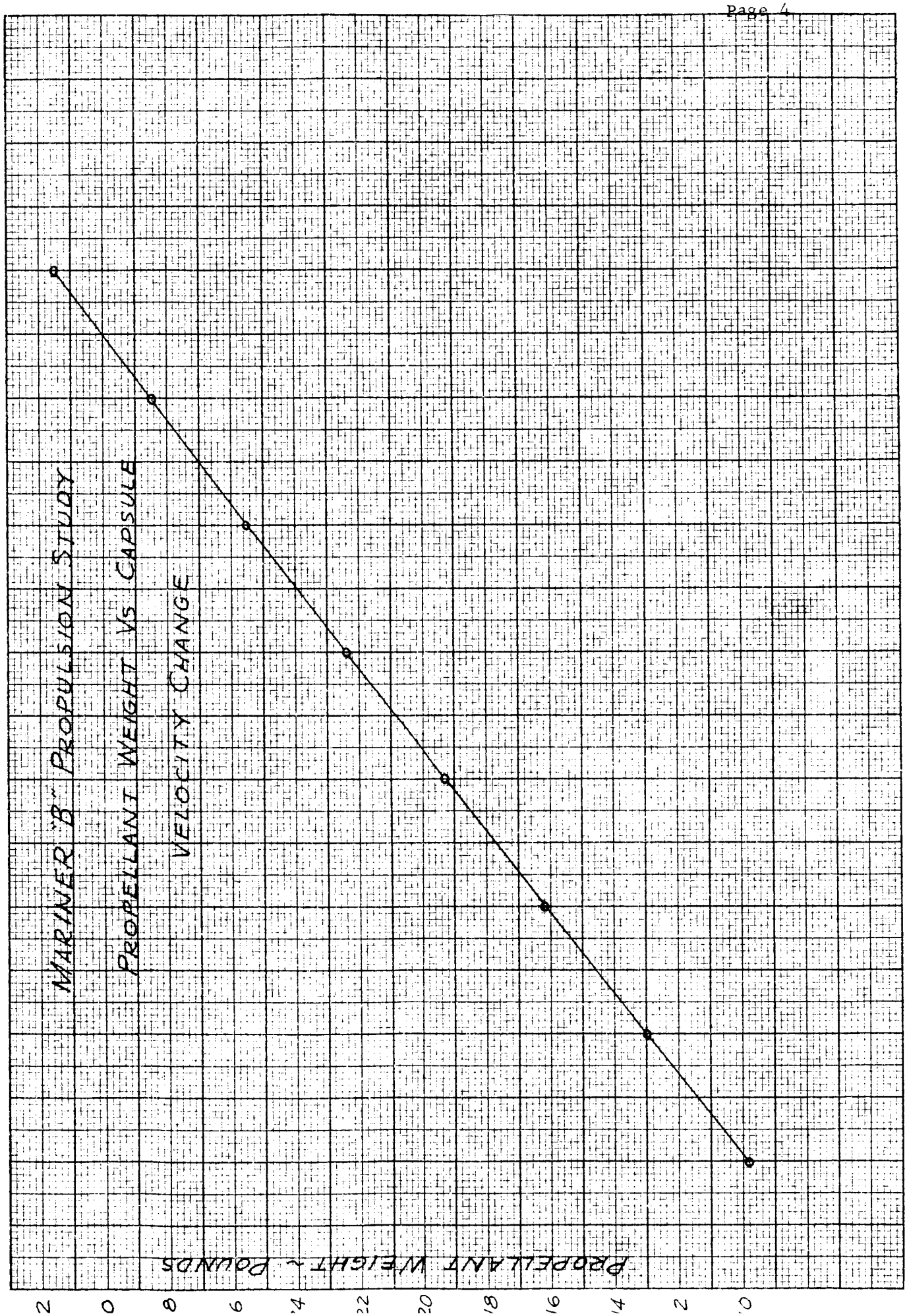

FIGURE 1

K+E 10 X 10 TO THE ½ INCH 359-11
KEUFFEL & ESSER CO. MADE IN U.S.A.

4. The thrust F acting at 48 inches to produce this torque is 118 lbs.

5. For a propellant having I_{sp} = 200 sec, the required propellant weight

$$W = \frac{F}{I_{sp}} = \frac{118}{200} = .59 \text{ lbs/sec}$$

say 0.6 lb. of propellant

W. T. Lemm

WTL:clm

Distribution

R. R. Auelmann
T. A. Bergstrahl
I. F. Blifford
M. G. Boobar
P. B. Bower
M. Caldwell
D. M. Conrad
F. G. Denison
E. Durand
R. M. Foster
A. A. Gammas
K. C. Harder
W. W. Hawley
V. H. Henderson
J. Housego
J. A. Jansen
S. Lampert
F. A. Losee
G. R. Miczaika
R. P. Nagorski
R. F. Nease
T. W. Neumann
J. J. Oslake
D. Rodriquez
W. H. Schilling
I. F. Sobczak
D. Stimpson

APPENDIX I

SPACE ENVIRONMENT AND PLANET PHYSICAL CHARACTERISTICS

Ford Motor Company AERONUTRONIC DIVISION

Intra-Company Communication

SUBJECT: MARINER B CAPSULE STUDY
SPACE ENVIRONMENT

October 5, 1961

FROM: Irving H. Blifford

TO: Distribution

Unless the capsule is protected by the carrier vehicle structure, it will be subjected to space environmental conditions during flight and in the case of the landed capsule, to those on the surface of Mars. The principal effect will almost certainly be due to the solar radiation received. The solar energy flux at the Earth's mean distance from the sun (1 A.U.) is approximately 440 BTU/hr-ft^2 $\pm$ 2%. At Mars the flux would be reduced to

$$\frac{440}{(1.52)^2} = 190 \text{ BTU hr}^{-1} \text{ ft}^{-2} .$$

The solar radiation approximates that of a 6,000°K blackbody except in the region of the ultraviolet below 2500 Å. The intensity in this latter region is strongly dependent on solar disturbances but contributes little to the total radiation flux. However the radiation is relatively energetic and may affect the surface or mechanical properties of sensitive materials. The variation in the solar energy flux (taken from de Vaucouleurs) is illustrated in the accompanying figure. In calculating the surface flux account has been taken of scattering and absorption in the atmosphere.

In space the principal effect of the solar radiation will be that to capsule interior, assuming again that it will be unprotected by the bus vehicle. The heating will be controlled by the amount of thermal radiation absorbed and reflected by the outer shell as well as the thermal conduction from inside to outside. For calculation of the effects however it will be necessary to have knowledge of the materials of construction, their properties and the geometrical configuration.

The reflectivity and absorptivity of material is quite dependent on the surface properties. The latter may be altered by high energy solar radiations and especially by micrometeorite bombardment.

According to an analysis of micrometeorite impacts by Singer (Phys. & Med. of the Atmos. & Space, Wiley, 1960) the erosion of the vehicle skin will be of the order of 10^{-5} cm per year. Since this is only about

1,000 Å and less than the wavelength of the average solar flux, little change in the reflectivity is likely over the much shorter time of the Earth to Mars flight. A summary of the effects of various space environment parameters is given in Table I which is taken from Aeronutronic Report No. U-910, Contract Nr AF 33(616)-6641, May 1960.

Distribution:

R. Auelman	V. Henderson
T. Bergstralh	J. Housego
M. Boobar	J. Kemmerly
P. Bower	S. Lampert
M. Caldwell	F. Losee
E. Durand	T. Neumann
R. Foster	J. Oslake
A. Gammal	D. Rodriquez
K. Harder	L. Stimpson

TABLE I

SUMMARY ESTIMATES OF MAXIMUM MAGNITUDE OF SPACE ENVIRONMENT PARAMETERS OF IMPORTANCE TO MATERIAL BEHAVIOR

Effect	Section For Detailed Discussion	Lower Limit	Upper Limit	Factors That Influence Magnitude of Effect	Thickness of Al Required To Minimize Effect
Vehicle Skin	3	$-150^{\circ}F$	$+400^{\circ}F$	α/ϵ ratio; orbit; orientation of vehicle; density, heat capacity & thickness of vehicle skin	N.A.
Vacuum	-	10^{-11} mm Hg	760 mm Hg	See Minzer & Ripley (Ref. 4-1)	Mechanical strength for P_{max} = 14.7 psi
Meteorites	5	Mass 10^{-10} gm. V = 15 km/sec	Mass 10^{-2} gm. V = 72 km/sec	Mass, velocity, frequency & orbit.	0.1"-1.0"
Radiation:	7				
Electron	7	30 Kev	1 Mev	Maximum completely absorbed by 0.15 cm Al	0.06"
Proton	7	*<10 protons/cm^{2}sec @ >23 Mev	*<1 protons/cm^{2}sec @ > 52 Mev	Solar flare activity. Orbit. Low atomic no. materials better for proton shield.	0.45" see p. 184
Neutron	7	Negligible	Very small		
Very short Wavelength Electromagnetic Radiation	7	Negligible	Very small	Solar X-rays completely absorbed by 0.01 cm Al.	0.004"
Near Ultraviolet, Visible, & Infrared	-		2 cal cm^{-2} min^{-1}	α/ϵ ratio for UV	N.A.

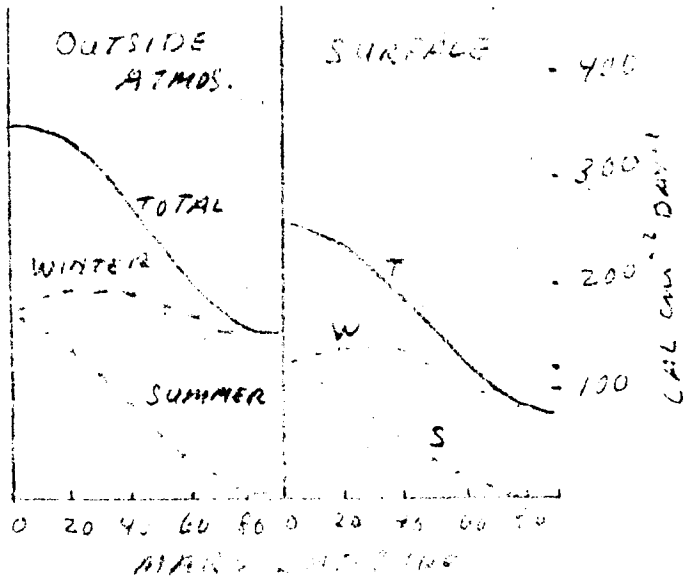

VARIATION IN TOTAL SOLAR ENERGY FLUX

SUBJECT: MARINER-B CAPSULE STUDY
MARS PHYSICAL CHARACTERISTICS

October 23, 1961

FROM: Irving H. Blifford TO: Distribution

Surface and Climate

All of the information regarding Mars' surface has been obtained from telescopic observation. Since the resolution is about 300-400 km even under the most favorable conditions, little can be said about surface conditions on a scale that seems very useful for landing operations. Measurements made spectroscopically or photometrically however have provided a certain body of information from which it is possible to draw a few conclusions.

For example, the slope of the photometric curve is much flatter for Mars than for the Moon and is taken as evidence that Mars is relatively level. Since it is assumed that meteorite bombardment of the surface would produce features similar to the lunar craters, some erosion may have taken place.

In general, the planet Mars appears to be a neutral gray with traces of brown and perhaps green. Earlier reports of clearly defined green areas are no longer accepted. Seasonal effects are observed, the most clearly defined being the formation of polar caps and their subsequent disappearance with approaching spring and summer. Polarization measurements indicate that the polar caps are deposits of frost formed under reduced atmospheric pressure. Bright white spots which appear in the polar regions appear to be clouds, about 100 km in diameter, of ice crystals. Some of the smaller ones remain in place for several days which may indicate mountains or hills in these regions.

Dark markings particularly surrounding the polar caps which change in a regular planet-wide way with the seasons are also observed. The polarization measurements do not agree with the hypothesis that contrast changes are due to an evaporating ice crystal layer. Actually the observations are consistent with the assumption that opaque granules representing life forms are the cause of the seasonal growth of these dark fringes.

Characteristic rectilinear markings which under high resolution can be broken up into complex detail are observed. These bands are believed to be related to the Martian geology but present opinion seems to discount former observations of geometric patterns (canals).

Yellow clouds (yellow veil) are observed at lower levels than the white clouds and are believed to be composed of dust particles 2 to 5 microns in diameter. Polarization measurements indicate that this dust is highly absorbing and may consist of carbon particles.

Besides the yellow and white clouds, blue clouds are observed. The normal condition on Mars seems to be one in which a thin blue layer of transparent microscopic particles, but nothing else is present. These clouds appear at the morning and evening edge of the planet, disappear at noon, and reappear at sunset.

The above phenomena can provide only hints as to the surface features although there seems to be an unknown degree fine structure on a scale of about 100 km.

In summary, one is left with a vague picture of a rather flat and monotonous landscape similar to terrestrial mountain plateaus. Some haze is usually present, light clouds appear in the morning and evening, and occasional dust storms sweep the surface. In winter the northern and southern regions are covered by a thin layer of ice crystals which gradually disappear with the coming of summer. At the edge of the receding front layer, a low dark form of vegetation replaces the ice. Some opinion has been offered to the effect that this process leads to the production of a certain amount of dust.

The climate of Mars is appreciably more severe than that of the earth with temperature variations at the surface from 10° to 20°C in tropical latitudes in summer and from -80 to -100°C at the poles in winter. There have been suggestions also that strong convection occurs as a result of large diurnal variations in surface temperature. All in all, a picture emerges of a rather severe climatic regime with conditions at the surface quite similar to those of the terrestrial stratosphere.

Atmosphere of Mars

The atmosphere of Mars is of great scientific interest not only because something is known of it from telescopic observations but the meteorology is in fact simpler and easier to understand than that of the earth. The water vapor content is low and consequently the thermodynamic problems are more tractable. Likewise there are no large bodies of water or high mountains to modify circulation patterns. Therefore just as the moon is interesting because of its less complicated geology, the study of the meteorology of Mars can provide a model of terrestrial atmospheric processes that will lead to a better understanding of those on the earth.

Perhaps the practical problems of entry into the Martian atmosphere by probe vehicles, instrument operation and communications offer even more incentive to have as much quantitative information as possible. Heat shielding and even electronics operation under reduced atmospheric pressure requires more or less exact knowledge of composition and the state variables. The electrical condition of the atmosphere and propagation of

electromagnetic radiation through a possible ionosphere is obviously of great importance. The existence of a magnetic field and certain photochemical effects of course are central to this question.

The total mass of the Martian atmosphere has been determined by several methods. The most recent and probably best are those of Dollfuss and were obtained from polarimetric studies. He gives 250 $\pm$ 100 gm cm^{-2} or the equivalent of about 94 mb for the surface pressure. The temperature of the atmosphere near the surface has been measured telescopically and also derived theoretically from radiation balance considerations to be about 230°K.

In regard to composition, the only gas that has been positively identified is CO_2 which is present in about 2 percent by volume or 7.5 gm cm^{-2}. Water vapor may be present but is believed to be less than about 10^{-2} gm cm^{-2}. Spectroscopic evidence obtained from measurement of line shapes in the search for Doppler shifted components gives the O_2 content as less than 4 gm cm^{-2}. The bulk of the atmosphere is assumed to be nitrogen. The reasoning is partly by analogy to the atmosphere of the earth and partly from chemical considerations which indicate that the only inert gas that seems reasonable to postulate is nitrogen. A small amount of argon (3-13 gm cm^{-2}) is probably present if the abundance of potassium is the same on Mars as on the earth. The above composition would result in a mean molecular weight of 28.4 from which can be derived a dry adiabatic lapse rate of -3.8 deg km^{-1}.

While the change in the pressure, temperature and density with altitude is exceedingly important, these quantities are difficult to determine. There are no measurements available from which stratospheric temperatures can be estimated and therefore the existence of a tropopause can only be conjectured. There are, however, several ways in which a model of the atmosphere can be formulated based on the principles of dynamic meteorology. Convective equilibrium can be assumed to obtain with essentially adiabatic conditions, which results in a maximum tropopause height of about 70 km. Another model has been formulated in which isothermal equilibrium is assumed above the tropopause. Additional models can be constructed based on absorption of solar radiation by atmospheric gases such as O_3 and CO_2 as is known to be the case on the earth. Estimates resulting from such calculations are subject to relatively large errors which increase markedly with height. For example the error in altitude at which the Mars pressure is equal to that on the earth, varies from about 17-26 km at 10 km to 42 - 85 km at 80 km on Mars.

Appendix I is a tabulation of Basic Data on Mars which have been abstracted from various sources. Appendix II contains a summary of information relative to the atmosphere of Mars obtained from RAND report RM-2817-JPL dated June 30, 1961.

Ford Motor Company AERONUTRONIC DIVISION

Intra-Company Communication

Mariner B. Capsule Study

SUBJECT: BASIC DATA ON MARS (From "Physics of the Planet Mars" by G. deVaucouleurs - London 1954)

September 26, 1961

FROM: I. H. Blifford TO: Distribution

	Miles	Km
Distance From Sun		
Mean (1.5237 A.U.)	141.5×10^6	228×10^6
Aphelion (1.6658 A.U.)	154.1	248
Perihelion (1.3826 A.U.)	128	206
Distance From Earth		
Perihelion opposition	34.8×10^6	56×10^6
Aphelion opposition	61.5	99
Aphelion conjunction	340	547
Orbital Velocity per Second		
Mean	14.98	24.11
At aphelion	13.64	21.95
At perihelion	16.45	26.37
Escape velocity per second	3.13	5.04
Velocity at surface	2.21	3.56
Equatorial diameter	4220	6780

177

Length of year (668.599 Mars days)	686.979 Earth days
Eccentricity of orbit	0.09336
Mean sidereal motion in 24 hours	1886.519"
Inclination of orbit to eccliptic	1° 50' 59.8"
Inclination of Martian equator to its orbit	25° 10'
Length of day	24 h 37 m 22.668 s (sidereal) 24 h 39 m 35.247 s (solar)

Seasons

No. Hemisphere	So. Hemisphere	Mars day
Spring	Fall	194.2
Summer	Winter	176.8
Fall	Spring	141.8
Winter	Summer	155.8

Mass (earth = 1)	0.108
Volume (earth = 1)	0.151
Density (earth = 1) (water = 1)	0.710 3.91
Surface area (earth = 1)	0.278
Gravity at surface (earth = 1)	0.38
Mean magnitude at opp.	-1.90 ± 0.02
Mean surface brightness	0.23 int. candle/cm^2
Visual abedo	0.15

Temperatures At Surface

	Perihelion	Aphelion
Tropic Summer	+ 10°C	+ 20°C
Tropic Winter	- 20	- 10
Temperate Summer	0	+ 20
Temperate Winter	- 50	- 30
Polar Summer	- 10	+ 10
Polar Winter	- 80	- 100

Atmosphere

Altitude (km)	Pressure mb
0	85
5	64
10	48
15	36
20	27
25	20
30	15

Atmospheric Composition

Gas	Thickness (m, NTP)	Volume (%)	
N_2	1800	98.5	(inferred)
O_2	<2	<0.1	det. limit
A	22	1.2	inferred
CO_2	4.4	0.25	spectroscopic
H_2O	<200 cm	<0.15	det. limit

Atmospheric Composition --Continued

Gas	Thickness (m, NTP)	Volume (%)	
CH_4	< 10 cm	--	det. limit
C_2H_4	< 2 cm	--	det. limit
C_2H_6	< 1 cm	--	det. limit
NH_3	< 2 cm	--	det. limit
H_2	0	--	theoretical
He	0		theoretical
O_3	low, if at all		

List of Oppositions of Mars (1960 - 1975)

Year	Date	Nearest Distance To Earth	Largest Apparent Diam.
1960	12/29	56.2×10^6 miles	15.4"
1963	2/3	61.8	14.0
1965	3/8	61.8	14.0
1967	4/13	56.2	15.4
1969	5/29	45.3	19.1
1971	8/6	34.6	25.0
1973	10/21	40.6	21.6
1975	12/13	53.1	16.5

Distribution:

R. Auelmann
T. Bergstralh
M. Caldwell
E. Durand
R. Foster
A. Gammal
J. Hanrahan
K. Harder
V. Henderson
J. Jansen
J. Kemmerly
S. Lampert
F. Losee
R. Morrow
G. Miczaika
R. Nagorski
T. Newmann

Ford Motor Company

AERONUTRONIC DIVISION

Intra-Company Communication

SUBJECT: MARINER B CAPSULE STUDY
MARS ATMOSPHERE

October 2, 1961

FROM: I. H. Blifford

TO: Distribution

From RAND report RM-2817-JPL, June 30, 1961, the following information has been abstracted and is intended to form the basis for a working model of the atmosphere for design purposes. It must be recognized that the basic experimental information is meager and that widely differing interpretations are possible depending on the method of analysis. However for the present it is my opinion that the following values should be accepted.

		Lower Limit	Average	Upper Limit
Total mass/unit area (gm cm^{-2})		150	250	350
Surface acceleration (cm sec^{-2})		360	375	390
Surface pressure (gm cm^{-2})		150	250	350
	(millibars)	54	94	136
Mean temperature at surface (^{o}K)		210	230	260
Atmospheric Composition				
CO_2	(gm cm^{-2})	3.9	7.5	16.6
	(meters NTP)	20	38	84
	(Vol. %)	0.7	1.9	7.2
Argon	(gm cm^{-2})	3	--	13
H_2O	(gm cm^{-2})	10^{-3}	$5x10^{-3}$	$3.5x10^{-2}$
Oxygen	(gm cm^{-2})			<4
Mean molecular wt.		28.2	28.4	29.9
Dry adiabatic lapse rate (deg km^{-1})		-3.43	-3.75	-4.10
Temperature of stratosphere above tropopause (^{o}K)		130	180	250
Surface density (gm cm^{-3})		$7.5x10^{-5}$	$1.4x10^{-4}$	$2.2x10^{-4}$

MEAN STRATOSPHERIC SCALE HEIGHT

$$\beta = \frac{g_m M}{RT} \qquad H = \frac{1}{\beta}$$

	g_m (cm sec^{-2})	T (^oK)	β km^{-1}	H km
Upper Limit	360	220	5.6×10^{-2}	18
Average	375	160	8.0×10^{-2}	12.5
Lower Limit	390	120	1.1×10^{-1}	9

SPECIFIC HEATS BASED ON CALCULATIONS WITH N_2 (87-99%), CO_2 (1-7%) AND A (0-6%)

		CO_2 = 1 A = 0	CO_2 = 7 A = 6
Ratio =	γ = cp/cv	1.398	1.402
Specific heat at p = const.	cp	1.035	0.97

EXTREME RANGE OF EQUAL "PRESSURE ALTITUDES"
FOR EARTH AND MARS

Earth Alt. (km)	Pressure mb	Mars Alt. (km) Minimum	(Mod III)*	Maximum
10	265	0	0	0
20	55.3	0	8	18
30	11.85	16	36	49
40	3.0	28.3	62.8	76.5
50	0.879	37.8	89.4	101
60	0.256	47.4	119	126
70	0.0602	58.8	152.4	154.6
80	0.0101	72.6	181	190

* Conjectural model assuming ozone U-V absorption similar to earth.

Distribution:

R. Auelmann
T. Bergstralh
I. Blifford
M. Boobar
M. Caldwell
E. Durand
R. Foster
A. Gammal
K. Harder
V. Henderson
J. Housego
J. Jansen
S. Lampert
F. Losee
C. Miczaika
R. Nagorski
T. Neumann
P. Bower
J. Oslake
J. Kemmerly

Ford Motor Company

AERONUTRONIC DIVISION

Intra-Company Communication

SUBJECT: MARINER B CAPSULE STUDY

DATE: September 28, 1961

FROM: I. H. Blifford

TO: R. Auelmann, T. Bergstralh, M. Caldwell, R. Foster, A. Gammal, K. Harder, V. Henderson, J. Housego, J. Kemmerly, J. Jansen, S. Lampert, F. Losee, G. Miczaika, R. Nagorski, T. Neumann, P. Bower, J. Oslake, E. Durand

The enclosed curves were obtained by John Housego at the JPL meeting. They are abstracted from RAND Report RM-2817-JPL and do not seem to be in disagreement with other estimates. After we obtain the report it may be possible to determine some basis for choice among the several cases presented, if this is required for purposes of design analysis.

177

TEMPERATURE OF MARS ATMOSPHERE

Case	T_o	T_s	P_o
A	470	410	113
B	410	320	196
C	380	230	284
D	470	230	113
E	410	410	196
Units	°R	°R	$\frac{lb}{ft^2}$

Subscripts o—SURFACE s—STRATOSPHERE

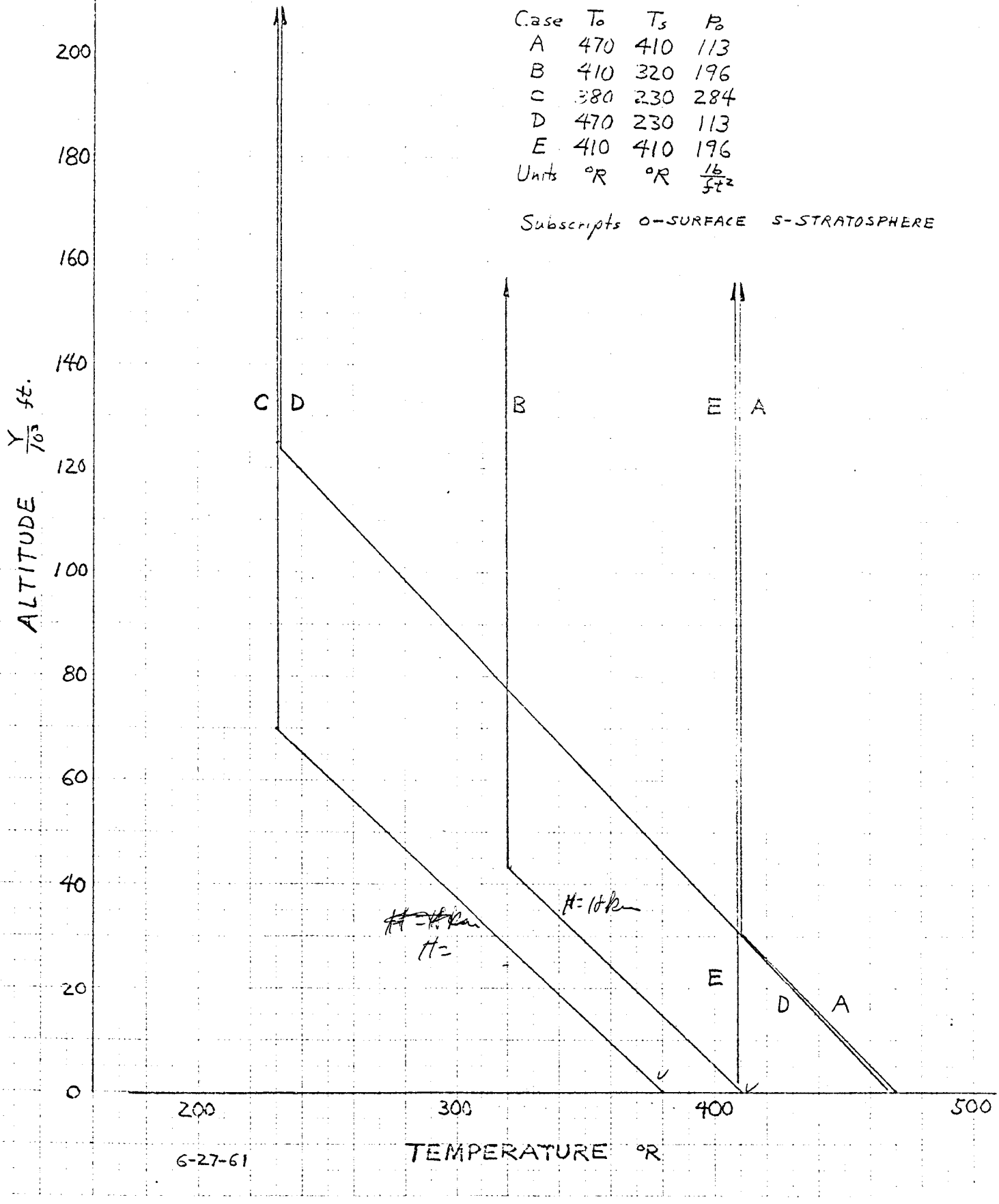

6-27-61

17

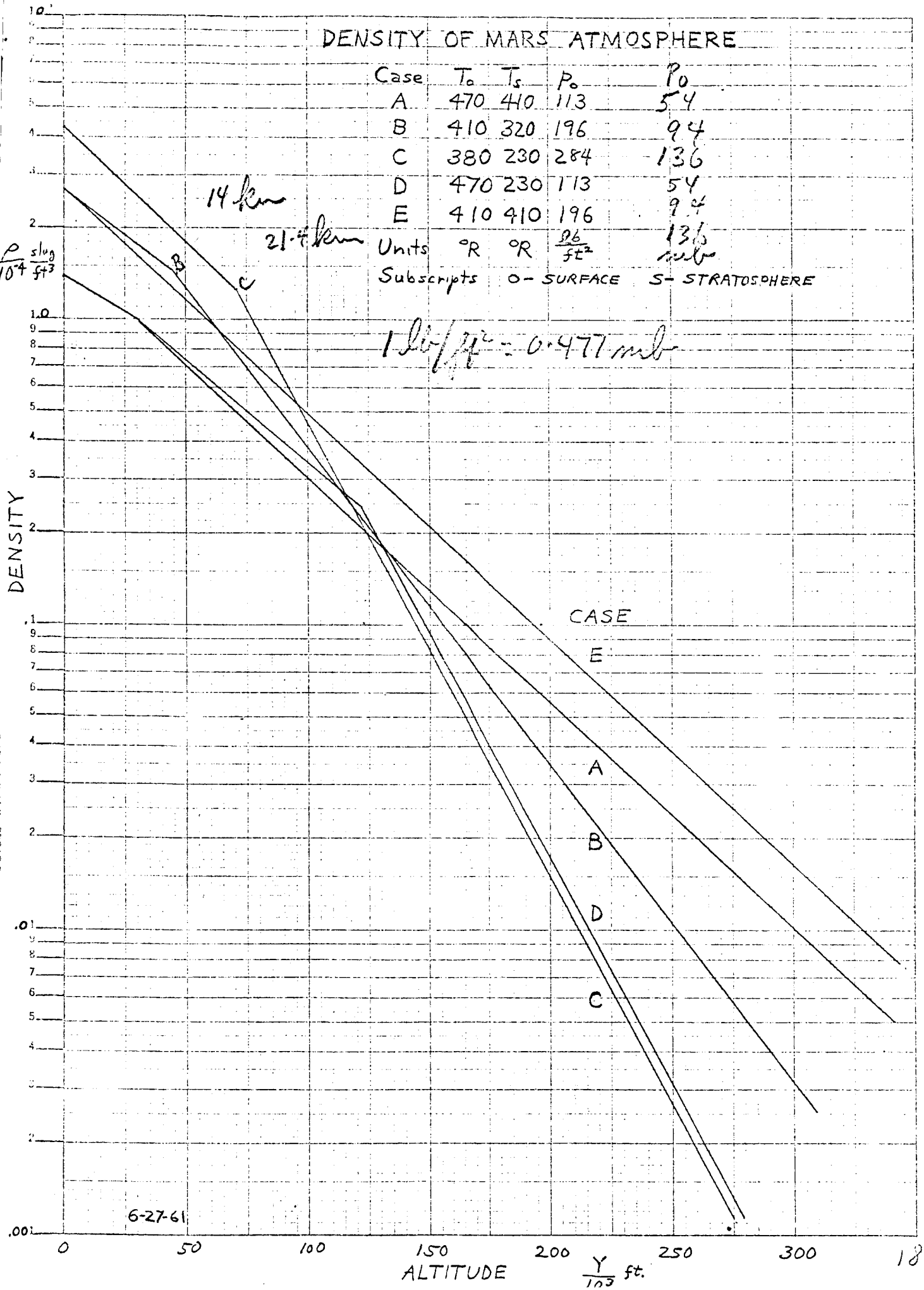
DENSITY OF MARS ATMOSPHERE
Case T_o T_s P_o P_o
A 470 440 113 54
B 410 320 196 94
C 380 230 284 136
D 470 230 113 54
E 410 410 196 94
Units °R °R lb/ft² mb
Subscripts 0 - SURFACE S - STRATOSPHERE
1 lb/ft² = 0.477 mb
14 km
21.4 km
B
C
CASE
E
A
B
D
C
DENSITY
ρ / 10^{-4} slug/ft³
ALTITUDE
Y / 10³ ft.
0
50
100
150
200
250
300
6-27-61

Intra-Company Communication

SUBJECT: MARINER B CAPSULE STUDY
MARS CAPSULE TV
SURFACE BRIGHTNESS OF MARS
(From de Vaucoulers)

October 2, 1961

FROM: I. H. Blifford TO: Distribution

The solar illumination E at Mars distance D is given by

$$E = \frac{I}{D^2}$$

where I is the solar intensity at 1.0 A.U. and D^2 is the distance of Mars to the Sun in A.U.

The brightness of a perfectly reflecting surface obeying Lambert's law is then

$$B = \frac{E}{\pi} = \frac{I}{\pi D^2} .$$

If i is the intensity of Mars at opposition and s its apparent semi-diameter the geometrical albedo K is (at zero phase)

$$K = \frac{i}{Is^2}$$

and the mean surface brightness is

$$B_o = kB = \frac{i}{\pi s^2 D^2} .$$

Since Log i = -0.4 (M_m - M_s) where M_m = mean stellar magnitude of Mars at opp.

177

After correcting for units the relationship between the mean magnitudes and the apparent angular diameter at opposition the following relationship can be written

$$\log B_o = 0.4\ (M_s - M_m) + 2\left[\log (D-1) - \log s\right] - 4.497.$$

de Vaucouleurs gives the following values:

$$s = 2.264 \pm 0.002 \times 10^{-5} \text{ radian}$$

$$M_m = -1.90 \pm 0.02$$

$$M_s = -14.32 \pm 0.02$$

which when put into the above equation give

$$B = 0.23 \pm 0.01 \text{ candle/cm}^2$$

when corrected for absorption in the Martian atmosphere.

The mean albedo of Mars is about 0.15 but both bright and dark areas are observed which differ from this value in reflecting power.

Fessenkoff's results (loc. cit.) for these areas are:

Wavelength Å	Albdeo Bright	Albdeo Dark
0.430	0.094	0.087
0.560	0.188	0.175
0.630	0.233	0.165
0.730	0.268	0.162

Television Camera and Optics

For purposes of discussion the model HE-431A Missileborne Slow-Scan TV camera manufactured by Hallamore Electronics Div., Siegler Corp. will be used. This unit employs a 7290 Westinghouse Vidicon camera tube.

Some of the characteristics of this system are:

Electrical:

Resolution	600-450 TV lines
Gray shades	8-10
Video output	1.4 V p-p
Total pwr	15 watts
Frame rate	1/2 cps
Target area	1/2" x 3/8"

Environmental:

Temp.	0-158°F
Rel. humidity	100%
Pressure	0.01μ - 30 mm Hg
Shock	50 G
Vibration	10G
Acceleration	10 G

Physical:

Camera	8" L x 2 1/2" D
Camera control	3-3/4" x 5" x 7"
Total weight	6 lb.

The manufacturer gives typical light transfer characteristics which indicate that an exposure of about 0.1 foot candle sec will be required. The output current is stated to remain approximately constant over the range of exposure times of 10 m sec to 30 sec if the quantity of light remains constant.

The spectral response of the Westinghouse 7290 Slow Scan Vidicon has a maximum at 4500 Å and drops to 20% at about 5600 Å. If this tube is used it appears that little change in luminance will be experienced due to the spectral and geographic variation of albedo.

It can be shown that the illumination E at the image plane of an optical system of aperture f, looking at a surface of luminance L is

$$E = \frac{\pi L}{4f^2} .$$

For the Vidicon being considered a lens of aperture f 1.0 is easily realisable and therefore the illuminance at the tube will be

$$E = \frac{\pi}{4} (0.23)$$

$$= 0.18 \text{ cm candle}$$

$$= 180 \text{ foot candles}$$

This will require an exposure time of only about 1/1000 sec. Figures for the exposure time for other apertures are given below:

f	t (sec)
1	0.56×10^{-3}
2	2.2
4	8.8
8	35
16	140

It may be concluded that there is sufficient illumination to make it possible to use a simple and light weight optical system. It is assumed that extremely high resolution will not be required. The exposure times determined above are realizable with mechanical shutters of the between the lens or focal plane types. Spaulding (J. SMPTE, Vol. 69, Jan 1960) describes an optical system with an 8 in. F.L. and f number 1.35 for lunar photography. However the estimated weight of 20 lb compared to a few oz. for the standard 35 mm or movie camera lens suggested here is probably excessive.

Resolution

The ground resolution R_G is given approximately by

$$R_G = h/25\ L_f\ R$$

where: h = height above ground in feet

L_f = focal length of lens in inches

R = resolution limit in lines per mm.

For the altitude of parachute deployment of 55,000 feet the ground resolution would be

$$R_G = \frac{55 \times 10^3}{25 \times 16} \simeq 140 \text{ ft.}$$

for L_f = 1" and R = 200 TV lines on a 0.5 inch frame = 16 lines per mm.

For diffraction limited optics and relative aperture $f = \frac{D_L}{L_f}$ the limiting aperture is given by

$$f = \frac{R}{1500} \simeq 100$$

for 16 /mm camera resolution. It may be concluded that there is little fear of image degradation due to lens diffraction even for large f numbers.

In terrestrial high altitude photographs atmospheric turbulence can be the principal limitation to the resolution. It is of interest to see whether this may be a factor in the proposed system. The angular deviation δ, due to terrestrial turbulent effects is often quoted as approximately 1 sec of arc. The displacement d of the image at the Vidicon tube face will be approximately

$$d = L_f \tan \delta$$

$$\simeq \delta L_f$$

$$\simeq 5 \times 10^{-6} \times 25$$

$$= 1.3 \times 10^{-4} \text{ mm}$$

or with 16 line/mm resolution a negligible amount. Of course this conclusion cannot be supported by any measurements of the Martian atmosphere and assumes that turbulence will be of the order of that on the Earth.

Number of Pictures

For a 200 line picture the number of bits will be about 1.2×10^5 using 8 gray levels and at a transmission capability of 10^3 bits/sec it will require 120 sec to transmit one picture. At the estimated capsule fall velocity of 50 ft/sec there will be about 1000 sec available or approximately 8 pictures may be obtained. Of course the short exposure times previously calculated indicate that at least several hundred pictures are feasible. In this case however it would be necessary to use some form of storage (memory core) on the capsule and to transmit the information after landing.